GEOMETRIC MODELING OF MANUFACTURIN PROCESSES USING SYMBOLIC AND COMPUTATIONAL CONJUGATE GEOMETRY

A Thesis Submitted
In Partial Fulfilment of the Requirements
for the Degree of
Doctor of Philosophy

by
Karunakara Poopathi, K.P.

to the
Department of Mechanical Engineering
INDIAN INSTITUTE OF TECHNOLOGY KANPUR
May, 1993

7 JUN 1994 ME
CENTRAL LIBRARY
KANPUR
Acc. No. A. 117852

ME-1993-D-KAR-GEO

Dedicated to
my parents, my wife and
my daughters

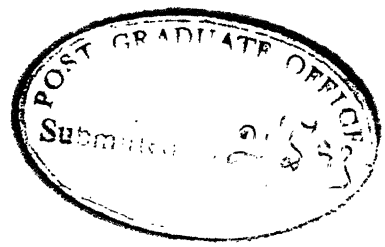

CERTIFICATE

This is to certify that the present work entitled GEOMETRIC MODELING OF MANUFACTURING PROCESSES USING SYMBOLIC AND COMPUTATIONAL CONJUGATE GEOMETRY was carried out by Karunakara Poopathi, K.P under my supervision and it has not been submitted elsewhere for a degree.

Dr Sanjay G. Dhande
Professor, ME & CSE
Head, Mechanical Engineering
IIT Kanpur

May 21, 1993

SYNOPSIS

GEOMETRIC MODELING OF MANUFACTURING PROCESSES
USING SYMBOLIC AND COMPUTATIONAL CONJUGATE GEOMETRY

A Thesis Submitted
in Partial Fulfilment of the Requirements
for the Degree of
Doctor of Philosophy
by

Karunakara Poopathi, K.P.

to the

Department of Mechanical Engineering
Indian Institute of Technology, Kanpur

May, 1993

All manufacturing processes are shape realization processes. How the shape is realized is as important as how it is designed. The present thesis addresses the problem of modeling the shape realization processes mathematically. Unified models for the geometry of a generic cutter as well as for the kinematic structure of a generic machine tool have been proposed using the concepts of envelope theory and conjugate geometry. The methodology adopted here is called *conjugate geometry formulation*. These models of the generic machine tool and the generic cutter have been implemented as symbolic algorithms using the symbolic manipulation package *MACSYMA* for modeling a variety of shape generating processes. It has been shown that several types of machine tool kinematic structures can be realized using the proposed unified model of the machine tool. Also, it has been shown that a variety of cutter geometries can be instantiated from the unified model of the cutter. Furthermore, one can automatically obtain the equations of the geometry of the machined surface for any combination of a cutting tool geometry and

a machine tool structure. The proposed methodology enables a manufacturing engineer to evaluate the likely outcome of a particular cutting tool/ machine tool assembly of a manufacturing process.

Any shape generation process has three constituents, viz., the geometry of the cutter, the geometry of the surface it produces on the blank and the relative motion between the cutter and the blank. The conjugate geometry formulation is based on the fact that the surface of the cutter and the machined surface are mutually enveloping surfaces. A coordinate frame is attached to each of these two surfaces and the positions and orientations of these two moving frames are given by twelve parameters with respect to a fixed global frame of reference. These twelve motion parameters are algebraic expressions as functions of time and the cutter surface and the blank surface will be expressed as algebraic expressions in the bi-parametric form. Homogeneous transformation matrices are used to map the instantaneous positions of the cutter surface and the blank surface from one frame to the other. Out of the three constituents of a machining process, if any two are known, the third constituent can be determined using the mapping functions and the condition of cutting. The condition of cutting is the orthogonolity condition between the relative velocity vector and the common normal of the cutter and blank surfaces at the point of cutting. The proposed model of a generic machine tool will be a useful tool for NC cutter path simulation, NC cutter path generation and selection of an appropriate combination of a machine tool and cutting tool to produce a given surface. In the traditional methods for cutter path simulation and cutter path generation, the blank is considered to be fixed and all the relative motions are imposed on the cutter by superimposing the reverse motion of the blank to both the cutter and the blank. In contrast to this, the degrees of freedom of both the cutter and the blank are directly used in the proposed conjugate geometry approach and hence when it is used for cutter path generation, the output is in terms of the joint coordinates of the machine

tool thus alleviating the need for post-processing and when it is used for cutter path simulation, the surface obtained is more realistic and free from post-processing inaccuracies. Added to this, the output of the symbolic programs will be algebraic expressions which can be reduced to numeric form of any desired accuracy.

The models of the generic cutter uses nine parameters to define a two-dimensional profile. This profile consists of a set of three straight line and a circular arc segments. By appropriately sweeping this planar profile, the bi-parametric definition of the cutter surface is obtained.

The usefulness of the two models of the generic machine tool and the generic cutter have been demonstrated by modeling a number of manufacturing processes. Modeling of gear manufacture using a gear planing process with a rack cutter and using a gear hobbing process has been illustrated. The proposed methodology will be helpful for a manufacturing engineer to evaluate alternative machining strategies in order to choose the optimum one. By simply changing the values of the nine parameters describing the cutter surface and the twelve motion parameters, an engineer can obtain the machined surface and can visualize it using a graphic display. Three alternative strategies to produce a helicoidal surface have been modelled to illustrate this. Two different ways of producing a hyperbolic paraboloidal surfaces are also given. Finally, a cylindrical cam and follower mechanism has been modelled. For a given cylindrical translating follower, the surface of the slot on the cam has been obtained using the proposed models. It is interesting to note that the same set of input and output will describe the manufacture of the cam surface using an end milling cutter.

An extensive case study has been carried out for the design and manufacture of extruder screw surfaces. This case study establishes that the methodology proposed in

this thesis for modeling the manufacturing processes can also be useful for the geometrical design of extruder screws. First, the procedure for the design of one of the surfaces of the extruder screw pair is explained by considering it to be a set of contiguous arc segments. Since the relative motion between the screws is known and both the screw surfaces are mutually enveloping, the other screw surface can be determined using the generic model of a machine tool with twelve degrees of freedom. Examples for the design of extruder screws of all three types, viz., symmetrical screw pairs, unsymmetrical screw pairs of equal diameters and unsymmetrical screws of unequal diameters have been given.

It is found that only the root and flank arc segments of an extruder screw influence the cutter design for the manufacture of the extruder screws since the tip segment is realized in the preparation of the cylindrical blank itself. A procedure to determine the characteristic cutter profile for any screw surface geometry has been developed. This characteristic profile is the intersection curve between the helical slot of the screw and a plane that is normal to the helix. The axial position of this plane is chosen such that the full slot is captured in it. The extruder screw which is basically a helicoidal surface can be machined using a turning process with a form tool. It can also be produced by a milling process with an end milling cutter, a side-and-face milling cutter or by a side milling cutter. The procedure to obtain the surfaces of the turning tool, end milling cutter and disc type of cutter have been explained with the help of examples. The design of the side milling cutter has been studied in detail and it was found that except for very simple helicoidal surfaces, such a cutter does not exist. However, a procedure has been given using which a side milling cutter can be designed if such a cutter exists and this procedure has been explained with an example.

ACKNOWLEDGEMENTS

I am immensely grateful to Professor Sanjay G. Dhande. He was not only my guide; he is my mentor as well. He did not restrict himself to supervising the thesis alone. Whenever I was in trouble, he was there to help me. He used to spend his precious weekends with me in discussing the research work. When I was transferred from Kanpur to Nasik, I chose to continue my research at IIT and resigned my job at HAL. During the period of uncertainty and agony after the resignation, the encouragement and support extended by Professor Dhande is unforgettable. I am highly indebted to him and his family.

I would like to place on record my sincere gratitude to the authorities in HAL, particularly, Mr G.S. Singhal, General Manager of Kanpur Division and Mr N.R. Mohanty, General Manager of Nasik Division who went out of the way to help me. I am very thankful to Professor B. Sahay for his help during the initial period of my research. My thanks are also due to my best friend at HAL, Mr Appu.

My wife has an unshakable faith in me and readily concurs all my decisions. She is ready to undergo any amount of sufferings for my benefit. Her constant support and encouragement during the course of this program was the source of energy to achieve my goal. She never complained even though she had to undergo great amount of difficulties and our daughters followed her footsteps. I am proud of them. My parents believe that I am mature enough to take decisions but still watched my moves with fear and prayed for me all the time. But for their prayers and blessings, I doubt whether this thesis work would have been possible. During the last eight months, my brother Chamna stayed with me and helped me in the report preparation and household works. I wish him success in his endeavors.

I am very thankful to my friends Mr B.K. Misra, Mr P.V.M. Rao, Mr J. Venkatesh, Dr P.S. Avadhani and others for the fruitful discussions I had with them. I am grateful to Mr Satish Vamburkar, Mrs S. Biswas, Mr B.S.S. Pradhan, Dr A. Chawla and Mr Gagan Saksena for their help and company.

I also would like to thank the employees of CAD-Project, Mr C.P. Singh, Mr S. Gupta and Mr Babu Lal who helped me in several ways during the last four years.

- K. P. Karunakaran

TABLE OF CONTENTS

LIST OF FIGURES

LIST OF TABLES

LIST OF SYMBOLS

Σ_1 - Surface of the cutter.

Σ_2 - Surface of the blank.

S_1 - Coordinate system attached to the cutter.

S_2 - Coordinate system attached to the blank.

S_0 - Fixed global cordinate system.

$S_{\bar{1}}$ - Initial position of the coordinate system S_1.

$S_{\bar{2}}$ - Initial position of the coordinate system S_2.

a_1 - Distance of O_1 from O_0 along X_0 axis.

b_1 - Distance of O_1 from O_0 along Y_0 axis.

c_1 - Distance of O_1 from O_0 along Z_0 axis.

θ_1 - Rotation of coodinate system S_1 about X_0 axis.

ϕ_1 - Rotation of coodinate system S_1 about Y_0 axis.

ψ_1 - Rotation of coodinate system S_1 about Z_0 axis.

a_2 - Distance of O_2 from O_0 along X_0 axis.

b_2 - Distance of O_2 from O_0 along Y_0 axis.

c_2 - Distance of O_2 from O_0 along Z_0 axis.

θ_2 - Rotation of coodinate system S_2 about X_0 axis.

ϕ_2 - Rotation of coodinate system S_2 about Y_0 axis.

ψ_2 - Rotation of coodinate system S_2 about Z_0 axis.

u, v - Parameters describing the Σ_1.

$^1\underset{\sim}{p}$ - Point P with reference to the tool coordinate system S_1.

$^2\underset{\sim}{p}$ - Point P with reference to the blank coordinate system S_2.

$^1\underset{\sim}{n}_{P,1}$ - Unit normal vector of the cutter surface Σ_1 at point P with reference to coordinate system S_1.

$^0\underset{\sim}{n}_{P,1}$ - Unit normal vector of the cutter surface Σ_1 at point P with reference to coordinate system S_0.

$^2\underset{\sim}{n}_{P,2}$ - Unit normal vector of the blank surface Σ_2 at point P with reference to coordinate system S_2.

$^0\underset{\sim}{n}_{P,2}$ - Unit normal vector of the blank surface Σ_2 at point P with reference to coordinate system S_0.

$[^0_1M]$ - Homogeneous transformation matrix of a vector from the coordinate system S_1 to S_0 .

$[^0_2M]$ - Homogeneous transformation matrix of a vector from the coordinate system S_2 to S_0.

$^0\underset{\sim}{n}_{P,1}$ - Unit normal vector of the cutter surface Σ_1 at point P with reference to coordinate system S_0.

$^0\underset{\sim}{n}_{P,2}$ - Unit normal vector of the cutter surface Σ_2 at point P with reference to coordinate system S_0.

$^0\underset{\sim}{V}_{P,1}$ - Velocity of the surface of the cutter with reference to coordinate system S_0.

$^0\underset{\sim}{V}_{P,2}$ - Velocity of the surface of the blank with reference to coordinate system S_0.

$^0\underset{\sim}{V}_{P,12}$ - Relative velocity vector between the tool and blank with reference to coordinate system S_0.

Chapter 1

INTRODUCTION

1.1 Geometric Modeling in Design & Manufacturing

Until recently the primary focus in geometric modeling has been on modeling of the basic geometry and topology of a component. As design engineers continue to evolve powerful definitions of free form surfaces using these geometric modeling techniques, the problem of manufacturing such surfaces becomes a challenging task. Hence emphasis is now shifting towards the development of computer-based models of product shapes which take into account aspects of physical realizability in addition to its basic geometry and topology for representing a component. Computer-based models which take into account the shape generating capabilities of machining processes are essential to evaluate the manufacturability of a design. What is now referred to as "Design for Manufacture", "Concurrent Design" or "Simultaneous Engineering" is increasingly becoming relevant to the total life cycle value of a component.

Physical realizability of a designed shape is a primary concern of any manufacturing activity. If the surface is to be realized using a milling-like process then it is necessary to select the most appropriate geometry of the cutting tool as well as the most suitable kinematic structure of the machine tool or the machining center. In some cases, a manufacturing engineer may have alternative options of cutting tool geometries and machine tool structures available for realizing a given designed surface. In such a case, it is necessary to find, before hand, the most appropriate combination of a machine tool type and a cutting tool geometry. Furthermore, a manufacturing engineer is usually called upon to define the law of relative motion between the cutting tool and the blank for a given type of kinematic structure of the machine tool. This is necessary since many a machines are now being controlled using CNC controllers. All such problems are now being considered as an important class of problems in the area of design for manufacture (Grossman, 1986; Dixon, 1989a, 1989b). Design for manufacture involves many aspects such as ease of manufacture, process planning, ease of inspection, design of tolerances,

design for reliability, testability and maintainability. Research interests in this area are growing. Many researchers are using the feature based representations to carry out these tasks of designing.

Design, analysis and manufacturing constitute three basic components of any cycle of product development. The process of design in general, and engineering design in particular, requires simultaneous considerations of engineering analysis as well as considerations of realization or manufacturing. As the technology of Computer Aided Design started becoming available at a reasonable cost to a designer, it became obvious that the developments would be directed to make the CAD tools more effective and relevant to the needs of a designer. After an initial phase of development where considerations of geometric modeling played a significant role, it appears that this initial development has triggered research in several different areas of design and manufacturing.

Behavioral scientists, computer science experts and engineers are trying to develop an appropriate design theory and methodology (Finger and Dixon, 1989a, 1989b). Descriptive, prescriptive and cognitive models are being used for developing such design theories. Engineers are trying to model all stages of the design process, viz., conceptual design, configurational design and detail design. There is also a considerable effort in developing new languages for design and manufacture. In the area of engineering analysis, considerable work is underway to develop interfaces between analysis and design processes. Many designers are incorporating different methods of optimization for improving a design. A quick review of the literature (Wozny et al., 1990) shows that design implications of manufacturing have started to emerge as an important consideration in the process of engineering design (Figure 1-1).

In order to be able to visualize and evaluate the geometry of machined surfaces generated by employing alternative machining strategies, unified symbolic models and algorithms for conventional milling-like processes have been developed in the present work. In these models, the cutter is considered to be a biparametric axisymmetric surface. The machined surface is assumed to be a conjugate surface generated by the cutting tool surface due to the relative motion between the blank and the cutting tool. In order to unify different types of kinematic structures of machine tools, it has been proposed to model the relative motion using a twelve degrees of freedom model of a machine tool. The symbolic algorithm of machining enables the manufacturing engineer to obtain the biparametric equation of the machined surface (Symbolics, Inc, 1988; Wallis et al., 1989). One can visualize and evaluate computationally the accuracy of this surface before finalizing the manufacturing process.

In the present work, unified models for the geometry of a generic cutter as well as for the kinematic structure of a generic machine tool have been proposed using the

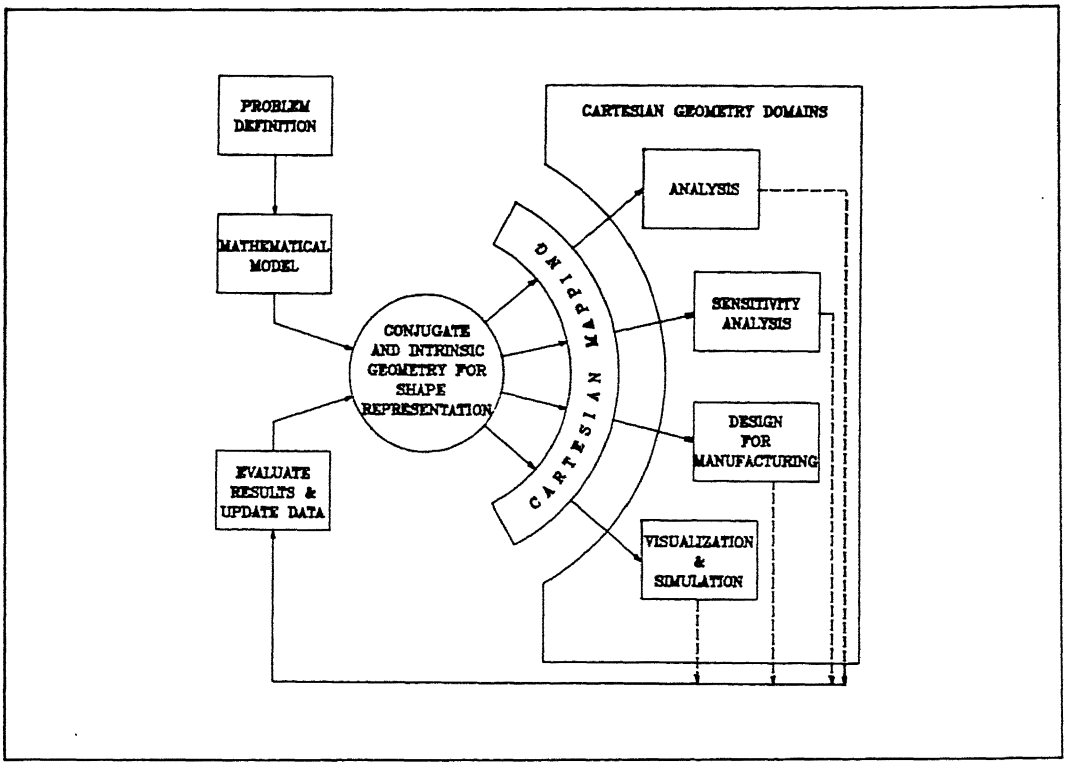

Figure 1-1. Model of Shape Synthesis Tools Based on Conjugate and Intrinsic Geometry Formulation.

concepts of *envelope theory* and *conjugate geometry*. The three basic determinants of a manufacturing process as identified in this model are geometry of the cutter, geometry of the machined surface and description of the relative motion between these two surfaces. The twelve degrees of freedom model of a manufacturing process proposed here can be used to find any one of the three determinants of a manufacturing process if the other two are known. Such a unified model will be useful for cutter path simulation, cutter path generation and selection of an appropriate combination of machine tool and cutting tool to produce a given surface. It can also be used in the design of cams, gears, extruder screws etc. which involve a pair of enveloping surfaces.

1.2 Literature Review

Recent developments in the area of geometric modeling in general, and solid modeling in particular, have provided design and manufacturing engineers with an elegant and precise definition of a component or a product that needs to be designed (Mortenson,

1985; Mäntylä, 1988; Voelcker and Requicha, 1977; Faux and Pratt, 1983). Based on these definitions of a component, several research workers have developed methodologies to generate process plans for manufacturing the designed components (Chang and Wysk, 1985; Kanumury and Chang, 1991; Joshi and Chang, 1988; Perng et al., 1990; Shah, 1991; Srinivasan and Ferreira, 1990). The process plans are generally based on the geometric features of a component on one hand and the capability of a manufacturing process to produce those features on the other hand. Such process plans do not generally take into account a micro-level geometric model of the tool and the blank along with the kinematic structure of the machine tool used for the manufacturing process. Researchers in the area of manufacturing processes have studied the physics and the mechanics of several processes (Acherkan et al., 1973; Ghosh and Mallik, 1981; Ber et al., 1988; Sen and Bhattacharyya, 1969; Pande and Shah, 1980). However, it has been found that except in the area of gear manufacturing, there is very little in the literature to model either symbolically or computationally the geometry of several manufacturing processes.

Simulation of machining processes is one of the major areas of research in manufacturing. In order to model a machining process, one needs to take into account several factors such as the geometry of the cutting tool, the kinematic structure of the machine tool, the cutting speed and the feed rate, the material properties of the cutting tool and the material being cut, the cutting forces of the machining process, the energy required for machining, etc. Srinivasan and Ferreira (1990) have proposed two levels for modeling a machining process. The lower level takes into account the kinematic chain of the machine tool and the upper level takes into account each component of the cutting and feed motions. Such a classification is helpful for feature definition and process selection activity of *Computer Aided Process Planning* (CAPP).

The problem of defining the geometry of a machined surface is essentially a problem of defining the boundary of the swept volume of the cutter. Wang and Wang (1986a, 1986b) have defined the swept volume using the envelope theory approach. They however do not model explicitly the kinematic structure of the machine tool. Yap (1988) has described some algorithms for computing three dimensional tool paths for planar and non-planar machined surfaces. Dhande et al. (1990, 1992) have shown how the geometry of a machined surface can be derived for a non-traditional manufacturing process such as wire EDM. The discrete simulation of machining sculptured surfaces has been studied by Drysdale and Jerard (1989). An approach to define the swept volume using the sweep differential equations has been proposed by Blackmore and Leu (1990). All these works do not take into account explicitly the kinematic structure of the machine tool.

The problem of conjugate geometry between a pair of moving as well as contacting surfaces is termed as a higher pair contact problem in kinematics (Boltyanskii, 1964; Dudley and Darle, 1962; Chakraborty and Dhande, 1977). Such problems have been

analyzed by designers for design of cams and gears. Dhande and Chakraborty (1977) have described the methodology of defining the kinematics of relative motion as well as the geometry of the contacting surfaces for three dimensional cams. Several researchers have studied the problem of conjugate geometry for planar and spatial gear mechanisms (Dudley, 1962; Dhande and Chakraborty, 1977). One can see that there is some amount of similarity between the conjugate geometry problems encountered in machining processes on one hand and for gear and cam design on the other.

One of the major computational difficulties in formulating and analyzing the problems of conjugate geometry is that for every given situation of a pair of contacting surfaces and their relative motion, one has to derive the biparametric equations of the surfaces every time. This can be improved by using the symbolic manipulation approach for the problems of conjugate geometry especially for modeling different manufacturing processes. Reinholtz and Dhande et al.(1990) have described an approach of how symbolic manipulation can be used for defining the machined surfaces. They have considered only a three degrees of freedom model to show how helically swept surfaces can be manufactured using alternative machining strategies. A model with more degrees of freedom such as the twelve degrees of freedom model proposed in this thesis, it is believed, can be used for instantiating a variety of machine tool structures. The proposed symbolic model of the generic cutter along with this model of the machine tool assembly provides a unified approach for modeling a variety of manufacturing situations.

1.3 Envelope Theory

A brief summary of the important results of the envelope theory are described in the present section. A family of curves can be specified in an implicit form by the equation

$$f(x, y, \alpha) = 0 \qquad \alpha_{min} \leq \alpha \leq \alpha_{max} \tag{1-1}$$

where x and y are the Cartesian coordinates of a generic point and α is a parameter (Figure 1-2). By giving a specific numerical value of α, say α_i, one can obtain the equation of a member of the family as

$$f(x, y, \alpha_i) = 0 \tag{1-2}$$

It is assumed that every member of the family is a C^1-continuous curve. Furthermore, it is assumed that successive members of the family intersect at a finite point. Each of these points of intersections, it is assumed, has a limiting position when the successive member curves are considered infinitesimally close and approaching a limit

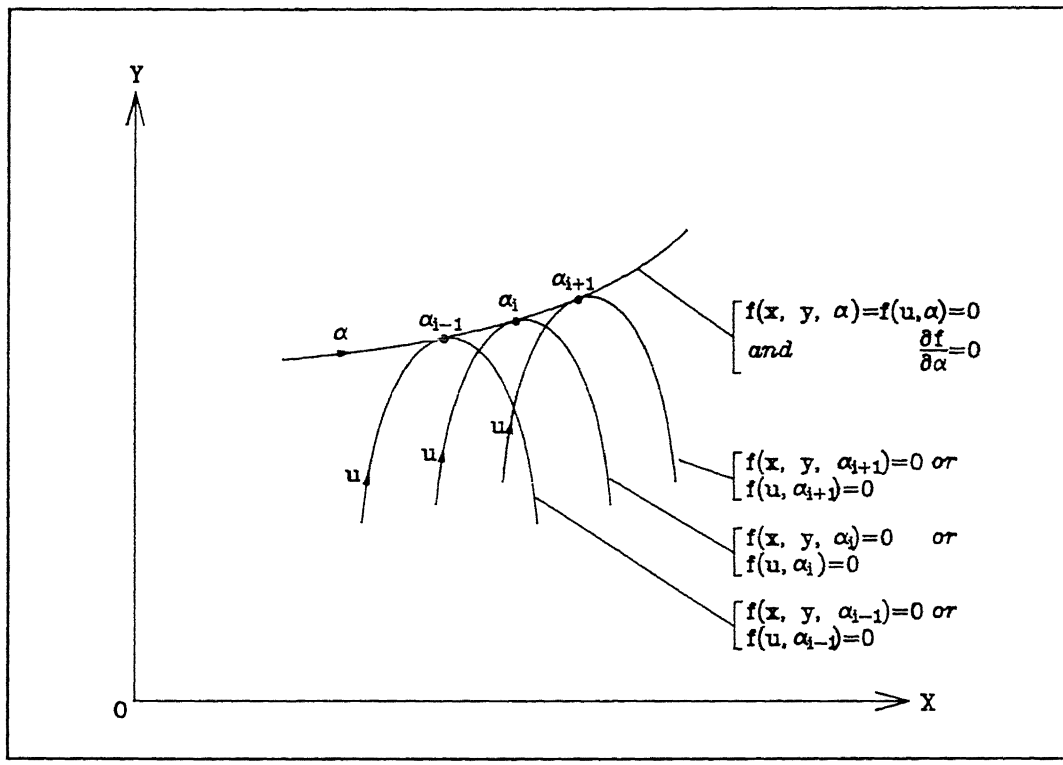

Figure 1-2. Envelope of a Family of Curves.

(Boltyanskii, 1964). The point of intersection of a pair of infinitesimally close member curves can be obtained by solving the equations

$$\begin{aligned} f(x, y, \alpha_i) &= 0 \\ f(x, y, \alpha_i+\Delta\alpha) &= 0 \end{aligned} \tag{1-3}$$

$\Delta\alpha$ being an infinitesimal increase in α. The limiting position of this point of intersection can be obtained by eliminating α from the following equations:

$$\begin{aligned} f(x, y, \alpha) &= 0 \\ \frac{\partial f}{\partial \alpha} &= 0 \end{aligned} \tag{1-4}$$

All such limiting positions, in turn, define the envelope to the family of curves.

In parametric form, this equation of a family of curves is given by

$$f(u, \alpha) = 0 \tag{1-5}$$

and a generic point P of this family can be expressed as

$$\underset{\sim}{p}(u, \alpha) = [\, x(u, \alpha) \quad y(u, \alpha)] \tag{1-6}$$

where $u_{min} \le u \le u_{max}$ and $\alpha_{min} \le \alpha \le \alpha_{max}$. In parametric form, the limiting positions of the points of intersections can be obtained by considering the collinearity of the vectors $\dfrac{\partial \underset{\sim}{p}}{\partial u}$ and $\dfrac{\partial \underset{\sim}{p}}{\partial \alpha}$. In other words, the equation of the envelope in the parametric form can be obtained by eliminating the parameter u between the following two equations (Chakraborty and Dhande, 1977):

$$\begin{aligned} f(u, \alpha) &= 0 \\ \underset{\sim}{n} \cdot \underset{\sim}{V} &= 0 \end{aligned} \tag{1-7}$$

where $\underset{\sim}{V} = \dfrac{\partial \underset{\sim}{p}}{\partial \alpha}$ and $\underset{\sim}{n} \cdot \left(\dfrac{\partial \underset{\sim}{p}}{\partial u} \right) = -1$.

It will be useful to give a physical interpretation of Equation (1-7). If the parameter α represents time then $\underset{\sim}{V}$ and $\underset{\sim}{n}$ will be the velocity and normal vectors at any point. When a curve is being swept, every point on the curve is moving along the direction of its velocity. If this velocity vector is orthogonal to the normal vector at any point on the curve, then that point (of the curve) is the point defining the envelope curve at that instant. All other points of the curve will lie within the swept area of the curve.

In many cases, it is required to find the envelope of a curve or surface in another moving frame of reference rather than a fixed frame of reference. Furthermore, the parametric form allows us to describe the envelope of either a curve or a surface in a symbolic manner. Taking these two aspects into account, a general model of two mutually enveloping surfaces has been developed which is considered as a conjugate geometry model (Chapter 2).

1.4 Symbolic Computation

Computers have been used traditionally to solve problems which could be expressed numerically, i.e., all symbols used in the problem are bound to numerical values before they are referred. On the other hand, some problems can be expressed best in symbolic terms, or perhaps can be expressed only that way. Solving such problems where the variables are manipulated even when they do not have numerical bindings is called *symbolic computation*. It is also known by many other names such as symbolic algebra, symbolic mathematics, symbolic manipulation, analytic calculation, computer algebra, algebraic manipulation, formula manipulation etc.

The idea that computers, or calculating engines as they were known, could perform algebraic rather than numerical calculations was first suggested nearly 150 years ago by Lady Ada Lovelace[1]. However, only after 1960, the hardware and software capabilities became reasonably adequate to permit the development of useful computer algebra systems. Since this time, the systems developed for symbolic computation can be divided into three notional groups, viz., Group I, Group II and Group III (Table 1-1). Initially the packages were written to solve problems of specific areas such as general relativity, quantum theory, celestial mechanics and high energy physics. Since the usefulness of these packages for other areas also was realized, general purpose symbolic algebra systems were developed. They were very general and hence they required very huge memory and they also were very sluggish. The early symbolic algebra systems were not interactive. To-day, the speed of computers have gone up by virtue of the latest technologies like *RISC* and parallel processing. The symbolic packages such as *MathCAD* and *MACSYMA* are available for a variety of platforms including personal computers. They are highly user-friendly as they make use of sophisticated user-interfaces like *Windows*. In view of this, symbolic computing is competing with even numerical computing.

The symbolic manipulation systems can perform a variety of operations. They can perform matrix algebra and trigonometric calculations, solve a system of equations and find roots of an expression. They can also solve problems involving differentiation and integration. Some of the packages like *MACSYMA* can also find the numerical solutions wherever required. It can evaluate a function as one of its arguments approaches a specified limit. The results of the calculations are output in more readable multi-line format. These packages also have graphic capabilities with automatic scaling etc. for depicting the results graphically. Most of the symbolic packages can generate output in

[1] Lady Ada Lovelace was patron of Charles Babbage who is usually credited with the development of World's first computer.

Notional Group	Characteristics	Examples with Salient Features			
I	i) Tends to solve specialized problems such as General Relativity, Quantum Theory, Celestial Mechanics and High Energy Physics and ii) Requires of large main frame.	*SCHOONSHIP* Non-interactive	*CAMAL* Non-interactive	*CLAM* Non-interactive	*ASHMEDAI* Non-interactive
II	i) Too much general, ii) Sacrificed performance to achieve generality, iii) Better user-interface and iv) Requires only smaller main frame or work station.	*REDUCE* - Rand Corp. - Available for several O.S., - Few built-in functions, - Non-interactive.	*MACSYMA* - Symbolics Inc., - Available for fewer O.S., - Large number of built-in functions, - Non-interactive.	*SMP* - Inference Corp., - Fairly good number of built-in functions.	*SCRATCHPAD* - IMB Corp., - Available for IBM O.S., - Non-interactive.
III	i) Restricted generality, ii) Smaller memory requirements, iii) Simple to use due very user-friendly interactive environment and iv) Wide range of built-in fuctions.	*MAPLE* - Watcom Products, - Available for a variety of platforms at work station level.	*muMATH* - Software Warehouse Inc., - Runs on micro-computers with CP/M or DOS and main frames.	*MathCAD* - MathSoft Inc., - Available for microcomputers and main frames, - Very user-friendly.	

Table 1-1. Classification of Symbolic Computation Systems

the format acceptable to other systems like *FORTRAN* and *C* compilers.

The advantages of symbolic computing can be listed as given below.

a) The purpose of computing is insight and not numbers. If we write $\left(\frac{x}{a}\right)^2 + \left(\frac{y}{b}\right)^2 = 1$, it immediately occurs to a mathematician that it is an ellipse. This is a symbolic expression. On the other hand, if the coordinates of a set of points lying on this ellipse are given, one cannot visualize it as an ellipse unless he plots these points and performs a curve-fitting. Thus computing symbolically helps fulfill the purpose of providing analytical rather than numerical answers. In other words, an algebraic solution is usually more succinct and meaningful than a numerical solution.

b) When a computation is performed symbolically, the algorithm maintains the generality of computation. Hence the symbolic system is inherently well-suited for developing generic algorithms. Dhande (1976) has derived the expressions for the conjugate surfaces of more than 20 different cases of planar and spacial cam mechanisms. All those computations can be solved by a single symbolic algorithm. In fact, this was the motivation for the selection of the symbolic approach for implementing the models of the generic machine tool and the generic cutter.

c) Numerical systems operate with floating point approximations whose precision is limited by the hardware whereas the algebraic solutions are always exact. Rounding-off can be delayed till the last step to minimize its influence on the final result when symbolic computation is used. The symbolic algorithms can deal with zero and infinity more elegantly.

d) A symbolic algorithm can solve an analytical problem in a few minutes which could be taxing a capable mathematician for several months. One wonders how many tractable problems remain unsolved or have been forgotten about simply because they were making excessive demands on a researcher's time and sanity. Moreover, the solution will be free from errors caused due to fatigue.

e) Symbolic algebra minimizes the need for tables of solutions to specific problems. Indeed, one of the triumphs of these systems is that they have highlighted several errors in tables of integrals used by engineers and scientists. Hence, one can concentrate on the problem formulation rather than

remembering various numeric techniques for solving the problem.

f) For some problems where the analytical solution may not exist, it is preferable to simplify the expressions using the symbolic system to produce more efficient and accurate results.

Mani (1989) has demonstrated the use of a hybrid system consisting of the symbolic manipulation system *MACSYMA* and the numerical compiler *FORTRAN* for the analysis of mechanical systems such as a robot arm. As the speed of computers increases, it is expected that more and more applications will make use of the symbolic approach which were hitherto solved numerically.

1.5 Organization of the Work

The objective of the present work is to develop the mathematical formulation and the symbolic algorithms required for the geometric modeling of manufacturing processes in a unified way. The methodology proposed here can be used in developing a user-friendly menu-driven software that a manufacturing engineer can use effectively. This report consists of eight chapters. In Chapter 1, brief descriptions of envelope theory and symbolic computation are presented following an extensive literature review.

Chapters 2, 3 and 4 deal with the conjugate geometry formulation. In Chapter 2, mathematical interpretation of Acherkan's four methods of obtaining the generatrix and directrix of a manufacturing process is given (Section 2.2) followed by several examples of manufacturing processes identifying the generatrix, directrix and the degrees of freedom involved in each case (Section 2.3). After this, the conjugate geometry formulation and its symbolic algorithm are described in Section 2.4. The instantiation of the generic model of the machine tool for a variety of machine tools is presented in Chapter 3. Also given is the illustration of the model for machining an extruder screw surface. A generic model of the cutter and its instances are described in Chapter 4.

In Chapter 5, the usefulness of the conjugate geometry model of a machine tool and the model of the generic cutter have been demonstrated by means of examples such as gear hobbing and shaping. Alternative machining strategies of a helicoidal and hyperbolic paraboloidal surfaces have also been modeled using the proposed models. It is concluded with an example on design and manufacture of a cylindrical cam and follower mechanism.

The use of the proposed methodology for the design and manufacture of extruder screws has been investigated in Chapters 6 and 7. In Chapter 6, the procedure for the

design of a pair of extruder screws of different types is given. Chapter 7 is for the manufacture of extruder screws. Procedures for the design of cutter to machine a given screw surface and for the determination of the screw surface for a given cutter profile are given in this chapter.

Finally, the conclusions and future extensions of this work are presented in Chapter 8.

Chapter 2

CONJUGATE GEOMETRY MODEL OF A MACHINING PROCESS

2.1 Introduction

The proposed methodology of a generic machine tool model is based on the premise that all manufacturing processes are essentially *shape realization* processes. Furthermore, all such shape realization processes can be classified into two groups, viz., (i) shape generation processes and (ii) shape formation or shape transformation processes. The shape generation processes are those processes which involve realization of a surface by removal of material. Generally, such material removal requires movement of a cutter through the volume of the blank. Processes such as milling, hobbing and shaping can be classified as shape generation processes (Figure 2-1a). Another class of shape realization processes involves transformation of a given volume from one state to another state. Such transformations generally involve plastic deformation of the material. Processes such as deep drawing, forging etc. can be cited as examples of this category (Figure 2-1b).

To begin with, a shape can be considered as the mathematical description of the extrinsic and intrinsic geometry of the boundary of a closed *regular set*. Let $\boldsymbol{S}$ be a closed regular set of points in either a 2-D or a 3-D space. Let $\boldsymbol{b(S)}$ be the set of points belonging to a closed regular set and defining the boundary of that set. The extrinsic properties are the properties such as the Cartesian coordinates of the points on the boundary of a set while the intrinsic properties are the properties such as the arc length and the curvature at a point on the boundary of that set.

It should be kept in mind that a mathematical description of the shape can be specified depending on the purpose of its use. For instance, if a shape is to be displayed on a computer-controlled display device then a parametric definition is appropriate (Figures 2-2b & 2-3b). If a shape is to be specified for some analysis procedure then an explicit or an implicit closed-form expression in Cartesian coordinates is useful (Figures

2-2a & 2-3a). However, if a shape is to be realized by a generation process then neither of these definitions are useful.

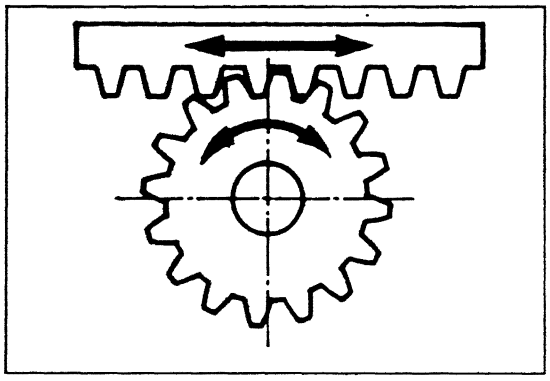

(a) Example of a Shape Generation Process

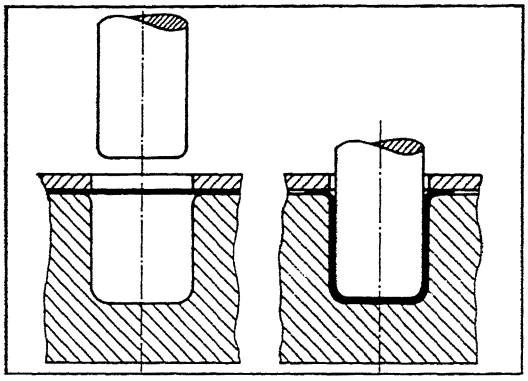

(b) Example of a Shape Transformation Process

Figure 2-1. Shape Generation and Shape Transformation Processes for Shape Realization.

Consider a case of generating a circle from a 2-D lamina. In order to realize the circular shape, one way could be to employ a series of straight line cuts (for example, using a pair of scissors). These straight line cuts constitute a family of curves (Figure 2-2c). An envelope to this family is the shape generated. In this case, it happens to be a circle. Similarly, if one needs to display a straight line then it can be defined in a parametric form (Figure 2-3b). However, if one needs to realize a straight line shape then it can be generated as an envelope of a family of circles. The family is generated by moving the center of the circle on a linear path (Figure 2-3c). Interestingly, it can be seen that in the examples shown in Figure 2-2 and Figure 2-3 a family of straight lines is generating a circular shape while a family of circles is generating a linear shape. This observation is important for a manufacturing engineer. It shows that a shape specified by a designer is realized by a generation scheme. This generation scheme employs a shape that is not necessarily the same but a different one, called as the conjugate shape, for the realization of the designed shape. It is also important to note that the manner in which the family of curves or shapes is defined is as important as the definition of the conjugate shape for designing a shape generating process. Generally, the manner in which the family of curves or surfaces of the cutting tool is defined is determined by the kinematic structure of the machine tool.

Traditionally, the envelope theory formulation finds the definition of an enveloping curve or a surface in a fixed frame of reference (Boltyanskii, 1964; Wang and Wang, 1986). This is not as useful for modeling several manufacturing processes. In many

(a)

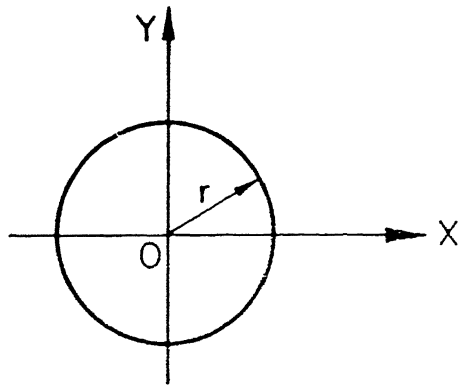

$x^2 + y^2 = r^2$

(b)

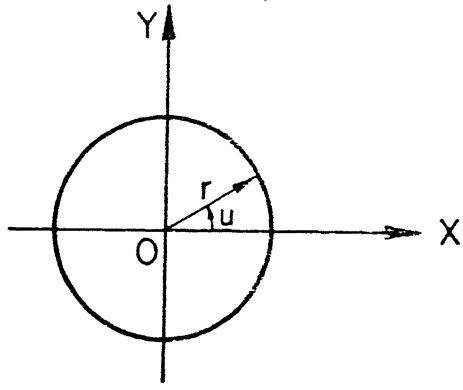

$x = r \cos \theta$
$y = r \sin \theta$
$0 \leq u \leq 2\pi$

(c)

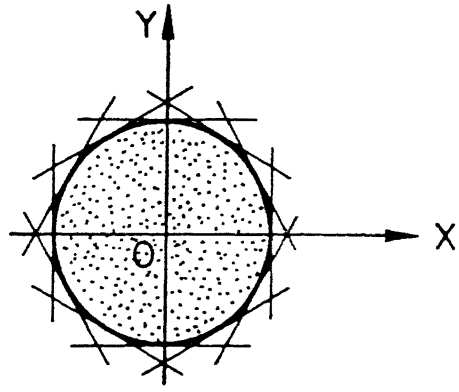

Envelope of

a family of straight lines

Figure 2-2 Definition, Display and Realization of a Circular Shape
(a) Mathematical Definition - Implicit Form
(b) Display Definition - Parametric Form and
(c) Realization Definition - Envelope Form

(a)

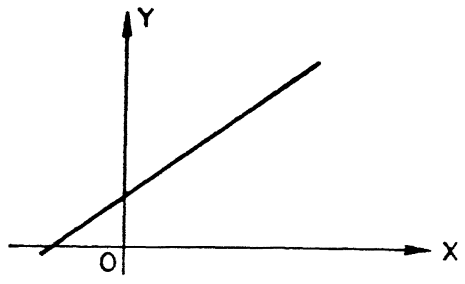

$$y = m\,x + c$$

(b)

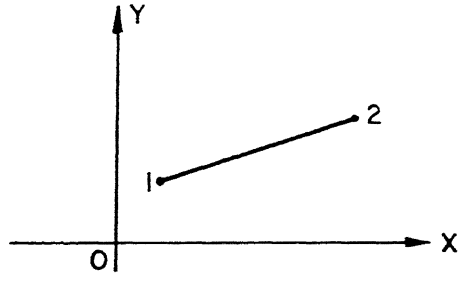

$$x = (1 - u)\,x_1 + u\,x_2$$
$$y = (1 - u)\,y_1 + u\,y_2$$
$$0 \leq u \leq 1$$

(c)

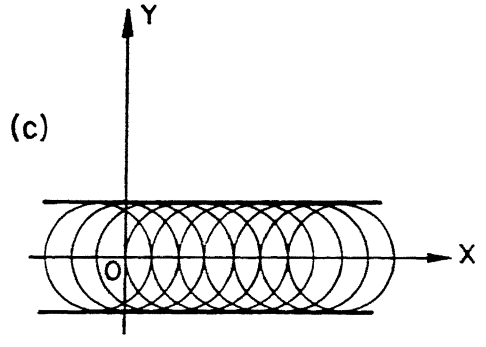

Envelope of

a family of circles

Figure 2-3 Definition, Display and Realization of a Straight Line Shape
(a) Mathematical Definition - Implicit Form
(b) Display Definition - Parametric Form and
(c) Realization Definition - Envelope Form

manufacturing processes, both the cutter as well as the blank may be moved in order to realize a surface. In such cases, it is necessary to find the envelope of the tool geometry (curve or surface) in another moving frame of reference attached to the blank body. The kinematics of the machine tool determines the relative motion between the tool and the blank. Such an extension of the envelope theory formulation can be termed as the *conjugate geometry formulation*. The conjugate geometry formulation defines the envelope in one moving frame of reference due to a family generated by another shape (curve or surface) and due to the relative motion between these two shapes, i.e., the cutter and the blank. This conjugate geometry model which is an extension of the envelope theory is the mathematical basis for modeling the geometry of several shape generating processes.

2.2 Shaping of Geometrical and Real Surfaces

Acherkan et al. (1973) have classified surfaces as geometrical and real surfaces. A geometrical surface is the one conceived by a designer. It can be defined as the trace or the sweep obtained due to the motion of one geometrical generating line, the generatrix, with respect to another geometrical generating line, the directrix. Alternatively, a geometrical surface can also be thought of as the boundary of a set resulting from the Minkowski addition of a set of points belonging to the generatrix and the set of points belonging to the directrix. If $\boldsymbol{A}$ and $\boldsymbol{B}$ are two closed regular sets of geometric points then the Minkowski addition of $\boldsymbol{A}$ and $\boldsymbol{B}$ is defined as a set-theoretic union of all the mapping of the set $\boldsymbol{A}$ when it is copied at every element of $\boldsymbol{B}$ (Ghosh and Mudur, 1984; Kaul, 1992). In the present case, the set $\boldsymbol{A}$ is the generatrix curve and the set $\boldsymbol{B}$ is the directrix curve. This definition of a geometrical surface is inadequate for defining surfaces realized in several manufacturing processes. For this purpose, it is necessary to consider the definition of real surfaces.

Real surfaces are obtained on a solid body by any one of the several methods of metal working. All these methods produce a real surface by shaping or removing material with the aid of *auxiliary material elements* which could be either points, lines (i.e. straight or curved) or real surfaces. The designed geometrical surfaces are produced due to the relative motions of these real auxiliary material elements. These relative motions are called *formative motions*. In practice the shaping of a material surface involves realization of the geometrical generating line through the auxiliary material element. The designed surface is produced due to the formative motions of the geometrical generating lines.

There are four methods of realizing geometrical generating lines from the auxiliary material elements which may be in the form of a line or a point. These are (i) forming method, (ii) generating method, (iii) tracing method and (iv) tangent method.

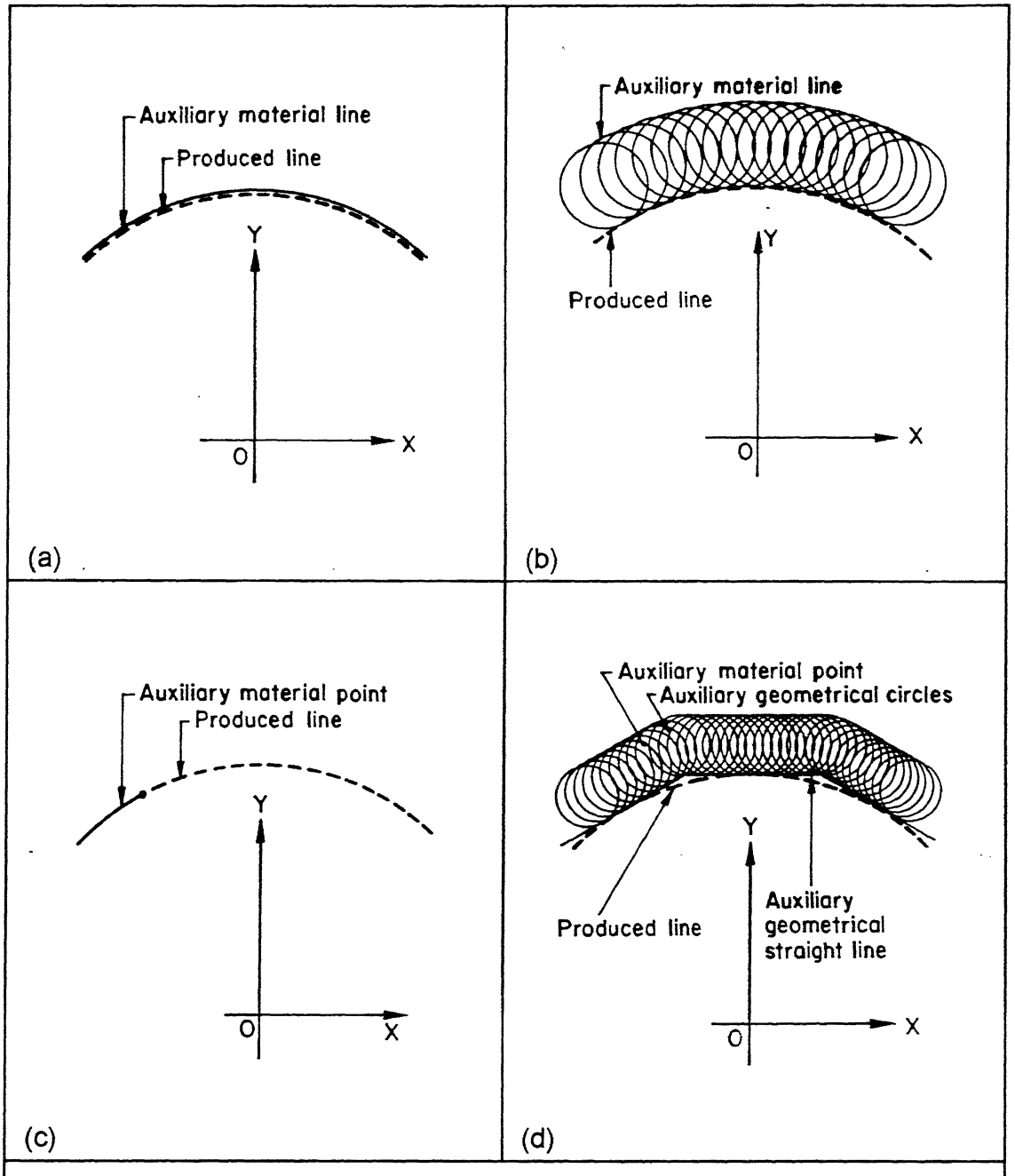

Figure 2-4 Methods of Producing Geometrical Surfaces
(a) Forming Method
(b) Generating Method
(c) Tracing Method and
(d) Tangent Method

2.2.1 Forming Method (Figure 2-4a)

In this method, the geometrical generating line is produced without any formative motion since it is a copy of the auxiliary material line. The geometrical generating line coincides with the shape and extent of the auxiliary material line. The geometrical generating line can be defined as,

$$f(x, y) = 0 \tag{2-1}$$

where $f(x, y) = 0$ is the geometry of the auxiliary line.

2.2.2 Generating Method (Figure 2-4b)

In this method, the geometrical generating line is obtained as an envelope of the auxiliary material line when the latter rolls along the line being produced. As such, only one formative motion is involved in the process. If i_1 is the parameter of the rolling motion then the geometrical generating line is an envelope of a family of curves due to the motion i_1. The equation of the enveloping geometrical generating line is obtained by eliminating the parameter i_1 from the following equations,

$$\begin{aligned} f(x, y, i_1) &= 0 \\ \frac{\partial f}{\partial i_1} &= 0 \end{aligned} \tag{2-2}$$

2.2.3 Tracing Method (Figure 2-4c)

The auxiliary element in this method is in the form of a material point. The geometrical generating line is found as the trace of the material point in its motion. Since a line or a curve can be described as a uni-variate geometrical entity, it can be said that the generating line is produced with a single formative motion. In practice, the material point will have a short length of the tool. However, it is assumed to be sufficiently small so as to idealize it as a point. If i_2 is the formative motion then their geometrical generating line can be described as,

$$\begin{aligned} x &= x(i_2) \\ y &= y(i_2) \end{aligned} \tag{2-3}$$

Processing Method	Formative Tool	Type of Auxiliary Element	Method of Obtaining Geometrical Generating Lines		Number of Formative Motions
			Generatrix	Directrix	
Casting	Foundry moulds	Surface	Forming	Forming	0
Die forging	Dies	Surface	Forming	Forming	0
Blanking	Dies	Line	Forming	Tracing	1
Knurling and rolling	Knurls or rolls	Line	Forming	Generating	1
Ball burnishing	Ball	Surface	Generating	Generating	2
Metal cutting (machining)	Cutting Edge	Line or point	Tangent	Generating tracing or tangent	1 to 3
Grinding	Grinding wheel	Line or point	Tangent	Generaring tracing or tangent	2 or 3
Honing	Abrasive sticks	Point	Tracing	Tracing	2
Abrasive vapour blasting	Abrasive slurry	Surface	Forming	Tracing	1
Buffing	Buffing wheel	Point	Tangent	Tangent	3
Lapping	Lap	Point	Tracing	Tracing	2
Super-finishing	Abrasive stones	Point	Tangent	Tangent or tracing	3
Ball hole-burnishing	Ball	Line	Forming	Tracing	1
Electric discharge machining	Electrode	Line	Forming	Tracing	1
Plastic moulding	Moulds	Surface	Forming	Forming	0
Metallizing	Work piece	Surface	Forming	Forming	0
Chromium and nickel electroplating to size	Work piece	Surface	Forming	Forming	0
Ultrasonic machining	Sonic contour	Line	Forming	Tracing	1
Wire-drawing	Drawing die	Line	Forming	Tracing	1

Table 2-1 Interrelation between the Processing Method and the Method of Geometrically Shaping a Surface.

2.2.4 Tangent Method (Figure 2-4d)

In this method, the geometrical generating line is tangent to a series of supplementary auxiliary lines produced by the material point either by the tracing method (Figure 2-4c) or by the tangent method (Figure 2-4d). In either case, this method requires two or more formative motions.

In Figure 2-4d, the auxiliary material point produces the auxiliary geometrical circle by a rotational formative motion described by the parameter u by the tracing method. The family of the auxiliary geometrical circles produces the auxiliary geometrical straight lines by an oscillatory formative motion described by the parameter i_3 which is the generating method. The family of the auxiliary geometrical straight lines generates a circle by yet another rotational formative motion described by the parameter i_4 by the generating method. Thus, as shown in Figure 2-4d, the generating line is produced by one tracing method and two generating methods. If the equation of the material point at any instant is represented as,

$$f(x, y, u, i_3, i_4) = 0 \tag{2-4}$$

then the produced line (shown as dotted line in Figure 2-4d) is obtained by eliminating the parameters u, i_3 and i_4 from the following equations:

$$\begin{aligned} f(x, y, u, i_3, i_4) &= 0 \\ \frac{\partial f}{\partial u} = \frac{\partial f}{\partial i_3} &= \frac{\partial f}{\partial i_4} = 0 \end{aligned} \tag{2-5}$$

2.3 Shaping of Real Surfaces

The foregoing discussion shows that a real surface can be obtained by defining a geometrical line for the generatrix as well as another one for the directrix of a surface. Since a geometrical line can be defined by any one of these four methods, one can conceive sixteen different conceptual schemes for shaping a real surface. These have been described by Acherkan et al. (1973). Schematic diagram of this classification is given in Table 2-1.

As shown in Figure 2-5, manufacturing processes such as casting and die-forging

belong to the category where the generatrix as well as the directrix are realized by forming methods. It should be noted, however, that one auxiliary motion is required for setting the material curve or surface in its final position. Furthermore, there is no manufacturing process where the generatrix is realized by either the generating, tracing or tangent method and the directrix is realized by the forming method. Hence, in the present work these three cases will not be considered further.

Manufacturing processes such as thread rolling and knurling belong to the category where the generatrix is realized by the forming method and the directrix is realized by the generating method. From Figure 2-6, one can see that the thread profile is the generatrix and the rolling and axial motion of the roll is the directrix. It should be noted that this manufacturing process has only one formative motion or the degree of freedom since the roll and the blank have a relative motion of pure rolling.

Figure 2-7 shows the manufacturing process of ball burnishing. In this method, both the generatrix and the directrix are realized by the generating method. The ball has two formative motions and the resulting enveloping surface is the burnished contour surface.

The manufacturing of spur gears using a circular shaping cutter is shown in Figure 2-8. In this class of processes, the generatrix is realized by the tracing method and the directrix is realized by the generating method. The linear motion of the cutter is the formative motion for realizing the generatrix and the planetary motion of the cutter is the formative motion for realizing the directrix.

If a disk type grinding wheel is used for grinding the involute shaped cylindrical surface of a spur gear then the process can be classified in a class where the generatrix is realized by the tangent method and the directrix is realized by the generating method. As shown in Figure 2-9, this manufacturing process has three formative motions. A variety of grinding processes belong to the category where the generatrix is realized by the tangent method and the directrix is realized either by the generating or the tracing or the tangent method.

The case of cutting a thread on a cylindrical blank with a form tool using the screw cutting lathe belongs to a category where the generatix is realized by the forming method and the directrix is realized by the tracing method. As shown in Figure 2-10, such a method requires only one formative motion. A large number of conventional and advanced machining processes belong to this category. Processes such as ultrasonic machining, electric discharge machining, wire drawing, blanking and ball hole-burnishing belong to this category. In almost all these cases, one formative motion is required.

A relatively less frequently occurring category is the situation where the generatrix is realized by the generating process and the directrix is realized by the tracing process. The familiar process of gear hobbing belongs to this category (Figure 2-11). In this case, the rotations of the blank and the hob produce the generatrix. Here, the generatrix is the involute curve and the directrix is realized due to the linear motion of the hob along the axis of the blank. In this class of processes, the total number of formative motions required is two. It should also be noted that in this process the auxiliary material line responsible for generating the involute profile is a straight line cutting edge of the hob.

Manufacturing processes such as honing and surface relieving belong to the category where the generatrix as well as directrix are realized by the tracing method. In case of generating the relief surfaces on the helical teeth of a plain milling cutter, a pointed tool traces a curve in the space due to two formative motions (Figure 2-12). The first motion generates an Archimedean spiral and the second motion is responsible for generating helix. In this class of manufacturing processes, the auxiliary material element can be idealized as a point or a short line representing the cutting edge of the tool.

Manufacturing processes such as super-finishing using abrasive stones, some categories of grinding and some processes of metal cutting belong to the category where the generatrix is realized by the tangent method and the directrix is realized by the tracing method. Figure 2-13 shows the case of grinding a generalized cylindrical surface using a disk type grinding wheel. In this case, three formative motions are required.

When a thread is milled with a single thread cutter, the generatrix is realized using the forming method and the directrix is realized by the tangent method (Figure 2-14). In this case, the directrix realization requires two formative motions. The realization of the generatrix requires one formative motion. However, the formative motion for realization of generatrix coincides with one of the formative motions required for the realization of the directrix. Since, these two motions are coinciding, the net number of the formative motions required for this process is two.

Another class of manufacturing processes which is rarely encountered in practice is the category where the generatrix is realized by the generating method and the directrix is realized by the tangent method. The case of grinding the flank surfaces of a spur gear using a helically profiled worm-type grinding wheel belongs to this category. For this process, one would normally require three formative motions, one for the grinding wheel rotation, one for the longitudinal feed and one for the generation of involute. However, the grinding wheel rotation cannot be independent of the motion required for involute generation (Figure 2-15). Hence, the resulting number of formative motions required in this case is two.

(a)

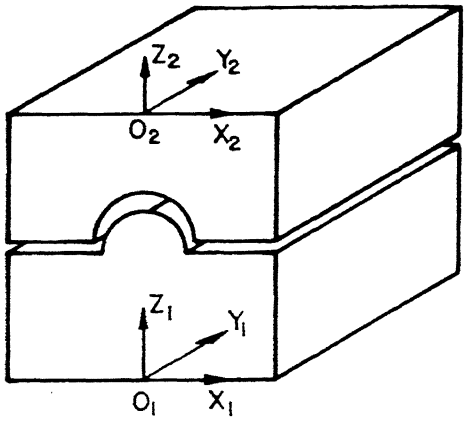

(b)

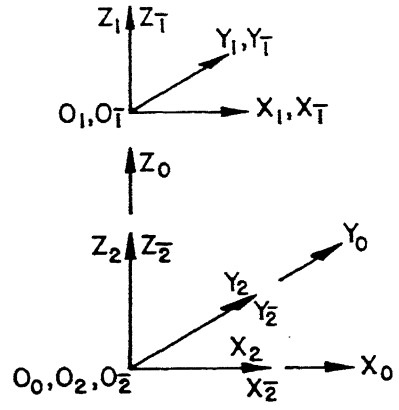

(c)

	a_1	b_1	c_1	θ_1	ϕ_1	ψ_1	a_2	b_2	c_2	θ_2	ϕ_2	ψ_2
Status	X	X	X	X	X	X	X	X	X	X	X	X
D. O. F.	0	0	0	0	0	0	0	0	0	0	0	0
Function	0	0	c_1	0	0	0	0	0	0	0	0	0

Legend : F - Full d. o. f. X - No d. o. f.

Figure 2-5 A Manufacturing Process where both the Generatrix and the Directrix are Produced by the Forming Method.
(a) Schematic Diagram of the Process
(b) Coordinate Systems for the Conjugate Geometry Model and
(c) Table of the Degrees of Freedom.

(a)

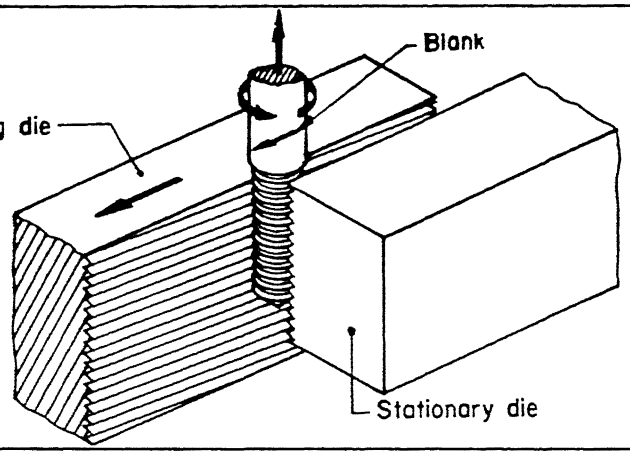

(b)

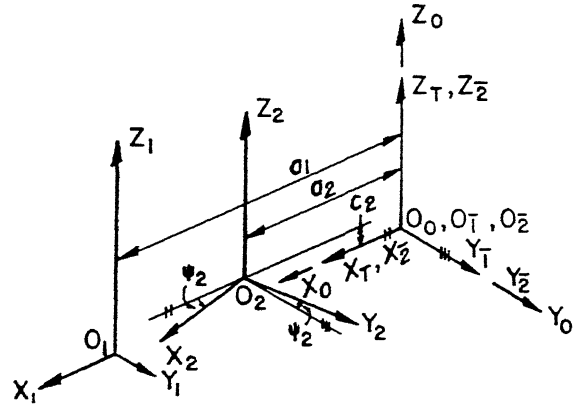

(c)

	a_1	b_1	c_1	Θ_1	Φ_1	Ψ_1	a_2	b_2	c_2	Θ_2	Φ_2	Ψ_2
Status	F	X	X	X	X	X	X	X	X	X	X	X
D.O.F.	1	0	0	0	0	0	0	0	0	0	0	0
Function	←	0	0	0	0	0	←	0	$(t/\pi d)\rho$	0	0	$2t/d$

Legend: F - Full d.o.f. X - No d.o.f.

Figure 2-6 A Manufacturing Process where the Generatrix is Produced by the Forming Method and the Directrix is Produced by the Generating Method.
(a) Schematic Diagram of the Process
(b) Coordinate Systems for the Conjugate Geometry Model and
(c) Table of the Degrees of Freedom.

(a)

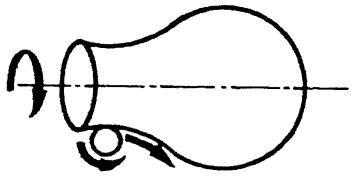

(b)

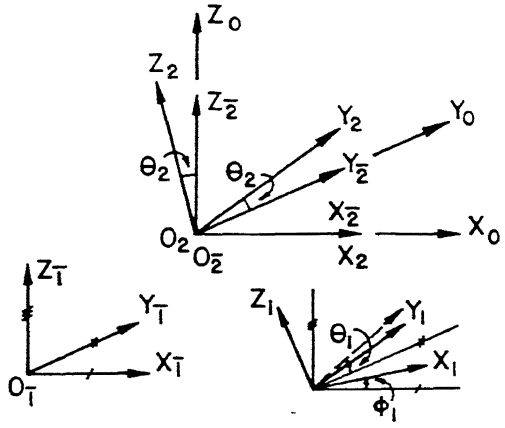

(c)

	a_1	b_1	c_1	θ_1	ϕ_1	ψ_1	a_2	b_2	c_2	θ_2	ϕ_2	ψ_2
Status	X	X	X	F	F	X	X	X	X	X	X	X
D.O.F.	0	0	0	1	1	0	0	0	0	0	0	0
Function	$a_1(\theta_1)$	0	$c_1(\phi_1)$	$\theta_1(t)$	$\phi_1(t)$	0	0	0	0	$\theta_2(\theta_1)$	0	0

Legend : F-Full d.o.f. X-No d.o.f.

Figure 2-7 A Manufacturing Process where the Generatrix is Produced by the Generating Method and the Directrix is Produced by the Generating Method.
(a) Schematic Diagram of the Process
(b) Coordinate Systems for the Conjugate Geometry Model and
(c) Table of the Degrees of Freedom.

(a)

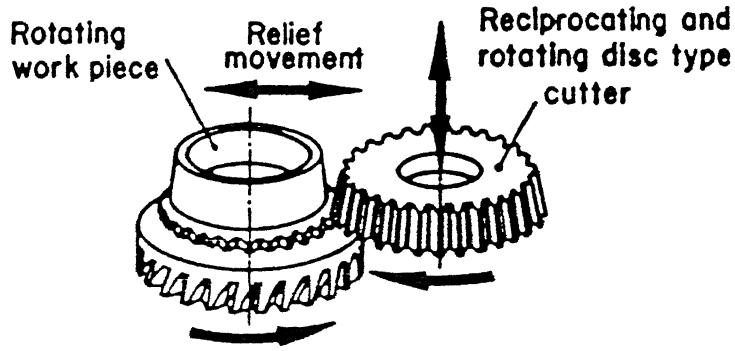

(b)

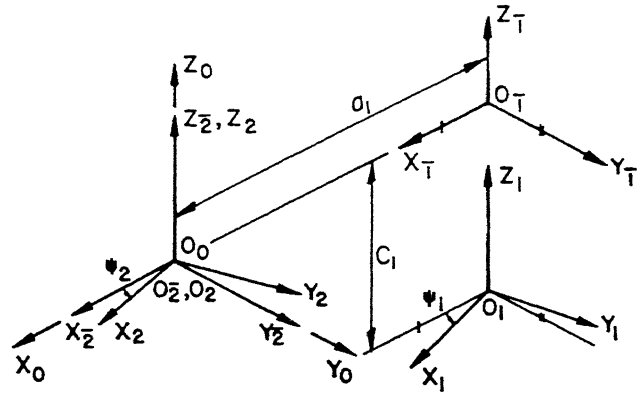

(c)

	a_1	b_1	c_1	Θ_1	Φ_1	Ψ_1	a_2	b_2	c_2	Θ_2	Φ_2	Ψ_2
Status	X	X	F	X	X	F	X	X	X	X	X	X
D.O.F	0	0	1	0	0	1	0	0	0	0	0	0
Function	$(d_1+d_2)/2-d_t$	0	$(1/2)\sin(at)$	0	0	t	0	0	0	0	0	$(d_1/d_2)t$

Legend : F - Full d.o.f. X - No d.o.f.

Figure 2-8 A Manufacturing Process where the Generatrix is Produced by the Tracing Method and the Directrix is Produced by the Generating Method.
(a) Schematic Diagram of the Process
(b) Coordinate Systems for the Conjugate Geometry Model and
(c) Table of the Degrees of Freedom.

(a)

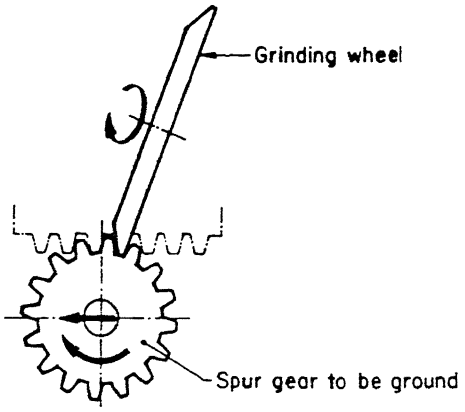

(b)

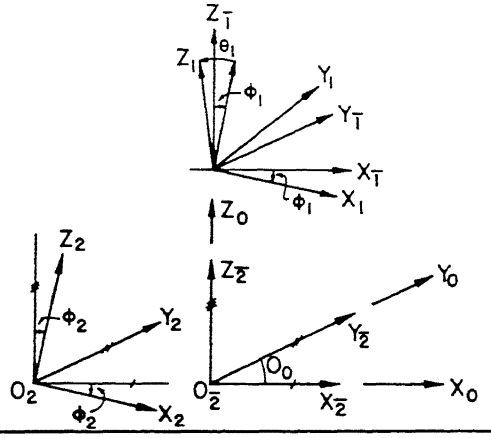

(c)

	a_1	b_1	c_1	θ_1	Φ_1	Ψ_1	a_2	b_2	c_2	θ_2	Φ_2	Ψ_2
Status	X	F	X	F	X	X	X	X	X	X	F	X
D.O.F.	0	1	0	1	0	0	0	0	0	0	1	0
Function	$a_{\bar{1}}$	$b_1(t)$	$c_{\bar{1}}$	$\theta_1(t)$	$\Phi_{\bar{1}}$	0	$a_2(\Phi_2)$	0	$c_{\bar{2}}$	0	$\Phi_2(t)$	0

Legend : F – Full d.o.f. X – No d.o.f.

Figure 2-9 A Manufacturing Process where the Generatrix is Produced by the Tangent Method and the Directrix is Produced by the Generating Method.
(a) Schematic Diagram of the Process
(b) Coordinate Systems for the Conjugate Geometry Model and
(c) Table of the Degrees of Freedom.

(a)

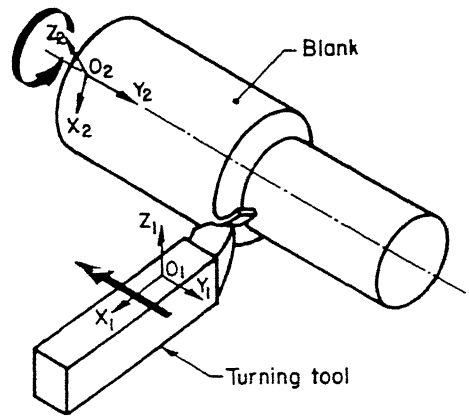

(b)

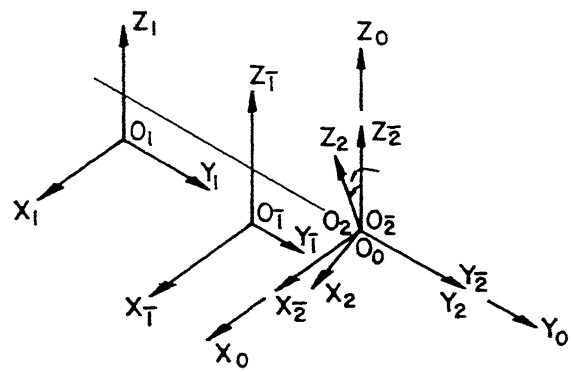

(c)

	a_1	b_1	c_1	θ_1	ϕ_1	ψ_1	a_2	b_2	c_2	θ_2	ϕ_2	ψ_2
Status	X	X	X	X	X	X	X	X	X	X	F	X
D.O.F.	0	0	0	0	0	0	0	0	0	0	1	0
Function	$a_{\bar{1}}$	$b(\phi_2)$	0	0	0	0	0	0	0	0	←	0

Legend : F - Full d.o.f. X - No d.o.f.

Figure 2-10 A Manufacturing Process where the Generatrix is Produced by the Forming Method and the Directrix is Produced by the Tracing Method.
(a) Schematic Diagram of the Process
(b) Coordinate Systems for the Conjugate Geometry Model and
(c) Table of the Degrees of Freedom.

(a)

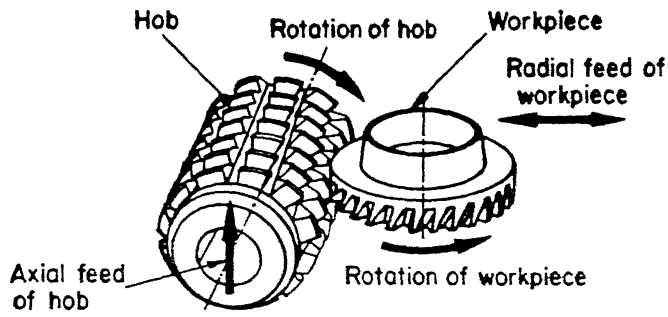

(b)

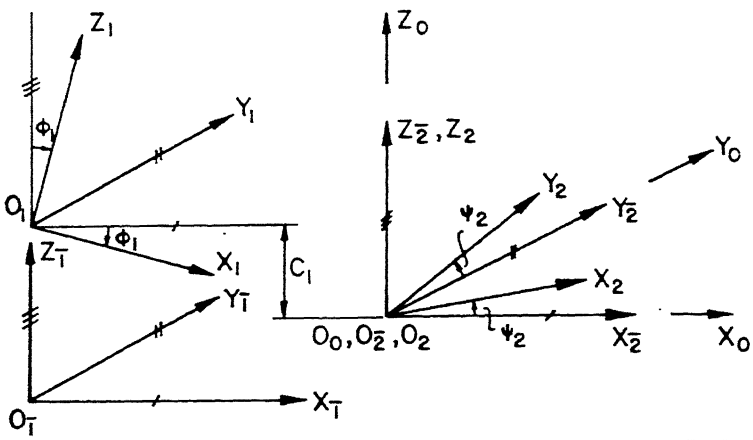

(c)

	a_1	b_1	c_1	θ_1	ϕ_1	ψ_1	a_2	b_2	c_2	θ_2	ϕ_2	ψ_2
Status	X	X	F	X	F	X	X	X	X	X	X	X
D.O.F.	0	0	0	0	1	0	0	0	0	0	0	0
Function	$(d_1+d_2)/2-d_t$	0	C_T+f_t	0	$2\pi n_1 t/60$	0	0	0	0	0	0	$2\pi n_2 t/60$

Legend: F-Full d.o.f. X-No d.o.f.

Figure 2-11 A Manufacturing Process where the Generatrix is Produced by the Generating Method and the Directrix is Produced by the Tracing Method.
(a) Schematic Diagram of the Process
(b) Coordinate Systems for the Conjugate Geometry Model and
(c) Table of the Degrees of Freedom.

(a)

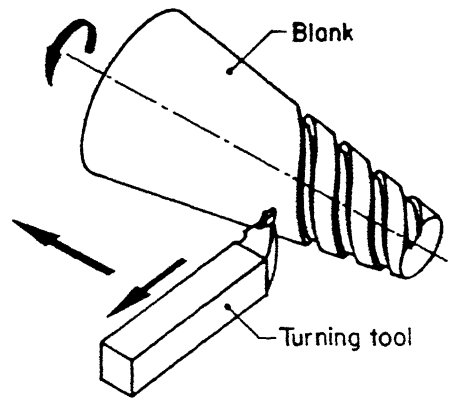

(b)

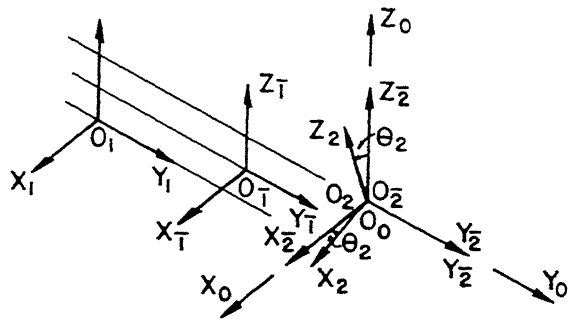

(c)

	a_1	b_1	c_1	Θ_1	Φ_1	Ψ_1	a_2	b_2	c_2	Θ_2	Φ_2	Ψ_2
Status	F	X	X	X	X	X	X	X	X	X	F	X
D.O.F.	1	0	0	0	0	0	0	0	0	0	1	0
Function	$a_1(t)$	$b_1(\Phi_2)$	$C_{\bar{1}}$	0	0	0	0	0	0	0	←	0

Legend : F-Full d.o.f. X-No d.o.f.

Figure 2-12 A Manufacturing Process where the Generatrix is Produced by the Tracing Method and the Directrix is Produced by the Tracing Method.
(a) Schematic Diagram of the Process
(b) Coordinate Systems for the Conjugate Geometry Model and
(c) Table of the Degrees of Freedom.

(a)

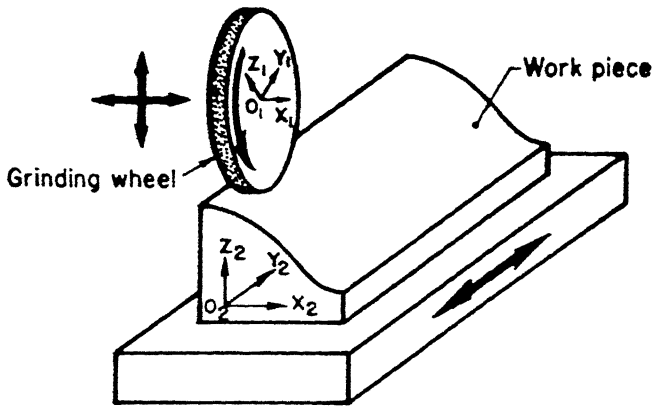

(b)

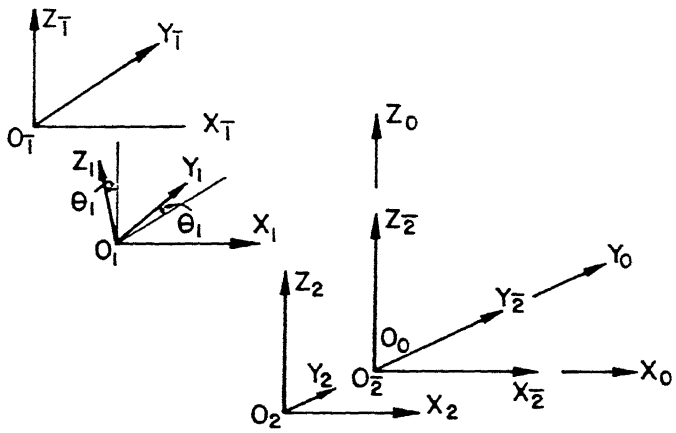

(c)

	a_1	b_1	c_1	θ_1	ϕ_1	ψ_1	a_2	b_2	c_2	θ_2	ϕ_2	ψ_2
Status	F	X	X	F	X	X	X	F	X	X	X	X
D.O.F.	1	0	0	1	0	0	0	1	0	0	0	0
Function	$a_1(t)$	$b_{\bar{1}}$	$c_1(a_1)$	$2\pi n_1 t/60$	0	0	0	$b_2(t)$	0	0	0	0

Legend : F - Full d. o. f. X - No d. o. f.

Figure 2-13 A Manufacturing Process where the Generatrix is Produced by the Tangent Method and the Directrix is Produced by the Tracing Method.
(a) Schematic Diagram of the Process
(b) Coordinate Systems for the Conjugate Geometry Model and
(c) Table of the Degrees of Freedom.

(a)

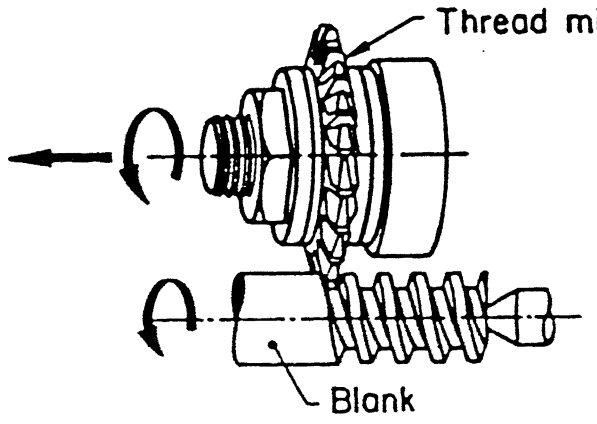

(b)

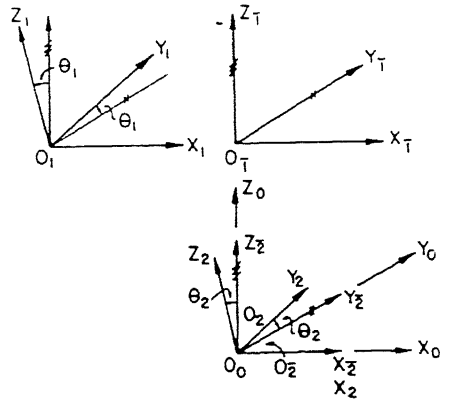

(c)

	a_1	b_1	c_1	θ_1	Φ_1	ψ_1	a_2	b_2	c_2	θ_2	ϕ_2	ψ_2
Status	X	X	X	F	X	X	X	X	X	F	X	X
D.O.F.	0	0	0	1	0	0	0	0	0	1	0	0
Function	$-n_2\,pt/60$	0	0	$2\pi\,n_1 t/60$	0	0	0	0	0	$2\pi\,n_2 t/60$	0	0

Legend: F - Full d. o. f. X - No d. o. f.

Figure 2-14 A Manufacturing Process where the Generatrix is Produced by the Forming Method and the Directrix is Produced by the Tangent Method.
(a) Schematic Diagram of the Process
(b) Coordinate Systems for the Conjugate Geometry Model and
(c) Table of the Degrees of Freedom.

(a)

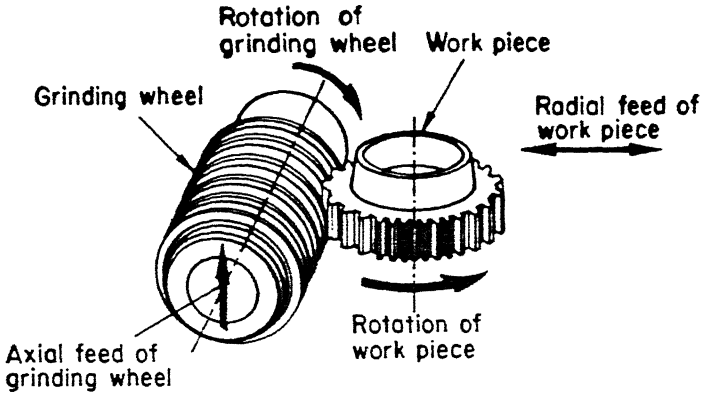

(b)

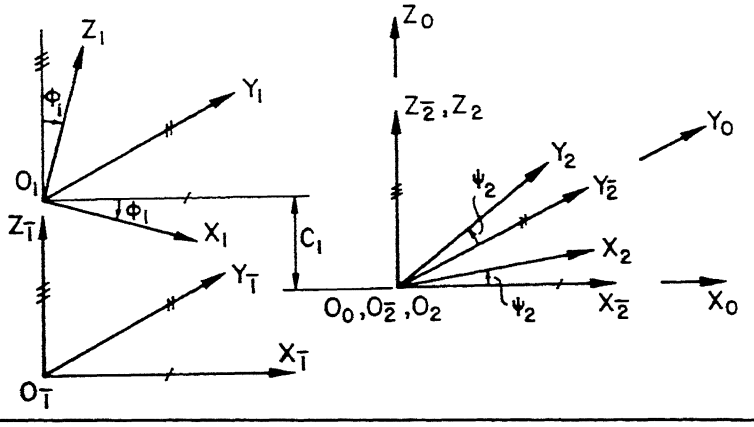

(c)

	a_1	b_1	c_1	Θ_1	Φ_1	Ψ_1	a_2	b_2	c_2	Θ_2	Φ_2	Ψ_2
Status	X	X	F	X	F	X	X	X	X	X	X	X
D.O.F.	0	0	0	0	1	0	0	0	0	0	0	0
Function	$(d_1+d_2)/2-d_t$	0	$C_{\bar{1}}+ft$	0	$2\pi n_1 t/60$	0	0	0	0	0	0	$2\pi n_2 t/60$

Legend: F - Full d.o.f. X - No d.o.f.

Figure 2-15 A Manufacturing Process where the Generatrix is Produced by the Generating Method and the Directrix is Produced by the Tangent Method.
(a) Schematic Diagram of the Process
(b) Coordinate Systems for the Conjugate Geometry Model and
(c) Table of the Degrees of Freedom.

(a)

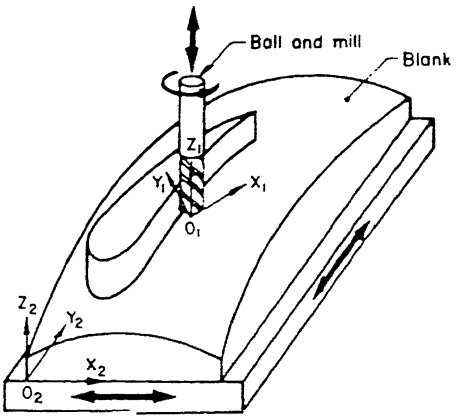

(b)

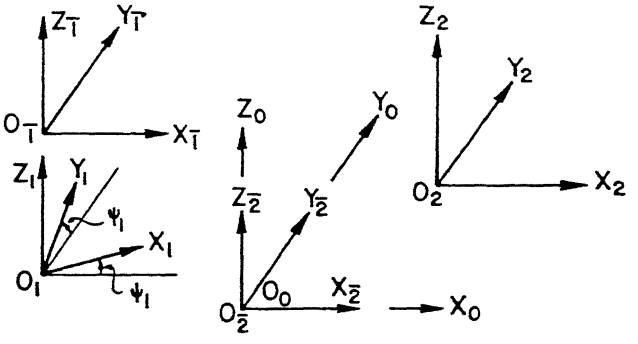

(c)

	a_1	b_1	c_1	θ_1	ϕ_1	ψ_1	a_2	b_2	c_2	θ_2	ϕ_2	ψ_2
Status	X	X	X	X	X	F	F	F	X	X	X	X
D.O.F.	0	0	0	0	0	1	1	1	0	0	0	0
Function	$a_{\bar{1}}$	$b_{\bar{1}}$	$c_1(a_2, b_2)$	0	0	$2\pi n_1 t/60$	$a_2(t)$	$b_2(t)$	0	0	0	0

Legend : Full d.o.f. X-No d.o.f.

Figure 2-16 A Manufacturing Process where the Generatrix is Produced by the Tangent Method and the Directrix is Produced by the Tangent Method.
(a) Schematic Diagram of the Process
(b) Coordinate Systems for the Conjugate Geometry Model and
(c) Table of the Degrees of Freedom.

As indicated by Acherkan et al. (1973), the category of shaping of surfaces where the generatrix is realized by the tracing method and the directrix is realized by the tangent method has found no application as yet in its true form, hence, this category will not be dealt with any further in our present analysis.

The last class of manufacturing processes belongs to the category where the generatrix as well as the directrix are realized by the tangent method. Some of the machining processes belong to this category which is also referred to as the double tangent method. The case of milling a doubly curved surface with an end mill using a tracer controlled duplicating machine belongs to this category (Figure 2-16). In general, the double tangent method requires four formative motions, two for realizing the generatrix family of curves and two for realizing the directrix family of curves. However, the cutting motion is common in both the cases and at any given time, only one curve is generated. Hence, the formative motions required are two at any given time. The manufacturing process of buffing also belongs to this category of double tangent method.

The foregoing review of the manufacturing processes on one side and their characterization as one of the sixteen shape realization processes on the other side shows that different schemes of kinematic structures and tool geometries are employed to realize simple and complex surfaces.

2.4 Definition of the Conjugate Geometry Model of a Generic Machine Tool

There are basically three elements involved in any machining process. The first one is the surface of the cutting tool denoted as Σ_1 and the second is the surface that is to be produced denoted as Σ_2 (Figure 2-17). The third element is the relative motion between these two surfaces which will be constrained by the type of kinematic chain of the machine tool. To produce the surface Σ_2 correctly, it is essential that the two surfaces Σ_1 and Σ_2 are conjugate to each other. In other words, these two surfaces will maintain a higher pair contact throughout the cutting motion. Using this principle of conjugate geometry and envelope theory, a unified model of the machine tool with twelve degrees of freedom has been proposed in the present thesis. Among the three elements of a machining process, viz., the cutter surface Σ_1, the surface to be machined Σ_2 and their relative motion, if any two are known, the third one can be determined using this model of the generic machine tool. Such a model can be used for the determination of the NC cutter path wherein the cutter surface Σ_1 and the surface to be machined Σ_2 are known and their relative motion is required to be determined. This model can also be used for NC path simulation which is required for off-line NC tape proving, error analysis of the produced surface, NC code optimization etc. The former will fall in the category of the reverse kinematic problem and the latter is a forward kinematic problem. Also one can

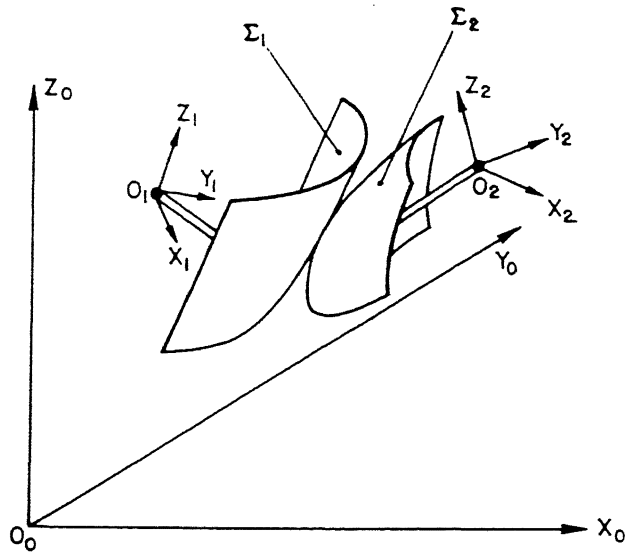

Figure 2-17 A Pair of Conjugate Surfaces in a Shape Generation Process

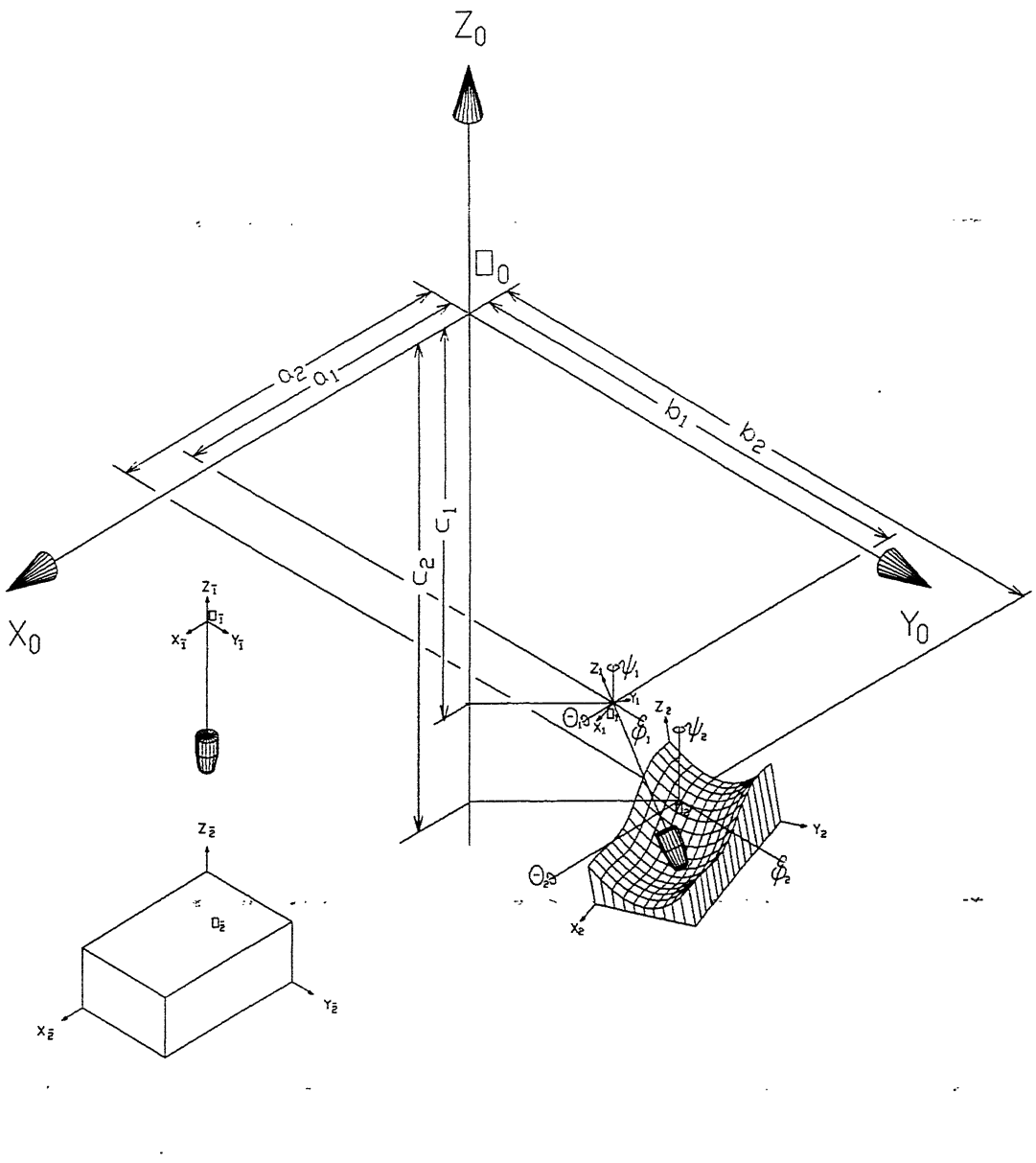

Figure 2-18 Description of a Generic Machine Tool with Twelve Degrees of Freedom

use the proposed conjugate geometry model for choosing the optimal combination of the machine tool and the cutting tool by an iterative process.

A generic model of a machine tool is essentially a representation of the kinematic structure of the machine tool (Acherkan, 1973). A kinematic structure of a machine tool describes the kinematic chain necessary for providing the cutting motion to the cutter and the feed motions to the cutter and/or the blank. In this model, the cutter and the blank are considered to be two free bodies in space and hence their position and orientation can be described by six degrees of freedom each. These twelve degrees of freedom are expressed with respect to a fixed frame of reference S_0 (O_0 - X_0, Y_0, Z_0). A coordinate system S_2 (O_2 - X_2, Y_2, Z_2) is considered to be attached to the blank and another coordinate system S_1 (O_1 - X_1, Y_1, Z_1) to the cutter (Figure 2.18). The initial positions of the coordinate systems S_1 and S_2 are denoted as $S_{\bar{1}}$ ($O_{\bar{1}}$ - $X_{\bar{1}}$, $Y_{\bar{1}}$, $Z_{\bar{1}}$) and $S_{\bar{2}}$ ($O_{\bar{2}}$ - $X_{\bar{2}}$, $Y_{\bar{2}}$, $Z_{\bar{2}}$) (Figure 2-19). Let (a_1, b_1, c_1) and (a_2, b_2, c_2) denote the translation of the origins O_1 and O_2 of the moving coordinate frames and let (θ_1, ϕ_1, ψ_1) and (θ_2, ϕ_2 and ψ_2) denote the rotations of the coordinate frames S_1 and S_2 respectively. As these twelve parameters of motion, viz., a_1, b_1, c_1, θ_1, ϕ_1, ψ_1, a_2, b_2, c_2, θ_2, ϕ_2 and ψ_2 as shown in Figure 2-18 represent the kinematic arrangement of the machine tool, they can be expressed as functions of time t. Since we assume that the cutter is rigid and the joints and links of the machine tool are perfect (i.e., no play and no deflection), the tool surface Σ_1 and the surface produced on the blank Σ_2 will be time-invariants. The known surface among the two surfaces can be expressed as a biparametric surface in u and v. Since the two surfaces Σ_1 and Σ_2 are in higher pair contact, at the point of contact P,

$$ {}^1\underset{\sim}{p}\left[{}^0_1M\right] = {}^2\underset{\sim}{p}\left[{}^0_2M\right] \qquad \textbf{(2-6)} $$

and

$$ {}^1\underset{\sim}{n}\left[{}^0_1M\right] = \pm\,{}^2\underset{\sim}{n}\left[{}^0_2M\right] \qquad \textbf{(2-7)} $$

where,

${}^1\underset{\sim}{p}$ - Point P with reference to the cutter coordinate system S_1.

${}^2\underset{\sim}{p}$ - Point P with reference to the blank coordinate system S_2.

${}^1\underset{\sim}{n}_{P,1}$ - Unit normal vector of the cutter surface Σ_1 at point P with reference to coordinate system S_1.

$\underset{\sim}{{}^{2}n}_{P,2}$ - Unit normal vector of the blank surface Σ_2 at point P with reference to coordinate system S_2.

$\left[{}^{0}_{1}M\right]$ - Homogeneous transformation matrix for transforming a vector from the coordinate system S_1 to S_0 .

$\left[{}^{0}_{2}M\right]$ - Homogeneous transformation matrix for transforming a vector from the coordinate system S_2 to S_0.

It is to be noted that all vectors such as position vectors, normal vectors and velocity vectors are expressed as row vectors in the homogeneous coordinate system. Hence the fourth element of any position vector is unity and it is zero for the normal and velocity vectors.

The surface Σ_2 is the boundary of the *swept volume* of the cutter surface Σ_1 which is nothing but the envelope to the various instances of the cutter surface. In order to identify the point on the cutter surface Σ_1 which is cutting the blank and producing (or generating) the surface Σ_2 at any given time, it is necessary to establish some additional constraints. This constraint is called as the *condition of cutting* or the *condition of contact* or the *condition of envelope*. It can be said that in order to ensure a smooth contact or cutting at any given time, the relative velocity vector between the cutter and the blank must be orthogonal to the common normal at the point of cutting (Chakraborty and Dhande, 1977). Mathematically, this condition can be expressed as,

$$\underset{\sim}{{}^{0}n}_{P,1} \cdot \underset{\sim}{{}^{0}V}_{P,12} = 0 \qquad \textbf{(2-8)}$$

and

$$\underset{\sim}{{}^{0}n}_{P,2} \cdot \underset{\sim}{{}^{0}V}_{P,12} = 0 \qquad \textbf{(2-9)}$$

where,

$\underset{\sim}{{}^{0}n}_{P,1}$ - Unit normal vector of the cutter surface Σ_1 at point P with reference to coordinate system S_0.

$\underset{\sim}{{}^{0}n}_{P,2}$ - Unit normal vector of the cutter surface Σ_2 at point P with reference to coordinate system S_0.

$\underset{\sim}{{}^{0}V}_{P,12}$ - Relative velocity vector between the tool and blank with reference to

coordinate system S_0.

The condition of contact is a scalar equation relating parameters u, v and t. Thus, at any given instant of time t, the condition of contact reduces to a relation between u and v. For any value of u within its feasible range, one can find the corresponding value of the parameter v. Thus, one can locate a set of points or a curve on the surface Σ_1 which defines the surface curve for Σ_2 as well. The corresponding points of the surface Σ_2 can be obtained using the equation,

$$\underset{\sim}{{}^2p} = \underset{\sim}{{}^ip} \left[{}^0_1M \right] \left[{}^2_0M \right] \qquad \textbf{(2-10)}$$

A symbolic algorithm, that can be programmed in any of the algebraic manipulation systems such as *MACSYMA*, *MathCAD* or *REDUCE* can now be stated as follows:

1. Define the position vector $\underset{\sim}{{}^1p}$ of a generic point P on the cutter surface Σ_1 as a biparametric surface in u and v such that

$$\underset{\sim}{{}^1p}\ (u, v) = \left[x_1(u, v) \quad y_1(u, v) \quad z_1(u, v) \quad 1 \right] \qquad \textbf{(2-11)}$$

2. Define the twelve parameters of motion a_1, b_1, c_1, θ_1, ϕ_1, ψ_1, a_2, b_2, c_2, θ_2, ϕ_2 and ψ_2 in terms of time t.

3. Calculate the matrices $\left[{}^0_1M \right]$ and $\left[{}^0_1\dot{M} \right]$ as follows:

$$\left[{}^0_1M \right] = \left[{}^0_1R_x \right] \left[{}^0_1R_y \right] \left[{}^0_1R_z \right] \left[{}^0_1T \right] \qquad \textbf{(2-12)}$$

where,

$$\left[{}^{0}_{1}R_{x}\right] = \begin{bmatrix} 1 & 0 & 0 & 0 \\ 0 & \cos\theta_1 & \sin\theta_1 & 0 \\ 0 & -\sin\theta_1 & \cos\theta_1 & 0 \\ 0 & 0 & 0 & 1 \end{bmatrix} \qquad \left[{}^{0}_{1}R_{y}\right] = \begin{bmatrix} \cos\phi_1 & 0 & -\sin\phi_1 & 0 \\ 0 & 1 & 0 & 0 \\ \sin\phi_1 & 0 & \cos\phi_1 & 0 \\ 0 & 0 & 0 & 1 \end{bmatrix}$$

$$\left[{}^{0}_{1}R_{z}\right] = \begin{bmatrix} \cos\psi_1 & \sin\psi_1 & 0 & 0 \\ -\sin\psi_1 & \cos\psi_1 & 0 & 0 \\ 0 & 0 & 1 & 0 \\ 0 & 0 & 0 & 1 \end{bmatrix} \qquad \left[{}^{0}_{1}T\right] = \begin{bmatrix} 1 & 0 & 0 & 0 \\ 0 & 1 & 0 & 0 \\ 0 & 0 & 1 & 0 \\ a_1 & b_1 & c_1 & 1 \end{bmatrix}$$

Matrix $\left[{}^{0}_{1}\dot{M}\right]$ is the time-differential of matrix $\left[{}^{0}_{1}M\right]$.

4. Calculate the matrices $\left[{}^{0}_{2}M\right]$, $\left[{}^{2}_{0}M\right]$ and $\left[{}^{0}_{2}\dot{M}\right]$ as follows:

$$\left[{}^{0}_{2}M\right] = \left[{}^{0}_{2}R_{x}\right]\left[{}^{0}_{2}R_{y}\right]\left[{}^{0}_{2}R_{z}\right]\left[{}^{0}_{2}T\right] \tag{2-13}$$

where,

$$\left[{}^{0}_{2}R_{x}\right] = \begin{bmatrix} 1 & 0 & 0 & 0 \\ 0 & \cos\theta_2 & \sin\theta_2 & 0 \\ 0 & -\sin\theta_2 & \cos\theta_2 & 0 \\ 0 & 0 & 0 & 1 \end{bmatrix} \qquad \left[{}^{0}_{2}R_{y}\right] = \begin{bmatrix} \cos\phi_2 & 0 & -\sin\phi_2 & 0 \\ 0 & 1 & 0 & 0 \\ \sin\phi_2 & 0 & \cos\phi_2 & 0 \\ 0 & 0 & 0 & 1 \end{bmatrix}$$

$$\left[{}^{0}_{2}R_{z}\right] = \begin{bmatrix} \cos\psi_2 & \sin\psi_2 & 0 & 0 \\ -\sin\psi_2 & \cos\psi_2 & 0 & 0 \\ 0 & 0 & 1 & 0 \\ 0 & 0 & 0 & 1 \end{bmatrix} \qquad \left[{}^{0}_{2}T\right] = \begin{bmatrix} 1 & 0 & 0 & 0 \\ 0 & 1 & 0 & 0 \\ 0 & 0 & 1 & 0 \\ a_2 & b_2 & c_2 & 1 \end{bmatrix}$$

$$\left[{}^{2}_{0}M \right] = \left[{}^{0}_{2}M \right]^{-1} \tag{2-14}$$

Matrix $\left[{}^{0}_{2}\dot{M} \right]$ is the time-differential of matrix $\left[{}^{0}_{2}M \right]$.

5. Derive the position vector ${}^{2}\underset{\sim}{p}$.

$${}^{2}\underset{\sim}{p} = \left[x_2 \quad y_2 \quad z_2 \quad 1 \right]$$

$${}^{2}\underset{\sim}{p} = {}^{1}\underset{\sim}{p} \left[{}^{0}_{1}M \right] \left[{}^{2}_{0}M \right] \tag{2-15}$$

6. Derive the normal vector ${}^{1}\underset{\sim}{N}_{P,1}$.

$${}^{1}\underset{\sim}{N}_{P,1} = \frac{\partial\, {}^{1}\underset{\sim}{p}}{\partial u} \; x \; \frac{\partial\, {}^{1}\underset{\sim}{p}}{\partial v} \tag{2-16}$$

where,

$\dfrac{\partial\, {}^{1}\underset{\sim}{p}}{\partial u}$ and $\dfrac{\partial\, {}^{1}\underset{\sim}{p}}{\partial v}$ are the partial derivatives of ${}^{1}\underset{\sim}{p}$ with respect to u and v respectively. Therefore,

$$\frac{\partial\, {}^{1}\underset{\sim}{p}}{\partial u} = \left[\frac{\partial x_1}{\partial u} \quad \frac{\partial y_1}{\partial u} \quad \frac{\partial z_1}{\partial u} \quad 0 \right] \qquad \frac{\partial\, {}^{1}\underset{\sim}{p}}{\partial v} = \left[\frac{\partial x_1}{\partial v} \quad \frac{\partial y_1}{\partial v} \quad \frac{\partial z_1}{\partial v} \quad 0 \right]$$

When the vectors $\dfrac{\partial\, {}^{1}\underset{\sim}{p}}{\partial u}$ and $\dfrac{\partial\, {}^{1}\underset{\sim}{p}}{\partial v}$ are expressed in Cartesian coordinates, the normal vector ${}^{1}\underset{\sim}{n}_{P,1}$ is defined as

$$ {}^{1}\underset{\sim}{n}_{P,1} = \begin{vmatrix} i & j & k \\ \dfrac{\partial x_1}{\partial u} & \dfrac{\partial y_1}{\partial u} & \dfrac{\partial z_1}{\partial u} \\ \dfrac{\partial x_1}{\partial v} & \dfrac{\partial y_1}{\partial v} & \dfrac{\partial z_1}{\partial v} \end{vmatrix} $$

The same can be redefined when the vectors $\dfrac{\partial {}^{1}\underset{\sim}{p}}{\partial u}$ and $\dfrac{\partial {}^{1}\underset{\sim}{p}}{\partial v}$ are expressed in homogeneous coordinates as

$$ {}^{1}\underset{\sim}{n}_{P,1} = \begin{vmatrix} i & j & k & l \\ \dfrac{\partial x_1}{\partial u} & \dfrac{\partial y_1}{\partial u} & \dfrac{\partial z_1}{\partial u} & 0 \\ \dfrac{\partial x_1}{\partial v} & \dfrac{\partial y_1}{\partial v} & \dfrac{\partial z_1}{\partial v} & 0 \\ 0 & 0 & 0 & 1 \end{vmatrix} $$

7. Calculate the unit normal vector ${}^{1}\underset{\sim}{n}_{P,1}$.

$$ {}^{1}\underset{\sim}{n}_{P,1} = \frac{{}^{1}\underset{\sim}{N}_{P,1}}{\| \ {}^{1}\underset{\sim}{N}_{P,1} \ \|} \qquad \textbf{(2-17)} $$

where $\| \ {}^{1}\underset{\sim}{N}_{P,1} \ \|$ is the magnitude of ${}^{1}\underset{\sim}{N}_{P,1}$.

8. Calculate the unit normal vector ${}^{0}\underset{\sim}{n}_{P,1}$ in the global coordinate system.

$$ {}^{0}\underset{\sim}{n}_{P,1} = {}^{1}\underset{\sim}{n}_{P,1} \left[{}^{0}_{1}M \right] \qquad \textbf{(2-18)} $$

9. Calculate the relative velocity vector ${}^0\underset{\sim}{V}_{P,12}$.

$$ {}^0\underset{\sim}{V}_{P,12} = {}^0\underset{\sim}{V}_{P,2} - {}^0\underset{\sim}{V}_{P,1} \qquad \textbf{(2-19)} $$

where

$$ {}^0\underset{\sim}{V}_{P,1} = {}^1\underset{\sim}{p}\left[{}^0_1\dot{M}\right] \quad \text{and} \quad {}^0\underset{\sim}{V}_{P,2} = {}^2\underset{\sim}{p}\left[{}^0_2\dot{M}\right] $$

10. Reduce symbolically the condition of contact

$$ {}^0\underset{\sim}{n}_{P,1} \cdot {}^0\underset{\sim}{V}_{P,12} = 0 \qquad \textbf{(2-20)} $$

11. ${}^2\underset{\sim}{p}$ obtained in step 5 will be a function of u, v and t. Use the condition of contact obtained in step 10 to eliminate either of u and v. This will yield the surface Σ_2.

It has been stated earlier that based on the method of obtaining the generatrix and directrix, the manufacturing processes can be classified into sixteen groups out of which only twelve are encountered in practice. An example for each of these twelve manufacturing processes has been given in Figures 2-5 through 2-16. Part (a) of these figures gives the schematic diagram of the process. The fixed global coordinate frame S_0, the moving coordinate frames S_1 and S_2 and their initial positions $S_{\bar{1}}$ and $S_{\bar{2}}$ are depicted in part (b). Part (c) contains a table in which the expressions for the twelve motion parameters are given as functions of time t. Out of these twelve motion parameters, it may be observed that at the most only six will be independent of each other and the rest of the parameters can be expressed as constants or as functions of these independent parameters. This is because of the fact that the cutter surface is always in contact with the blank surface. Furthermore, for a milling process, the number of independent motion parameters are limited to five since the sixth independent parameter, viz., the spindle rotation, is a passive degree of freedom as far as the present conjugate geometry model is concerned (In a way, it can be said that the spindle rotation is related to the sweep parameter v in the definition of the cutter surface for a milling process - see Chapter 4). This is the reason why most of the CNC machines have only upto five axes. The generic model with twelve degrees of freedom assumes the characteristics of a given machine tool when the twelve motion parameters pertaining to this machine are defined.

In the next chapter, the conjugate geometry formulation has been explained with

the help of an example. Also the instantiation of the generic model of a machine tool for five different types of machine tools is illustrated.

Chapter 3

INSTANCES OF THE GENERIC MACHINE TOOL

3.1 Introduction

The model of a generic machine tool with twelve degrees of freedom was proposed in the previous chapter. Even though the proposed model is designed to handle twelve degrees of freedom, such a machine with twelve independent degrees of motion cannot exist in reality. The fact that the surfaces Σ_1 and Σ_2 are in continuous contact implies that there could be only six relative degrees of freedom, in other words, independent degrees of freedom, at the most. And for a milling-like process, one cannot think of a machine tool which has more than five independent motion parameters since the sixth motion which is the spindle rotation is a passive degree of freedom. It will be obvious from the following chapter that the spindle rotation may be used to describe the generatrix profile in the biparametric definition of the cutter surface. Even though all twelve degrees of freedom will not be used by a single process, by incorporating the highest number of degrees of freedom in this model, the greatest amount of versatility is achieved in order that any kind of machine tool can be instantiated using this model. The need for a unified model of this kind can be justified as follows:

Other classical methods such as the *APT* algorithm for cutter path generation assume a machine tool which has a fixed table and five degrees of freedom for the cutter. The cutter path generated from these systems is a series of tool tip positions along with the corresponding direction cosines of the tool axis. The task of converting this cutter path called *CL data* into the joint coordinates (kinematic parameters) of a particular machine tool has to be performed by another program called *post-processor*. The design of the post-processor becomes more complicated when it is required to customize the CL data for a machine tool which has few degrees of freedom for the table also since it has to

perform interpolation in order to adhere to the *LINTOL*[1] limits. In the conjugate geometry model, the kinematic information of the machine tool is inherently taken care of thus alleviating the need for post-processing[2].

The output in the APT paradigm is discrete and numerical whereas the proposed conjugate geometry model generates the output surface in terms of the joint coordinates in the form of algebraic equations which can be reduced to any desired accuracy.

Today, most of the NC programming packages come with built-in path simulation routines. There are several packages such as *VeriCUT* which are exclusively for NC program verification. But all these simulation programs take the CL file as input. Hence even if the CL file appears satisfactory during the simulation, one cannot be sure that the same surface would be produced during the actual machining since errors such as wrong start-up and retraction and LINTOL interpolation errors could creep in at the post-processing stage. The simulation based on the conjugate geometry formulation will be free from these problems.

3.2 Instances of the Generic Machine Tool

Figure 3-1 to Figure 3-5 illustrate the instantiation of the conjugate geometry model of the generic machine tool for five different kinds milling machines. The table given in each of these figures is the kinematic data of the corresponding machine tool input to the symbolic algorithm.

3.2.1 Instantiation of a 4 Axis Vertical Milling Machine

Figure 3-1 shows a four axis CNC vertical milling machine. In this machine, the translation along the X_2 and Z_2 directions are effected by the table movement and the Y_1 movement is due to the movement of the spindle assembly. It also has a rotary table about the Z_2 axis. Thus it has three degrees of freedom for the blank and one degree of freedom for the cutter. Hence there are four entries viz., b_1, a_2, c_2 and ψ_2 in the table

---

[1] *LINTOL* is a post-processor command which is an acronym for LINear TOLerance. The post-processor generates additional points between adjacent pairs of blocks of CL file in order to ensure that the path followed by the tool tip does not deviate beyond this tolerance band.

[2] The post-processing consists of two step. The first step is the mapping of CL data into the joint coordinate space and the second one is to generate output in the required format. The second step will still be required to be performed.

which are time-dependant and the rest are constant values. It may be noted that θ_1 which is related to the spindle rotation is entered as zero for all milling machines since it is a passive degree of freedom.

3.2.2 Instantiation of a 5 Axis Horizontal Milling Machine with Two Rotary Tables

A 5 axis CNC machine with the table capable of moving in the X_2 and Y_2 directions and the spindle head contributing to the Z_1 movement is shown in Figure 3-2. This machine has a rotary table about the X_2 axis in addition to the conventional rotary table about the Z_2 axis. Thus it has four degrees of freedom for the blank and one degree of freedom for the cutter. Hence c_1, a_2, b_2, θ_2 and ψ_2 are the five time-dependant values and the rest are constants.

3.2.3 Instantiation of a 5 Axis Milling Machine with a Rotary Tables and a Tilting Tool Head

Another 5 axis CNC machine shown in Figure 3-3 has the X_2 and Y_2 movements for the table and the Z_1 movement for the spindle head. Apart from the conventional rotary table about the Z_2 axis, its spindle head also can be tilted about the X_1 axis. Thus there are three degrees of freedom for the blank and two degrees of freedom for the cutter. Hence c_1, θ_1, a_2, b_2 and ψ_2 are the five time-dependant entries in the table while the other seven are constants.

3.2.4 Instantiation of a 5 Axis Milling Machine with Spindle Head Swivel Capability about Two Principal Directions

The 5 axis CNC milling machine illustrated in Figure 3-4 is very similar to the machine shown in Figure 3-3 except that it has a tilting mechanism for the spindle head about the Y_1 axis instead of the rotary table about the Z_2 axis. Thus there are two degrees of freedom for the blank and three degrees of freedom for the cutter. Hence c_1, θ_1, ϕ_1, a_2 and b_2 are the five time-dependant entries in the input table while the other seven are constants. This machine is capable of producing two identical parts simultaneously since it has got two spindle heads. However, in this modeling, we are concerned with the spindle head on the right side only.

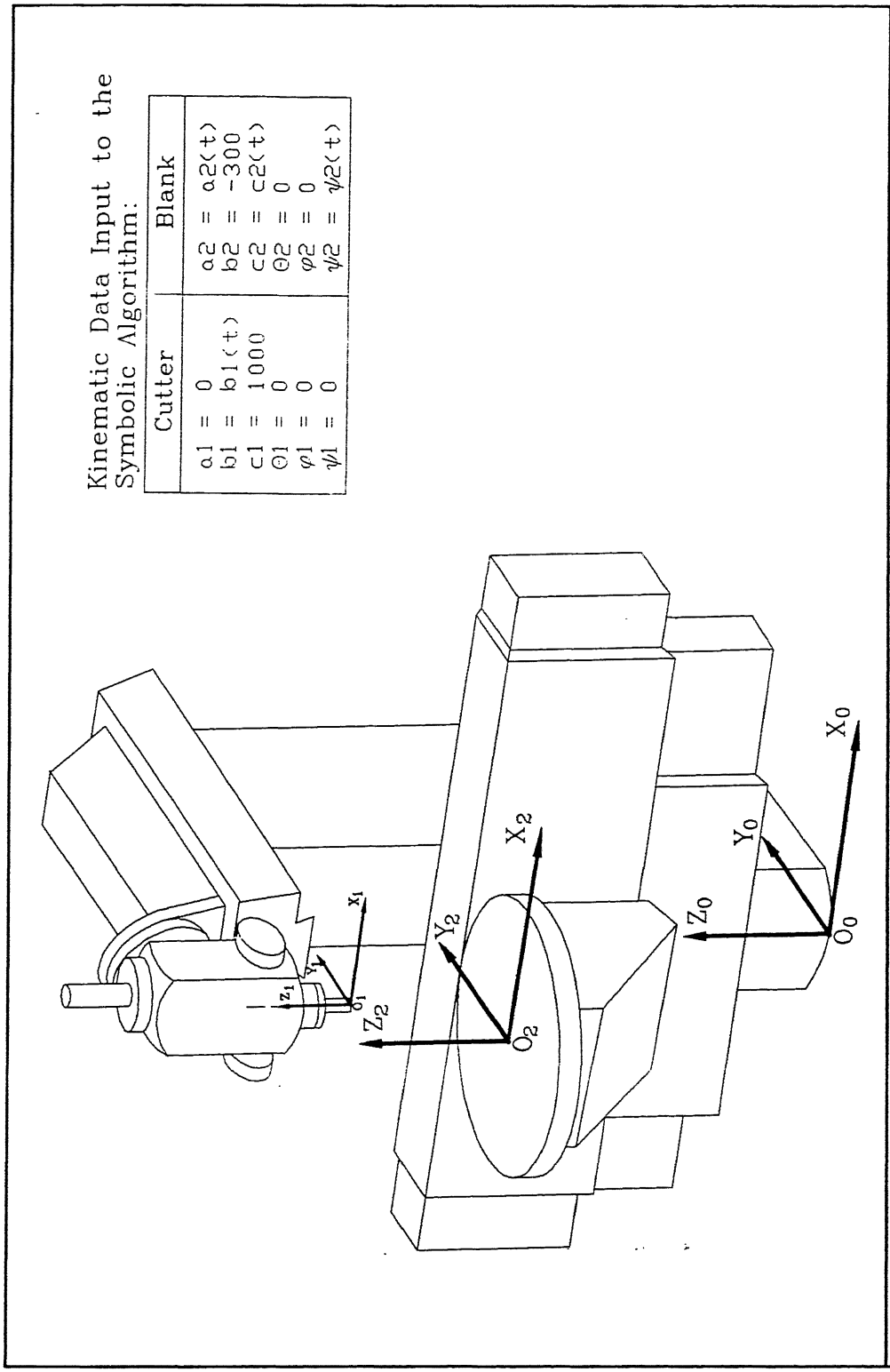

Figure 3-1 Instantiation of the Generic Machine Tool for a 4 Axis Milling Machine with a Rotary Table.

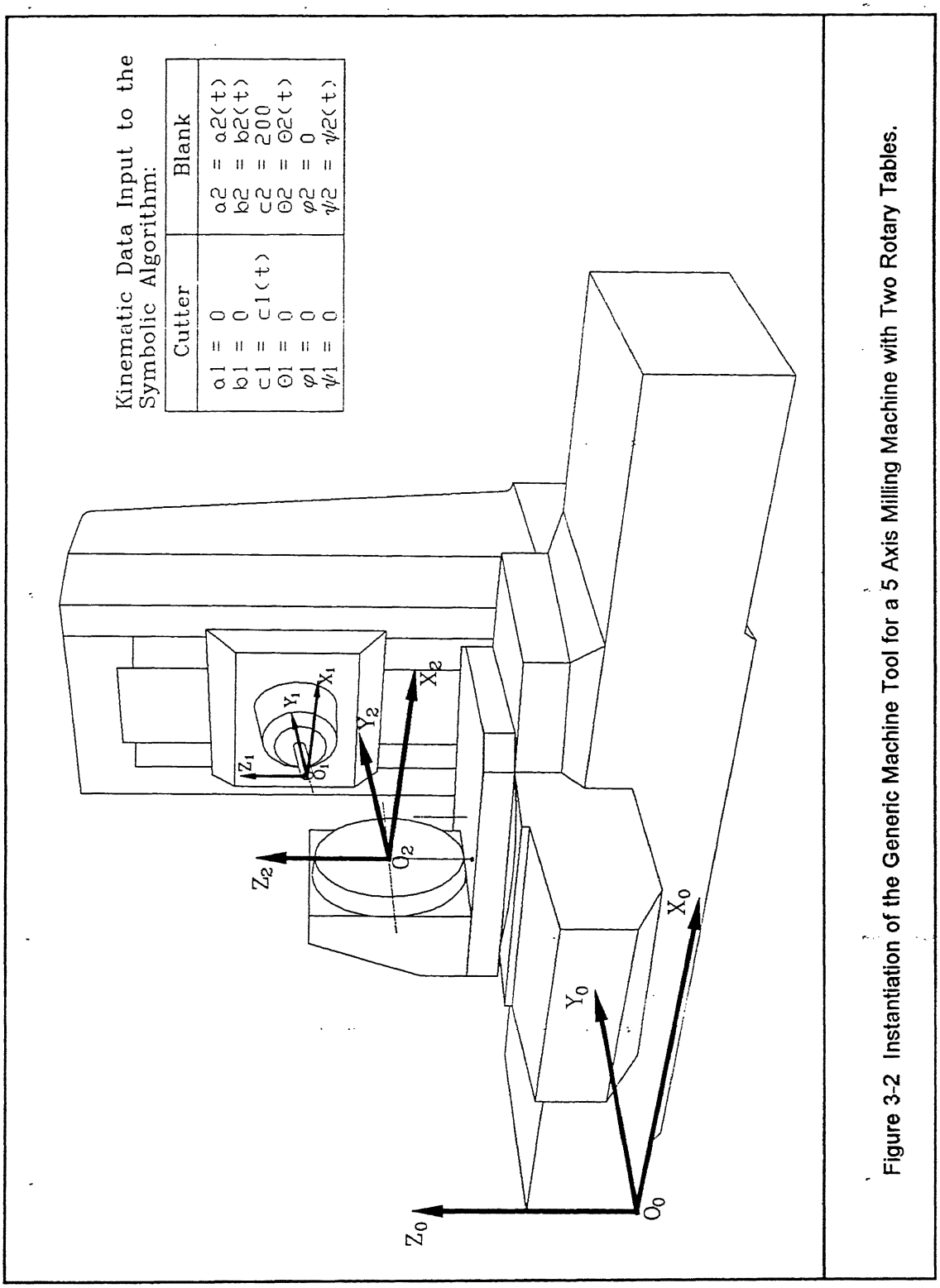

Figure 3-2 Instantiation of the Generic Machine Tool for a 5 Axis Milling Machine with Two Rotary Tables.

I. I. T. KANPUR
Acc. No. A. 117852

Kinematic Data Input to the Symbolic Algorithm:

Cutter	Blank
a1 = 500	a2 = a2(t)
b1 = 400	b2 = b2(t)
c1 = c1(t)	c2 = 300
Θ1 = Θ1(t)	Θ2 = 0
φ1 = 0	φ2 = 0
ψ1 = 0	ψ2 = ψ2(t)

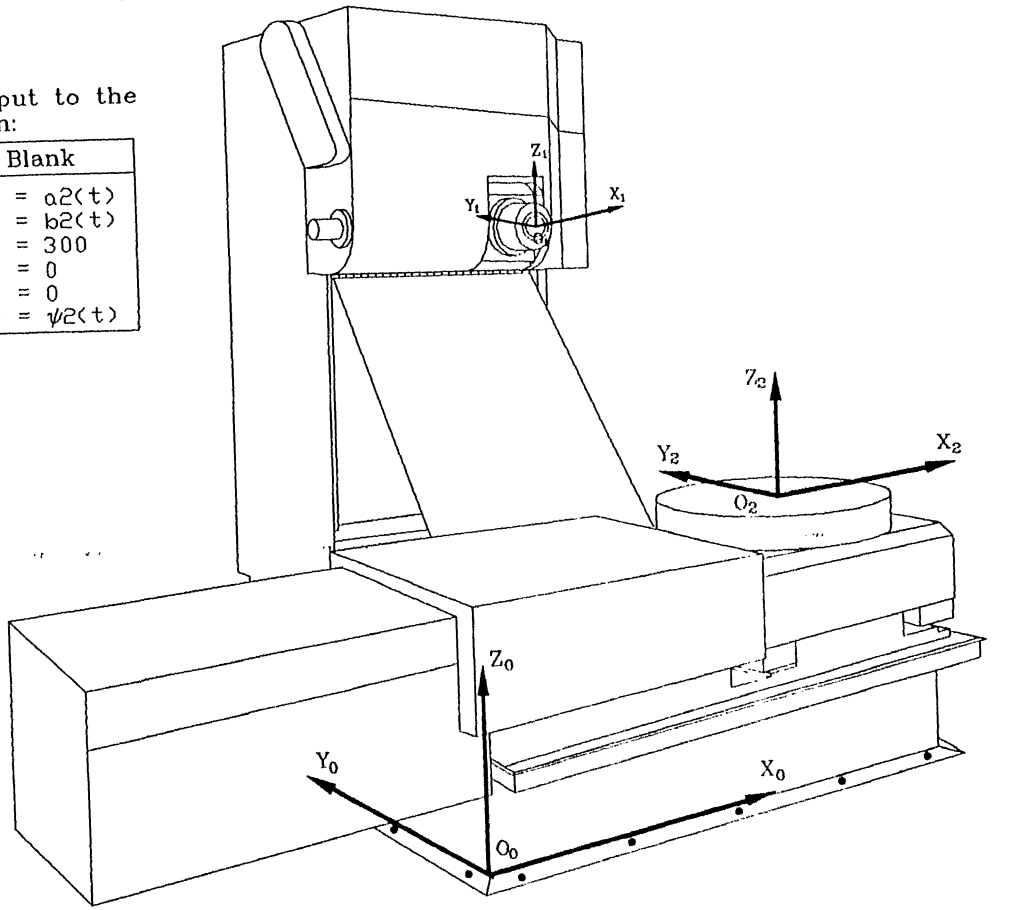

Figure 3-3 Instantiation of the Generic Machine Tool for a 5 Axis Milling Machine with a Rotary Table and a Tilting Spindle Head.

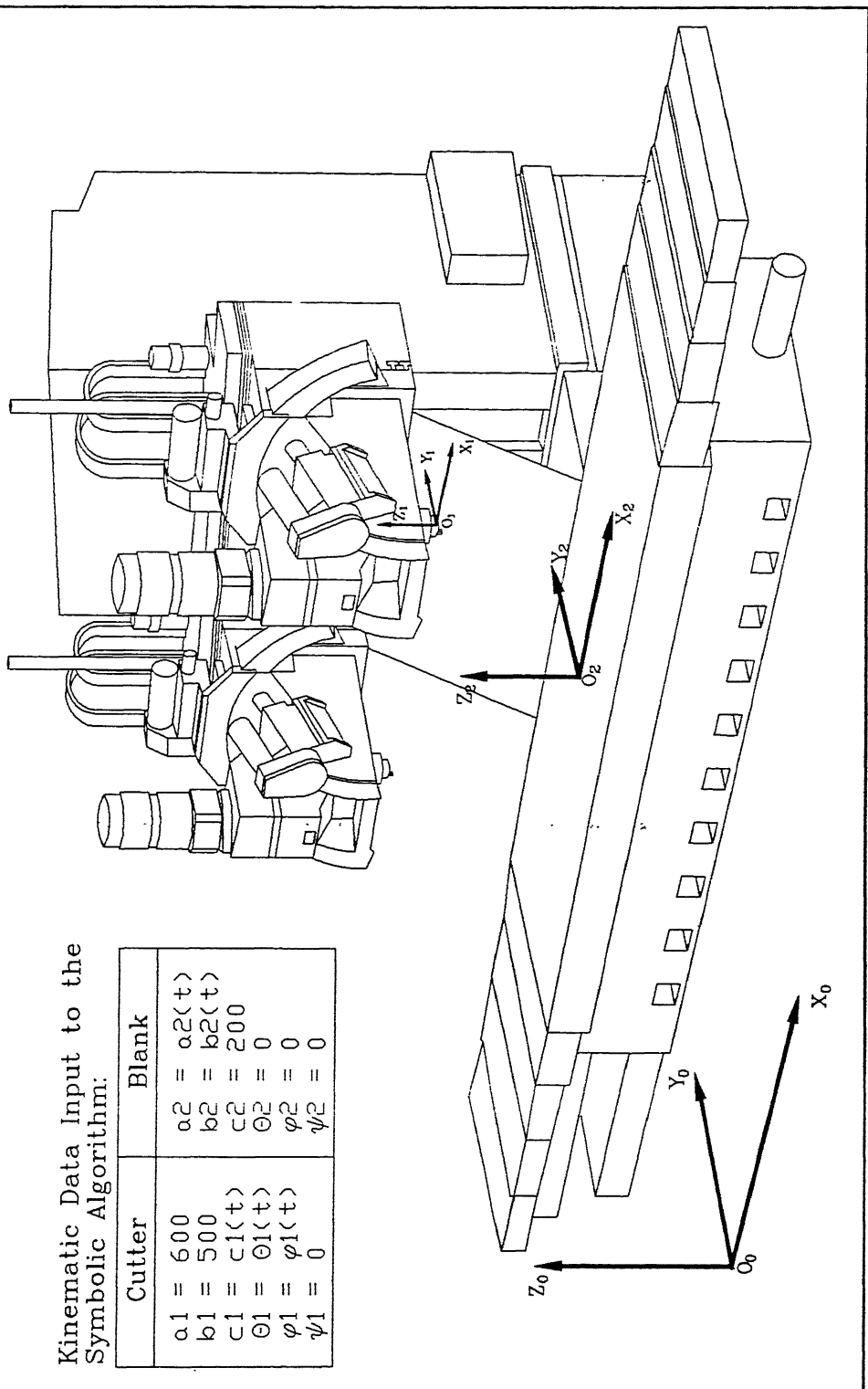

Figure 3-4 Instantiation of the Generic Machine Tool for a 5 Axis Milling Machine with Spindle Head Swivel Capability about Two Principal Directions.

3.2.5 Instantiation of a 5 Axis Milling Machine with Spindle Head Swivel Capability about Two Arbitrary Directions

The four machine tools illustrated so far have their rotary motions about the principal directions. Since the ultimate aim of the two rotary movements in any machine tool is to orient the cutter in any desired direction, one can also think of machine tools with these two rotary motions about any two arbitrary axes. One such machine is shown in Figure 3-5. In this machine, the table is grouted to the floor and hence it has no degree of freedom. The cutter has all the five degrees of freedom. One of the rotary movements is about the A axis which is parallel to the Z_0 axis. The other rotary movement is about an axis called B axis which makes an angle δ with the A axis. For this machine, a_1, b_1, c_1, θ_1 and ϕ_1 only will be the time-dependant variables. ψ_1 will be a function of θ_1 and ϕ_1 and the rest six parameters will be constants. It may be noted that the purpose of B axis is to cause a throw or a tilt of the tool axis from its initial vertical position. Hence the effect of rotation about A axis is not felt when the tool axis is vertical since it will be equivalent to a change in the spindle rotation at this condition. If α is the angle of rotation about the A axis and β is the angle of rotation about the B axis then, α and β are related to the angles θ_1, ϕ_1 and ψ_1 as follows:

$$\left.\begin{aligned} \theta_1 &= 0 \\ \varphi_1 &= \cos^{-1}[1 - \sin^2\delta(1 - \cos\beta)] \\ \psi_1 &= \tan^{-1}\left\{\frac{\cos\delta \sin\alpha (1 - \cos\beta) - \cos\alpha \sin\beta}{\cos\delta \cos\alpha (1 - \cos\beta) + \sin\alpha \sin\beta}\right\} \end{aligned}\right] \quad \textbf{(3-1)}$$

Figure 3-6 describes the configuration of these two rotations. Figure 3-7 shows the cutter orientation for various values of β for $\alpha = 0$. When $\beta = 0$, the rotation about the A axis has no influence in the orientation of the cutter. When the B axis is rotated, the cutter describes a tilted cone of fixed base diameter, say cone B, causing the cutter to deviate from its vertical position. When the A axis also rotates, the cone B itself rotates about the A axis. The enveloping cone may be called cone A whose apex angle is a function of β. Figure 3-8 shows the orientation of the cutter along with the corresponding cone A and cone B for various combinations of α and β. For these illustrations, δ is assumed to be $\pi/8$.

For a given cutter and the required surface Σ_2, the path generated by the conjugate geometry model will be directly in terms of the joint coordinates x, y, z, α and β. In the case of the conventional APT method, the CL file will be generated which will contain the path information in terms of x, y, z, i, j and k where i, j and k are the directional cosines of the cutter axis. The post processor will have to map these into the joint space

using the following relations obtained from Equation (3-1):

$$\begin{aligned} x_{new} &= x_{prev} + L \cos a \sin b \\ y_{new} &= y_{prev} + L \sin a \sin b \\ z_{new} &= z_{prev} - L(1 - \cos b) \end{aligned} \tag{3-2a}$$

$$\beta_{new} = 2 \tan^{-1} \left(\frac{\sin \frac{b}{2}}{\sqrt{\sin^2 \delta - \sin^2 \frac{b}{2}}} \right) \tag{3-2b}$$

$$\alpha_{new} = \frac{\pi}{2} + a + \tan^{-1} \left(\frac{\cos \delta \ (1 - \cos \beta_{new})}{\sin \beta_{new}} \right)$$

where

$$a = \tan^{-1} \frac{j}{i}$$
$$b = \cos^{-1} k$$

and L is the distance between the cutter tip and the fulcrum point and the subscripts *new* and *prev* respectively refer to the new and the previous joint coordinate positions. The APT processor generates CL data such that between any two consecutive positions, when x, y, z, $\cos^{-1}i$, $\cos^{-1}j$ and $\cos^{-1}k$ are linearly varied, the resulting surface will represent the desired surface within the *TOLER*, *INTOL* and *OUTOL*[3] limits. However, that the desired surfaces will be produced within these limits cannot be guaranteed when the joint coordinates x, y, z, α and β of the corresponding pair of CL data are linearly varied. In order to get the correct surface, the post-processor is required to calculate additional points between the two end positions and inserts them in the NC program.

[3] *INTOL*, *OUTOL* and *TOLER* are APT commands for specifying the tolerance of the generated surface with respect to the desired surface. These stand for INside TOLerance, OUTside TOLerance and TOLERance.

Kinematic Data Input to the Symbolic Algorithm:

Cutter	Blank
a1 = a1(t)	a2 = 0
b1 = b1(t)	b2 = 0
c1 = c1(t)	c2 = 0
Θ1 = Θ1(t)	Θ2 = 0
φ1 = φ1(t)	φ2 = 0
ψ1 = ψ1(Θ1, φ1)	ψ2 = 0

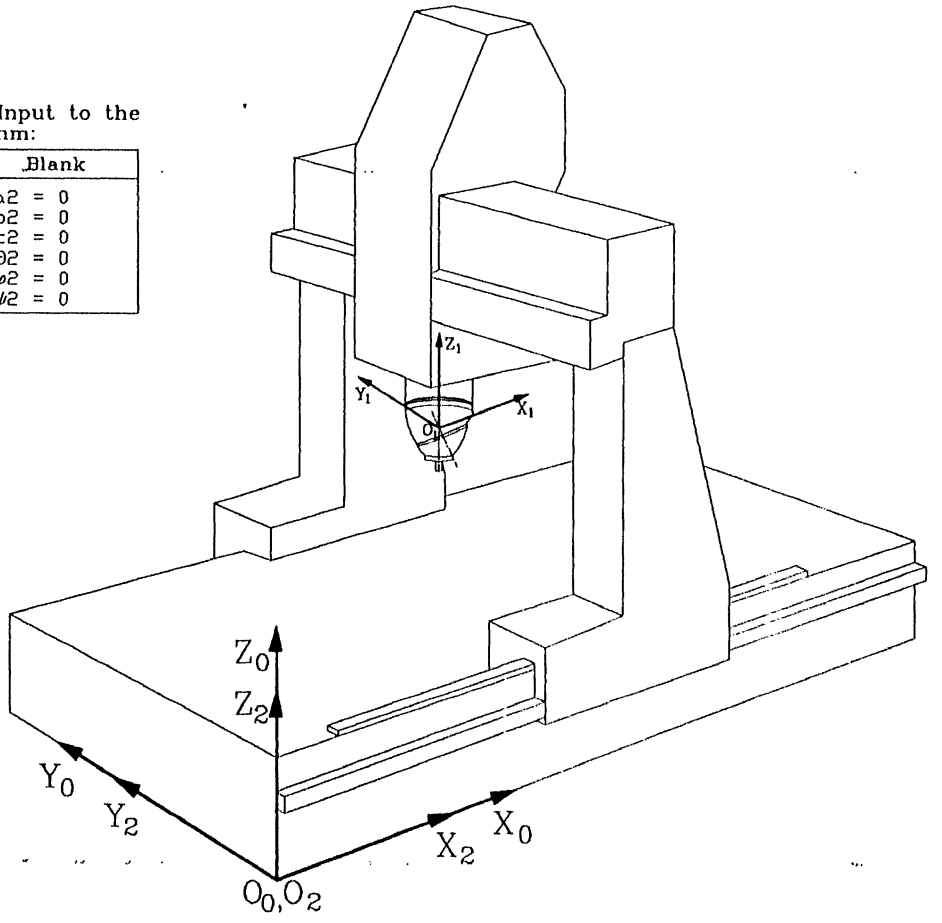

Figure 3-5 Instantiation of the Generic Machine Tool for a 5 Axis Milling Machine with Spindle Head Swivel Capability about Two Arbitrary Directions.

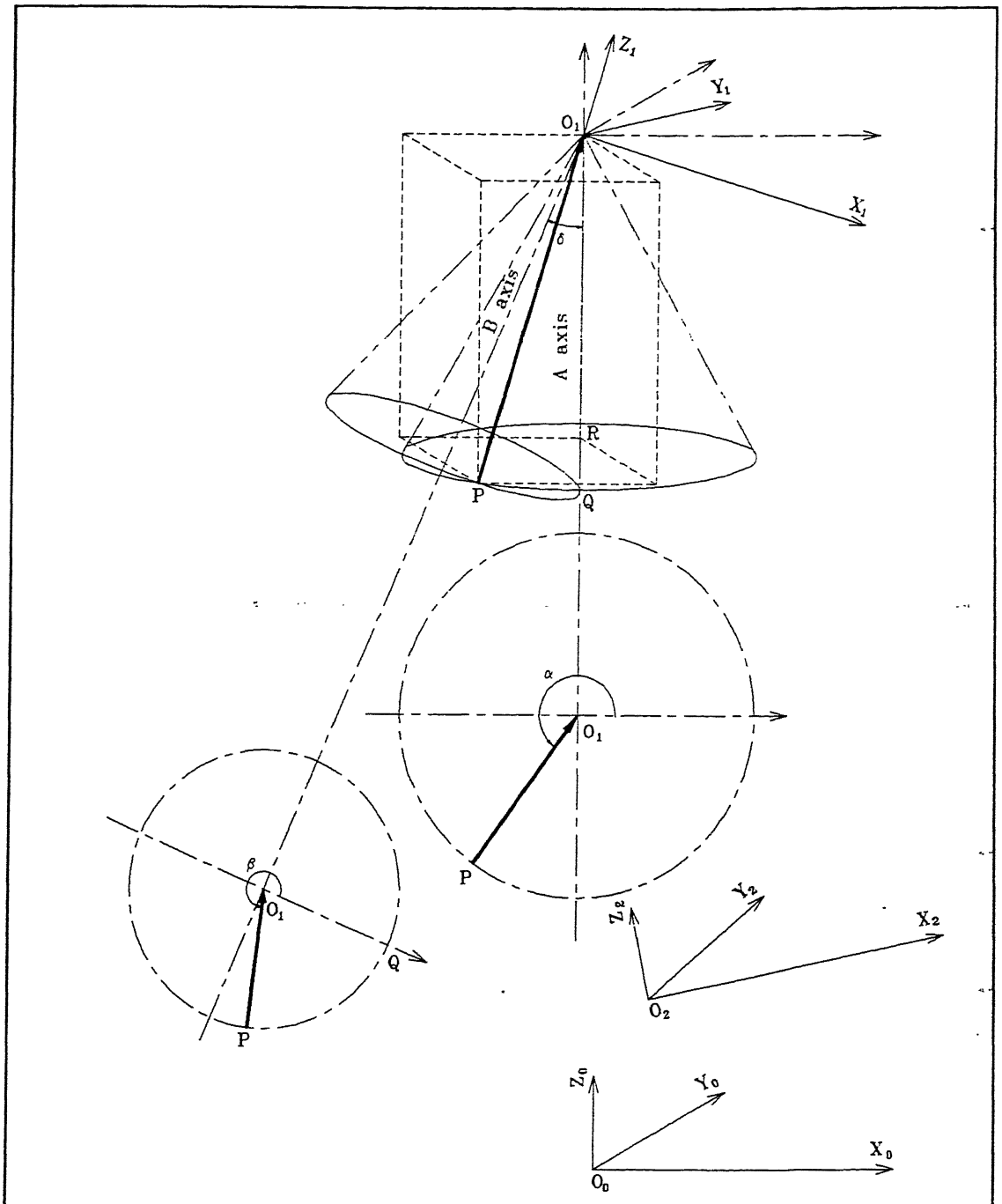

Figure 3-6 Spindle Configuration of the 5 Axis Profiler Shown in Figure 3-5.

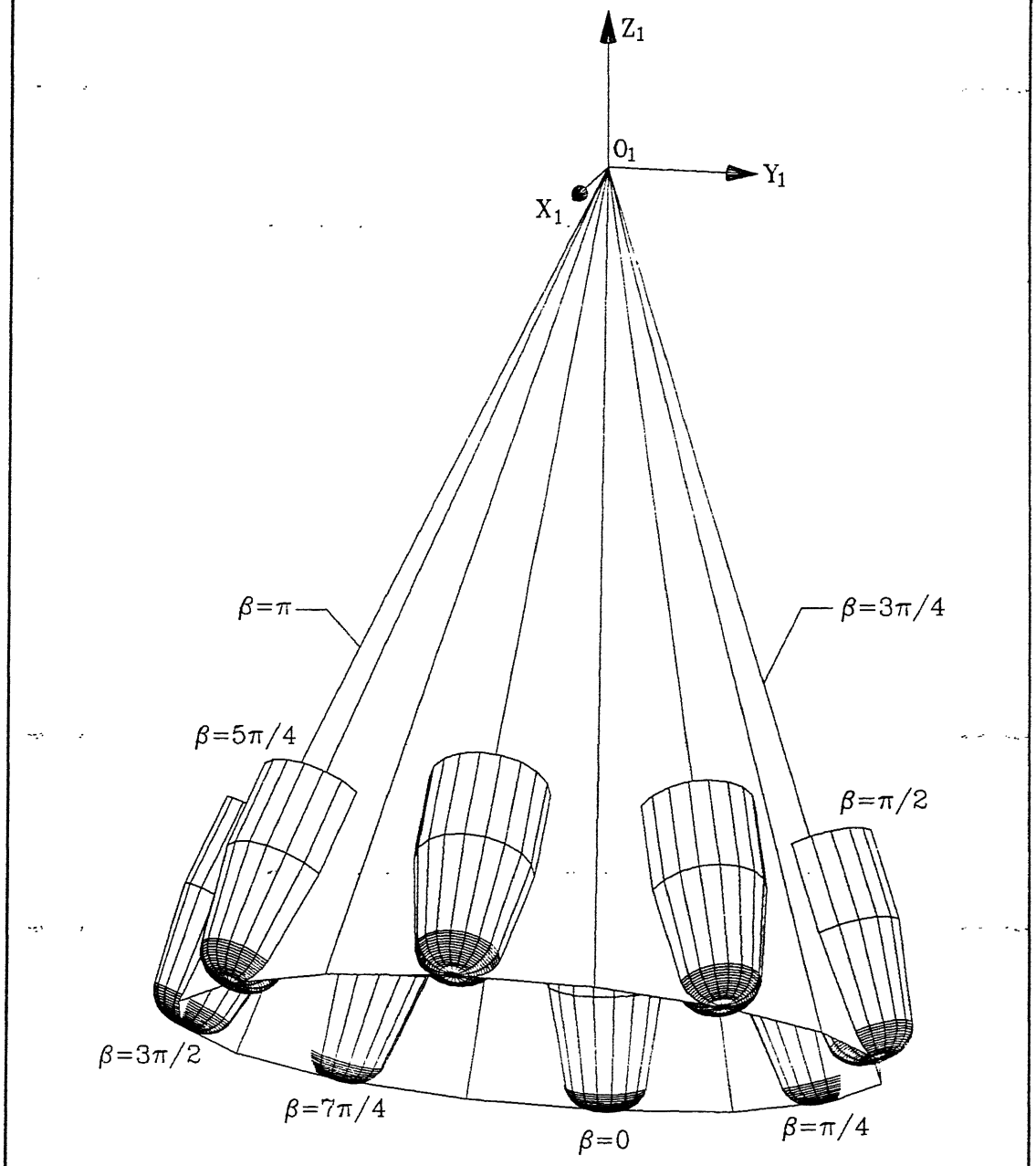

Figure 3-7 Tool Orientation for Various Values of β at α=0 for the 5 Axis Profiler Shown in Figure 3-5.

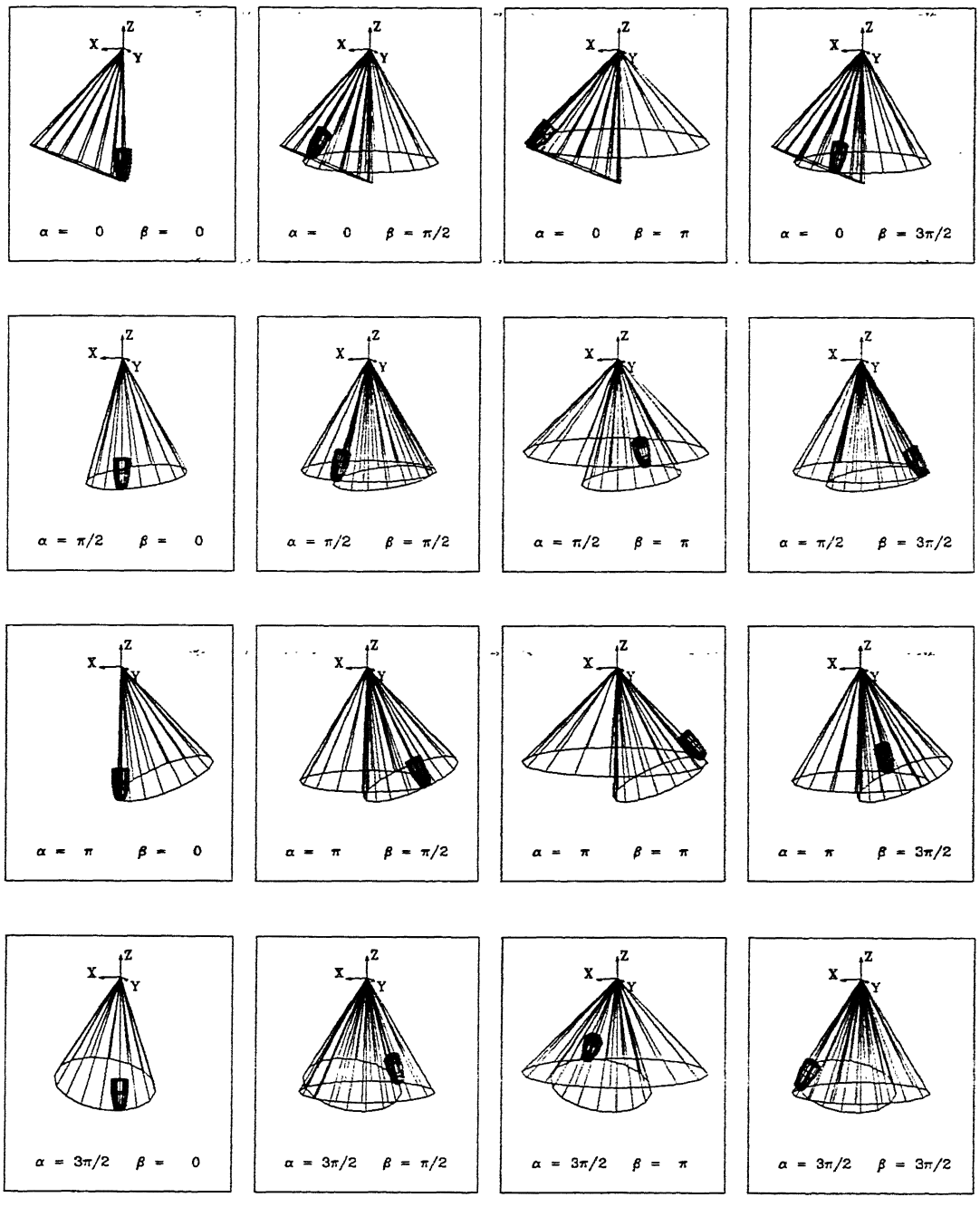

Figure 3-8 Tool Orientation for Various Combinations of α and β for the 5 Axis Profiler Shown in Figure 3-5.

3.3 Illustrative Example

Let us consider an example of machining a helicoidal surface using a horizontal milling machine with an end milling cutter of the required form. The biparametric definition of one such cutter in u and v is as follows:

$$\left.\begin{aligned} x_1 &= u \cos v \\ y_1 &= u \sin v \\ z_1 &= a u^2 + b u + c \end{aligned}\right] \qquad (3\text{-}3)$$

where

$$0 \le u \le 5.33903e{+}01$$
$$0 \le v \le 2\pi$$

$$a = 1.68979e{-}02$$
$$b = 1.02956e{-}06 \text{ and}$$
$$c = 4.91379e{+}01$$

Figure 3-9a shows the kinematic scheme of this process. The cutter is stationary and the blank rotates about X_0 axis at the rate of ω radian/second while it translates along $-X_0$ axis at the rate of $p\omega/2\pi$ meter/second where p is the pitch of the helicoidal surface. The twelve parameters of motion for this case will be:

Cutter	Blank
$a_1 = 0$	$a_2 = -\dfrac{p\,\omega\,t}{2\pi}$
$b_1 = 0$	$b_2 = 0$
$c_1 = 0$	$c_2 = 0$
$\theta_1 = -\dfrac{\pi}{2}$	$\theta_2 = \omega t$

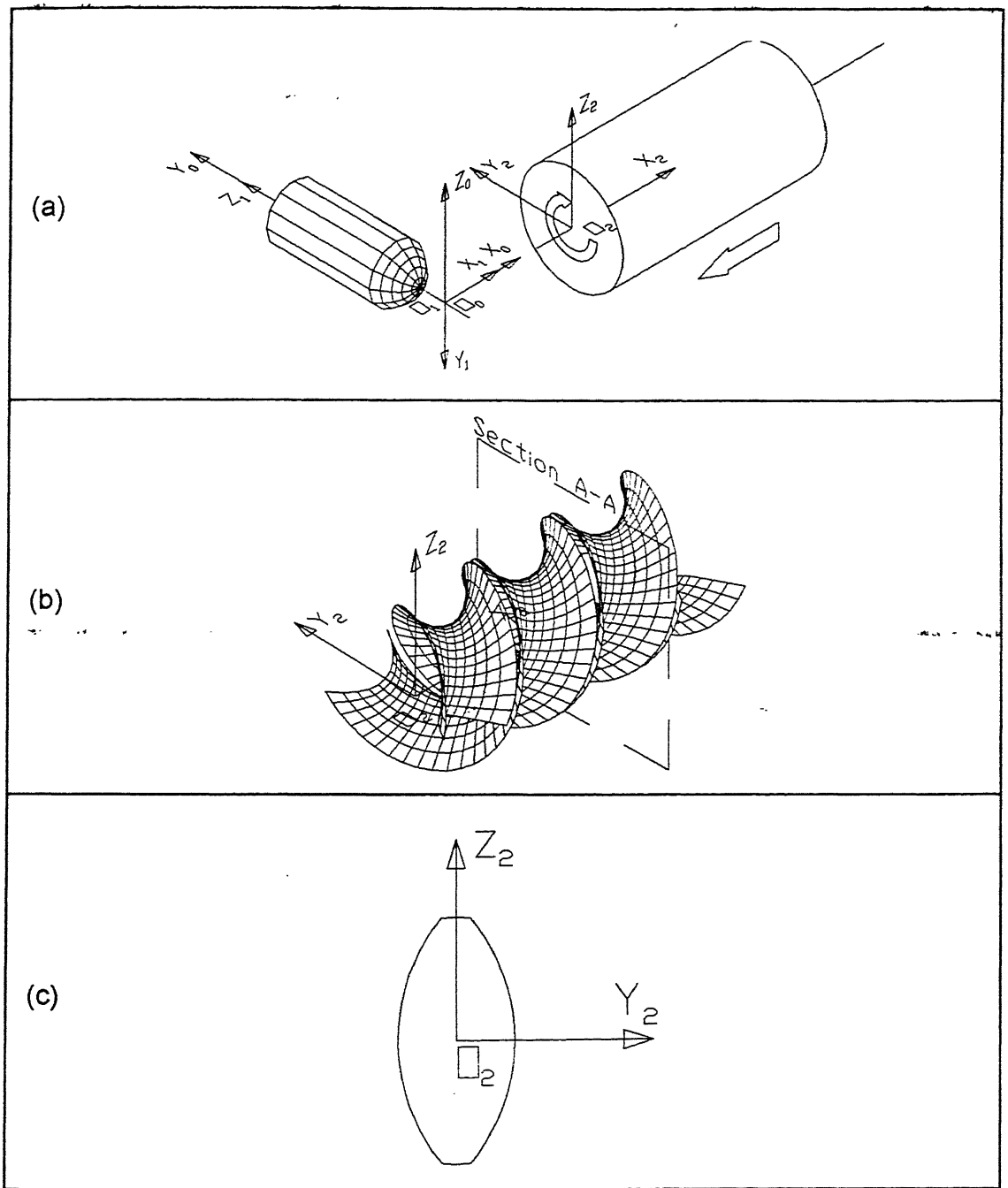

Figure 3-9 Modeling of a Milling Process to Generate a Helicoidal Surface.
(a) Kinematic Arrangement of the Process
(b) Machined Surface Σ_2 and
(c) Cross-section of the Machined Surface Σ_2 at Section A-A.

$\phi_1 = 0$	$\phi_2 = 0$
$\psi_1 = 0$	$\psi_2 = 0$

Table 3-1. Parameters Describing the Relative Motion in a Milling Process

Having known the surface of the cutter Σ_1 and the twelve parameters of motion for the cutter and the blank, one can predict the machined surface Σ_2 using the algorithm described in the previous chapter.

Step 1: The biparametric definition of the cutter surface is given below:

$$ {}^1\underset{\sim}{p} = [\, x_1 \quad y_1 \quad z_1 \quad 1 \,] $$

$$ {}^1\underset{\sim}{p} = [u\cos v \quad u\sin v \quad au^2 + bu + c \quad 1] \qquad \textbf{(3-4)} $$

Step 2: The twelve parameters of motion are described in Table 3-1.

Step 3: The transformation matrix $\left[{}^0_1M\right]$ for transforming the position vector ${}^1\underset{\sim}{p}$ and the normal vector ${}^1\underset{\sim}{n}_{P,1}$ from the cutter coordinate system S_1 to the global coordinate system S_0 is

$$ \left[{}^0_1M\right] = \begin{bmatrix} 1 & 0 & 0 & 0 \\ 0 & 0 & -1 & 0 \\ 0 & 1 & 0 & 0 \\ 0 & 0 & 0 & 1 \end{bmatrix} \qquad \textbf{(3-5)} $$

Matrix $\left[{}^0_1\dot{M}\right]$ is the time-differential of the matrix $\left[{}^0_1M\right]$ which converts the position vector ${}^1\underset{\sim}{p}$ in the cutter coordinate system S_1 into velocity vector ${}^0\underset{\sim}{V}_{P,1}$ in the global coordinate system S_0.

$$\left[{}^{0}_{1}\dot{M} \right] = \begin{bmatrix} 0 & 0 & 0 & 0 \\ 0 & 0 & 0 & 0 \\ 0 & 0 & 0 & 0 \\ 0 & 0 & 0 & 0 \end{bmatrix} \tag{3-6}$$

Step 4: The transformation matrices $\left[{}^{0}_{2}M \right]$ and $\left[{}^{2}_{0}M \right]$ for transforming the position vector ${}^{2}\underset{\sim}{p}$ from the blank coordinate system S_2 to the global coordinate system S_0 and vice-versa are respectively:

$$\left[{}^{0}_{2}M \right] = \begin{bmatrix} 1 & 0 & 0 & 0 \\ 0 & \cos \omega t & \sin \omega t & 0 \\ 0 & -\sin \omega t & \cos \omega t & 0 \\ -\frac{p \omega t}{2 \pi} & 0 & 0 & 1 \end{bmatrix} \tag{3-7}$$

$$\left[{}^{2}_{0}M \right] = \begin{bmatrix} 1 & 0 & 0 & 0 \\ 0 & \cos \omega t & -\sin \omega t & 0 \\ 0 & \sin \omega t & \cos \omega t & 0 \\ \frac{p \omega t}{2 \pi} & 0 & 0 & 1 \end{bmatrix} \tag{3-8}$$

Matrix $\left[{}^{0}_{2}\dot{M} \right]$ is the time-differential of the matrix $\left[{}^{0}_{2}M \right]$ which converts the position vector ${}^{2}\underset{\sim}{p}$ in the blank coordinate system S_2 into velocity vector ${}^{0}\underset{\sim}{V}_{P,2}$ in the global coordinate system S_0.

$$\left[{}^{0}_{2}\dot{M} \right] = \begin{bmatrix} 0 & 0 & 0 & 0 \\ 0 & -\omega \sin \omega t & \omega \cos \omega t & 0 \\ 0 & -\omega \cos \omega t & -\omega \sin \omega t & 0 \\ -\dfrac{p\,\omega}{2\,\pi} & 0 & 0 & 0 \end{bmatrix} \tag{3-9}$$

Step 5: The position vector ${}^{2}\underset{\sim}{p}$ is

$${}^{2}\underset{\sim}{p} = \begin{bmatrix} x_2 & y_2 & z_2 & 1 \end{bmatrix}$$

$${}^{2}\underset{\sim}{p} = {}^{1}\underset{\sim}{p} \left[{}^{0}_{1}M \right] \left[{}^{2}_{0}M \right]$$

$${}^{2}\underset{\sim}{P} = \begin{bmatrix} u \cos v + \dfrac{p\,\omega\,t}{2\,\pi} \\ (a\,u^2 + b\,u + c) \cos \omega t - u \sin v \sin \omega t \\ -(a\,u^2 + b\,u + c) \sin \omega t - u \sin v \cos \omega t \\ 1 \end{bmatrix}^{T} \tag{3-10}$$

Step 6: The normal vector ${}^{1}N_{P,1}$ of the cutter surface is obtained as follows:

$$\frac{\partial\, {}^{1}\underset{\sim}{p}}{\partial u} = \begin{bmatrix} \cos v & \sin v & (2\,a\,u + b) & 0 \end{bmatrix}$$

$$\frac{\partial\, {}^{1}\underset{\sim}{p}}{\partial v} = \begin{bmatrix} -u \sin v & u \cos v & 0 & 0 \end{bmatrix}$$

$$ {}^{1}\underset{\sim}{N}_{P,1} = \frac{\partial\, {}^{1}\underset{\sim}{p}}{\partial u} \times \frac{\partial\, {}^{1}\underset{\sim}{p}}{\partial v} $$

$$ {}^{1}\underset{\sim}{N}_{P,1} = \begin{bmatrix} -(2au + b)\, u \cos v \\ -(2au + b)\, u \sin v \\ u \\ 0 \end{bmatrix}^{T} \qquad \textbf{(3-11)} $$

Step 7: The unit normal vector ${}^{1}\underset{\sim}{n}_{P,1}$ of the cutter surface is obtained as follows:

$$ \| \; {}^{1}\underset{\sim}{N}_{P,1} \; \| = \sqrt{1 + (2au + b)^2}\; u $$

$$ {}^{1}\underset{\sim}{n}_{P,1} = \frac{{}^{1}\underset{\sim}{N}_{P,1}}{\| \; {}^{1}\underset{\sim}{N}_{P,1} \; \|} $$

$$ {}^{1}\underset{\sim}{n}_{P,1} = \begin{bmatrix} -\dfrac{(2au + b)}{\sqrt{1 + (2au + b)^2}} \cos v \\ -\dfrac{(2au + b)}{\sqrt{1 + (2au + b)^2}} \sin v \\ \dfrac{1}{\sqrt{1 + (2au + b)^2}} \\ 0 \end{bmatrix}^{T} \qquad \textbf{(3-12)} $$

Step 8: The normal vector ${}^{0}\underset{\sim}{n}_{P,1}$ of the cutter surface in the global coordinate system is:

$$ {}^{0}\underset{\sim}{n}_{P,1} = {}^{1}\underset{\sim}{n}_{P,1} \left[{}^{0}_{1}M \right] $$

$$ {}^{0}\underset{\sim}{n}_{P,1} = \begin{bmatrix} -\dfrac{(2au + b)}{\sqrt{1 + (2au + b)^2}} \cos v \\ \dfrac{1}{\sqrt{1 + (2au + b)^2}} \\ \dfrac{(2au + b)}{\sqrt{1 + (2au + b)^2}} \sin v \\ 0 \end{bmatrix}^T \qquad \textbf{(3-13)} $$

Step 9: The relative velocity vector ${}^{0}\underset{\sim}{V}_{P,12}$ in the global coordinate system can be now calculated as:

$$ \begin{aligned} {}^{0}\underset{\sim}{V}_{P,1} &= {}^{1}\underset{\sim}{P} \left[{}^{0}_{1}\dot{M} \right] \\ {}^{0}\underset{\sim}{V}_{P,1} &= \begin{bmatrix} 0 & 0 & 0 & 0 \end{bmatrix} \end{aligned} \qquad \textbf{(3-14)} $$

$$ \begin{aligned} {}^{0}\underset{\sim}{V}_{P,2} &= {}^{2}\underset{\sim}{P} \left[{}^{0}_{2}\dot{M} \right] \\ {}^{0}\underset{\sim}{V}_{P,2} &= \begin{bmatrix} -\dfrac{p\,\omega}{2\pi} & \omega\, u \sin v & \omega\,(a u^2 + b u + c) & 0 \end{bmatrix} \end{aligned} \qquad \textbf{(3-15)} $$

$$ \begin{aligned} {}^{0}\underset{\sim}{V}_{P,12} &= {}^{0}\underset{\sim}{V}_{P,2} - {}^{0}\underset{\sim}{V}_{P,1} \\ {}^{0}\underset{\sim}{V}_{P,12} &= \begin{bmatrix} -\dfrac{p\,\omega}{2\pi} & \omega\, u \sin v & \omega\,(a u^2 + b u + c) & 0 \end{bmatrix} \end{aligned} \qquad \textbf{(3-16)} $$

Step 10: The condition of contact ${}^{0}\underset{\sim}{n}_{P,1} \cdot {}^{0}\underset{\sim}{V}_{P,12} = 0$ yields the following relation between u and v:

$$\tan v = \frac{-\frac{p}{2\pi}(2au + b)}{u + (2au + b)(au^2 + bu + c)} \tag{3-17}$$

Step 11: Surface Σ_2 can be now represented as a biparametric equation in u and t as given below which can be graphically represented as shown in Figure 3-9b.

$$\left.\begin{aligned} x_2 &= u\cos v + \frac{p\omega t}{2\pi} \\ y_2 &= (au^2 + bu + c)\cos\omega t - u\sin v\sin\omega t \\ z_2 &= -(au^2 + bu + c)\sin\omega t - u\sin v\cos\omega t \end{aligned}\right] \tag{3-18}$$

where

$$\tan v = \frac{-\frac{p}{2\pi}(2au + b)}{u + (2au + b)(au^2 + bu + c)}$$

Incidentally, this happens to be the screw surface of a twin-screw extruder used in the polymer industry. This is a bi-lobed screw with zero minor the cross-sectional profile of which is shown in Section A-A of Figure 3-9c.

Chapter 4

SYMBOLIC DEFINITION OF A GENERIC CUTTER

4.1 Introduction

The geometry of a cutter can be modelled as an axisymmetric, biparametric surface. The axis of symmetry depends on whether the cutter is an end mill type cutter, a side mill type cutter, a face mill type cutter or any combination of some of these basic types. In the present work, a model of a generic cutter is developed in which the generatrix curve is a planar curve consisting of a set of contiguous straight line and circular fillet segments. The directrix motion is the axisymmetric sweep of this curve around an axis in the plane of the generatrix curve. In numerical control literature, a generic cutter is defined using seven parameters and the generatrix curve consists of two straight line segments forming the tip flank as well as the side flank and a circular fillet between these straight line segments (Chang, 1989). In this thesis, an extension of this concept is used. The generatrix curve is assumed to be a piecewise continuous curve consisting of three straight line segments and a circular fillet between the tip flank and the side flank lines (see Figure 4-1). This generatrix curve can be defined by means of eight parameters, viz., d, r, e, f, a, b, h and h_1 as shown in Figure 4-1. The cutter surface can be obtained by rotating the generatrix curve either along the Z_1 axis or along the X_1 axis as shown in Figure 4-2. When the sweep is a rotation about the Z_1 axis, one can generate the geometry of various types of end milling cutters used in 3 to 5 axis machining and also the cutters used in the non-traditional machining processes such as laser beam, water jet and wire of an EDM process. If the rotation is about the X_1 axis, then a disc type of cutting tool geometry is generated which will represent a side-and-face milling cutter or a grinding wheel. If the generatrix curve is swept in a helical manner, then the geometry of a gear hob or a tapping tool can be obtained. Thus by choosing appropriate values of the parameters describing the planar curve and the sweep motion, one can obtain a variety of conventional and non-traditional cutting tools.

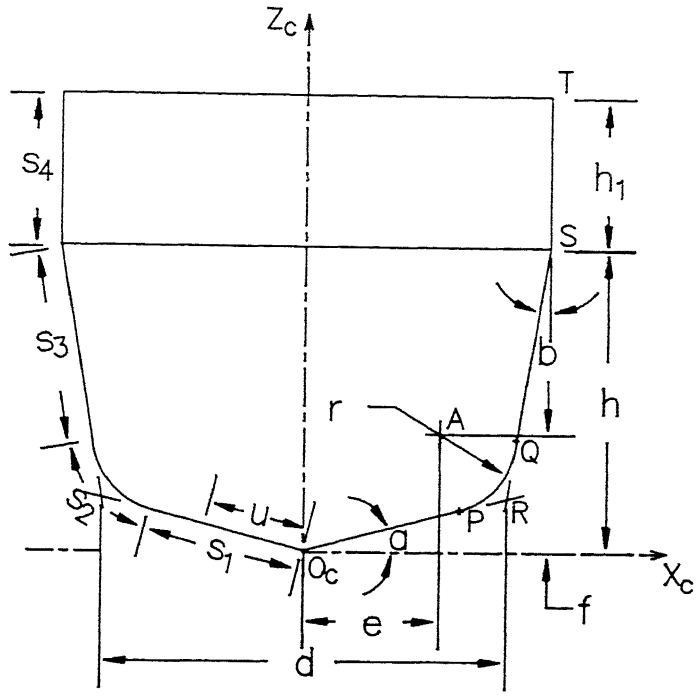

Figure 4-1. Definition of a Generic Cutter

(i) Sweep Matrix to Generate an End Mill Type Cutters (Rotation about Z_1 axis) :

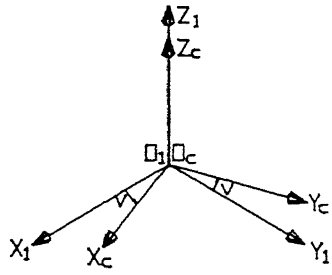

$$\left[{}^{1}_{c}M\right] = \begin{bmatrix} \cos v & \sin v & 0 & 0 \\ -\sin v & \cos v & 0 & 0 \\ 0 & 0 & 1 & 0 \\ 0 & 0 & 0 & 1 \end{bmatrix}$$

(ii) Sweep Matrix to Gnerate a Disc Type Cutters (Rotation about an Axis Parallel to X_1 axis and at a distance of q from X_1 Axis) :

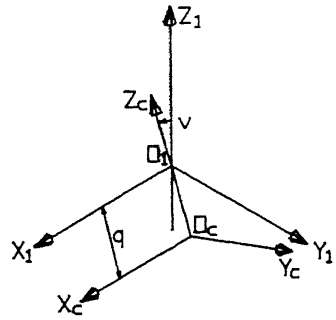

$$\left[{}^{1}_{c}M\right] = \begin{bmatrix} \cos v & \sin v & 0 & 0 \\ -\sin v & \cos v & 0 & 0 \\ 0 & 0 & 1 & 0 \\ 0 & 0 & 0 & 1 \end{bmatrix}$$

(iii) Sweep Matrix to Generate a Gear Hob or a Tap Type Cutters (Helical Sweep along X_1 axis with Lead l and Radius of Helix q) :

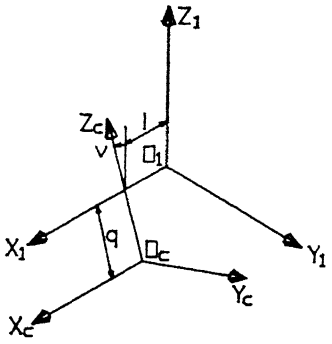

$$\left[{}^{1}_{c}M\right] = \begin{bmatrix} 1 & 0 & 0 & 0 \\ 0 & \cos v & \sin v & 0 \\ 0 & -\sin v & \cos v & 0 \\ \dfrac{l\,v}{2\pi} & q\sin v & -q\cos v & 1 \end{bmatrix}$$

Figure 4-2. Examples of the Sweep Matrix $\left[{}^{1}_{c}M\right]$

4.2 Description of the Generic Cutter

The planar curve of the generic cutter surface consists of three straight line segments and a circular arc segment (Figure 4-1). For the case of an end mill type cutter, the first and second straight line segments will generate the tip and the side flanks of the cutter while the third straight line segment will generally represent the shank of the cutter. The circular arc segment will generate the corner radius of the end mill. A coordinate system S_c (O_c - X_c, Y_c, Z_c) is considered to be attached to this cutter profile. This planar curve of the cutter profile can be represented by means of a parameter u which is the profile length of any point on the profile with respect to the origin O_c. The cutter surface Σ_1 is obtained by sweeping this generatrix profile along a directrix curve which can be circular, helical, etc. This sweep motion is represented by means of a homogeneous transformation matrix $\left[{}_c^1M\right]$ whose elements will be functions of a parameter v. The four segments of the generatrix curve can be algebraically expressed as

$$\left.\begin{aligned} O_cP &: z_c = x_c \tan a \\ PQ &: (x_c - e)^2 + (z_c - f) = r^2 \\ QS &: x_c = z_c \tan b - \frac{d}{2}\tan a \tan b + \frac{d}{2} \\ ST &: x_c = h \tan b - \frac{d}{2}\tan a \tan b + \frac{d}{2} \end{aligned}\right] \qquad (4\text{-}1)$$

where

O_cP - First straight line segment,

PQ - The circular segment with center at A,

QS - Second straight line segment,

ST - Third straight line segment,

R - Point of intersection of the first segment O_cP and the third segment QS,

d - Diameter of the cutter measured at R,

r - Radius of the circular segment. This is positive for a convex arc and negative for a concave arc,

a - Angle of segment O_cP measured from X_c axis. $-\pi/2 < a < \pi/2$,

b - Angle of segment QS measured from Z_c axis. $-\pi/2 \leq b < \pi/2$,

e - X coordinate of point A in the coordinate system S_c,

f - Z coordinate of point A in the coordinate system S_c,

h - Nonparallel height of the cutter,

h_1 - Parallel height of the cutter,

is_fillet_radius - Flag which is to be set to *TRUE* when the circular segment PQ is tangent to both the straight line segments O_cP and QS and *FALSE* otherwise,

u - Parameter which is the profile length of any generic point P on the profile measured from O_c,

v - Parameter which describes the sweep of the two dimensional profile,

$\left[{}^{1}_{c}M\right]$ - Homogeneous transformation matrix which describes the sweep of the two dimensional profile,

s_1 - Length of the first straight line segment O_cP,

s_2 - Length of the circular arc segment PQ,

s_3 - Length of the second straight line segment QS,

s_4 - Length of the third straight line segment ST,

${}^{c}\underset{\sim}{p}$ - Position vector of a generic point P on the two dimensional profile of the cutter in S_c coordinate system in terms of u and

${}^{1}\underset{\sim}{p}$ - Position vector of a generic point P on the surface of the cutter in S_1 coordinate system in terms of u and v.

The parametric equation of the generatrix curve ${}^{c}\underset{\sim}{p}(u)$ can be defined in a generic manner with respect to a coordinate system S_c (O_c - X_c, Y_c, Z_c) as follows :

$$ {}^{c}\underset{\sim}{p}(u) = \left[\, x_c(u) \quad y_c(u) \quad z_c(u) \quad 1 \,\right] \tag{4-2} $$

where,

$$ \textit{for the interval } 0 \le u < s_1, $$
$$ \left.\begin{aligned} x_c(u) &= u \cos a \\ y_c(u) &= 0 \\ z_c(u) &= u \sin a \,, \end{aligned}\right] \tag{4-3} $$

$$ \textit{for the interval } s_1 \le u < s_1+s_2, $$
$$ \left.\begin{aligned} x_c(u) &= e + abs(r) \cos\left\{\tan^{-1}\left(\frac{s_1 \sin a - f}{s_1 \cos a - e}\right) + \left(\frac{u - s_1}{r}\right)\right\} \\ y_c(u) &= 0 \\ z_c(u) &= f + abs(r) \sin\left\{\tan^{-1}\left(\frac{s_1 \sin a - f}{s_1 \cos a - e}\right) + \left(\frac{u - s_1}{r}\right)\right\} , \end{aligned}\right] \tag{4-4} $$

$$ \textit{for the interval } s_1+s_2 \le u < s_1+s_2+s_3, $$
$$ \left.\begin{aligned} x_c(u) &= [u - (s_1+s_2+s_3)] \sin b + x_c^S \\ y_c(u) &= 0 \\ z_c(u) &= [u - (s_1+s_2+s_3)] \cos b + z_c^S \end{aligned}\right] \tag{4-5} $$

$$ \textit{and for the interval } s_1+s_2+s_3 \le u \le s_1+s_2+s_3+s_4, $$
$$ \left.\begin{aligned} x_c(u) &= x_c^S \\ y_c(u) &= 0 \\ z_c(u) &= [u - (s_1+s_2+s_3)] + z_c^S \,. \end{aligned}\right] \tag{4-6} $$

Having known the planar profile ${}^{c}p(u)$ and the sweep, the biparametric definition of the cutter surface Σ_1 can be obtained from the equation

$$\underset{\sim}{{}^{1}p}(u, v) = \underset{\sim}{{}^{c}p}(u) \cdot \left[{}^{1}_{c}M\right] \tag{4-7}$$

where $\left[{}^{1}_{c}M\right]$ is the matrix describing the sweep motion. The algorithm of this generic cutter described in Section 4.3 has been implemented in the symbolic manipulation system *MACSYMA* and the results obtained for a 27 cutters are shown in Figure 4-3 to Figure 4-29.

4.3 Algorithm to Derive the Biparametric Equation of the Generic Cutter

The symbolic algorithm to derive the biparametric equation of the surface Σ_1 from the nine parameters of the cutter profile and the sweep matrix has been implemented in *MACSYMA*. It may be noted that all the nine parameters of the generic cutter may not be required in all cases. For instance, when the flag *is_fillet_radius* is *TRUE* and b is zero, only d,r,a,b and h_1 are required and when *is_fillet_radius* is *TRUE* and b is nonzero, then only d,r,a,b,h_1 and h are needed. The algorithm can now be stated as follows:

1. Calculate e and f if *is_fillet_radius* = *TRUE*.

$$e = \frac{d}{2} - r\left(\frac{\cos a - \sin b}{\cos (a+b)}\right)$$
$$f = \frac{r + e \sin a}{\cos a} \tag{4-8}$$

2. Calculate point P.

$$x_c^P = (e + f \tan a) \cos^2 a - \sqrt{\left[(e + f \tan a) \cos^2 a\right]^2 - (e^2+f^2-r^2) \cos^2 a}$$
$$z_c^P = x_c^P \tan a \tag{4-9}$$

3. Calculate point Q.

$$\left.\begin{aligned} z_c^Q &= \left\{ f + \left[e + \frac{d}{2}(\tan a \tan b - 1) \right] \tan b \right\} \cos^2 b \\ &+ \sqrt{\left[\left\{ f + \left[e + \frac{d}{2}(\tan a \tan b - 1) \right] \tan b \right\} \cos^2 b \right]^2 - \left\{ f^2 + \left[e + \frac{d}{2}(\tan a \tan b - 1) \right]^2 - r^2 \right\} \cos^2 b} \\ x_c^Q &= z_c^Q \tan b - \frac{d}{2}(\tan a \tan b - 1) \end{aligned}\right] \quad (4\text{-}10)$$

4. Calculate h if *is_fillet_radius* = *TRUE* and $b = 0$.

$$h = z_c^Q \quad (4\text{-}11)$$

5. Calculate point S.

$$\begin{aligned} x_c^S &= h \tan b - \frac{d}{2} \tan a \tan b + \frac{d}{2} \\ z_c^S &= h \end{aligned} \quad (4\text{-}12)$$

6. Calculate s_1, s_2, s_3 and s_4.

$$\left.\begin{aligned} s_1 &= \sqrt{\left(x_c^P\right)^2 + \left(z_c^P\right)^2} \\ s_2 &= r \left\{ \tan^{-1}\left(\frac{z_c^Q - f}{x_c^Q - e} \right) - \tan^{-1}\left(\frac{z_c^P - f}{x_c^P - e} \right) \right\} \\ s_3 &= \sqrt{\left(x_c^S - x_c^Q\right)^2 + \left(z_c^S - z_c^Q\right)^2} \\ s_4 &= h_1 \end{aligned}\right] \quad (4\text{-}13)$$

7. Define the parametric equation ${}^{c}\underset{\sim}{p}(u)$ of the two dimensional profile of the cutter in terms of the parameter u.

$$ {}^{c}\underset{\sim}{p}(u) = \begin{bmatrix} x_c(u) & y_c(u) & z_c(u) & 1 \end{bmatrix} \qquad \textbf{(4-14)} $$

where,

for the interval $0 \le u < s_1$,

$$ \left.\begin{aligned} x_c(u) &= u \cos a \\ y_c(u) &= 0 \\ z_c(u) &= u \sin a \end{aligned}\right] $$

for the interval $s_1 \le u < s_1 + s_2$,

$$ \left.\begin{aligned} x_c(u) &= e + abs(r) \cos\left\{\tan^{-1}\left(\frac{s_1 \sin a - f}{s_1 \cos a - e}\right) + \left(\frac{u - s_1}{r}\right)\right\} \\ y_c(u) &= 0 \\ z_c(u) &= f + abs(r) \sin\left\{\tan^{-1}\left(\frac{s_1 \sin a - f}{s_1 \cos a - e}\right) + \left(\frac{u - s_1}{r}\right)\right\} \end{aligned}\right] $$

for the interval $s_1 + s_2 \le u < s_1 + s_2 + s_3$,

$$ \left.\begin{aligned} x_c(u) &= [u - (s_1 + s_2 + s_3)] \sin b + x_c^S \\ y_c(u) &= 0 \\ z_c(u) &= [u - (s_1 + s_2 + s_3)] \cos b + z_c^S \end{aligned}\right] $$

and for the interval $s_1 + s_2 + s_3 \le u \le s_1 + s_2 + s_3 + s_4$,

$$ \left.\begin{aligned} x_c(u) &= x_c^S \\ y_c(u) &= 0 \\ z_c(u) &= [u - (s_1 + s_2 + s_3)] + z_c^S \end{aligned}\right] $$

8. Define the sweep matrix $\left[{}^{1}_{c}M\right]$
(*See examples in Figure 4-2*)

9. Define ${}^{1}\underset{\sim}{p}(u, v)$.

$$ {}^{1}\underset{\sim}{p}(u, v) = {}^{c}\underset{\sim}{p}(u) \cdot \left[{}^{1}_{c}M \right] \qquad (4\text{-}15) $$

4.4 Instances of the Generic Cutter

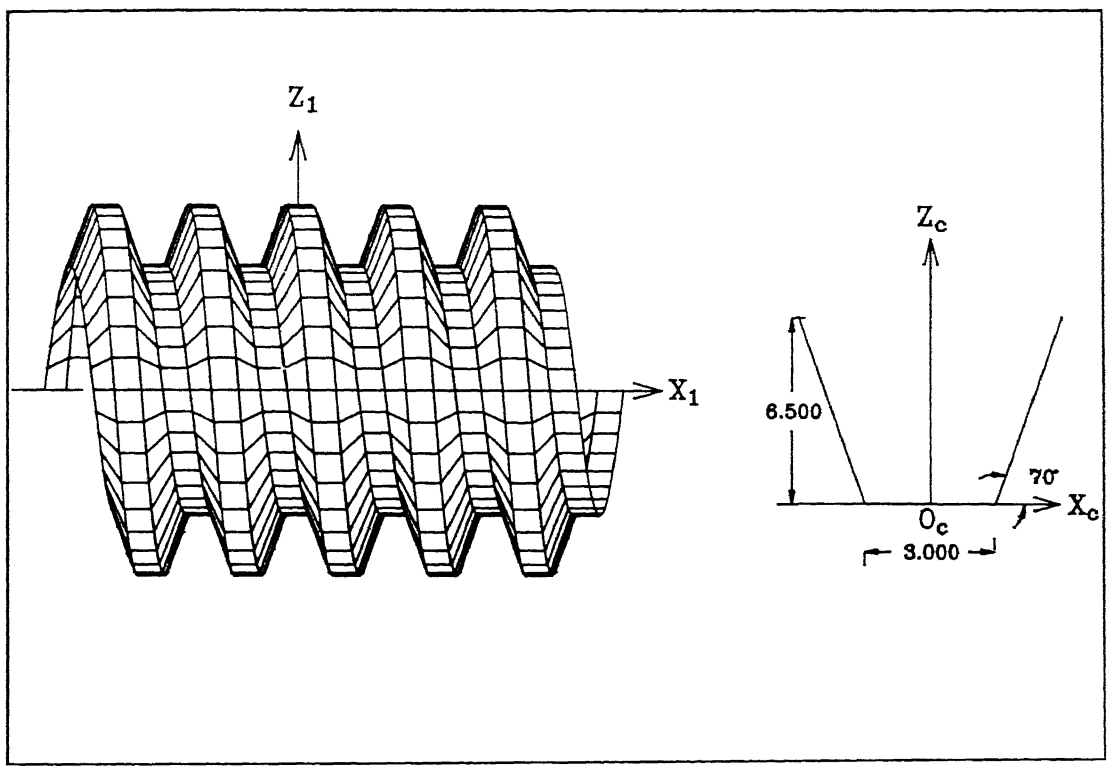

Figure 4.3 Instantiation of a Gear Hob Using the Model of the Generic Cutter

Hobbing is gear manufacturing process for mass production. A typical gear hobbing process has been illustrated in Figure 2-11. In this section, it will be shown how the parametric equation of one such gear hob can be obtained using the model of the generic cutter. It is to be noted that the surface that will be considered in this modeling is a continuous surface as shown in Figure 4-3 and does not represent the flutes. The tooth profile of the hob and the coordinate frames S_c and S_1 are also depicted in Figure 4-3. The tooth profile can be obtained by substituting the values given in the table 4-1 in the definition of the generic cutter.

Is arc tangential	d	r	a	b	h_1	e	f	h
yes	3.000	0.000	0.000	20.000	0.000	(1.500)	(0.000)	6.500

Table 4-1. Input Data to Instantiate a Gear Hob.

Thus the parametric equation of the cross-sectional profile of the hob is:

$$ {}^{c}\underline{p}(u) = \begin{bmatrix} x_c(u) & y_c(u) & z_c(u) & 1 \end{bmatrix} \qquad \textbf{(4-16)} $$

where,

$$ \textit{for the interval } 0 \le u < 1.500, \quad \left.\begin{aligned} x_c(u) &= u \\ y_c(u) &= 0 \\ z_c(u) &= 0 \end{aligned}\right] $$

$$ \textit{and for the interval } 1.500 \le u \le 8.417, \quad \left.\begin{aligned} x_c(u) &= 0.342\,(u - 1.500) + 1.500 \\ y_c(u) &= 0 \\ z_c(u) &= 0.939\,(u - 1.500)\,. \end{aligned}\right] $$

This profile is given a helical sweep to obtain the surface of the hob. The transformation matrix describing this sweep is

$$ \left[{}^{1}_{c}M\right] = \begin{bmatrix} 1 & 0 & 0 & 0 \\ 0 & \cos v & \sin v & 0 \\ 0 & -\sin v & \cos v & 0 \\ \dfrac{l\,v}{2\pi} & q \sin v & -q \cos v & 1 \end{bmatrix} \qquad \textbf{(4-17)} $$

where l is the lead of the hob and q is the distance of the origin O_c from the axis X_1 as shown in Figure 4-2c. Hence, the biparametric surface obtained from Equation (4-15) is

$$ {}^{1}\underset{\sim}{p}(u,\ v) = \left[\ x_1(u,\ v) \quad y_1(u,\ v) \quad z_1(u,\ v) \quad 1\ \right] \tag{4-18} $$

where

$$ x_1(u,\ v) = x_c(u) + \frac{l\,v}{2\pi} $$

$$ y_1(u,\ v) = y_c(u)\cos v - z_c(u)\sin v + q\sin v $$

$$ z_1(u,\ v) = y_c(u)\sin v + z_c(u)\cos v - q\cos v $$

This definition of the cutter surface Σ_1 can be used in the conjugate geometry model of the generic machine tool described in the previous chapter in order to determine the gear profile produced on the blank.

In addition to the example of a gear hob, There are 26 examples shown in Figures 4-4 through 4-29. These are several types of drills, end mills, T-slot cutters, side and face milling cutters, flange cutters, wire of the EDM process, laser beam, etc. Each of these figures consists of three parts. The first part of is the graphic representation of the two dimensional profile of the cutting tool. The second part gives the table of the parameters defining the cutter. This will be the input data for the symbolic algorithm. It may be noted that the values within the parentheses need not be provided as the algorithm will calculate them from the tangency conditions. The third part in these figures is the output from the symbolic algorithm which is the biparametric equation of the cutter surface ${}^{1}\underset{\sim}{p}$ in terms of u and v. In all the examples, the lengths are given in millimeter and angles are given in degrees.

(a) Profile of the Cutter :

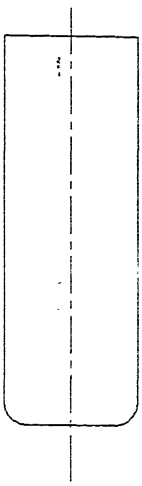

(b) Input Data to the Symbolic Algorithm :

Is arc tangential	d	r	a	b	h_1	e	f	h
yes	25.000	4.000	0.000	0.000	66.000	(8.500)	(4.000)	(4.000)

(c) Output from the Symbolic Model :

Range of u	x_c	y_c	z_c
$0 \le u \le 8.500$	u	0	0
$8.500 \le u \le 14.783$	4 cos [0.250(u-8.500)-1.571] + 8.500	0	4 sin [0.250(u-8.500)-1.571] + 4.000
-	-	-	-
$14.783 \le u \le 80.783$	12.500	0	u - 10.783

Figure 4.4 Instantiation of a 25 dia. 4R Dome End Mill

(a) Profile of the Cutter :

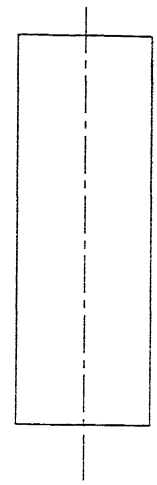

(b) Input Data to the Symbolic Algorithm :

Is arc tangential	d	r	a	b	h_1	e	f	h
yes	25.000	0.000	0.000	0.000	70.000	(12.500)	(0.000)	(0.000)

(c) Output from the Symbolic Model :

Range of u	x_c	y_c	z_c
$0 \le u \le 12.500$	u	0	0
-	-	-	-
-	-	-	-
$12.500 \le u \le 82.500$	12.500	0	u - 12.500

Figure 4.5 Instantiation of a 25 dia. 0R End Mill

(a) Profile of the Cutter :

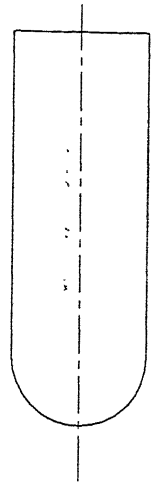

(b) Input Data to the Symbolic Algorithm :

Is arc tangential	d	r	a	b	h_1	e	f	h
yes	25.000	12.500	0.000	0.000	57.500	(0.000)	(12.500)	(12.500)

(c) Output from the Symbolic Model :

Range of u	x_c	y_c	z_c
-	-	-	-
$0.000 \leq u \leq 19.635$	12.500 cos [0.080 u-1.571]	0	12.500 sin [0.080 u-1.571]
-	-	-	-
$19.635 \leq u \leq 77.135$	12.500	0	u - 7.135

Figure 4.6 Instantiation of a 25 dia. Ball Nose End Mill

(a) Profile of the Cutter :

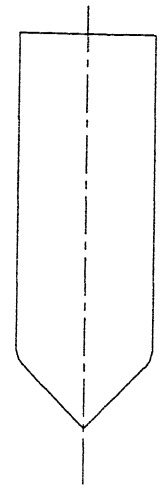

(b) Input Data to the Symbolic Algorithm :

Is arc tangential	d	r	a	b	h_1	e	f	h
yes	25.000	4.000	45.000	0.000	55.843	(8.500)	(14.157)	(5.561)

(c) Output from the Symbolic Model :

Range of u	x_c	y_c	z_c
$0 \le u \le 16.021$	0.707 u	0	0.707 u
$16.021 \le u \le 19.162$	4 cos [0.250 (u-16.021)-0.785] + 0.508	0	4 sin [0.250(u-16.021)-0.785]+14.157
-	-	-	-
$19.162 \le u \le 75.006$	12.500	0	u - 5.006

Figure 4.7 Instantiation of a 25 dia. 90 deg. Tool

(a) Profile of the Cutter :

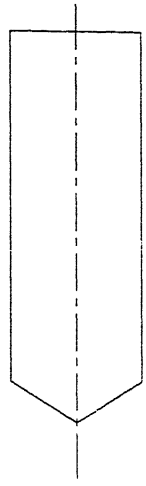

(b) Input Data to the Symbolic Algorithm :

Is arc tangential	d	r	a	b	h_1	e	f	h
yes	25.000	0.000	31.000	0.000	62.489	(12.500)	(2.204)	(7.511)

(c) Output from the Symbolic Model :

Range of u	x_c	y_c	z_c
$0 \le u \le 14.583$	0.857 u	0	0.515 u
-	-	-	-
-	-	-	-
$14.583 \le u \le 77.072$	12.500	0	u - 7.072

Figure 4.8 Instantiation of a 25 dia. Drill

(a) Profile of the Cutter :

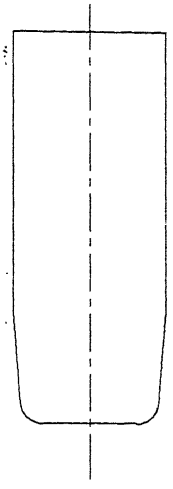

(b) Input Data to the Symbolic Algorithm :

Is arc tangential	d	r	a	b	h_1	e	f	h
yes	25.000	4.000	0.000	5.000	50.000	(8.835)	(4.000)	20.000

(c) Output from the Symbolic Model :

Range of u	x_c	y_c	z_c
$0 \le u \le 8.835$	u	0	0
$8.835 \le u \le 14.769$	4 cos [0.250(u-8.835)-1.571] + 8.835	0	4 sin [0.250(u-8.835)-1.571] + 4.000
$14.769 \le u \le 31.180$	0.087 (u-31.180) + 14.250	0	0.996 (u-31.180) + 20.000
$31.180 \le u \le 81.180$	14.250	0	u - 11.180

Figure 4.9 Instantiation of a 25dia. 4R Side Angle Cutter

(a) Profile of the Cutter :

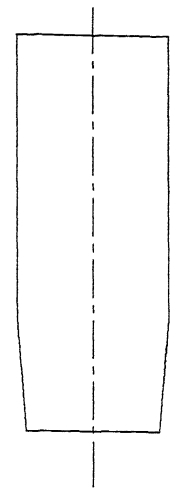

(b) Input Data to the Symbolic Algorithm :

Is arc tangential	d	r	a	b	h_1	e	f	h
yes	25.000	0.000	0.000	5.000	50.000	(12.500)	(0.000)	20.000

(c) Output from the Symbolic Model :

Range of u	x_c	y_c	z_c
0u≤12.500	u	0	0
-	-	-	-
12.500≤u≤32.576	0.087 (u-32.576) + 14.250	0	0.996 (u-32.576) + 20.000
32.576≤u≤82.576	14.250	0	u - 12.576

Figure 4.10 Instantiation of a 25dia. 0R Side Angle Cutter

(a) Profile of the Cutter :

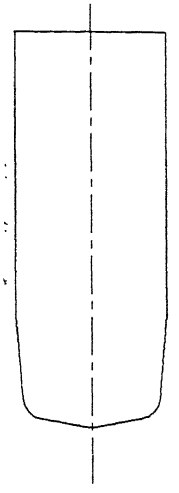

(b) Input Data to the Symbolic Algorithm :

Is arc tangential	d	r	a	b	h_1	e	f	h
yes	25.000	4.000	10.000	5.000	50.000	(8.782)	(5.610)	20.000

(c) Output from the Symbolic Model :

Range of u	x_c	y_c	z_c
$0 \le u \le 9.624$	0.985 u	0	0.174 u
$9.624 \le u \le 14.860$	4 cos [0.250(u-9.624)-1.396] + 8.783	0	4 sin [0.250(u-9.624)-1.396] + 5.610
$14.860 \le u \le 29.654$	0.087 (u-29.654) + 14.057	0	0.996 (u-29.654) + 5.610
$29.654 \le u \le 79.654$	14.057	0	u - 9.654

Figure 4.11 Instantiation of a 25 dia. 4R Side & Bottom Angle Cutter

(a) Profile of the Cutter :

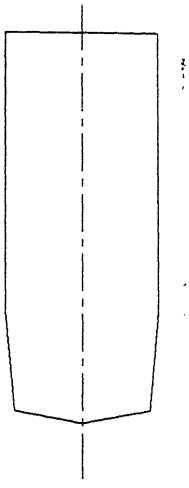

(b) Input Data to the Symbolic Algorithm :

Is arc tangential	d	r	a	b	h_1	e	f	h
yes	25.000	0.000	10.000	5.000	50.000	(12.500)	(2.204)	20.000

(c) Output from the Symbolic Model :

Range of u	x_c	y_c	z_c
$0 \le u \le 12.693$	0.985 u	0	0
-	-	-	-
$12.693 \le u \le 30.557$	0.087 (u-30.557) + 14.057	0	0.996 (u-30.557) + 20.000
$30.557 \le u \le 80.557$	14.057	0	u - 10.557

Figure 4.12 Instantiation of a 25 dia. 0R Side & Bottom Angle Cutter

(a) Profile of the Cutter :

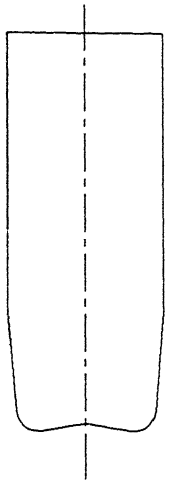

(b) Input Data to the Symbolic Algorithm :

Is arc tangential	d	r	a	b	h_1	e	f	h
yes	25.000	4.000	-10.000	5.000	50.000	(8.896)	(2.493)	20.000

(c) Output from the Symbolic Model :

Range of u	x_c	y_c	z_c
$0 \le u \le 8.328$	0.985 u	0	-0.174 u
$8.328 \le u \le 14.960$	4 cos [0.250 (u-8.328)-1.745] + 8.896	0	4 sin [0.250 (u-8.328)-1.745] + 2.493
$14.960 \le u \le 32.884$	0.087 (u-32.884) + 14.443	0	0.996 (u-32.884) + 20.000
$32.884 \le u \le 82.884$	14.443	0	u - 12.884

Figure 4.13 Instantiation of a 25 dia. 4R Side & Bottom Angle Cutter

(a) Profile of the Cutter :

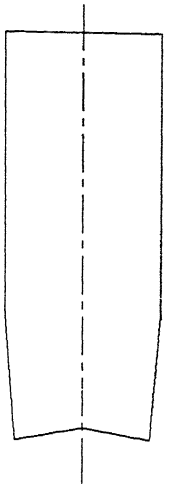

(b) Input Data to the Symbolic Algorithm :

Is arc tangential	d	r	a	b	h_1	e	f	h
yes	25.000	0.000	-10.000	5.000	50.000	(12.500)	(-2.204)	20.000

(c) Output from the Symbolic Model :

Range of u	x_c	y_c	z_c
$0 \le u \le 12.693$	0.985 u	0	-0.174 u
-	-	-	-
$12.693 \le u \le 34.982$	0.087 (u-34.982) + 14.443	0	0.996 (u-34.982) + 20.000
$34.982 \le u \le 84.982$	14.443	0	u - 14.982

Figure 4.14 Instantiation of a 25 dia. 0R Side & Bottom Angle Cutter

(a) Profile of the Cutter :

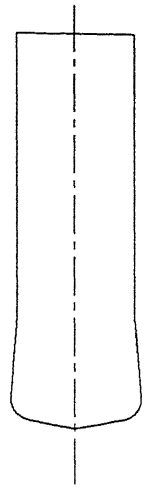

(b) Input Data to the Symbolic Algorithm :

Is arc tangential	d	r	a	b	h_1	e	f	h
yes	25.000	4.000	10.000	-5.000	50.000	(8.196)	(5.507)	20.000

(c) Output from the Symbolic Model :

Range of u	x_c	y_c	z_c
$0 \le u \le 9.028$	0.985 u	0	0.174 u
$9.028 \le u \le 14.962$	4 cos [0.250 (u-9.028)-1.396] + 8.196	0	4 sin [0.250 (u-9.028)-1.396] + 5.507
$14.962 \le u \le 29.160$	-0.087 (u-29.160) + 10.943	0	0.996 (u-29.160) + 20.000
$29.160 \le u \le 79.160$	10.943	0	u - 9.160

Figure 4.15 Instantiation of a 25 dia. 4R Side & Bottom Angle Cutter

(a) Profile of the Cutter :

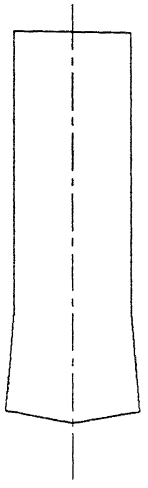

(b) Input Data to the Symbolic Algorithm :

Is arc tangential	d	r	a	b	h_1	e	f	h
yes	25.000	0.000	10.000	-5.000	50.000	(12.500)	(2.204)	20.000

(c) Output from the Symbolic Model :

Range of u	x_c	y_c	z_c
$0 \le u \le 12.693$	0.985 u	0	0.174 u
-	-	-	-
$12.693 \le u \le 30.557$	-0.087 (u-30.557) + 10.943	0	0.996 (u-30.557) + 20.000
$30.557 \le u \le 80.557$	10.943	0	u - 10.557

Figure 4.16 Instantiation of a 25 dia. 0R Side & Bottom Angle Cutter

(a) Profile of the Cutter :

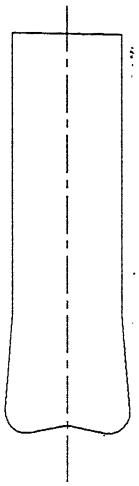

(b) Input Data to the Symbolic Algorithm :

Is arc tangential	d	r	a	b	h_1	e	f	h
yes	25.000	4.000	-10.000	-5.000	50.000	(8.061)	(2.640)	20.000

(c) Output from the Symbolic Model :

Range of u	x_c	y_c	z_c
$0 \le u \le 7.480$	0.985 u	0	-0.174 u
$7.480 \le u \le 14.810$	4 cos [0.250 (u-7.480)-1.745] + 8.061	0	4 sin [0.250 (u-7.480)-1.745] + 2.640
$14.810 \le u \le 31.886$	-0.087 (u-31.886) + 10.557	0	0.996 (u-31.886) + 20.000
$31.886 \le u \le 81.886$	10.557	0	u - 11.886

Figure 4.17 Instantiation of a 25 dia. 4R Side & Bottom Angle Cutter

(a) Profile of the Cutter :

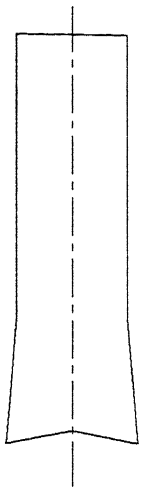

(b) Input Data to the Symbolic Algorithm :

Is arc tangential	d	r	a	b	h_1	e	f	h
yes	25.000	0.000	-10.000	-5.000	50.000	(12.500)	(-2.204)	20.000

(c) Output from the Symbolic Model :

Range of u	x_c	y_c	z_c
$0 \le u \le 12.693$	0.985 u	0	-0.174 u
-	-	-	-
$12.693 \le u \le 34.982$	-0.087 (u-34.982) + 10.557	0	0.996 (u-34.982) + 20.000
$34.982 \le u \le 84.982$	10.557	0	u - 14.982

Figure 4.18 Instantiation of a 25 dia. 0R Side & Bottom Angle Cutter

(a) Profile of the Cutter :

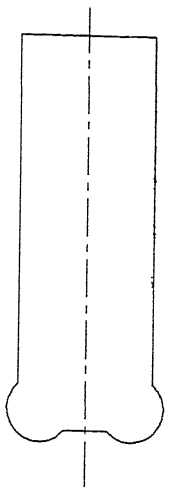

(b) Input Data to the Symbolic Algorithm :

Is arc tangential	d	r	a	b	h_1	e	f	h
no	25.000	6.000	0.000	0.000	61.528	8.500	4.000	(8.472)

(c) Output from the Symbolic Model :

Range of u	x_c	y_c	z_c
$0 \le u \le 4.028$	u	0	0
$4.028 \le u \le 23.545$	6 cos [0.167 (u-4.028)-2.412] + 8.500	0	6 sin [0.250 (u-4.028)-2.412] + 4.000
-	-	-	-
$23.545 \le u \le 85.073$	12.500	0	u - 15.073

Figure 4.19 Instantiation of a 25 dia. 6R Non-Fillet Type End Mill

(a) Profile of the Cutter :

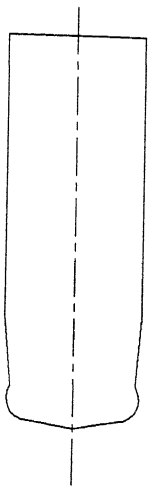

(b) Input Data to the Symbolic Algorithm :

Is arc tangential	d	r	a	b	h_1	e	f	h
no	25.000	4.000	10.000	5.000	50.000	8.100	5.400	20.000

(c) Output from the Symbolic Model :

Range of u	x_c	y_c	z_c
$0 \le u \le 8.077$	0.985 u	0	0.174 u
$8.077 \le u \le 16.876$	4 cos [0.250 (u-8.077)-1.607] + 8.100	0	4 sin [0.250 (u-8.077)-1.607] + 5.400
$16.876 \le u \le 29.289$	0.087 (u-29.289) + 12.500	0	0.996 (u-29.289) + 20.000
$29.289 \le u \le 79.289$	12.500	0	u-9.289

Figure 4.20 Instantiation of a 25dia. 4R Non-Fillet Type Side & Bottom Angle Cutter

(a) Profile of the Cutter :

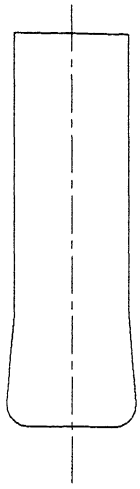

(b) Input Data to the Symbolic Algorithm :

Is arc tangential	d	r	a	b	h_1	e	f	h
yes	25.000	4.000	0.000	-5.000	50.000	(8.135)	(4.000)	20.000

(c) Output from the Symbolic Model :

Range of u	x_c	y_c	z_c
$0 \le u \le 8.135$	u	0	0
$8.135 \le u \le 14.767$	4 cos [0.250 (u-8.135)-1.571] + 8.135	0	4 sin [0.250 (u-8.135)-1.571] + 4.000
$14.767 \le u \le 30.478$	-0.087 (u-30.478) + 10.750	0	0.996 (u-30.478) + 20.000
$30.478 \le u \le 80.478$	10.750	0	u-10.478

Figure 4.21 Instantiation of a 25 dia. 4R Pick-feed Cutter

(a) Profile of the Cutter :

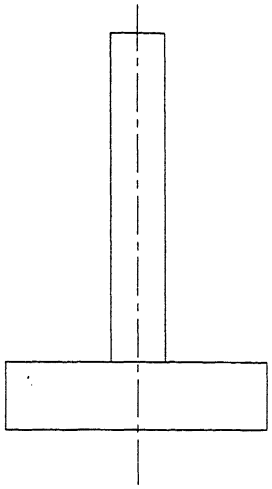

(b) Input Data to the Symbolic Algorithm :

Is arc tangential	d	r	a	b	h_1	e	f	h
no	∞	∞	0.000	-90.000	50.000	$\frac{-\infty}{+12.500}$	6.000	12.000

(c) Output from the Symbolic Model :

Range of u	x_c	y_c	z_c
0≤u≤12.500	u	0	0
12.500≤u≤24.500	12.500	0	u-12.500
24.500≤u≤32.000	-(u-24.500) + 12.500	0	12.000
32.000≤u≤82.000	5.000	0	u-20.000

Figure 4.23 Instantiation of a 25 dia. 0R Woodruff Cutter

(a) Profile of the Cutter :

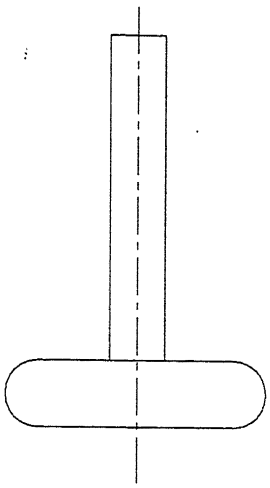

(b) Input Data to the Symbolic Algorithm :

Is arc tangential	d	r	a	b	h_1	e	f	h
no	∞	6.000	0.000	-90.000	58.000	19.000	6.000	12.000

(c) Output from the Symbolic Model :

Range of u	x_c	y_c	z_c
0≤u≤19.000	u	0	0
19.000≤u≤37.857	6 cos [0.167 (u-19.000)+1.571] + 19.000	0	6 sin [0.167 (u-19.000)+1.571] + 6.000
37.857≤u≤51.857	-(u-37.857) + 19.000	0	12.000
51.857≤u≤109.857	5.000	0	u-39.857

Figure 4.24 Instantiation of a 25 dia. 6R Woodruff Cutter

(a) Profile of the Cutter :

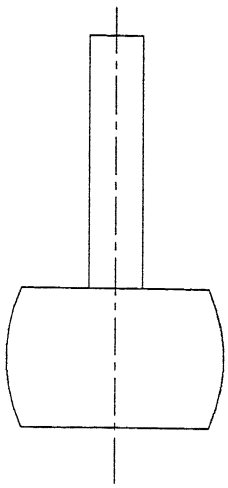

(b) Input Data to the Symbolic Algorithm :

Is arc tangential	d	r	a	b	h_1	e	f	h
no	∞	30.000	0.000	-90.000	45.000	-10.000	12.500	25.000

(c) Output from the Symbolic Model :

Range of u	x_c	y_c	z_c
0≤u≤17.272	u	0	0
17.272≤u≤43.058	30 cos [0.033 (u-17.272)-0.429] - 10.000	0	30 sin [0.033 (u-17.272)-0.429] + 12.500
43.058≤u≤55.330	-(u-55.330) + 5.000	0	25.000
55.330≤u≤100.330	5.000	0	u-30.330

Figure 4.25 Instantiation of a 25 dia. Flange Milling Cutter for Pick-feed Machining

(a) Profile of the Cutter :

(b) Input Data to the Symbolic Algorithm :

Is arc tangential	d	r	a	b	h_1	e	f	h
yes	1.000	0.000	0.000	0.000	70.000	(0.500)	(0.000)	(0.000)

(c) Output from the Symbolic Model :

Range of u	x_c	y_c	z_c
-	-	-	-
-	-	-	-
-	-	-	-
$0.500 \leq u \leq 70.500$	0.500	0	u-0.500

Figure 4.26 Instantiation of a Wire of an EDM Process

(a) Profile of the Cutter :

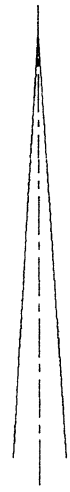

(b) Input Data to the Symbolic Algorithm :

Is arc tangential	d	r	a	b	h_1	e	f	h
yes	0.500	0.000	0.000	-0.050	0.000	(0.250)	(0.000)	70.000

(c) Output from the Symbolic Model :

Range of u	x_c	y_c	z_c
-	-	-	-
-	-	-	-
0.250 ≤u≤70.250	8.727e-04 (u-70.250) + 0.189	0	0.999 (u-70.250) + 70.000
-	-	-	-

Figure 4.27 Instantiation of a Beam in a Laser Cutting Process

(a) Profile of the Cutter :

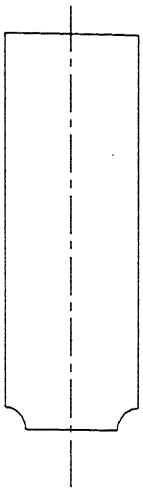

(b) Input Data to the Symbolic Algorithm :

Is arc tangential	d	r	a	b	h_1	e	f	h
no	25.000	-4.000	0.000	0.000	66.000	12.5000	0.000	(4.000)

(c) Output from the Symbolic Model :

Range of u	x_c	y_c	z_c
$0 \le u \le 8.500$	u	0	0
$8.500 \le u \le 14.783$	4 cos [-0.250 (u-8.500) + 1.571] + 12.500	0	4 sin [-0.250 (u-8.500) + 1.571]
-	-	-	-
$14.783 \le u \le 80.783$	12.500	0	u-10.783

Figure 4.28 Instantiation of a 25 dia. 4R Concave Cutter

(a) Profile of the Cutter :

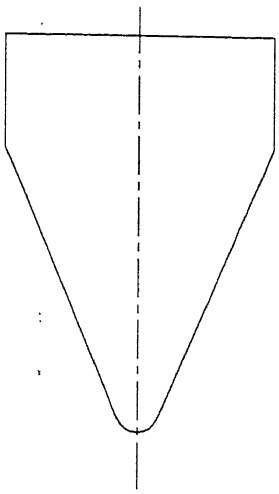

(b) Input Data to the Symbolic Algorithm :

Is arc tangential	d	r	a	b	h_1	e	f	h
yes	5.181	4.000	0.000	24.141	20.000	(0.000)	(4.000)	50.000

(c) Output from the Symbolic Model :

Range of u	x_c	y_c	z_c
-	-	-	-
$0.000 \leq u \leq 4.608$	4 cos [0.025 u-1.571]	0	4 sin [0.025 u-1.571]
$4.608 \leq u \leq 56.809$	-0.837 (u-56.809) + 25.000	0	0.548 (u-56.809) + 50.000
$56.809 \leq u \leq 76.809$	25.000	0	u-6.809

Figure 4.29 Instantiation of a Conical Cutter Used in 5 axis Machining

Chapter 5

ILLUSTRATIVE EXAMPLES

5.1 Introduction

The conjugate geometry model described in Chapter 2 along with the model of a generic cutter explained in Chapter 4 can be effectively used for modeling a variety of manufacturing processes. A manufacturing engineer generally has a set of machine tools and a collection of cutting tools and he will be required to produce the given surface within the tolerance specifications at the minimum cost by appropriately choosing a machine tool and a cutting tool. These models will aid him in evaluating the various alternatives available to him without performing the actual cutting. In this chapter, the use of these models has been demonstrated by means of several examples in design and manufacture.

5.2 Modeling of Gear Manufacturing Processes

Gear is one of the most common machine elements. They are manufactured using forming processes such as casting and blanking. They are also produced by a variety of machining processes such as milling, shaping, planing, hobbing, wire EDM etc. The selection of the manufacturing process depends on the size and the shape of the gear, the quantity required and the accuracy dictated by the application.

The teeth of a gear can be cut either by a *direct process* or by a *generating process*. In a direct process, cutting is performed with form-cutters which must have the form of the space between the teeth. Figure 5-1a shows the milling of a gear using a disk-type gear milling cutter and the milling of gear with a *Diametral Pitch cutter* is shown in Figure 5-1b. These two processes are direct processes. In the direct process, the size and the shape of the space between the teeth of a gear is different for different number of teeth even for the same pitch. Since it is uneconomical to have a separate cutter for

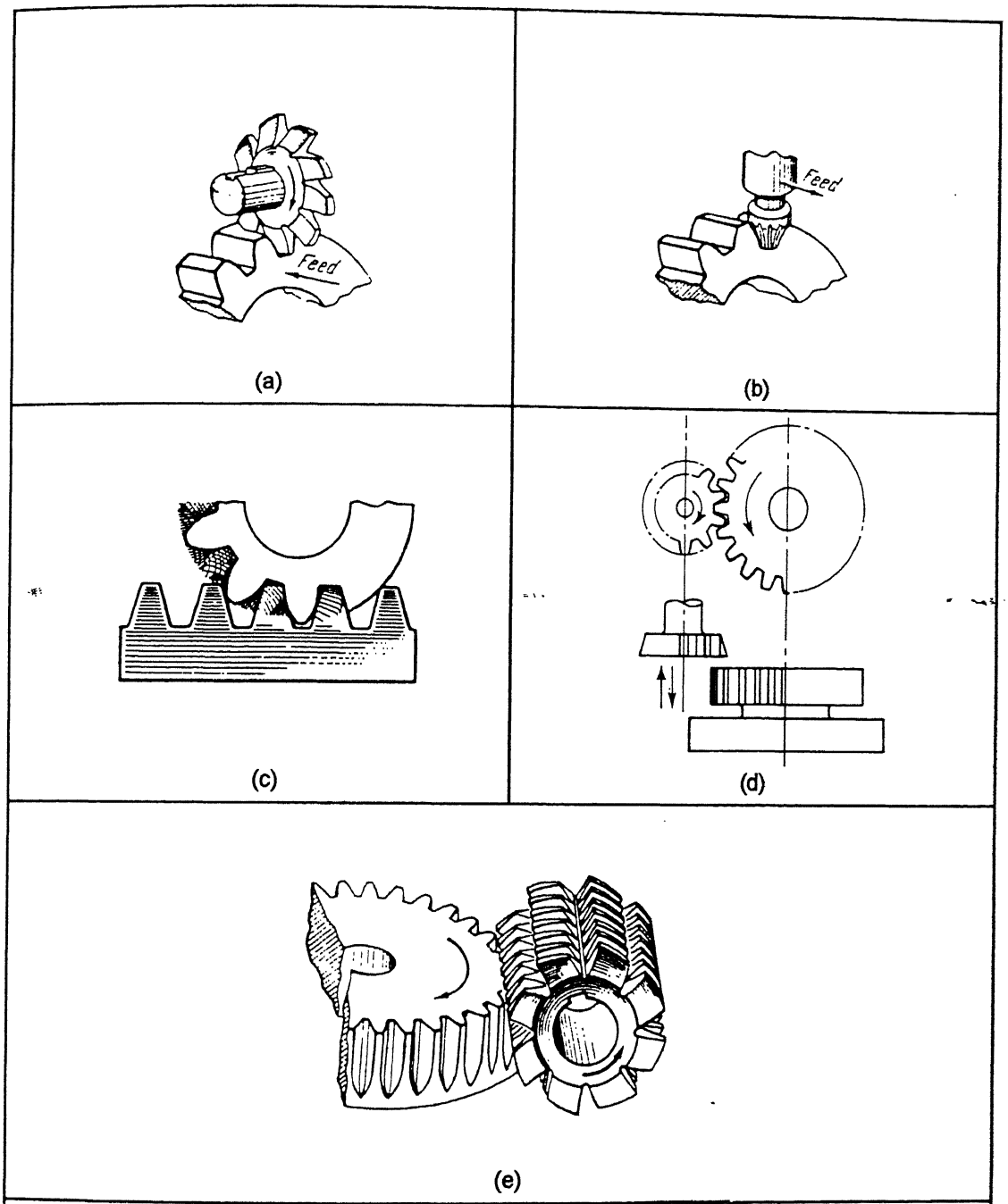

Figure 5-1. Processes of Gear Machining.
(a) Gear Milling Using a Disc Type Shape-Cutter,
(b) Gear Milling Using an End Mill Type Shape-Cutter,
(c) Gear Planing/ Shaping Using a Rack Type Cutter,
(d) Gear Shaping Using a Pinion Type Cutter and
(e) Gear Hobbing.

each combination of module and number of teeth, generally a set of cutters is used with each cutter catering to a range of module regardless of the number of teeth. Hence, the profile of the gear produced by such a cutter will be exact only for a particular value of the module and number of teeth and for all other values it will be approximate. Moreover, the direct method is very slow due to indexed motion.

The generating processes use screw-type cutters with profiles identical to the basic rack corresponding to the pitch and module of the gear. This process is more accurate as it generates the correct involute profile regardless of the number of teeth. Furthermore, the cutting in most of the generating processes is continuous and hence more productive. Gear planing with a rack cutter, gear shaping and gear hobbing are some of the gear generating processes used for the mass production of gears. In this section, two gear generating processes, viz., gear planing with a rack cutter and gear hobbing will be illustrated using the proposed conjugate geometry model.

5.2.1 Modeling of a Gear Planing Process with a Rack Cutter

Planing by means of rack type cutters is one of the oldest methods of gear production that is still extensively used for large gears. This is a true generating process since it utilizes the principle that an involute curve can be formed by a straight line generator when a circle is made to roll without slip relative to the generator. It is, perhaps, the simplest practical method of demonstrating the application of the basic rack to gear tooth generation.

In this process of planing a spur gear, the blank is made to rotate about its axis at a suitable speed and the cutter is moved longitudinally at the same linear speed as the blank. The teeth of the rack are straight and are relieved to form the cutting edges. The cutting action is obtained by reciprocating the cutter parallel to the axis of the gear blank. During the working stroke the rotation of the blank and the longitudinal translation of the cutter proceed continuously while on the return stroke the cutter is moved out of contact with the work to prevent rubbing. After a tangential advance of the cutter for a distance slightly exceeding one pitch, rotation of the blank is stopped, the cutter moves back the amount it has advanced and the process is repeated until the blank has completed one revolution. The gear is formed by sinking the cutter deeper into the blank until the required depth and tooth thickness are obtained.

The first step in modeling this gear planing process is to obtain the biparametric equation of the trapezoidal profile of the rack tooth shown in Figure 5-2. This equation can be obtained using the generic cutter definition for the values given in Table 5-1.

(a)

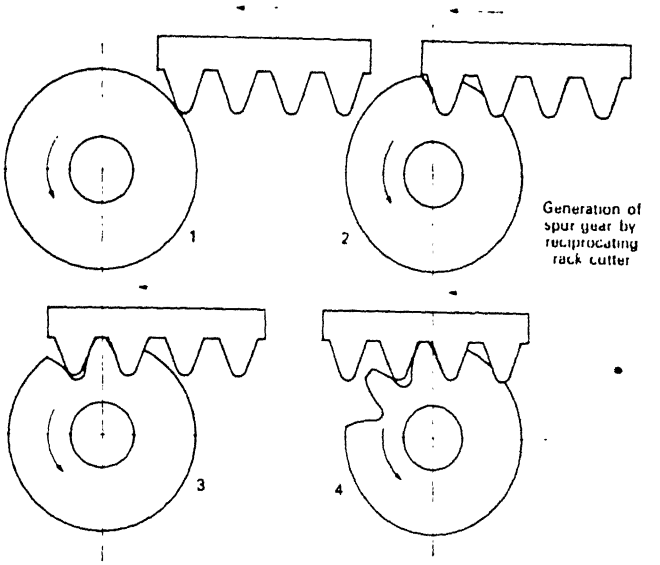

(b)

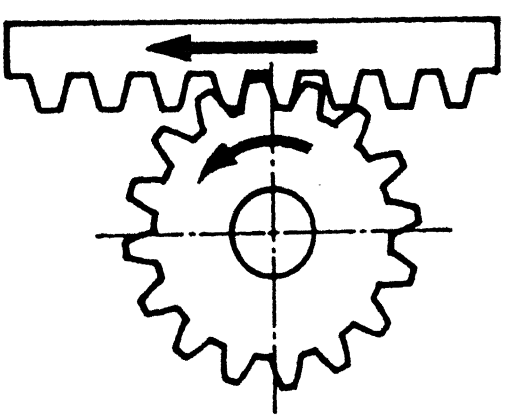

Figure 5-2. Modeling of a Gear Planing Process with a Rack Cutter.
(a) Generation of a Spur Gear and
(b) Schematic Diagram of the Gear Planing Process.

Is arc tangential	d	r	a	b	h_1	e	f	h
yes	3.000	0.000	0.000	20.000	0.000	(1.500)	(0.000)	6.500

Table 5-1. Input Data to Instantiate a Rack Cutter

Since the coordinate frames S_c and S_1 in the definition of the cutter are apart by a distance $h/2$ along Y direction, the matrix $\left[{}_c^1M\right]$ for this case will be

$$\left[{}_c^1M\right] = \begin{bmatrix} 1 & 0 & 0 & 0 \\ 0 & 0 & 1 & 0 \\ 0 & -1 & 0 & 0 \\ 0 & -\frac{h}{2} & 0 & 1 \end{bmatrix} \tag{5-1}$$

Therefore, the biparametric definition of the rack cutter will be

$$\underset{\sim}{{}^1p} = \begin{bmatrix} x_1 & y_1 & z_1 & 1 \end{bmatrix} \tag{5-2}$$

where

$$\text{for the interval } -\frac{w}{2} - \frac{h}{\cos\alpha} \le u \le -\frac{w}{2}$$

$$x_1 = -\frac{w}{2} + \left(u + \frac{w}{2}\right)\sin\alpha$$

$$y_1 = -\left(u + \frac{w}{2}\right)\cos\alpha - \frac{h}{2}$$

$$z_1 = v$$

$$\text{for the interval } -\frac{w}{2} \le u \le \frac{w}{2}$$

$$x_1 = u$$

$$y_1 = -\frac{h}{2}$$

$$z_1 = v$$

$$\text{and for the interval } \frac{w}{2} \le u \le \frac{w}{2} + \frac{h}{\cos\alpha}$$

$$x_1 = \frac{w}{2} + \left(u - \frac{w}{2}\right)\sin\alpha$$

$$y_1 = \left(u - \frac{w}{2}\right)\cos\alpha - \frac{h}{2}$$

$$z_1 = v$$

The axis of the gear blank is the Z_2 axis which coincides with the Z_0 axis of the global frame of reference. The blank rotates about its axis with a constant angular velocity of ω. The pitch line of the rack cutter is the X_1 axis and it is at a distance of r from the X_0 axis. The rack translates with a velocity of $-r\omega$ along the X_1 axis. After cutting a tooth in this forward stroke, it lifts to disengage from the blank and retracts exactly the same distance. The twelve parameters describing the relative motion between the gear blank and the rack cutter in the forward stroke are given in Table 5-2.

Cutter	Blank
$a_1 = -r\,\omega\,t$	$a_2 = 0$
$b_1 = r$	$b_2 = 0$
$c_1 = 0$	$c_2 = 0$
$\theta_1 = 0$	$\theta_2 = 0$

$\phi_1 = 0$	$\phi_2 = 0$
$\psi_1 = 0$	$\psi_2 = \omega t$

Table 5-2. Parameters Describing the Relative Motion in a Gear Planing Process

The tables 5-1 and 5-2 fully describe the surface of the cutter Σ_1 and the parameters of motion. These two inputs are used by the symbolic algorithm to determine the surface Σ_2 which is the surface of the gear produced in this process. The surface of a gear tooth is output as algebraic equations which are given below. There will be three equations corresponding to the three segments of the rack tooth, viz., the left flank, the tip flank and the right flank.

$$^2\underset{\sim}{p} = \begin{bmatrix} x_2 & y_2 & z_2 & 1 \end{bmatrix} \tag{5-3}$$

where

due to the left flank of the tooth

$$x_2 = \left[-\frac{w}{2} + \left(u + \frac{w}{2}\right)\sin\alpha - r\omega t\right]\cos\omega t + \left[-\left(u + \frac{w}{2}\right)\cos\alpha + \left(r - \frac{h}{2}\right)\right]\sin\omega t$$

$$y_2 = -\left[-\frac{w}{2} + \left(u + \frac{w}{2}\right)\sin\alpha - r\omega t\right]\sin\omega t + \left[-\left(u + \frac{w}{2}\right)\cos\alpha + \left(r - \frac{h}{2}\right)\right]\cos\omega t$$

$$z_2 = v$$

and $$u = -\frac{w}{2} + \left(\frac{w}{2} + r\omega t\right)\sin\alpha - \frac{h}{2}\cos\alpha$$

due to the tip flank of the tooth

$$x_2 = \left(r - \frac{h}{2}\right)\sin\omega t$$

$$y_2 = \left(r - \frac{h}{2}\right)\cos\omega t$$

$$z_2 = v$$

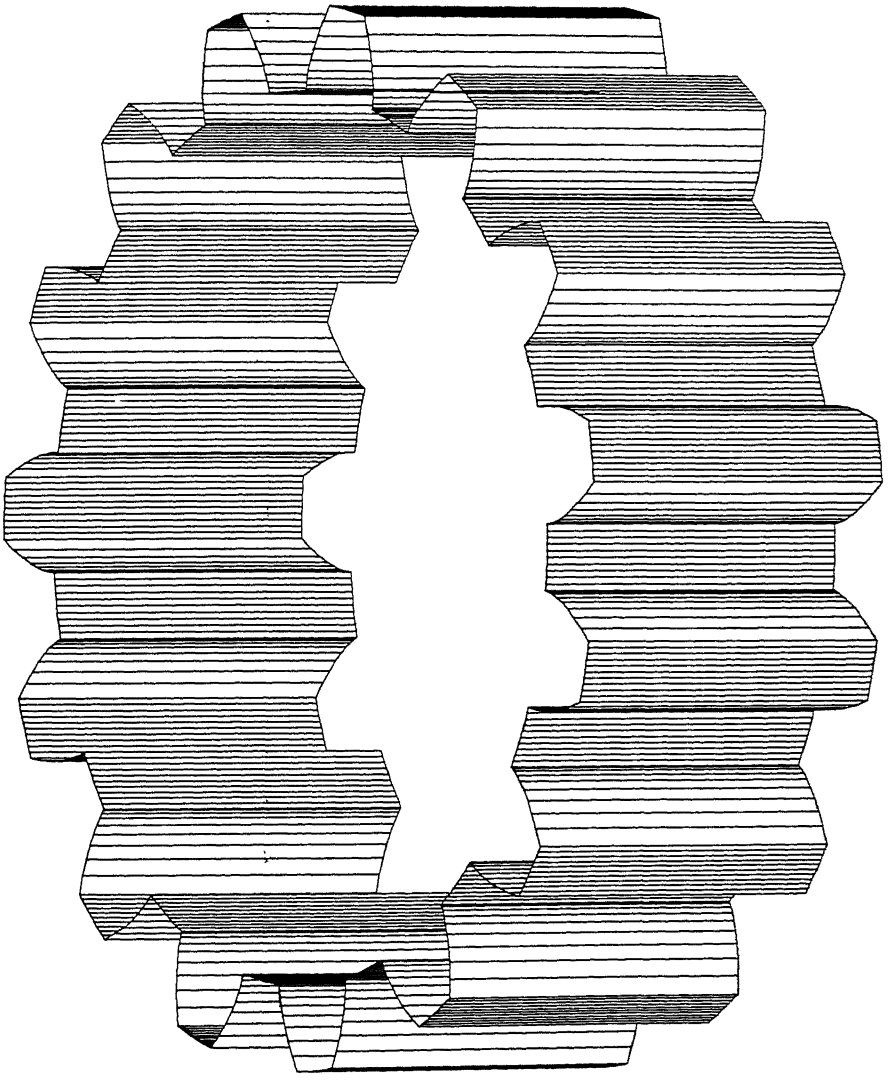

Figure 5-3. Surface of the Gear Obtained in a Gear Planing Process with Rack Cutter.

due to the right flank of the tooth

$$x_2 = \left[\frac{w}{2} + \left(u - \frac{w}{2}\right)\sin\alpha - r\omega t\right]\cos\omega t + \left[\left(u - \frac{w}{2}\right)\cos\alpha + \left(r - \frac{h}{2}\right)\right]\sin\omega t$$

$$y_2 = -\left[\frac{w}{2} + \left(u - \frac{w}{2}\right)\sin\alpha - r\omega t\right]\sin\omega t + \left[\left(u - \frac{w}{2}\right)\cos\alpha + \left(r - \frac{h}{2}\right)\right]\cos\omega t$$

$$z_2 = v$$

and $$u = \frac{w}{2} + \left(-\frac{w}{2} + r\omega t\right)\sin\alpha + \frac{h}{2}\cos\alpha$$

The gear surface described by these equations is plotted for $w = 3$, $h = 6.5$, $r = 25$, $\alpha = 20°$. It is shown in Figure 5-3.

5.2.2 Modeling of a Gear hobbing Process

Hobbing is regarded as the most accurate as well as the most productive process of gear machining. It is a generating process in which the hob teeth trace out the involute curves.

A typical gear hob and the schematic diagram of the gear hobbing process are shown in Figure 5-4a and 5-4b. The hob has basically the same shape as a screw with one or more threads and each thread is cut by a number of gashes to form the cutting edges. Both the gear blank and the hob rotate about their axes, the blank slowly and the hob faster. Since the hob has the shape of a screw, its threads appear to move in the direction of its axis so that they simulate the movement of a rack cutter. In addition, since the hob is rotating, the cutting faces move continuously in the tangential direction and this movement provides the cutting velocity. In order to cut each tooth across the entire face width of the gear, the hob is fed slowly in the direction parallel to the axis of the blank. The distance between the axes of the blank and the hob is set to get the required tooth depth on the blank.

In order that the cutter faces should meet the gear blank at the same angle as a rack, the hob is tipped over by a small angle as shown in Figure 5-4b. This angle is known as the swivel angle. The swivel angle is adjusted so that it is equal to the lead angle σ of the hob. The tangential velocities of the hob and the blank at the pitch diameter are same for spur gears. The helical gear is obtained by superimposing a compensatory motion to this basic motion by means of a differential gear arrangement.

Is arc tangential	d	r	a	b	h_1	e	f	h
yes	3.000	0.000	0.000	20.000	0.000	(1.500)	(0.000)	6.500

Table 5-3. Input Data to Instantiate a Gear Hob

The modeling of the gear hob using the generic cutter is illustrated in Chapter 4. The tooth profile of the hob can be obtained by substituting the values given in Table 5-3. The tooth profile of the hob tooth is given in the X_c - Z_c plane. The surface of the hob is obtained by performing a sweep operation which consists of the following three transformations :

a) a shift along Z_1 axis by a distance of $-d_1/2$ where d_1 is the diameter of the hob,
b) a twist about Z_1 axis by an angle of $-\sigma$ where σ is the lead angle of the hob
and c) a helical sweep about X_1 axis described by pitch p and the parameter v.

Therefore, the sweep matrix $\left[{}^{1}_{c}M\right]$ for this case will be

$$\left[{}^{1}_{c}M\right] = \begin{bmatrix} 1 & 0 & 0 & 0 \\ 0 & 1 & 0 & 0 \\ 0 & 0 & 1 & 0 \\ 0 & 0 & -\frac{d_1}{2} & 1 \end{bmatrix} \begin{bmatrix} \cos\sigma & -\sin\sigma & 0 & 0 \\ \sin\sigma & \cos\sigma & 0 & 0 \\ 0 & 0 & 1 & 0 \\ 0 & 0 & 0 & 1 \end{bmatrix} \begin{bmatrix} 1 & 0 & 0 & 0 \\ 0 & \cos v & \sin v & 0 \\ 0 & -\sin v & \cos v & 0 \\ \frac{l v}{2\pi} & 0 & 0 & 1 \end{bmatrix}$$

$$\left[{}^{1}_{c}M\right] = \begin{bmatrix} \cos\sigma & -\sin\sigma\cos v & -\sin\sigma\sin v & 0 \\ \sin\sigma & \cos\sigma\cos v & \cos\sigma\sin v & 0 \\ 0 & -\sin v & \cos v & 0 \\ \frac{l v}{2\pi} & \frac{d_1}{2}\sin v & -\frac{d_1}{2}\cos v & 1 \end{bmatrix} \quad \textbf{(5-4)}$$

Hence, the biparametric surface of the hob obtained from the definition of generic cutter is

$$ {}^{1}\underset{\sim}{p} = \begin{bmatrix} x_1 & y_1 & z_1 & 1 \end{bmatrix} \tag{5-5} $$

where

for the interval $-\frac{w}{2} - \frac{h}{\cos\alpha} \le u \le -\frac{w}{2}$

$$ x_1 = \left[-\frac{w}{2} + \left(u + \frac{w}{2} \right) \sin\alpha \right] \cos\sigma + \frac{l v}{2\pi} $$

$$ y_1 = -\left[-\frac{w}{2} + \left(u + \frac{w}{2} \right) \sin\alpha \right] \sin\sigma \cos v + \left[d_1 + \left(u + \frac{w}{2} \right) \cos\alpha \right] \sin v $$

$$ z_1 = -\left[-\frac{w}{2} + \left(u + \frac{w}{2} \right) \sin\alpha \right] \sin\sigma \sin v - \left[d_1 + \left(u + \frac{w}{2} \right) \cos\alpha \right] \cos v $$

for the interval $-\frac{w}{2} \le u \le \frac{w}{2}$

$$ x_1 = u \cos\sigma + \frac{l v}{2\pi} $$

$$ y_1 = -u \sin\sigma \cos v + d_1 \sin v $$

$$ z_1 = -u \sin\sigma \sin v - d_1 \cos v $$

for the interval $\frac{w}{2} \le u \le \frac{w}{2} + \frac{h}{\cos\alpha}$

$$ x_1 = \left[\frac{w}{2} + \left(u - \frac{w}{2} \right) \sin\alpha \right] \cos\sigma + \frac{l v}{2\pi} $$

$$ y_1 = -\left[\frac{w}{2} + \left(u - \frac{w}{2} \right) \sin\alpha \right] \sin\sigma \cos v + \left[d_1 - \left(u - \frac{w}{2} \right) \cos\alpha \right] \sin v $$

$$ z_1 = -\left[\frac{w}{2} + \left(u - \frac{w}{2} \right) \sin\alpha \right] \sin\sigma \sin v - \left[d_1 - \left(u - \frac{w}{2} \right) \cos\alpha \right] \cos v $$

The axis of the gear blank is the Z_2 axis which coincides with the Z_0 axis of the global frame of reference. The blank rotates about its axis with a constant angular velocity of ω. Initially, the plane X_2 - Y_2 coincides with the X_0 - Y_0 plane and as the blank rotates, it rises with a linear velocity of f. The axis of the hob is the X_1 axis and it is at a distance of $(d_1 + d_2 - 2h)/2$ where d_1 is the outer diameter of the hob, d_2 is the outer diameter of the blank and h is the tooth depth of the gear. The hob is tilted about Y_1 axis by a

constant angle of σ. The only movement that the hob has is the rotation about its own axis with an angular velocity of $n\omega$ where n is the number of teeth that will be cut using a single-start hob. The twelve parameters describing the relative motion between the gear blank and the hob for machining a spur gear are given in Table 5-2.

Cutter	Blank
$a_1 = 0$	$a_2 = 0$
$b_1 = \left(\frac{d_1 + d_2}{2} - h \right)$	$b_2 = 0$
$c_1 = s$	$c_2 = ft$
$\theta_1 = n\omega t$	$\theta_2 = 0$
$\phi_1 = \sigma$	$\phi_2 = 0$
$\psi_1 = 0$	$\psi_2 = \omega t$

Table 5-4. Parameters Describing Relative Motion of Gear Hobbing Process

The symbolic algorithm uses these data describing the hob surface and the relative motion to determine the surface of the gear generated. The equations describing this gear surface are given below :

$$^2\underset{\sim}{p} = \begin{bmatrix} x_2 & y_2 & z_2 & 1 \end{bmatrix} \qquad \textbf{(5-6)}$$

where

Due to the left flank of the tooth,

$$x_2 = \left\{ \begin{array}{l} \left[-\frac{w}{2} + \left(u + \frac{w}{2} \right) \sin\alpha \right] \cos^2\sigma \left[1 + \sin(n\omega t + v) \right] \\ -\left[\frac{d_1}{2} + \left(u + \frac{w}{2} \right) \cos\alpha \right] \sin\sigma \cos(n\omega t + v) \\ + \frac{lv}{2\pi} \cos\sigma \end{array} \right\} \cos\omega t$$

$$+ \left\{ \begin{array}{l} -\left[-\frac{w}{2} + \left(u + \frac{w}{2} \right) \sin\alpha \right] \sin\sigma \cos(n\omega t + v) \\ + \left[\frac{d_1}{2} + \left(u + \frac{w}{2} \right) \cos\alpha \right] \sin(n\omega t + v) \\ + \left[\frac{d_1 + d_2}{2} - h \right] \end{array} \right\} \sin\omega t$$

$$y_2 = -\left\{ \begin{array}{l} \left[-\frac{w}{2} + \left(u + \frac{w}{2} \right) \sin\alpha \right] \cos^2\sigma \left[1 + \sin(n\omega t + v) \right] \\ -\left[\frac{d_1}{2} + \left(u + \frac{w}{2} \right) \cos\alpha \right] \sin\sigma \cos(n\omega t + v) \\ + \frac{lv}{2\pi} \cos\sigma \end{array} \right\} \sin\omega t$$

$$+ \left\{ \begin{array}{l} -\left[-\frac{w}{2} + \left(u + \frac{w}{2} \right) \sin\alpha \right] \sin\sigma \cos(n\omega t + v) \\ + \left[\frac{d_1}{2} + \left(u + \frac{w}{2} \right) \cos\alpha \right] \sin(n\omega t + v) \\ + \left[\frac{d_1 + d_2}{2} - h \right] \end{array} \right\} \cos\omega t$$

$$z_2 = \left\{ \begin{array}{l} -\left[-\frac{w}{2} + \left(u + \frac{w}{2} \right) \sin\alpha \right] \sin\sigma \cos\sigma \left[1 + \sin(n\omega t + v) \right] \\ -\left[\frac{d_1}{2} + \left(u + \frac{w}{2} \right) \cos\alpha \right] \cos\sigma \cos(n\omega t + v) \\ -\frac{lv}{2\pi} \sin\sigma + s - ft \end{array} \right\}$$

where the condition of contact reduces to the following two constraints :

$$[1 + \sin(n\omega t + v)] = 0 \quad \text{and}$$

$$v = -\frac{\pi (d_2 - h)\, \omega t}{l \cos\alpha} .$$

due to the tip flank of the tooth

$$x_2 = -\left\{ \begin{array}{l} u \sin^2\sigma \left[1 + \sin(n\omega t + v)\right] \\ + \dfrac{d_1}{2} \sin\sigma \cos(n\omega t + v) \\ - \dfrac{l v}{2\pi} \cos\sigma - u \end{array} \right\} \cos\omega t + \left\{ \begin{array}{l} -u \sin\sigma \cos(n\omega t + v) \\ + \dfrac{d_1}{2} \left[1 + \sin(n\omega t + v)\right] \\ + \left[\dfrac{d_2}{2} - h\right] \end{array} \right\} \sin\omega t$$

$$y_2 = \left\{ \begin{array}{l} u \sin^2\sigma \left[1 + \sin(n\omega t + v)\right] \\ + \dfrac{d_1}{2} \sin\sigma \cos(n\omega t + v) \\ - \dfrac{l v}{2\pi} \cos\sigma - u \end{array} \right\} \sin\omega t + \left\{ \begin{array}{l} -u \sin\sigma \cos(n\omega t + v) \\ + \dfrac{d_1}{2} \left[1 + \sin(n\omega t + v)\right] \\ + \left[\dfrac{d_2}{2} - h\right] \end{array} \right\} \cos\omega t$$

$$z_2 = \left\{ \begin{array}{l} -u \sin\sigma \cos\sigma \left[1 + \sin(n\omega t + v)\right] \\ - \dfrac{d_1}{2} \cos\sigma \cos(n\omega t + v) \\ - \dfrac{l v}{2\pi} \sin\sigma + s - ft \end{array} \right\}$$

where the condition of contact reduces to the following two constraints :

$$[1 + \sin(n\omega t + v)] = 0 \quad \text{and}$$

$$v = -\frac{2\pi u}{l \cos\alpha}$$

Due to the right flank of the tooth,

$$x_2 = \left\{ \begin{array}{l} \left[\frac{w}{2} + \left(u - \frac{w}{2}\right)\sin\alpha\right]\cos^2\sigma\,[1 + \sin(n\omega t + v)] \\ -\left[\frac{d_1}{2} - \left(u - \frac{w}{2}\right)\cos\alpha\right]\sin\sigma\cos(n\omega t + v) \\ +\frac{lv}{2\pi}\cos\sigma \end{array} \right\} \cos\omega t$$

$$+ \left\{ \begin{array}{l} -\left[\frac{w}{2} + \left(u - \frac{w}{2}\right)\sin\alpha\right]\sin\sigma\cos(n\omega t + v) \\ +\left[\frac{d_1}{2} - \left(u - \frac{w}{2}\right)\cos\alpha\right]\sin(n\omega t + v) \\ +\left[\frac{d_1 + d_2}{2} - h\right] \end{array} \right\} \sin\omega t$$

$$y_2 = -\left\{ \begin{array}{l} \left[\frac{w}{2} + \left(u - \frac{w}{2}\right)\sin\alpha\right]\cos^2\sigma\,[1 + \sin(n\omega t + v)] \\ -\left[\frac{d_1}{2} - \left(u - \frac{w}{2}\right)\cos\alpha\right]\sin\sigma\cos(n\omega t + v) \\ +\frac{lv}{2\pi}\cos\sigma \end{array} \right\} \sin\omega t$$

$$+ \left\{ \begin{array}{l} -\left[\frac{w}{2} + \left(u - \frac{w}{2}\right)\sin\alpha\right]\sin\sigma\cos(n\omega t + v) \\ +\left[\frac{d_1}{2} - \left(u - \frac{w}{2}\right)\cos\alpha\right]\sin(n\omega t + v) \\ +\left[\frac{d_1 + d_2}{2} - h\right] \end{array} \right\} \cos\omega t$$

$$z_2 = \left\{ \begin{array}{l} -\left[\frac{w}{2} + \left(u - \frac{w}{2}\right)\sin\alpha\right]\sin\sigma\cos\sigma\,[1 + \sin(n\omega t + v)] \\ -\left[\frac{d_1}{2} - \left(u - \frac{w}{2}\right)\cos\alpha\right]\cos\sigma\cos(n\omega t + v) \\ -\frac{lv}{2\pi}\sin\sigma + s - ft \end{array} \right\}$$

where the condition of contact reduces to the following two constraints :

$$[1 + \sin(n\,\omega\,t + v)] = 0 \qquad \text{and}$$

$$v = -\frac{\pi\,(d_2 - h)\,\omega\,t}{l\cos\alpha}$$

Here again, we will get exactly the same equations for the surface of the gear as in the previous example of gear planing since the profile of the hob tooth and the rack tooth are same. The gear surface described by these equations is plotted for $w = 3$, $h = 6.5$, $r = 25$, $\alpha = 20°$. It is shown in Figure 5-3.

5.3 Simulation of Alternative Machining Strategies

A manufacturing engineer generally has a set of machine tools and a collection of cutting tools and he will be required to produce the given surface within the tolerance specifications at the minimum cost by appropriately choosing a machine tool and a cutter. Often, there will be more than one way to produce a component. Sometimes, the engineer has to explore alternate ways to manufacture a component because of the unavailability of the machine tool and/or the cutting tool (for which the component is earmarked) either due to a break-down or due to a busy schedule. These alternatives will have to be evaluated under the constraints of accuracy, time and cost in order to select the most optimal one. The selection of the most suitable alternative will be greatly simplified and speeded up if one can simulate the process using computer-based models such as the conjugate geometry model proposed in this thesis and perform evaluation of these alternative machining strategies with the aid of computers. In this section, the simulation of the alternative machining strategies for machining a helicoidal surface and a hyperbolic paraboloidal surface is discussed.

5.3.1 Alternative Machining Strategies to Produce a Helicoidal Surface

A helicoidal surface can be realized if the relative motion between the blank and the cutter consists of a rotation about the axis of the blank and a translation along the same axis. The manufacture of a helicoidal surface whose slot has a hemi-spherical cross-section across its helix is considered in this example. Three cases of realizing this helicoidal surface using the machine tools shown in Figures 3-1, 3-2 and 3-3 are discussed below. In each of these cases, the description of the expressions for the twelve degrees of freedom and the helicoidal surface produced are given.

Case (i) : In this case, a disc type of cutting tool similar to the one shown in Figure 4-24 is used on the 4 axis vertical milling machine shown in Figure 3-1. This disc type of cutter can be instantiated using the generic cutter model using the values given in Table 5-5.

Is arc tangential	d	r	a	b	h_1	e	f	h
yes	∞	5.000	0.000	-90.000	50.000	20.000	5.000	10.000

Table 5-5. Input Data to Instantiate a Disc Type Cutter

The resulting expressions for the cutter surface Σ_1 are given below :

$$ {}^1\underset{\sim}{p} = \begin{bmatrix} x_1 & y_1 & z_1 & 1 \end{bmatrix} \tag{5-7} $$

where

$$ \text{for the interval } \frac{d}{2} - r \le u \le \frac{d}{2} + r(\pi - 1) \text{ and } 0 \le v \le 2\pi $$

$$ x_1(u, v) = \left(r \sin \frac{u - \frac{d}{2} + r}{r} + \frac{d}{2} - r \right) \cos v $$

$$ y_1(u, v) = \left(r \sin \frac{u - \frac{d}{2} + r}{r} + \frac{d}{2} - r \right) \sin v $$

$$ z_1(u, v) = r \left(1 - \cos \frac{u - \frac{d}{2} + r}{r} \right) $$

and d is the diameter of the cutter and r is its corner radius.

The machining scheme is shown in Figure 5-5a. The blank is set on the rotary table such that their axes are collinear. The tool is held on the vertical spindle of the machine such that the axis of the disc is parallel to the table axis and offset from it along X direction so as to get the required depth of cut. The helical formative motion is obtained by rotating the rotary table and moving it along Z direction. Both these movements are coordinated to get the required lead of the helix.

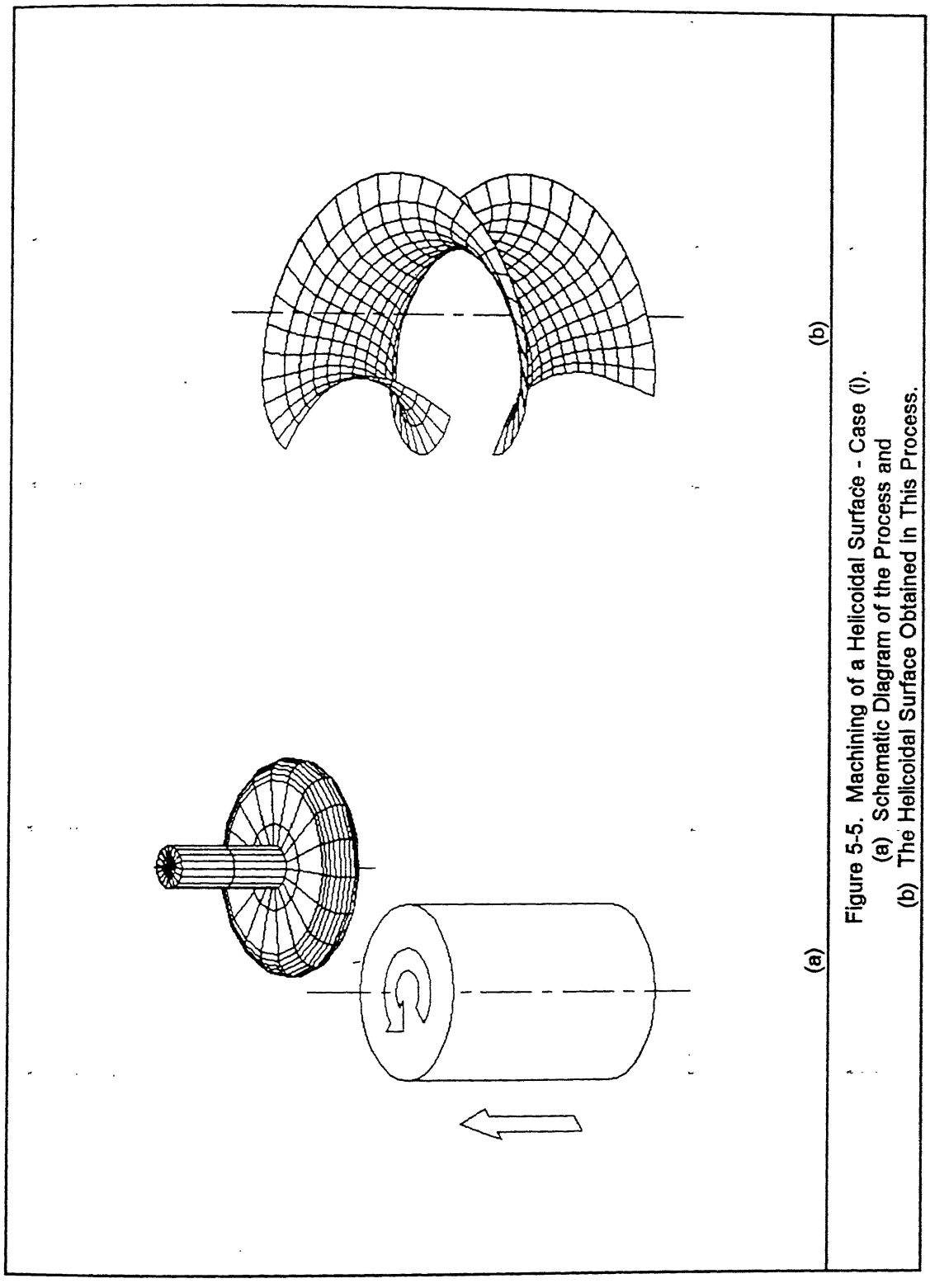

Figure 5-5. Machining of a Helicoidal Surface - Case (i).
(a) Schematic Diagram of the Process and
(b) The Helicoidal Surface Obtained in This Process.

Cutter	Blank
$a_1 = \frac{d_2 + d}{2} - r$	$a_2 = 0$
$b_1 = 0$	$b_2 = 0$
$c_1 = h_2$	$c_2 = \frac{p\,t}{2\,\pi}$
$\theta_1 = 0$	$\theta_2 = 0$
$\phi_1 = 0$	$\phi_2 = 0$
$\psi_1 = 0$	$\psi_2 = t$

Table 5-6. Parameters Describing Relative Motion in a Helical Milling Process - Case (i)

From the above, the geometry of the machined surface Σ_2 can be expressed as a biparametric equation in u and t as follows :

$$^2\underline{p} = \begin{bmatrix} x_2 & y_2 & z_2 & 1 \end{bmatrix} \qquad \textbf{(5-8)}$$

where

$$\text{for the interval } \frac{d}{2}-r \le u \le \frac{d}{2} + r(\pi-1) \text{ and } 0 \le t \le t_1$$

$$x_2(u, t) = \left\{\frac{d_2+d}{2} - r + \left(r \sin \frac{u+\frac{d}{2}-r}{r} + \frac{d}{2} - r\right) \cos v\right\} \cos t + \left(r \sin \frac{u+\frac{d}{2}-r}{r} + \frac{d}{2} - r\right) \sin v \sin t$$

$$y_2(u, t) = -\left\{\frac{d_2+d}{2} - r + \left(r \sin \frac{u+\frac{d}{2}-r}{r} + \frac{d}{2} - r\right) \cos v\right\} \sin t + \left(r \sin \frac{u+\frac{d}{2}-r}{r} + \frac{d}{2} - r\right) \sin v \cos t$$

$$z_2(u, t) = r\left(1 - \cos \frac{u-\frac{d}{2}+r}{r}\right) + h_2 - \frac{p\,t}{2\pi}$$

and

$$\sin v = \frac{p}{\pi(d_2+d-2r) \tan \frac{u-\frac{d}{2}+r}{r}}$$

The plot of this surface is given in Figure 5-5b.

Case (ii) : In this case, a ball-nose end milling cutter similar to the one shown in Figure 4-6 is used on the 5 axis horizontal milling machine shown in Figure 3-2. This cutter can be instantiated using the generic cutter model using the values given in Table 5-7.

Figure 5-6. Machining of a Helicoidal Surface - Case (II).
(a) Schematic Diagram of the Process and
(b) The Helicoidal Surface Obtained in This Process.

Is arc tangential	d	r	a	b	h_1	e	f	h
yes	10.000	5.000	0.000	0.000	50.000	(0.000)	(5.000)	10.000

Table 5-7. Input Data to Instantiate a Ball-Nose End Milling Cutter

The resulting expressions for the cutter surface Σ_1 are given below :

$$ {}^1\underset{\sim}{p} = \begin{bmatrix} x_1 & y_1 & z_1 & 1 \end{bmatrix} \tag{5-9} $$

where

$$ \text{for the interval } 0 \le u \le \frac{\pi r}{2} \text{ and } 0 \le v \le 2\pi $$

$$ x_1(u, v) = r \sin \frac{u}{r} \cos v $$

$$ y_1(u, v) = r \sin \frac{u}{r} \sin v $$

$$ z_1(u, v) = r \left(1 - \cos \frac{u}{r}\right) $$

The machining scheme is shown in Figure 5-6a. The blank is set on the horizontal rotary table such that their axes are collinear. The cutter is held on the horizontal spindle of the machine such that the axis of the cutter is perpendicular to the table axis and the tip of the cutter is offset from the table axis along Y direction so as to get the required depth of cut. The helical formative motion is obtained by rotating the rotary table and moving it along X direction. Both these movements are coordinated to get the required lead of the helix.

Cutter	Blank
$a_1 = 0$	$a_2 = -\frac{p\,t}{2\pi}$

$b_1 = \frac{d_2}{2} - r$	$b_2 = 0$
$c_1 = 0$	$c_2 = 0$
$\theta_1 = -\frac{\pi}{2}$	$\theta_2 = -t$
$\phi_1 = 0$	$\phi_2 = 0$
$\psi_1 = 0$	$\psi_2 = 0$

Table 5-8. Parameters Describing Relative Motion of Helical Milling Process - Case (ii)

From the above, the geometry of the machined surface Σ_2 can be obtained as a biparametric equation in u and t as follows :

$$ {}^2\underset{\sim}{p} = \begin{bmatrix} x_2 & y_2 & z_2 & 1 \end{bmatrix} \qquad \textbf{(5-10)} $$

where

for the interval $0 \le u \le \frac{\pi r}{2}$ and $0 \le t \le t_1$

$$ x_2(u, t) = r \sin\frac{u}{r} \cos v + \frac{p\,t}{2\pi} $$

$$ y_2(u, t) = -r \sin\frac{u}{r} \sin v \sin t + \left(\frac{d_2}{2} - r\cos\frac{u}{r}\right)\cos t $$

$$ z_2(u, t) = -r \sin\frac{u}{r} \sin v \cos t - \left(\frac{d_2}{2} - r\cos\frac{u}{r}\right)\sin t $$

where $\tan v = -\frac{p}{\pi\, d_2}$

The plot of this surface is given in Figure 5-6b.

Case (iii) : In this case also, the same ball-nose end milling cutter used in Case (ii) is used. However, the machine tool used here has a rotary table which has its axis vertical as shown in Figure 3-3. The cutter is described by Table 5-9 and the following equation which is exactly same as before.

Is arc tangential	d	r	a	b	h_1	e	f	h
yes	10.000	5.000	0.000	0.000	50.000	(0.000)	(5.000)	10.000

Table 5-9. Input Data to Instantiate a Ball-Nose End Milling Cutter

The resulting expressions for the cutter surface Σ_1 are given below :

$$ {}^1\underset{\sim}{p} = \begin{bmatrix} x_1 & y_1 & z_1 & 1 \end{bmatrix} \qquad \textbf{(5-11)} $$

where

$$ \textbf{for the interval } 0 \le u \le \frac{\pi r}{2} \textbf{ and } 0 \le v \le 2\pi $$

$$ x_1(u, v) = r \sin \frac{u}{r} \cos v $$

$$ y_1(u, v) = r \sin \frac{u}{r} \sin v $$

$$ z_1(u, v) = r \left(1 - \cos \frac{u}{r}\right) $$

The machining scheme is shown in Figure 5-7a. The blank is set on the vertical rotary table such that their axes are collinear. The cutter is held on the horizontal spindle of the machine such that the axis of the cutter is perpendicular to the table axis and the tip of the cutter is offset from the table axis along *Y* direction so as to get the required depth of cut. The helical formative motion is obtained by rotating the rotary table and moving it along *Z* direction. Both these movements are coordinated to get the required lead of the helix.

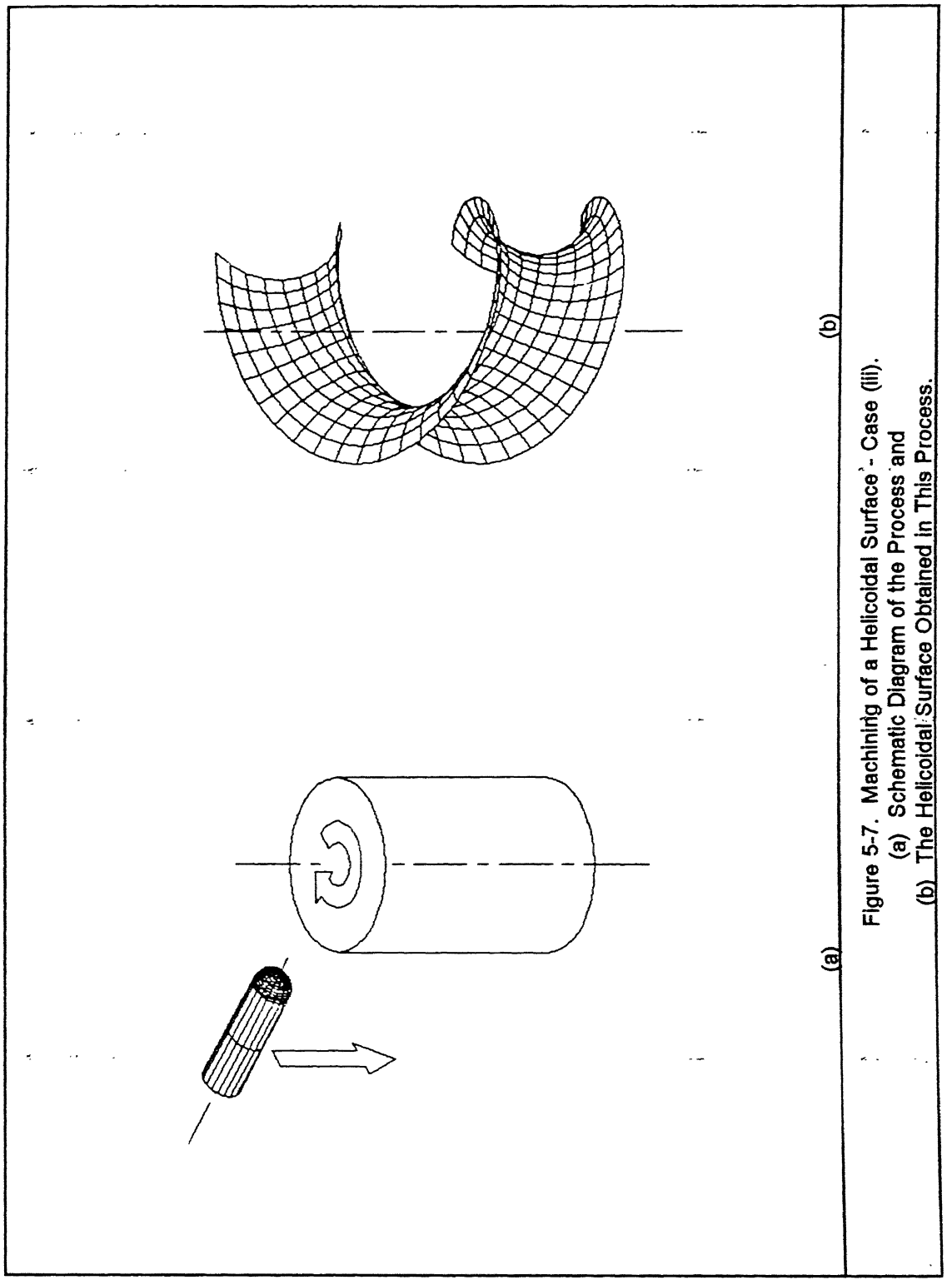

Figure 5-7. Machining of a Helicoidal Surface - Case (iii).
(a) Schematic Diagram of the Process and
(b) The Helicoidal Surface Obtained in This Process.

Cutter	Blank
$a_1 = 0$	$a_2 = 0$
$b_1 = \frac{d_2}{2} - r$	$b_2 = 0$
$c_1 = h_2 - \frac{p\,t}{2\pi}$	$c_2 = 0$
$\theta_1 = -\frac{\pi}{2}$	$\theta_2 = 0$
$\phi_1 = 0$	$\phi_2 = 0$
$\psi_1 = 0$	$\psi_2 = -t$

Table 5-10. Parameters Describing Relative Motion of Helical Milling Process - Case (iii)

From the above, the geometry of the machined surface Σ_2 can be expressed as a biparametric equation in u and t as follows :

$$^2\underline{p} = \begin{bmatrix} x_2 & y_2 & z_2 & 1 \end{bmatrix} \qquad \textbf{(5-12)}$$

where

for the interval $0 \le u \le \frac{\pi\, r}{2}$ and $0 \le t \le t_1$

$$x_2(u, t) = r \sin\frac{u}{r} \cos v \cos t - \left(\frac{d_2}{2} - r\cos\frac{u}{r}\right)\sin t$$

$$y_2(u, t) = r \sin\frac{u}{r} \cos v \sin t + \left(\frac{d_2}{2} - r\cos\frac{u}{r}\right)\cos t$$

$$z_2(u, t) = -r \sin\frac{u}{r} \sin v + h_2 - \frac{p\,t}{2\pi}$$

and

$$\tan v = \frac{\pi d_2}{p}$$

The plot of this surface is given in Figure 5-7b.

In case (ii) and case (iii), the helicoidal surfaces obtained are identical and they are exactly same as that of the desired surface which is a function of only the nose radius of the cutter. However, the surface obtained in case (i) is influenced by both the diameter d and corner radius r and hence it is an approximation to the desired surface. It can be seen that as the diameter d of the disc cutter approached twice the value of its fillet radius r, (i.e., d tends to $2r$), the error between the desired and produced surface decreases.

5.3.2 Alternative Machining Strategies to Produce a Hyperbolic Paraboloidal Surface

When a block of material is moving along a straight line with constant velocity, if an end mill type cutter is tilted with constant angular speed in a plane perpendicular to the movement of the blank, the resulting surface is called a hyperbolic paraboloid. Two alternative methods of realizing this surface is discussed in this section, using the 5 axis machines shown in Figures 3-4 and 3-5. These are described in Case (i) and Case (ii).

Case (i) : In this case, the cutter used is an end milling cutter. Only the side of the end mill is in contact with the material. The cylindrical surface of this cutter can be expressed in parametric form as

$$^1\underset{\sim}{p} = \begin{bmatrix} x_1 & y_1 & z_1 & 1 \end{bmatrix} \qquad \textbf{(5-13)}$$

where

$$\text{for the interval } 0 \le u \le h_f + r \text{ and } 0 \le v \le 2\pi$$
$$x_1(u, v) = r \cos v$$
$$y_1(u, v) = r \sin v$$
$$z_1(u, v) = u - h_f - r$$

Figure 3-4 shows the machine tool on which this surface is machined. It is a 5 axis machine with the tool head which can be tilted about the two principal directions X and

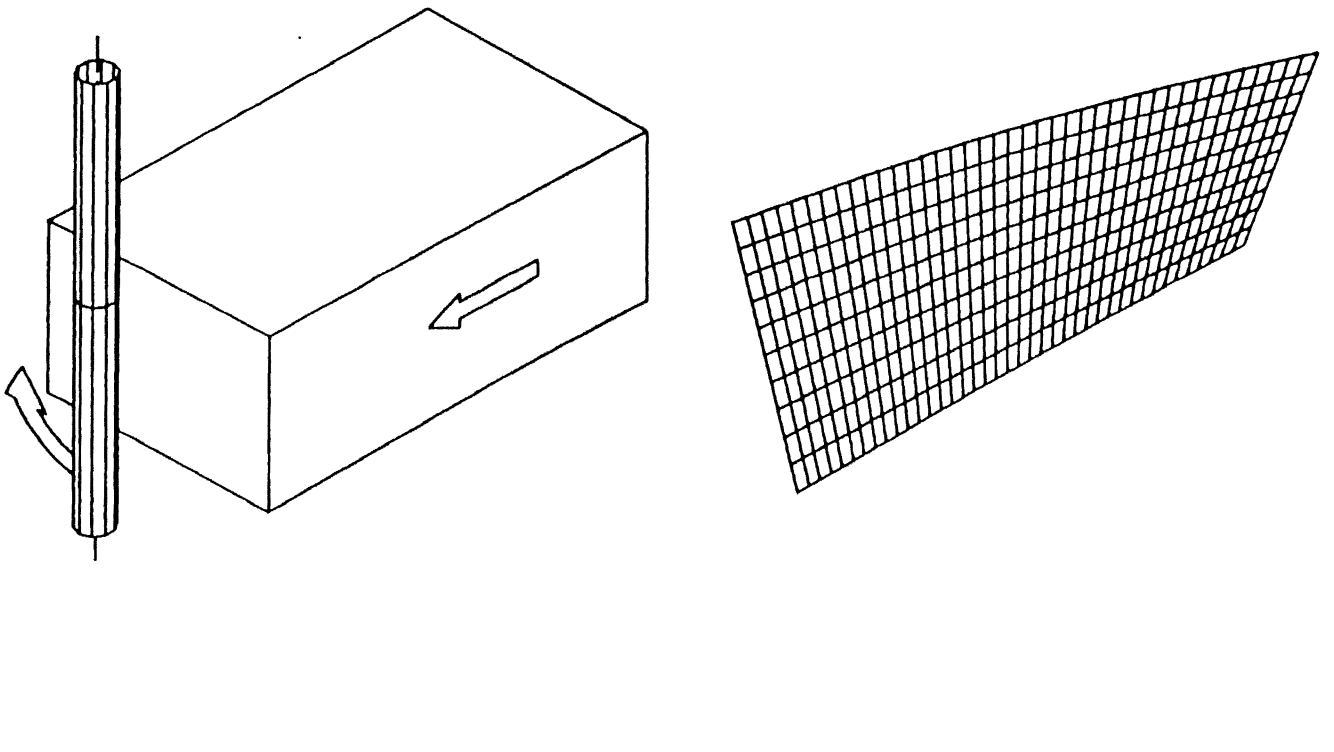

Figure 5-8. Modeling the Machining of a Hyperbolic Paraboloidal Surface - Case (i).
(a) Schematic Diagram of the Process and
(b) The Hyperbolic Paraboloidal Surface Obtained in This Process.

Y. The scheme of machining is shown in Figure 5-8a for this case. The blank is mounted on the table and the table moves along the *X* axis with unit velocity. At the same time, the cutter that is mounted on the spindle head swivels at an angular velocity of π/κ about the *X* axis. The twelve degrees of freedom for this process is described in Table 5-11.

Cutter	Blank
$a_1 = 0$	$a_2 = -t$
$b_1 = 0$	$b_2 = 0$
$c_1 = h_f$	$c_2 = 0$
$\theta_1 = \frac{\pi t}{\kappa}$	$\theta_2 = 0$
$\phi_1 = 0$	$\phi_2 = 0$
$\psi_1 = 0$	$\psi_2 = 0$

Table 5-11. Parameters Describing Relative Motion of a Milling Process - Case (i)

From the above, the geometry of the machined surface Σ_2 can be expressed as a biparametric equation in *u* and *t* as follows :

$$^2\underline{p} = \begin{bmatrix} x_2 & y_2 & z_2 & 1 \end{bmatrix} \qquad \textbf{(5-14)}$$

where

$$\text{for the interval } 0 \le u \le h_f + r \text{ and } t_1 \le t \le t_2$$

$$x_2(u, t) = r \cos v + t$$

$$y_2(u, t) = r \sin v \cos \frac{\pi t}{\kappa} - (u - h_f - r) \sin \frac{\pi t}{\kappa}$$

$$z_2(u, t) = r \sin v \sin \frac{\pi t}{\kappa} + (u - h_f - r) \cos \frac{\pi t}{\kappa} + h_f$$

and

$$\tan v = \frac{\kappa}{(u - h_f - r)\,\pi}$$

This hyperbolic paraboloidal surface is shown in Figure 5-8b.

Case (ii) : In this case, the cutter used is same as that of Case (i). Here also, only the side of the end mill is in contact with the material. Hence the equation of the cutter surface remains the same. However, the machine tool used here is a different one. Figure 3-5 shows the machine tool on which the same hyperbolic paraboloidal surface is machined. It is a 5 axis machine with the tool head which can be tilted about the two axes called *A* and *B* axes. The kinematic arrangement of this machine has been explained in detail in Chapter 3 by means of Figures 3-5 through 3-8. The scheme of machining is shown in Figure 5-9a for this case. The blank is mounted on the table. Since the table is fixed, the linear movement of the blank is replaced by the movement of the tool head in the opposite direction. At the same time, the cutter that is mounted on the spindle head swivels at an angular velocity of π/κ about the *X* axis. The twelve degrees of freedom for this process is described in Table 5-12.

Cutter	Blank
$a_1 = t$	$a_2 = 0$
$b_1 = 0$	$b_2 = 0$
$c_1 = h_f$	$c_2 = 0$

$\theta_1 = \frac{\pi t}{\kappa}$	$\theta_2 = 0$
$\phi_1 = 0$	$\phi_2 = 0$
$\psi_1 = 0$	$\psi_2 = 0$

Table 5-12. Parameters Describing Relative Motion of a Milling Process - Case (ii)

Since the rotary axes of the machine are not parallel to the principal directions, in order to get a tilt of the cutter about the X direction, the following relation between the α and β values (which are the joint coordinates pertaining to the rotary axes A and B of the machine tool) should be maintained.

$$\left.\begin{aligned} \beta &= \cos^{-1}\left(1 - \frac{1 - \cos\frac{\pi t}{\kappa}}{\sin^2\delta}\right) \\ \alpha &= \tan^{-1}\left(-\frac{\cos\delta\,(1 - \cos\beta)}{\sin\beta}\right) \end{aligned}\right] \qquad \textbf{(5-15)}$$

From the above, the geometry of the machined surface Σ_2 can be expressed as a biparametric equation in u and t as follows :

$$^2\underline{p} = \begin{bmatrix} x_2 & y_2 & z_2 & 1 \end{bmatrix} \qquad \textbf{(5-16)}$$

where

for the interval $0 \le u \le h_f + r$ and $t_1 \le t \le t_2$

$$x_2(u, t) = r\cos v + t$$

$$y_2(u, t) = r\sin v\cos\frac{\pi t}{\kappa} - (u - h_f - r)\sin\frac{\pi t}{\kappa}$$

$$z_2(u, t) = r\sin v\sin\frac{\pi t}{\kappa} + (u - h_f - r)\cos\frac{\pi t}{\kappa} + h_f$$

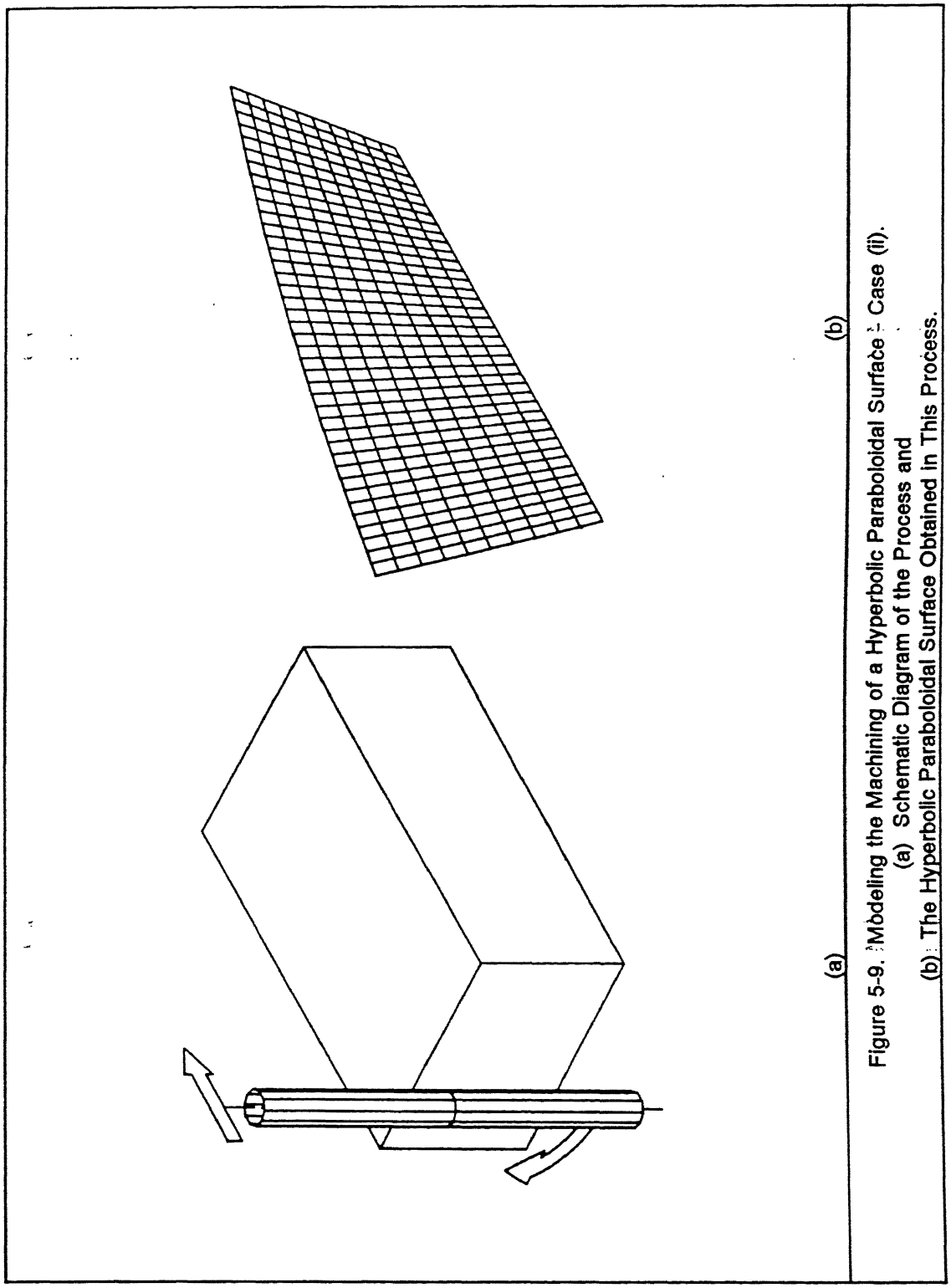

Figure 5-9. Modeling the Machining of a Hyperbolic Paraboloidal Surface - Case (ii).
(a) Schematic Diagram of the Process and
(b) The Hyperbolic Paraboloidal Surface Obtained in This Process.

and

$$\tan \nu = \frac{\kappa}{(u - h_f - r)\,\pi}$$

This hyperbolic paraboloidal surface is shown in Figure 5-9b.

Since the machine tool used in Case (i) has one of the rotary axes about the X direction, the hyperbolic paraboloidal surface can be machined exactly with a single NC block using this machine. However, several cutter path steps are required for the profiler used in Case (ii) in order to get the same surface to the required accuracy. In Case (ii), for each intermediate value of t, a_1, α and β should be calculated whereas in Case (i), the values of a_2 and θ_1 are to be calculated only for the end values of t. Even though the programming effort is more for the machine tool shown in Figure 3-5, its tool head is very compact and the working space of the cutter is axisymmetrical about the cutter axis whereas the tool head is more bulkier and the range of tool reach is not axisymmetrical for the machine shown in Figure 3-4.

5.4 Design and Manufacture of a Cylindrical Cam and Follower Mechanism

A cam mechanism is a three link mechanism with the cam and the follower in higher-pair contact. Since the contacting portions of the cam and follower surfaces are conjugate to each other, one can use the conjugate geometry formulation proposed in this thesis to analyze these mechanisms. As the proposed algorithm is symbolic, one can simulate a variety of two- and three-dimensional cam and follower mechanisms simply by changing the input values. In fact, the idea of attaching moving coordinate frames to the conjugate surfaces which is the basis of the proposed conjugate geometry formulation was conceived initially for the analysis of these mechanisms. In this example, a cylindrical cam with a cylindrical translating follower is considered.

For the purpose of modeling the cam and follower mechanism using the generic model of the machine tool, the follower and the cam are viewed respectively as an end milling cutter and a cylindrical blank respectively. Therefore, the follower's biparametric representation can be given as

$$^1\underset{\sim}{p} = \begin{bmatrix} x_1 & y_1 & z_1 & 1 \end{bmatrix} \qquad (5\text{-}17)$$

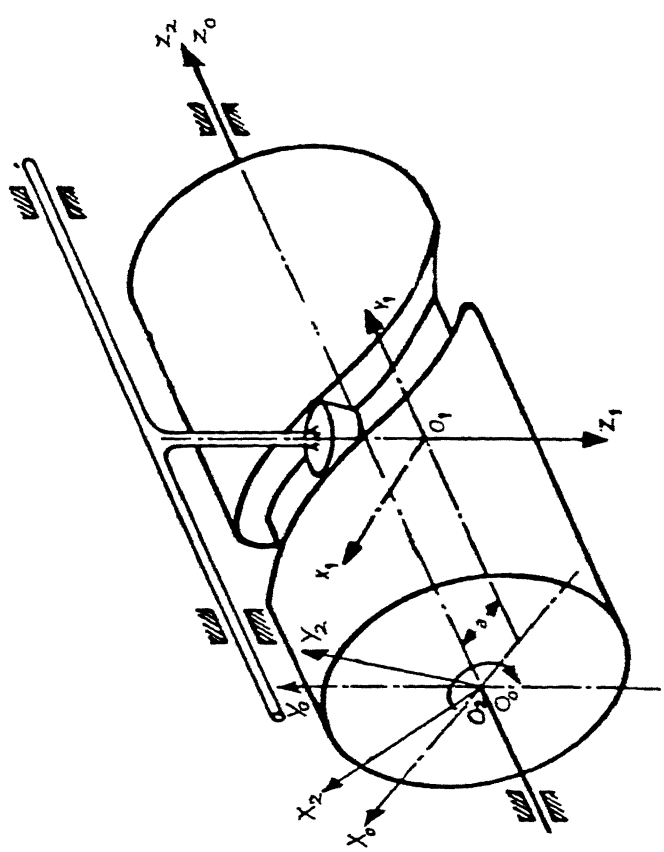

Figure 5-10. Modeling of a Cylindrical Cam and Follower Mechanism.

where

$$\text{for the interval } 0 \le u \le 2\pi \text{ and } 0 \le v \le v_1$$
$$x_1(u, v) = r \cos u$$
$$y_1(u, v) = r \sin u$$
$$z_1(u, v) = v$$

The axis of the cam and the Z_0 axis coincide and the cam is rotating about its axis with an angular velocity of unity. The axis of the follower (Z_1 axis) is parallel to and offset from the Y_0 axis by a distance of $-a$. It has the freedom to translate parallel to the Z_0 axis. The translation required in this case is assumed to be sinusoidal with an amplitude of $s/2$. The motions of these two elements of the mechanism can be described using the values given in the Table 5-13.

Follower	Cam
$a_1 = -a$	$a_2 = 0$
$b_1 = 0$	$b_2 = 0$
$c_1 = \frac{s}{2} \sin t$	$c_2 = 0$
$\theta_1 = \frac{\pi}{2}$	$\theta_2 = 0$
$\phi_1 = 0$	$\phi_2 = 0$
$\psi_1 = 0$	$\psi_2 = t$

Table 5-13. Parameters Describing Relative Motion of a Cylindrical Cam & Follower Mechanism

From the above data, the surface of the cam profile as determined by the conjugate geometry model is given below :

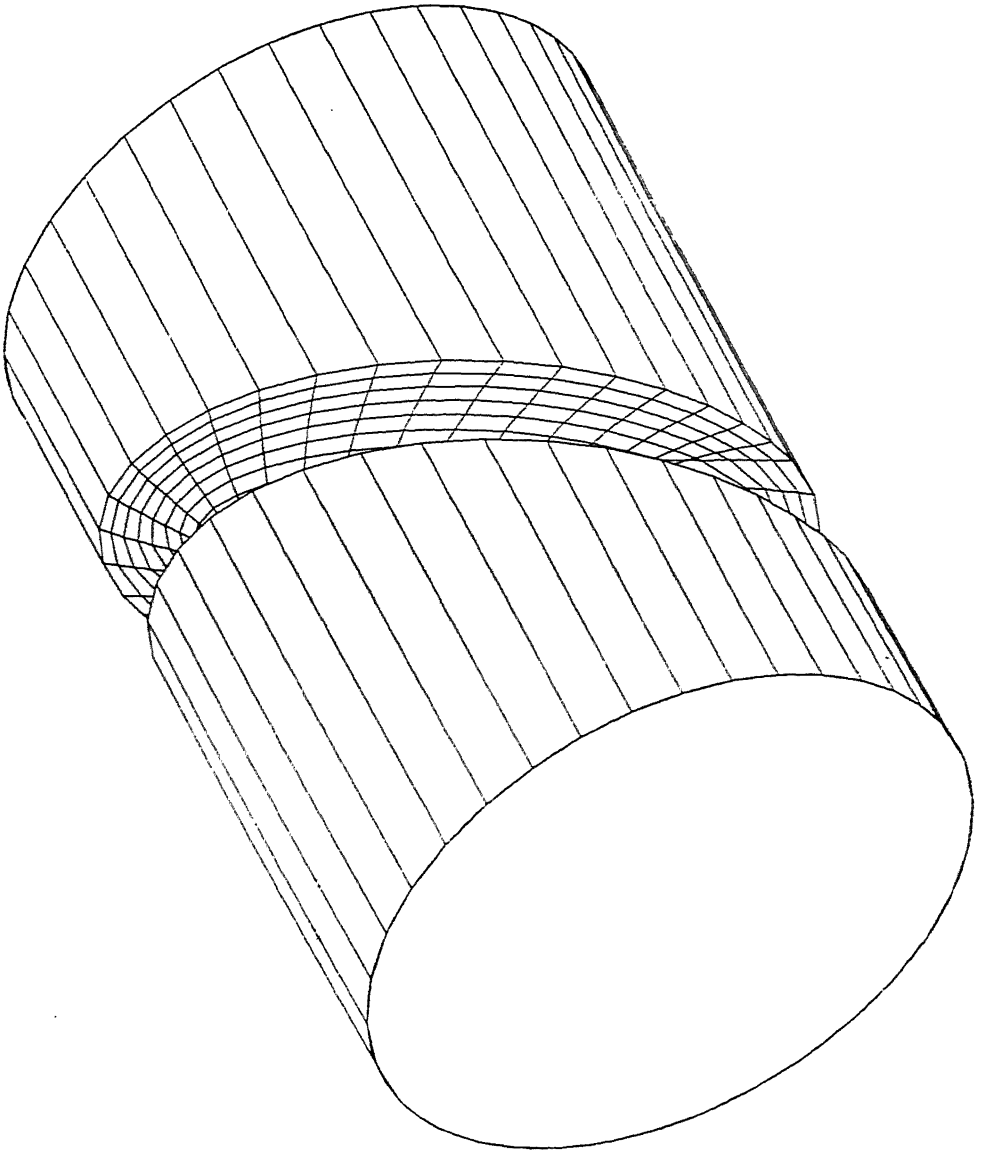

Figure 5-11. Surface of the Cylinrical Cam Obtained Using the Conjugate Geometry Formulation.

$$ {}^{2}\underset{\sim}{p} = \begin{bmatrix} x_2 & y_2 & z_2 & 1 \end{bmatrix} \tag{5-18} $$

where

$$ \text{for the interval } 0 \le v \le v_1 \text{ and } 0 \le t \le 2\pi $$
$$ x_2(u, t) = r \cos u \cos t - v \sin t - a \cos t $$
$$ y_2(u, t) = -r \cos u \sin t - v \cos t + a \sin t $$
$$ z_2(u, t) = r \sin u + \frac{s}{2} \sin t $$

and

$$ \tan u = \frac{2v}{s \cos t} $$

This surface is shown in Figure 5-11.

It is interesting to note that the manufacture of this cam profile can be modeled using the machine tool shown in Figure 3-2 or Figure 3-3 using exactly the same set of inputs where the follower will be replaced by an end milling cutter.

Chapter 6

DESIGN OF EXTRUDER SCREW SURFACES

6.1 Introduction

So far, we have discussed how conjugate geometry problems can be handled using symbolic, computational and graphical approaches. There are several types of free-form surfaces whose manufacturability needs to be evaluated before their design can be considered acceptable. One such case is that of design and manufacture of helicoidal surfaces (Saybold, 1992; Booy, 1978; Janssen, 1978; Battle et al., 1984). Flutes of twist drills, extruder screw surfaces and cylindrical cam surfaces are some examples of helicoidal surfaces. In the present chapter, it will be shown how helicoidal surfaces are designed keeping in mind the manufacturability constraint using the conjugate geometry model proposed in this thesis. In the next chapter, the specific problem of designing an end milling cutter and a side milling cutter for machining a helicoidal surface has been solved. The discussions in these chapters are focussed on the extruder screw surfaces which are used extensively in the polymer industry.

6.1.1 Definition of a Helicoidal Surface

Let $\underset{\sim}{g}(u)$ be a 2-D profile in X - Y plane which is the generatrix. When this generatrix is given a helical sweep, the surface generated by the edges of the generatrix profile will be a helicoidal surface. When the generatrix has rotated by an angle v about Z-axis from its initial position, at that instant, it would have moved by a distance $pv/2\pi$ along Z-axis where p is the pitch of the helix. Therefore, the helicoidal surface generated by the generatrix $\underset{\sim}{g}(u)$ can be expressed in homogeneous coordinate system as:

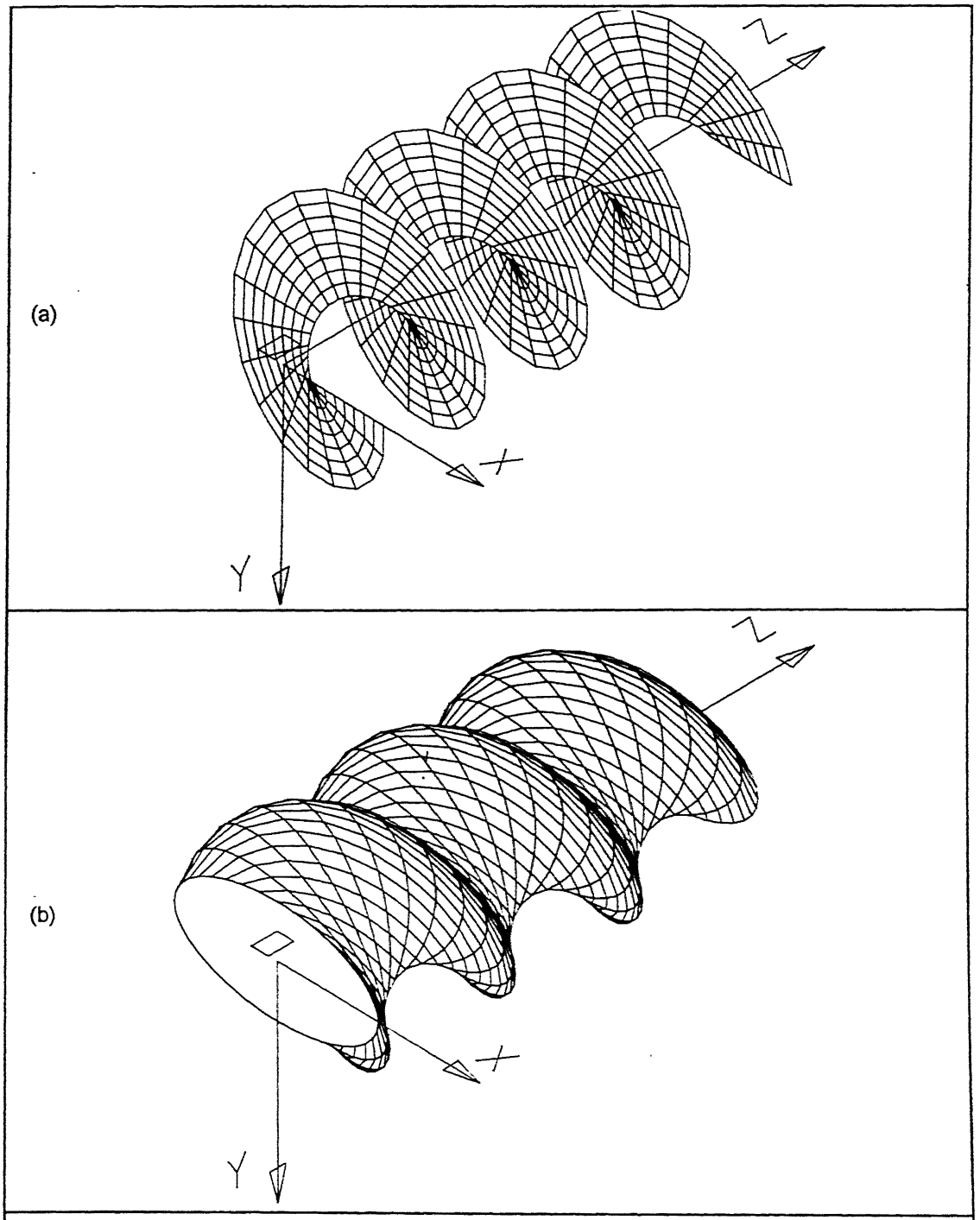

Figure 6-1. Examples of Helicoidal Surfaces.
(a) Due to a Straight Line Generatrix and
(b) Due to an Elliptical Generatrix

$$\underset{\sim}{p}(u, v) = \underset{\sim}{g}(u) \begin{bmatrix} \cos v & \sin v & 0 & 0 \\ -\sin v & \cos v & 0 & 0 \\ 0 & 0 & 1 & 0 \\ 0 & 0 & \frac{pv}{2\pi} & 1 \end{bmatrix} \tag{6-1}$$

Figure 6-1 shows a helicoidal surface obtained by sweeping a straight line generatrix

$$\underset{\sim}{g} = [\, u \quad 0 \quad 0 \quad 1 \,] \qquad 25 \le u \le 75 \tag{6-2}$$

and an elliptical generatrix

$$\underset{\sim}{g} = [\, a\cos u \quad b\sin u \quad 0 \quad 1 \,] \tag{6-3}$$

for $a = 100$, $b = 50$ and $p = 200$.

6.1.2 Description of Extruders

Twin-screw extruders are used in the polymer industry for extrusion and pumping of mass. In these equipments, one screw wipes its mate and vice-versa. It is this wiping action that makes the twin-screw equipment attractive for handling many polymers since it eliminates dead spots where polymer can collect, stagnate and return degraded to the mainstream.

The most common twin-screw extruder comprises a housing or a barrel, and two parallel shafts equipped with identical or opposite-hand screw or paddle elements (Figure 6-2). The identical screws rotate in the same direction at the same speed and the opposite-hand screws rotate at the same speed but in opposite directions. However, twin-screw equipments with unequal number of lobes and hence unequal speed ratio and/or unequal diameter ratio are not uncommon. The cross-section of a typical screw is shown in Figure 6-3. Each lobe of the screw consists of a tip segment, a root segment and two flank segments connecting these two segments.

Based on the geometry of the pair of screws, these twin-screw equipments may be classified into three categories. They are:

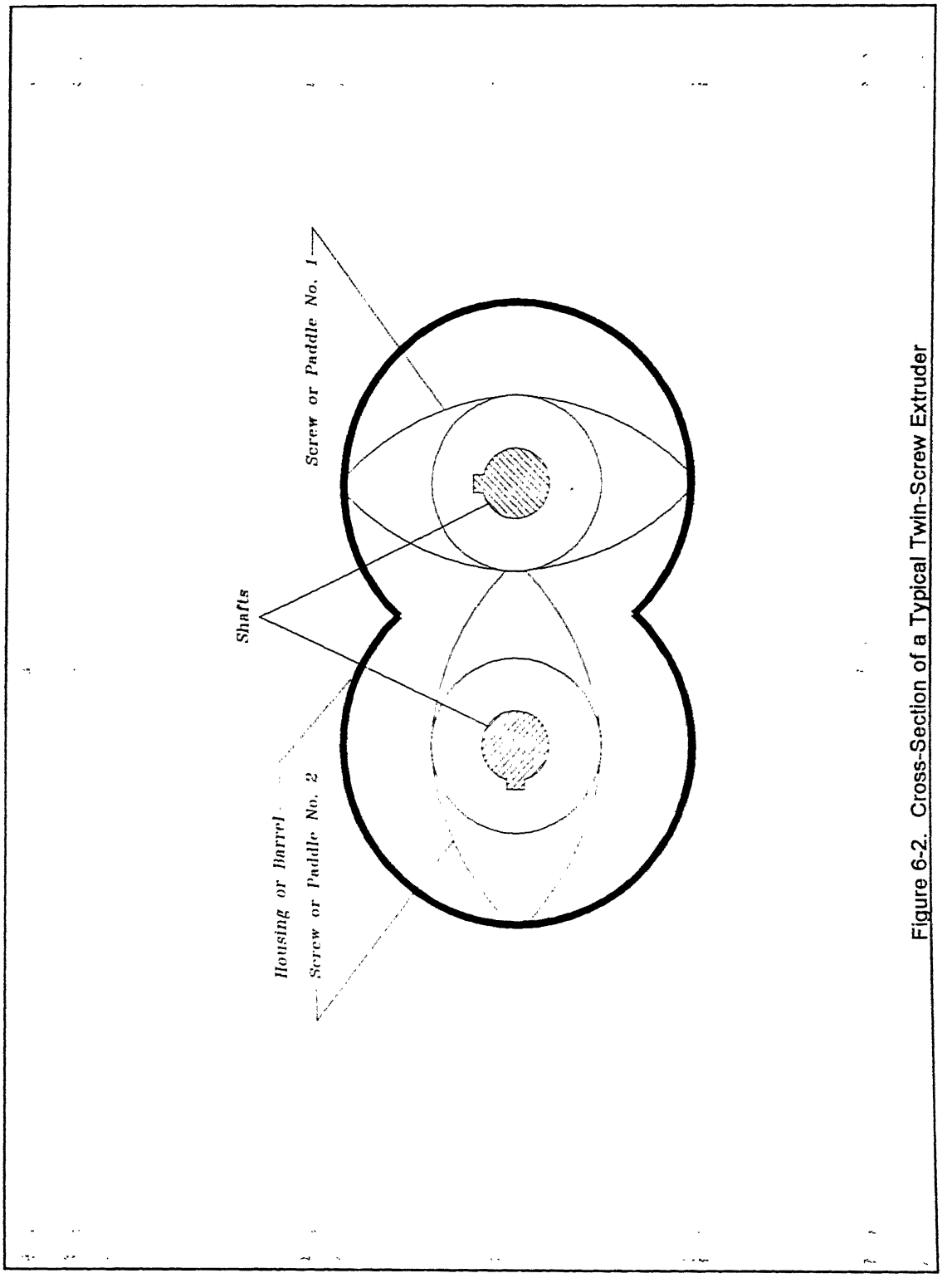

Figure 6-2. Cross-Section of a Typical Twin-Screw Extruder

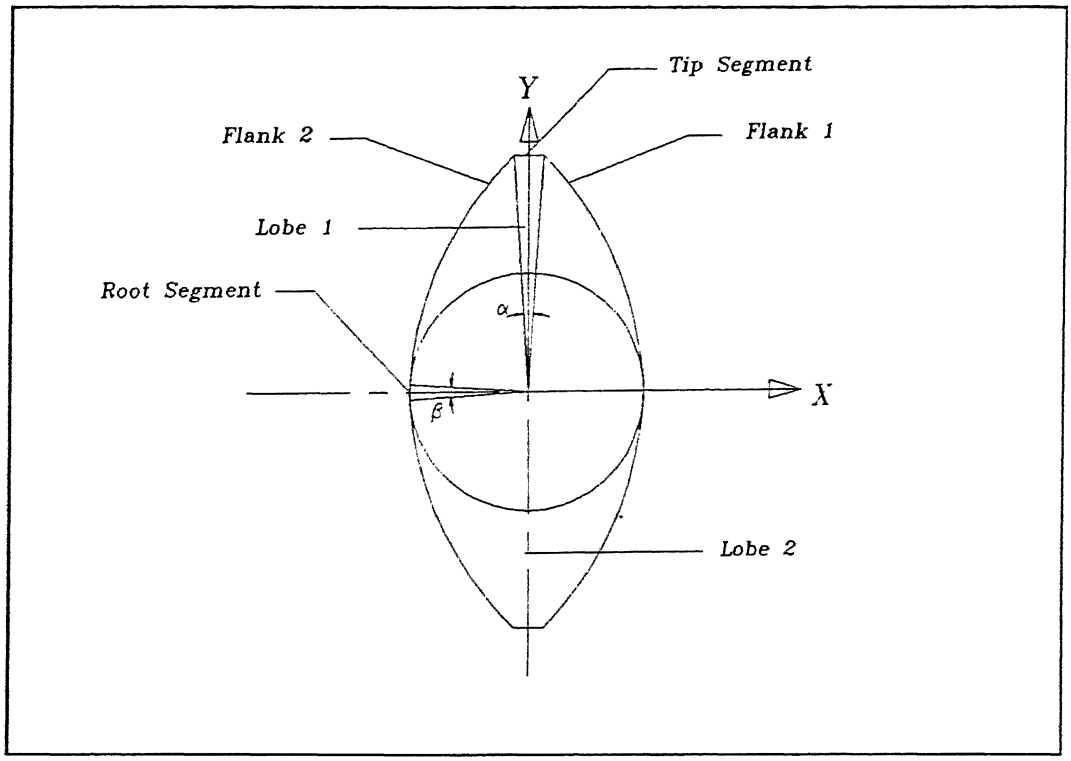

Figure 6-3. Cross-Section of a Typical Extruder Screw

i) Twin-screw equipments with identical screws,
ii) Twin-screw equipments with screws of unequal velocities but same diameters and
iii) Twin-screw equipments with screws of unequal velocities and unequal diameters.

In the first category, the shape and the size of both the screws are identical and hence they rotate at the same speed. In the second category, the number of lobes, velocity, etc. may be different for both the screws whereas in the third category, the screw diameters also will be different. In general, the cross-sections of the screws are composed of circular arcs. However, in the case of the third category, only one screw can be designed to have the cross-section composed of circular arcs and the flank curves of the other one will be non-circular.

Another major classification is based on an important geometric attribute of the pair of screws, viz., the clearance between the screws. They are:

i) Fully-wiped screws,

ii) Screws with constant clearance and
iii) Screws with variable clearance.

The fully-wiped screws have practically no clearance between them. These are used for the extrusion of highly homogeneous mass. Depending on the flow properties and homogeneity of the mass, one has to introduce the required clearance. In some screws, the clearance is designed to be variable so as to achieve the desired design specifications such as mass flow per revolution.

There are other less important classifications. The screws may be (i) Single-lobed screws, (ii) Bi-lobed screws, (iii) Tri-lobed screws etc. based on the number of lobes and (i) Co-rotating and (ii) Contra-rotating based on the direction of rotation.

The cross-section of a twin-screw has a unique shape for a given diameter, centerline distance and number of parallel channels because of the requirement that one screw must, in any position, wipe its mate. This unique shape is determined by means of a well-known kinematic principle. Kinematic analysis yields equations that relate the major design parameters and in graphical form, serve as the basis for design and selection of screw dimensions. Volumes and surface area can be calculated once the major parameters have been selected.

6.2 Design of Screw I of the Extruder

One can think of a screw with a given cross-section as being obtained by uniformly twisting a bar with that cross-section. Thus the screw is also an infinite set of infinitesimally thin discs, each rotated slightly with respect to its neighbor. Since all pairs of discs are fully wiped, we have to only study one pair to determine the cross-sectional screw cross section.

Let screw I rotate with an angular velocity of ω_1 about O_1 and screw II rotate with an angular velocity of ω_2 about O_2 (Figure 6.4). Let the center distance between O_1 and O_2 be r_0. Let PQ be the tip segment of disc I. We want to know the shape of disc II that is wiped by the tip PQ which means that we must construct the path or trajectory of PQ with respect to disc II. Constructing such a trajectory becomes simpler when we add a motion to the system of discs I and II which brings disc II to rest. Therefore the disc II becomes standstill when we superimpose a rotation $-\omega_2$ about O_0. As a result of this, disc I slows down to $(\omega_1 - \omega_2)$ and also goes round O_0 with an angular velocity of $-\omega_2$. Therefore, the trajectory of O_1 is a circle of radius r_0 with its center at O_0. Let r_1 and r_2 be the tip radii and n_1 and n_2 be the number of lobes of screws I and II respectively. Let k be the center-distance ratio of any screw which is the ratio of its tip radius and the

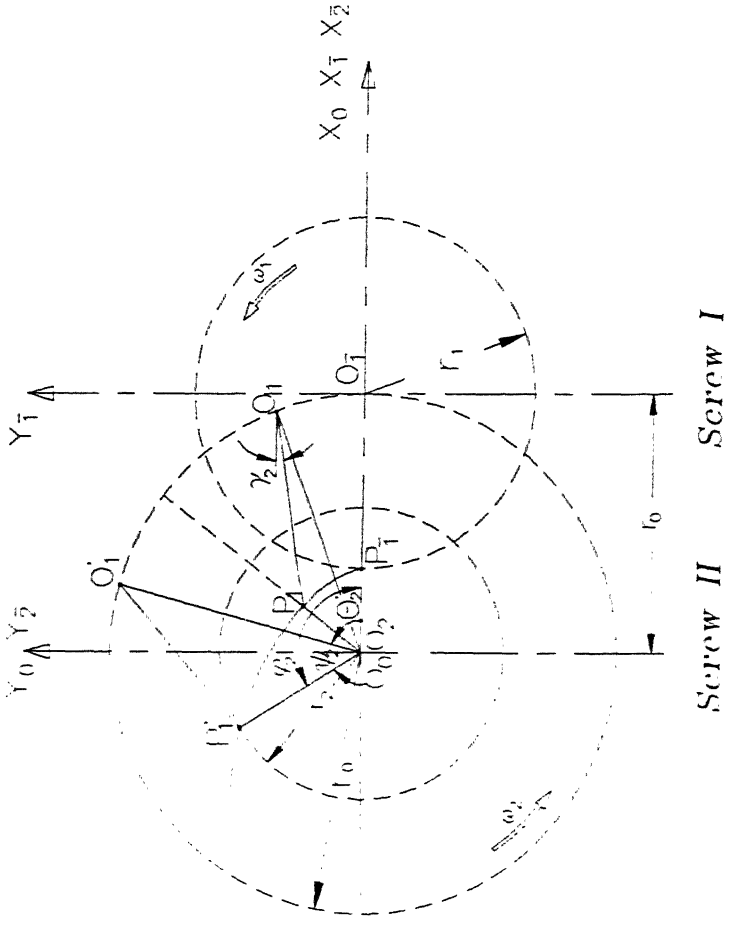

Figure 6-4. Kinematic Diagram of the Twin-Screw Mechanism

center distance of the pair of screws and m be the velocity ratio of the pair of screws. Therefore,

$$k_1 = \frac{r_1}{r_0} \tag{6-4}$$

$$k_2 = \frac{r_2}{r_0} \tag{6-5}$$

$$m = \frac{\omega_1}{\omega_2} = \frac{n_2}{n_1} \tag{6-6}$$

6.2.1 Determination of the Flank Curve

The line O_0O_1 rotates with an angular velocity of $-\omega_2$. Let P is any generic point on the tip segment of disc I and O_1 be the position occupied by O_1 at any instant. Also the line O_1P_1 rotates with an angular velocity of $(\omega_1 - \omega_2)$. Since it is a radial line of the tip segment, it has a length of r_1. Hence

$$\frac{\gamma_2}{\theta_2} = \frac{\omega_2 - \omega_1}{\omega_2} = 1 - m \tag{6-7}$$

Now the flank curve of the disc II which is the trajectory of the point P can be expressed in terms of the parameter θ as

$$\left.\begin{aligned} x_p &= r_0 \cos\theta_2 - r_1 \cos\gamma_2 = r_0 \cos\theta_2 - r_1 \cos[(1-m)\,\theta_2] \\ y_p &= r_0 \sin\theta_2 - r_1 \sin\gamma_2 = r_0 \sin\theta_2 - r_1 \sin[(1-m)\,\theta_2] \end{aligned}\right\} \tag{6-8}$$

In polar coordinates and in terms of the center-distance ratios, this can be written as

$$r_p = r_0 \left[1 + k_1^2 - 2k_1 \cos(m\,\theta_2)\right]^{\frac{1}{2}} \tag{6-9}$$

To determine the tip angle, we must know angle φ where the trajectory of P intersects the tip circle of disc I. At this point, $r = r_2$ and $\theta=\theta'$. Hence,

$$r_2 = r_0 \left[1 + k_1^2 - 2k_1 \cos\left(m\,\theta_2'\right)\right]^{\frac{1}{2}} \tag{6-10}$$

or

$$\theta_2' = \frac{1}{m} \cos^{-1}\left[\frac{1 + k_1^2 - k_2^2}{2\,k_1}\right] \tag{6-11}$$

Next, we must determine angle ψ_2. This is obtained by considering the triangle $O_0P_1'O_1'$. Therefore,

$$\psi_2 = \cos^{-1}\left[\frac{r_0^2 + r_2^2 - r_1^2}{2\,r_0\,r_2}\right] = \cos^{-1}\left[\frac{1 + k_2^2 - k_1^2}{2\,k_2}\right] \tag{6-12}$$

Therefore the flank angle φ_2 of disc II is

$$\begin{aligned}\phi_2 &= \psi_2 + \theta_2' \\ &= \cos^{-1}\left[\frac{1 + k_2^2 - k_1^2}{2\,k_2}\right] + \frac{1}{m}\cos^{-1}\left[\frac{1 + k_1^2 - k_2^2}{2\,k_1}\right]\end{aligned} \tag{6-13}$$

6.2.2 Relation between the Tip and the Root Angles

α_1 and α_2 are the tip angles and β_1 and β_2 are the root angles of discs I and II respectively. Since the tip segment of disc I wipes the root segment of disc II, during the period the point of contact between the tip segment of disc II and the root segment of disc I moves from one end of the tip segment of disc II to the other, the disc I would rotate by $(1 - m)\,\beta_2$. Therefore,

$$\begin{aligned}\alpha_1 &= \beta_2 - (1 - m)\,\beta_2 \\ &= m\,\beta_2\end{aligned} \tag{6-14}$$

Similarly,

$$\begin{aligned}\beta_1 &= \alpha_2 - (1 - m)\,\alpha_2 \\ &= m\,\alpha_2\end{aligned} \tag{6-15}$$

Equations (6-14) and (6-15) imply that

$$\frac{\alpha_1}{\beta_1} = \frac{\beta_2}{\alpha_2} \tag{6-16}$$

Thus the ratio of the root to tip angles of one disc is the inverse of its mate.

The disc I has n_1 lobes hence it has $2n_1$ flanks and similarly the disc II has $2n_2$ flanks. Hence,

$$\begin{aligned} n_1[\alpha_1 + \beta_1 + 2\phi_1] &= 2\pi \\ n_2[\alpha_2 + \beta_2 + 2\phi_2] &= 2\pi \end{aligned} \tag{6-17}$$

$$\begin{aligned} \alpha_2 + \beta_2 = \frac{2\pi}{n_2} &- 2\cos^{-1}\left[\frac{1 + k_2^2 - k_1^2}{2k_2}\right] \\ &- \frac{2}{m}\cos^{-1}\left[\frac{1 + k_1^2 - k_2^2}{2k_1}\right] \\ \alpha_1 + \beta_1 = \frac{2\pi}{n_1} &- 2m\cos^{-1}\left[\frac{1 + k_2^2 - k_1^2}{2k_2}\right] \\ &- 2\cos^{-1}\left[\frac{1 + k_1^2 - k_2^2}{2k_1}\right] \end{aligned} \tag{6-18}$$

From equation (6-16) and (6-18), we can arrive at α_1 and β_1 for the given parameters.

The following relation exists between the tip and root radii and the center distance:

$$r_0 = r_{t,1} + r_{r,2} = r_{t,2} + r_{r,1} \tag{6-19}$$

6.2.3 Algorithm for the Design of Disc I

The parameters that describe disc I are obtained from the following steps:

1. Calculate α_2 and β_2 from Equations (6-16) and (6-18). The ratio of the angles α_1/β_1 or β_2/α_1, n_1, n_2, m, r_1, r_2 and r_0 will be known from the design specification.

2. Calculate α_1 and β_1 from Equation (6-18).

3. Calculate ϕ_1 from Equation (6-13).

4. Define ${}^1\underset{\sim}{p}$, the position vector of a point P on the disc I for all the four arcs of each lobe. There will be $4n_1$ arc segments that form the disc I.

$$ {}^1\underset{\sim}{p} = \begin{bmatrix} x_1 & y_1 & 0 & 1 \end{bmatrix} \qquad \textbf{(6-20)} $$

where,

$$ \begin{aligned} x_1 &= p_i + r_i \cos u_i \\ y_1 &= q_i + r_i \sin u_i \\ u_{i1} &\le u_i \le u_{i2} \\ 1 &\le i \le 4n_1 \end{aligned} $$

6.3 Design of Screw II of the Extruder

6.3.1 Finding the Conjugate Segments of Disc II Corresponding to Each Segment of Disc I

The profile of disc I can be obtained from the algorithm given in the preceding section. The twelve parameters describing the motion of the disc I and disc II are also known. Since the two discs are fully-wiped, the profiles of the discs are conjugate to each other. Hence the profile of disc II can be determined using the conjugate geometry model with twelve degrees of freedom proposed in Chapter 2.

The steps involved in finding the profile of disc II are as follows:

1. Define ${}^1\underset{\sim}{p}$: This definition is given Equation (6-19).

2. Define the 12 parameters of motion: After superimposing a rotation of angular velocity ω_2 about Z_0 as described in Section 6.2, disc II is stationary and disc I rotates about Z_1 axis with an angular velocity of ω_1 - ω_2 and also goes round O_0 with an angular velocity of ω_2. The twelve parameters of motion for this case are given in Table 6-1.

Disc I	Disc II
$a_1 = r_0 \cos t$	$a_2 = 0$
$b_1 = r_0 \sin t$	$b_2 = 0$
$c_1 = 0$	$c_2 = 0$
$\theta_1 = 0$	$\theta_2 = 0$
$\phi_1 = 0$	$\phi_2 = 0$
$\psi_1 = (m-1)t$	$\psi = 0$

Table 6-1. Parameters Describing Relative Motion between the Two Screws.

3. The transformation matrix $\left[{}^0_1M\right]$ for transforming the position vector ${}^1\underset{\sim}{p}$ and the normal vector ${}^1\underset{\sim}{n}_{P,1}$ from the cutter coordinate system S_1 to the global coordinate system S_0 is:

$$\left[{}^0_1M\right] = \begin{bmatrix} \cos(m-1)t & \sin(m-1)t & 0 & 0 \\ -\sin(m-1)t & \cos(m-1)t & 0 & 0 \\ 0 & 0 & 1 & 0 \\ r_0 \cos t & r_0 \sin t & 0 & 1 \end{bmatrix} \qquad (6\text{-}21)$$

Matrix $\left[{}^0_1\dot{M}\right]$ is the time-differential of the matrix $\left[{}^0_1M\right]$ which converts the position vector ${}^1\underset{\sim}{p}$ in the cutter coordinate system S_1 into velocity vector ${}^0\underset{\sim}{V}_{P,1}$ in the global coordinate system S_0.

$$\left[{}_{1}^{0}\dot{M}\right] = \begin{bmatrix} -(m-1)\sin(m-1)t & (m-1)\cos(m-1)t & 0 & 0 \\ -(m-1)\cos(m-1)t & -(m-1)\sin(m-1)t & 0 & 0 \\ 0 & 0 & 0 & 0 \\ -r_0 \sin t & r_0 \cos t & 0 & 0 \end{bmatrix} \tag{6-22}$$

4. The transformation matrices $\left[{}_{2}^{0}M\right]$ and $\left[{}_{0}^{2}M\right]$ for transforming the position vector ${}^{2}\underset{\sim}{p}$ from the blank coordinate system S_2 to the global coordinate system S_0 and vice-versa are respectively:

$$\left[{}_{2}^{0}M\right] = \begin{bmatrix} 1 & 0 & 0 & 0 \\ 0 & 1 & 0 & 0 \\ 0 & 0 & 1 & 0 \\ 0 & 0 & 0 & 1 \end{bmatrix} \tag{6-23}$$

$$\left[{}_{0}^{2}M\right] = \begin{bmatrix} 1 & 0 & 0 & 0 \\ 0 & 1 & 0 & 0 \\ 0 & 0 & 1 & 0 \\ 0 & 0 & 0 & 1 \end{bmatrix} \tag{6-24}$$

Matrix $\left[{}_{2}^{0}\dot{M}\right]$ is the time-differential of the matrix $\left[{}_{2}^{0}M\right]$ which converts the position vector $\underset{\sim}{p}$ in the blank coordinate system S_2 into velocity vector ${}^{0}\underset{\sim}{V}_{P,2}$ in the global coordinate system S_0.

$$\left[{}_{2}^{0}\dot{M}\right] = \begin{bmatrix} 0 & 0 & 0 & 0 \\ 0 & 0 & 0 & 0 \\ 0 & 0 & 0 & 0 \\ 0 & 0 & 0 & 0 \end{bmatrix} \tag{6-25}$$

5. The position vector ${}^{2}\underset{\sim}{p}$ is

$$ {}^{2}\underset{\sim}{P} = \begin{bmatrix} p_i \cos(m-1)t - q_i \sin(m-1)t + r_i \cos[u_i + (m-1)t] \\ \qquad + r_0 \cos t \\ p_i \sin(m-1)t + q_i \cos(m-1)t + r_i \sin[u_i + (m-1)t] \\ \qquad + r_0 \sin t \\ 0 \\ 1 \end{bmatrix}^T \qquad (6\text{-}26) $$

6. The normal vector ${}^{1}\underset{\sim}{N}_{P,1}$ of the cutter surface is obtained as follows:

$$ \left.\begin{aligned} {}^{1}\underset{\sim}{p}_{u_i} &= [-r_i \sin u_i \quad r_i \cos u_i \quad 0 \quad 0] \\ {}^{1}\underset{\sim}{p}_{v} &= [\quad 0 \quad\quad 0 \quad\quad 1 \quad 0] \end{aligned}\right] \qquad (6\text{-}27) $$

$$ {}^{1}\underset{\sim}{N}_{P,1} = [\, r_i \cos u_i \quad\quad r_i \sin u_i \quad\quad 0 \quad\quad 0] \qquad (6\text{-}28) $$

7. The unit normal vector ${}^{1}\underset{\sim}{n}_{P,1}$ of the cutter surface is obtained as follows:

$$ \| \, {}^{1}\underset{\sim}{N}_{P,1} \, \| = r_i $$

$$ {}^{1}\underset{\sim}{n}_{P,1} = [\cos u_i \quad\quad \sin u_i \quad\quad 0 \quad\quad 0] \qquad (6\text{-}29) $$

8. The normal vector ${}^{0}\underset{\sim}{n}_{P,1}$ of the cutter surface in the global coordinate system is:

$$ {}^{0}\underset{\sim}{n}_{P,1} = [\cos[u_i + (m-1)t] \quad \sin[u_i + (m-1)t] \quad 0 \quad 0] \qquad (6\text{-}30) $$

9. The relative velocity vector ${}^{0}\underset{\sim}{V}_{P,12}$ in the global coordinate system can be now

or

$$u_i = \tan^{-1}\left(-\frac{\sin\,(m-2)\,t - \dfrac{(m-1)\,q_i}{r_0}}{\cos\,(m-2)\,t + \dfrac{(m-1)\,p_i}{r_0}} \right) \tag{6-35}$$

11. The profile Σ_2 of screw II can be now represented as a parametric equation in either u_i or t as given below:

$$\begin{aligned} x_2 &= p_i \cos\,(m-1)\,t - q_i \sin\,(m-1)\,t \\ &\quad + r_i \cos\,[u_i + (m-1)\,t] + r_0 \cos\,t \\ y_2 &= p_i \sin\,(m-1)\,t + q_i \cos\,(m-1)\,t \\ &\quad + r_i \sin\,[u_i + (m-1)\,t] + r_0 \sin\,t \end{aligned} \tag{6-36}$$

where

$$t = \frac{\sin^{-1}\left(-\dfrac{m-1}{r_0}\,[p_i \sin\,u_i - q_i \cos\,u_i] \right) - u_i}{m-2}$$

or

$$u_i = \tan^{-1}\left(-\frac{\sin\,(m-2)\,t - \dfrac{(m-1)\,q_i}{r_0}}{\cos\,(m-2)\,t + \dfrac{(m-1)\,p_i}{r_0}} \right)$$

and

$$\begin{aligned} u_{i1} \le u_i \le u_{i2} \\ 1 \le i \le 4n_1 \end{aligned}$$

6.3.2 Finding Conjugate Segments of Disc II Corresponding to the Cusps of Disc I

When the profile of disc I is a closed curve and has C^1-continuity throughout, then

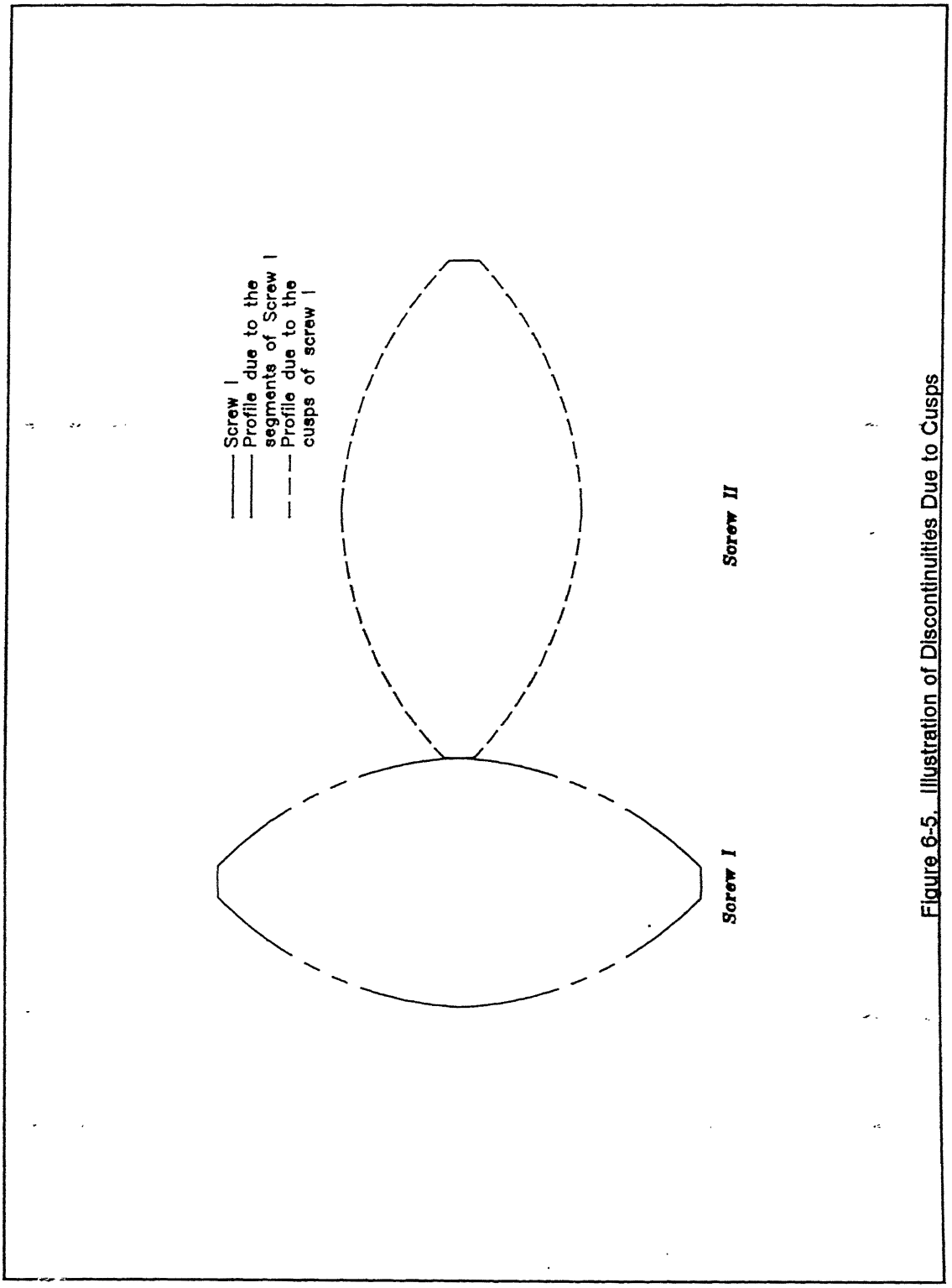

Figure 6-5. Illustration of Discontinuities Due to Cusps

(a)

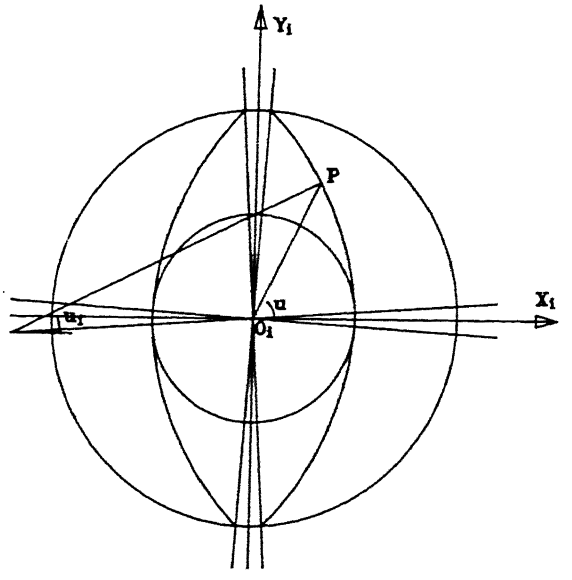

(b)

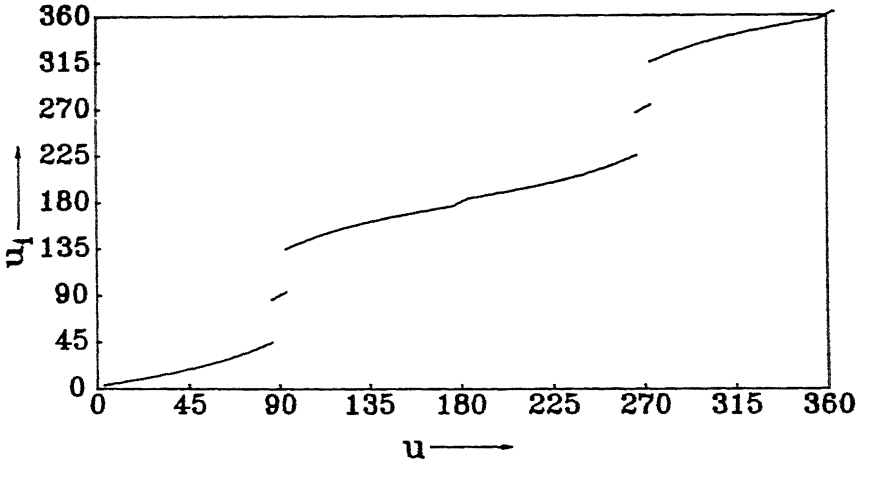

Figure 6-6. Identification of Cusps.
(a) Cross-Sectional Profile of Screw I and
(b) u versus u_1 Graph

the above eleven steps will yield the profile of disc II completely. However, since the disc I of the extruder is generally composed of circular segments, it does not satisfy this condition and hence there will be cusps. Cusp is a point that is common to both the preceding and the following curves which have different normals at that point. Hence, at the cuspoidal point, the normal abruptly changes. The procedure described in the previous section maps each point of profile of disc I and hence it considers each cusp for the two end values of its normal only and not for the values in-between. Hence the presence of a cusp is observed as a discontinuity in the Σ_2 profile obtained at Step 11. Mapping of each cusp will have to be done for each value of its normal. In order to do this, one needs to detect the presence of the cusps and then perform their mapping. Figure 6-5 shows the cross-section of Screw I and the cross-section of Screw II produced using the conjugate geometry formulation. In this figure, the solid lines are conjugate lines to the segments of the profile I and the dotted lines were generated by the cuspoidal points of this profile.

6.3.2.1 Detection of Cusps

In the definition of disc I as given in Equation (6-19), u_i which is the absolute angle of any point on an arc with respect to its center (p_i, q_i). Let u be a parameter which is the absolute angle of any point P on the profile of disc I with respect to O_1 (Figure 6-6a). The relation between u and u_i is given by:

$$u = \tan^{-1}\left(\frac{q_i + r_i \sin u_i}{p_i + r_i \cos u_i}\right) \qquad \textbf{(6-37)}$$

The plot of u versus u_i is shown in Figure 6-6b for the profile of disc I shown in Figure 6-6a. The data pertaining to the eight segments of disc I of this profile is given in Table 6-2.

i	p_i	q_i	r_i	u_{i1}	u_{i2}
1	-99.804	-6.262	150.000	0.06269	0.78540
2	0.000	0.000	100.000	1.50811	1.63349
3	99.804	-6.262	150.000	2.35619	3.07890
4	0.000	0.000	50.000	3.07890	3.20428
5	99.804	6.262	150.000	3.20428	3.92699

6	0.000	0.000	100.000	4.64970	4.77508
7	-99.804	6.262	150.000	5.49779	6.22049
8	0.000	0.000	50.000	6.22049	6.34587

Table 6-2. Biparametric Definition of the Profile Shown in Figure 6-6a.

It can be observed that there are four cusps and the graph shows the corresponding four discontinuities. This property can be used to collect the cusps as given below:

> Let u_{i1} and u_{i2} be the starting and ending values of u_i for the ith segment of the profile. If $u_{i2} \neq u_{(i+1)1}$, then the end point of the ith segment is a cuspoidal point.

6.3.2.2 Mapping of Cusps

Each cusp C_j identified earlier can be mapped onto the S_2 coordinate system using the following procedure:

1. At the cusp C_j which is the end point of segment i and starting point of segment $(i+1)$, the normal vector changes from that of the ith segment to that of $(i+1)$th segment. The interval in t, say, t_{j1} and t_{j2}, in which this change takes place is obtained by substituting the values of (u_{i2}, p_i, q_i and r_i) and ($u_{i+1,1}$, p_{i+1}, q_{i+1} and r_{i+1}) in Equation (6-34).

2. The cusp can be assumed to be an arc of zero radius. Hence, use Equation (6-35) for mapping the cusp for the interval t_{j1} to t_{j2} with (p_i, q_i) as the cuspoidal point in S_1, $r_i = 0$ and $u_i = 0$

6.4 Illustrative Examples

As mentioned earlier in Section 6.1.2, the pair of extruder screws are classified as symmetrical and unsymmetrical. The unsymmetrical screw pairs are further classified as equal diameter screw pairs and unequal diameter screw pairs. In this sections, several examples of symmetrical screw pairs and unsymmetrical screw pairs of both types are considered to illustrate the application of the conjugate geometry model for the design of these screws.

6.4.1 Design of a Twin-Screw Extruder of Symmetrical Screws

Since the screws of a symmetrical screw pair are identical,

$$\left.\begin{aligned} r_1 &= r_2 = r \\ \alpha_1 &= \alpha_2 = \alpha \\ \beta_1 &= \beta_2 = \beta \end{aligned}\right] \qquad \textbf{(6-38)}$$

As they rotate with equal speed,

$$\begin{aligned} n_1 &= n_2 = n \\ m &= 1 \end{aligned} \qquad \textbf{(6-39)}$$

Equations (6-14), (6-15), (6-38) and (6-39) can be reduced as

$$\alpha_1 = \beta_2 = \alpha_2 = \beta_1 = \alpha \text{ (say)} \qquad \textbf{(6-40)}$$

From the above, Equation (6-18) can be simplified as

$$\alpha = \frac{\pi}{n} - 2\cos^{-1}\left(\frac{r_0}{2r}\right) \qquad \textbf{(6-41)}$$

where $\alpha \geq 0$.

Therefore, the design procedure for this class of screws can be stated as follows:

From the given design specifications, determine the number of lobes n, the tip radius r, the tip angle δ and the center distance r_0 using Equations (6-41) and the following two equations which are applicable to all kinds of screw pairs :

$$r + r_r = r_0 \qquad \textbf{(6-42)}$$

Examples of five types of symmetrical screw pairs are explained in this section.

6.4.1.1 Design of a Twin-Screw Extruder of Mono-Lobed Symmetrical Screws

Given : The tip radius r = 100 mm.
root radius r_r = 25 mm.

Number of lobes $n = 1$.

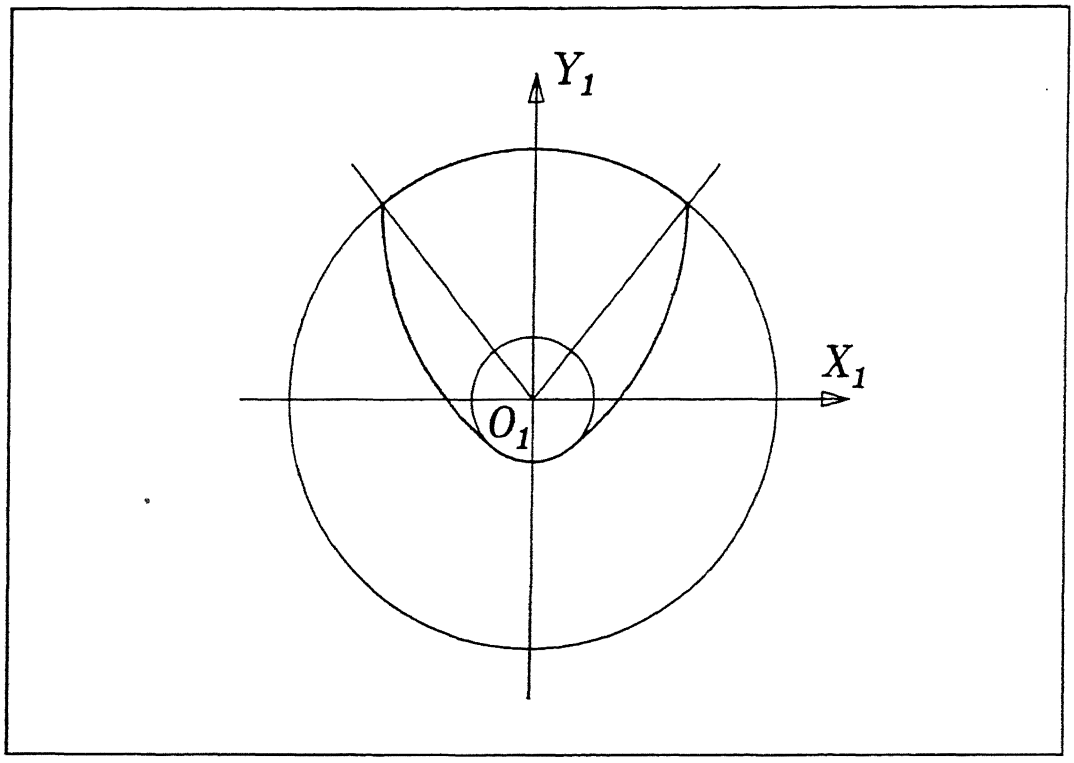

Figure 6-7. A Mono-Lobed Screw I.

The value of r_0 for this case as obtained from Equation (6-42) will be 125 mm. Therefore, the values of the tip and root angles $\alpha = \beta$ are calculated as 77.3648° from Equation (6-41). Table 6-3 describes the parametric equation of the profile of screw I as given in Equation (6-20). The plot of this profile is shown in Figure 6-7 and the generated the cross-sectional profile of screw II using the algorithm given in Section 6.3 is shown in Figure 6-8.

i	p_i	q_i	r_i	u_{i1}	u_{i2}
1	-62.500	78.063	125.000	5.38752	6.28319
2	0.000	0.000	100.000	0.89567	2.24593

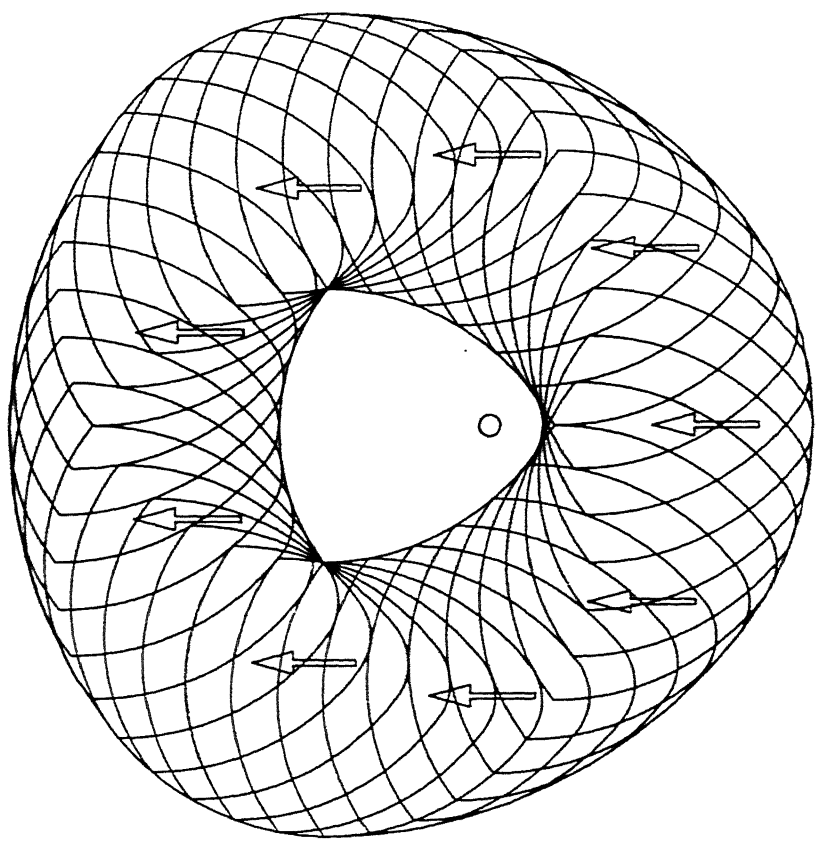

Figure 6-8. Generation of the Profile of Screw II for a Mono-Lobed Screw I

3	62.500	78.063	125.000	3.14159	4.03726
4	0.000	0.000	25.000	4.03726	5.38752

Table 6-3. Biparametric Definition of the Profile Shown in Figure 6-7.

6.4.1.2 Design of a Twin-Screw Extruder of Bi-Lobed Symmetrical Screws

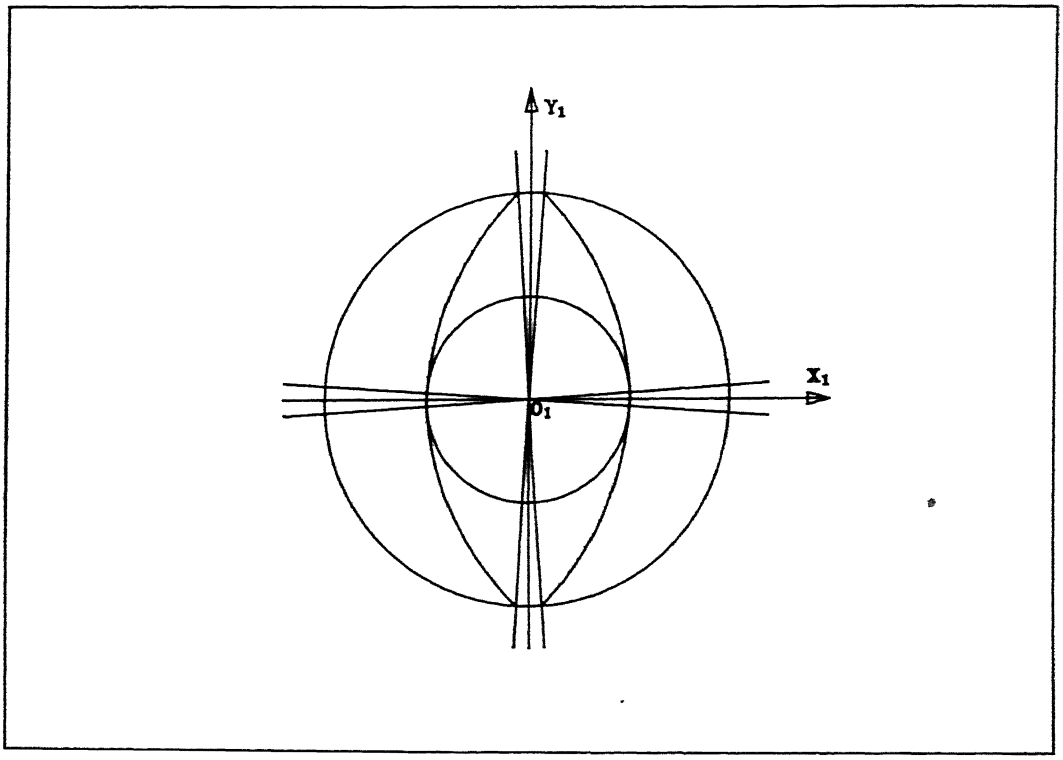

Figure 6-9. A Bi-Lobed Screw I.

Given : The tip radius r = 100 mm.
root radius r_r = 50 mm.
Number of lobes n = 2.

The value of r_0 for this case as obtained from Equation (6-42) will be 150 mm. Therefore, the values of the tip and root angles $\alpha = \beta$ are calculated as 7.18076° from Equation (6-41). Table 6-4 describes the parametric equation of the profile of screw I as

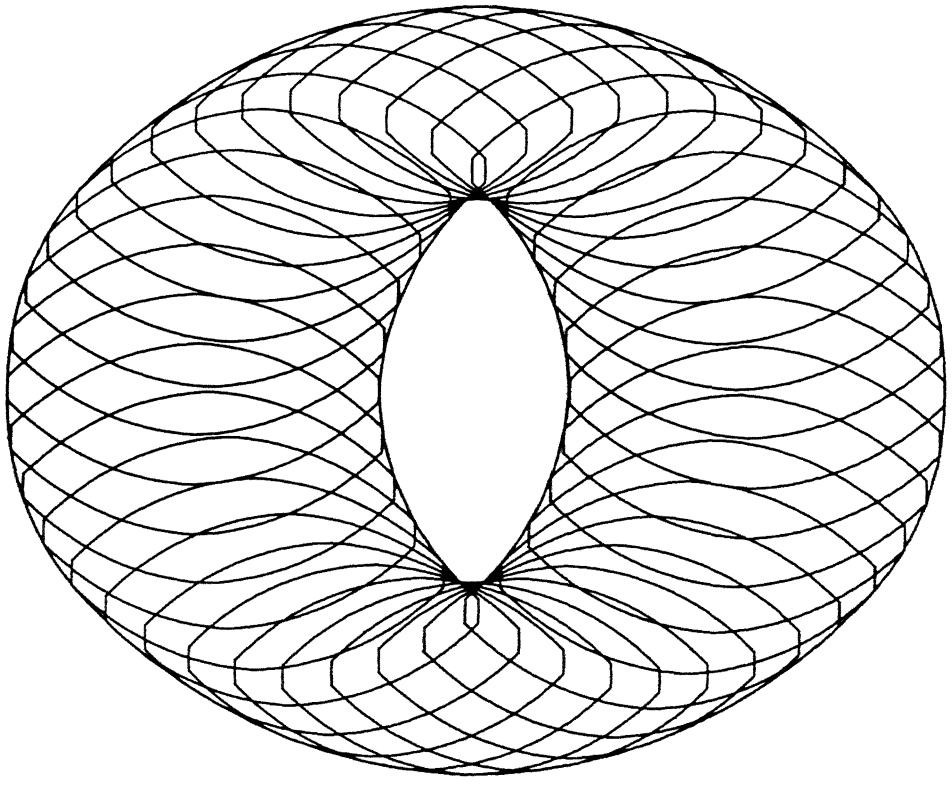

Figure 6-10. Generation of the Profile of Screw II for a Bi-Lobed Screw I

given in Equation (6-20). The plot of this profile is shown in Figure 6-9 and the generated the cross-sectional profile of screw II using the algorithm given in Section 6.3 is shown in Figure 6-10.

i	p_i	q_i	r_i	u_{i1}	u_{i2}
1	-99.804	-6.262	150.000	0.06269	0.78540
2	0.000	0.000	100.000	1.50811	1.63349
3	99.804	-6.262	150.000	2.35619	3.07890
4	0.000	0.000	50.000	3.07890	3.20428
5	99.804	6.262	150.000	3.20428	3.92699
6	0.000	0.000	100.000	4.64970	4.77508
7	-99.804	6.262	150.000	5.49779	6.22049
8	0.000	0.000	50.000	6.22049	6.34587

Table 6-4. Biparametric Definition of the Profile Shown in Figure 6-9.

6.4.1.3 Design of a Twin-Screw Extruder with Bi-Lobed Symmetrical Screws with Sharp Tips

Given : The tip radius $r = 100$ mm.
Tip angle $\alpha = 0°$
Number of lobes $n = 2$.

The value of r_0 for this case as obtained from Equation (6-41) will be 141.414 mm. Therefore, the values of the root diameter r_r of the screws is calculated as 41.414 mm. from Equation (6-42). Table 6-5 describes the parametric equation of the profile of screw I as given in Equation (6-20). The plot of this profile is shown in Figure 6-11 and the generated the cross-sectional profile of screw II using the algorithm given in Section 6.3 is shown in Figure 6-12.

i	p_i	q_i	r_i	u_{i1}	u_{i2}
1	-100.000	0.000	141.414	0.00000	0.78540
2	0.000	0.000	141.414	2.35619	3.14159
3	100.000	0.000	141.414	3.14159	3.92699
4	0.000	0.000	141.414	5.49779	6.28319

Table 6-5. Biparametric Definition of the Profile Shown in Figure 6-11

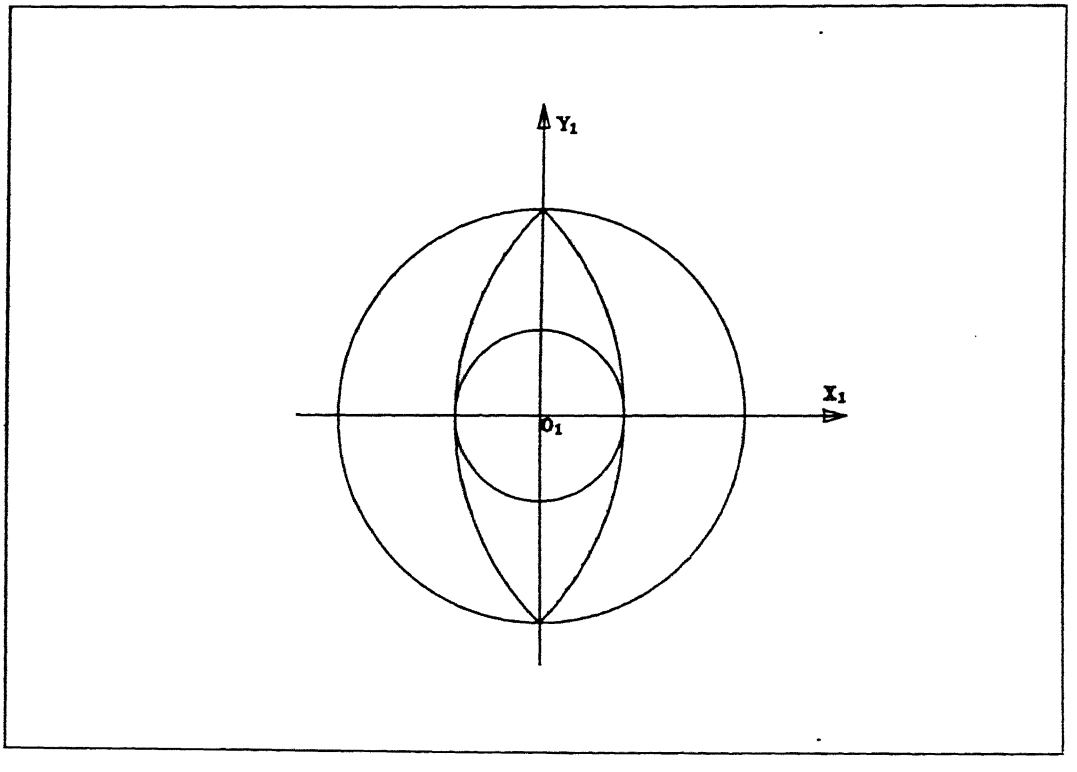

Figure 6-11. A Bi-Lobed Screw I with $\alpha = 0$.

6.4.1.4 Design of a Twin-Screw Extruder with Tri-Lobed Symmetrical Screws

Given : The tip radius r = 100 mm.
Tip angle α = 20°

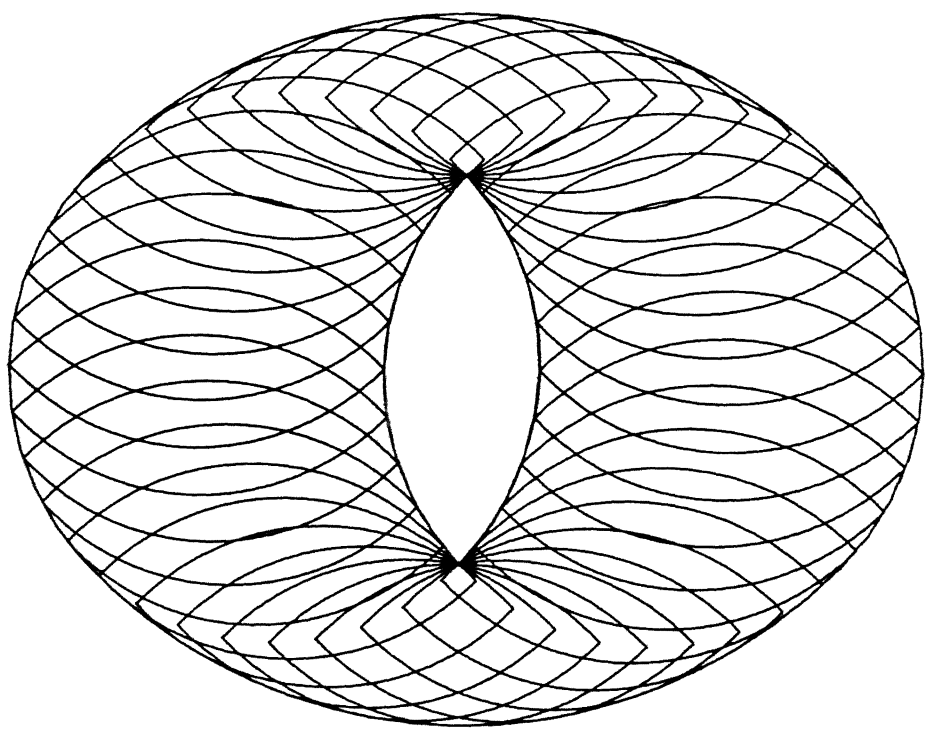

Figure 6-12. Generation of the Profile of Screw II for a Bi-Lobed Screw I

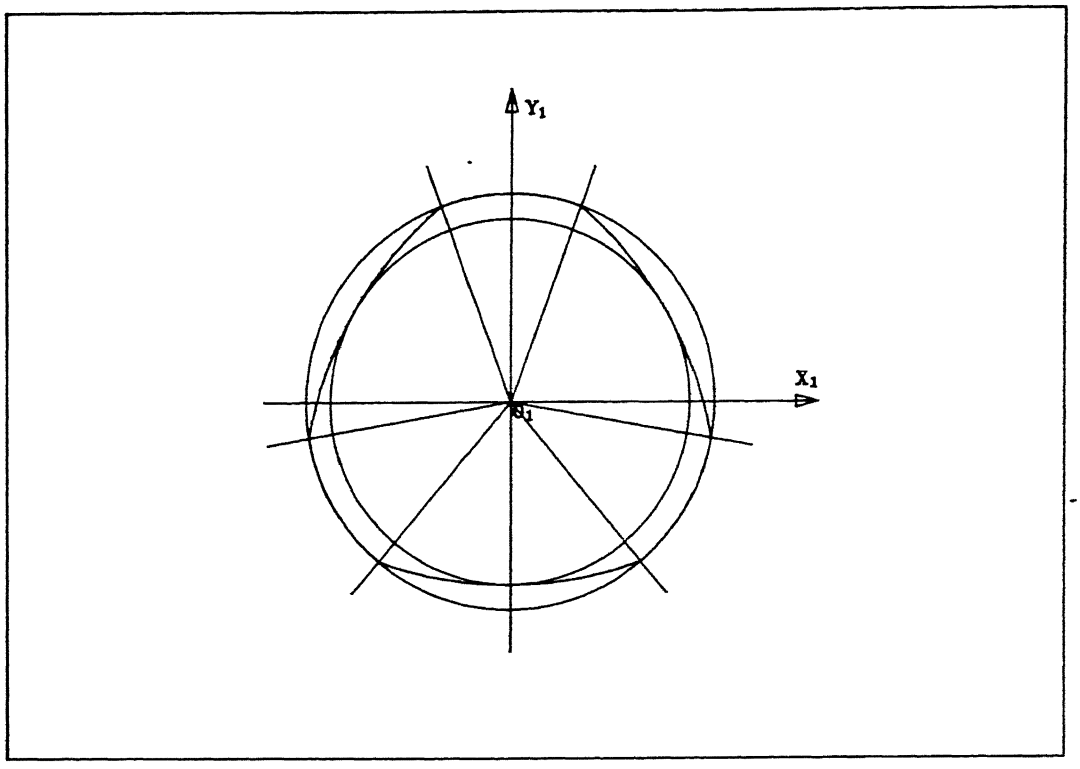

Figure 6-13. A Tri-Lobed Screw I.

Number of lobes $n = 3$.

The value of r_0 for this case as obtained from Equation (6-41) will be 187.939 mm. Therefore, the values of the root diameter r_r of the screws is calculated as 87.939 mm. from Equation (6-42). Table 6-6 describes the parametric equation of the profile of screw I as given in Equation (6-20). The plot of this profile is shown in Figure 6-13 and the generated the cross-sectional profile of screw II using the algorithm given in Section 6.3 is shown in Figure 6-14.

i	p_i	q_i	r_i	$u_{i,1}$	$u_{i,2}$
1	-76.604	-64.279	187.939	0.69813	1.04720
2	0.000	0.000	100.000	1.39626	1.74533
3	76.604	-64.279	187.939	2.09440	2.44346

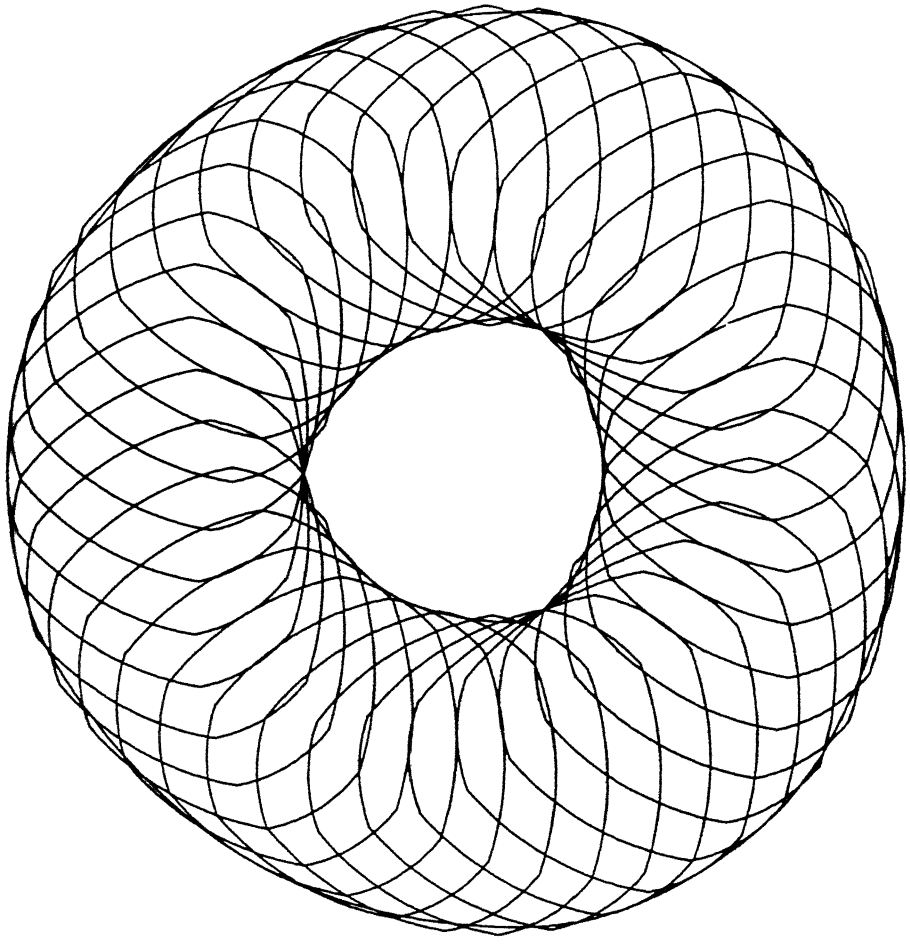

Figure 6-14. Generation of the Profile of Screw II for a Tri-Lobed Screw I

4	0.000	0.000	87.939	2.44346	2.79253
5	93.969	-34.202	187.939	2.79253	3.14159
6	0.000	0.000	100.000	3.49066	3.83972
7	17.365	98.481	187.939	4.18879	4.53786
8	0.000	0.000	87.939	4.53786	4.88692
9	-17.365	98.481	187.939	4.88692	5.23599
10	0.000	0.000	100.000	5.58505	5.93412
11	-93.969	-34.202	187.939	0.00000	0.34907
12	0.000	0.000	87.939	0.34907	0.69813

Table 6-6. Biparametric Definition of the Profile Shown in Figure 6-13.

6.4.1.5 Design of a Twin-Screw Extruder with Quadri-Lobed Symmetrical Screws

Given : The tip radius r = 100 mm.
Tip angle α = 10°
Number of lobes n = 4.

The value of r_0 for this case as obtained from Equation (6-41) will be 190.743 mm. Therefore, the values of the root diameter r_r of the screws is calculated as 90.743 mm. from Equation (6-42). Table 6-7 describes the parametric equation of the profile of screw I as given in Equation (6-20). The plot of this profile is shown in Figure 6-15 and the generated the cross-sectional profile of screw II using the algorithm given in Section 6.3 is shown in Figure 6-16.

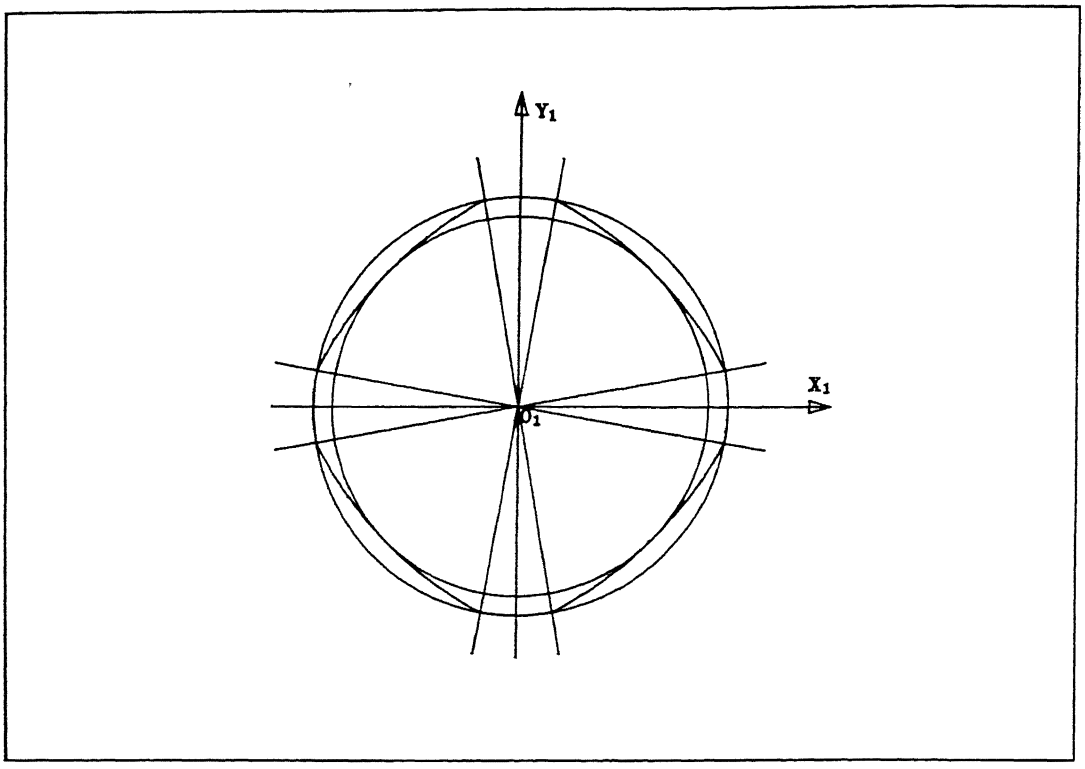

Figure 6-15. A Quadri-Lobed Screw I.

i	p_i	q_i	r_i	u_{i1}	u_{i2}
1	-64.281	-76.603	190.743	0.87264	1.17808
2	0.000	0.000	100.000	1.48352	1.65805
3	64.281	-76.603	190.743	1.96349	2.26893
4	0.000	0.000	90.743	2.26893	2.44344
5	76.603	-64.281	190.743	2.44344	2.74887
6	0.000	0.000	100.000	3.05431	3.22885
7	76.603	64.281	190.743	3.53429	3.83972
8	0.000	0.000	90.743	3.83972	4.01423

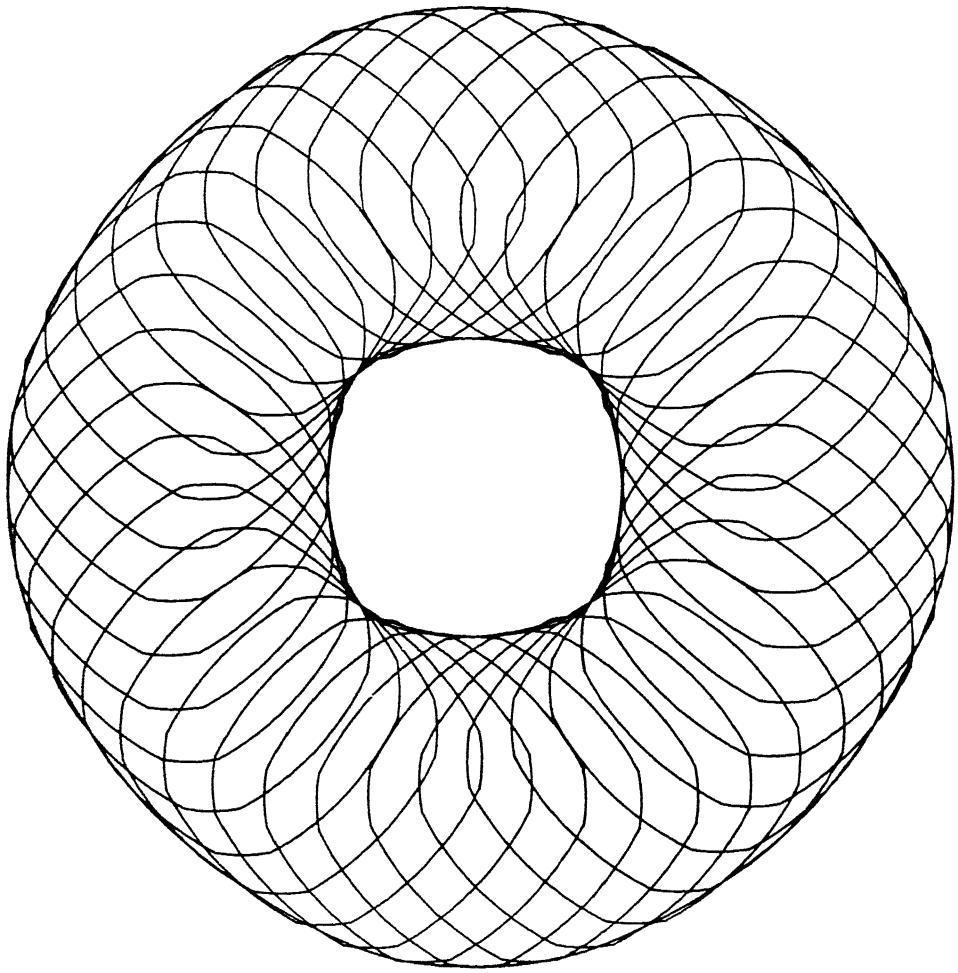

Figure 6-16. Generation of the Profile of Screw II for a Quadri-Lobed Screw I

9	64.281	76.603	190.743	4.01423	4.31967
10	0.000	0.000	100.000	4.62514	4.79964
11	-64.281	76.603	190.743	5.10508	5.41052
12	0.000	0.000	90.743	5.41052	5.58503
13	-76.603	64.281	190.743	5.58503	5.89047
14	0.000	0.000	100.000	6.19591	3.22884
15	-76.603	-64.281	190.743	0.39269	0.69813
16	0.000	0.000	90.743	0.69813	0.87264

Table 6-7. Biparametric Definition of the Profile Shown in Figure 6-15.

From the above five examples, it can be observed that the angular offset between the two screws of a symmetrical screw pair is

0 if n is odd and
π/n if n is even.

6.4.2 Design of a Twin-Screw Extruder of Unsymmetrical Screws of Equal Diameters

Since the diameters of the screws are equal,

$$r_1 = r_2 = r \tag{6-43}$$

As the shapes of these screws will be different, they rotate with unequal speed.

$$m = \frac{\omega_1}{\omega_2} = \frac{n_2}{n_1} \tag{6-44}$$

Therefore, Equations (6-14), (6-15), (6-43) and (6-44) yield

$$\frac{\alpha_1 + \beta_1}{2} = \frac{\pi}{n_1} - (m + 1)\cos^{-1}\left(\frac{r_0}{2r}\right) \qquad \textbf{(6-45)}$$

where $\alpha_1 \geq 0$ and $\beta_1 \geq 0$.

Therefore, the design procedure for this class of screws can be stated as follows:

From the given design specifications, determine the number of lobes n_1, n_2, the tip radius r, the tip and root angles α_1, β_1 and the center distance r_0 using Equation (6-42) and Equation (6-45). Example of a screw pair of this type is illustrated in this section.

6.4.2.1 Design of a Twin-Screw Extruder of Unsymmetrical Screws of Equal Diameters - Bi-Lobed Screw I

Given :

The tip radius	r	=	100 mm.
root radius	r_r	=	55 mm.
Number of lobes	n_1	=	2.
Number of lobes	n_2	=	1.

$$\alpha_1 = \beta_1$$

The value of r_0 for this case as obtained from Equation (6-42) will be 155.000 mm. and $m = 0.5$. From Equation (6-45), it is calculated that $\alpha_1 + \beta_1 = 62.415°$ and hence $\alpha_1 = \beta_1 = 31.208°$. Table 6-8 describes the parametric equation of the profile of screw I in the form given in Equation (6-19). The plot of this profile is shown in Figure 6-17 and the generated the cross-sectional profile of screw II using the algorithm given in Section 6.3 is shown in Figure 6-18.

i	p_i	q_i	r_i	u_{i1}	u_{i2}
1	-99.757	6.965	155.000	6.23824	0.61438
2	0.000	0.000	100.000	1.29846	1.84313
3	99.757	6.965	155.000	2.52722	3.18654
4	99.757	-6.965	155.000	3.09664	3.75597
5	0.000	0.000	100.000	4.44005	4.98473

6	-99.757	-6.965	155.000	5.66881	0.04495

Table 6-8. Biparametric Definition of the Profile Shown in Figure 6-17.

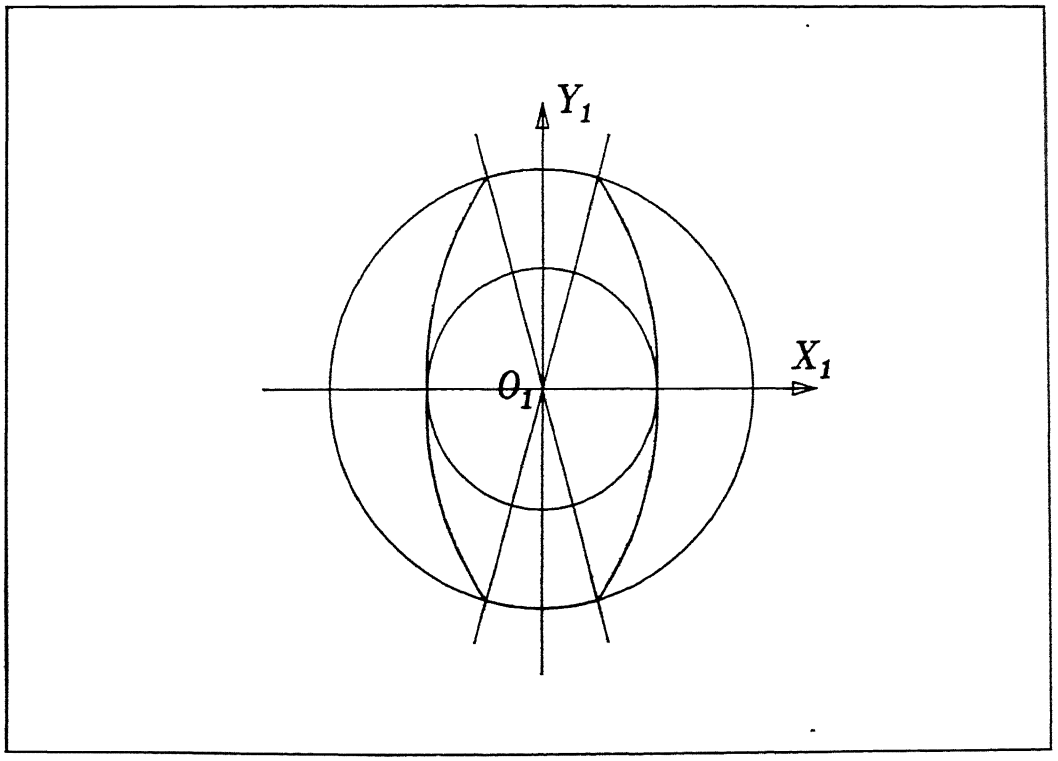

Figure 6-17. A Bi-Lobed Unsymmetrical Screw I.

6.4.3 Design of a Twin-Screw Extruder of Unsymmetrical Screws of Unequal Diameters and Unequal Speeds

These are more general case of screw pairs whose kinematic behavior is controlled by the Equations derived in Sections 6.2.1 and 6.2.2. The design procedure for this can be summarized as below:

From the given design specifications, determine the number of lobes n_1, n_2 the tip radii r_1, r_2, the tip and root angles α_1, β_1, α_2, β_2 and the center distance r_0 using Equations (6-14), (6-15, (6-16), (6-18) and (6-41). This has been explained with the help

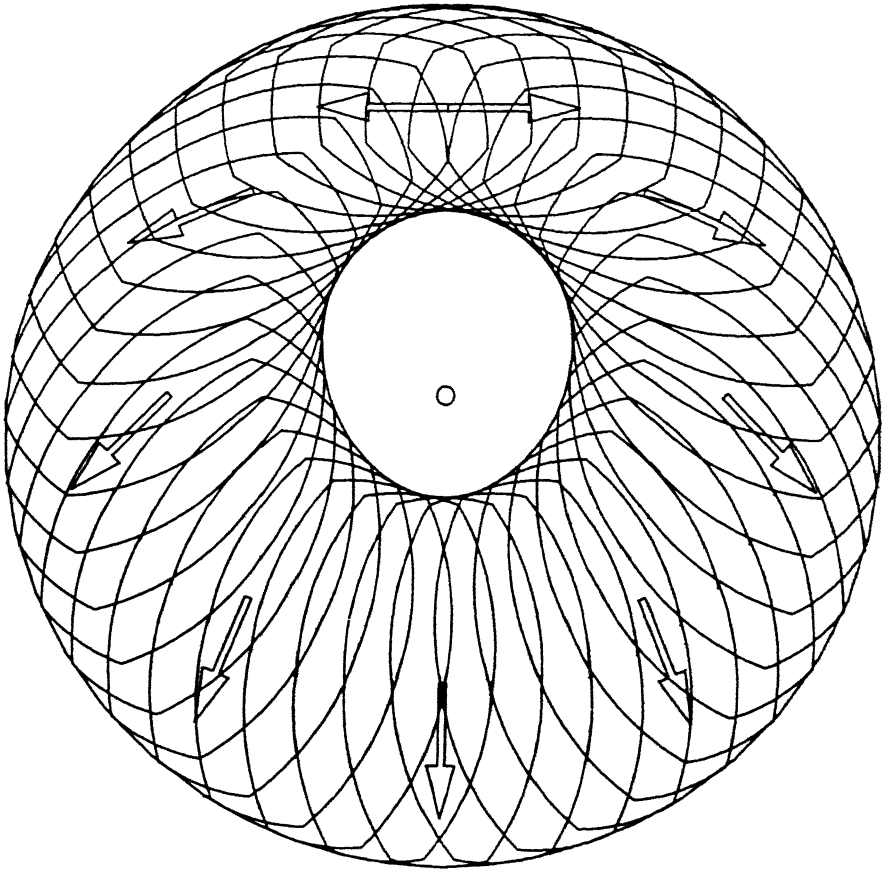

Figure 6-18. Generation of the Profile of Mono-Lobed Screw II for a Bi-Lobed Screw I

of three examples.

6.4.3.1 Design of a Twin-Screw Extruder of Unsymmetrical Screws of Unequal Diameters and Unequal Speeds - Mono-Lobed Screw I and Velocity Ratio m = 2

Given :

The tip radius of Screw I	$r_{t,1}$	= 100 mm.
The tip radius of Screw I	$r_{r,1}$	= 66.667 mm.
Center Distance	r_0	= 200 mm.
Number of lobes	n_1	= 1.
Number of lobes	n_2	= 2.
	$\alpha_1 = \beta_1$	

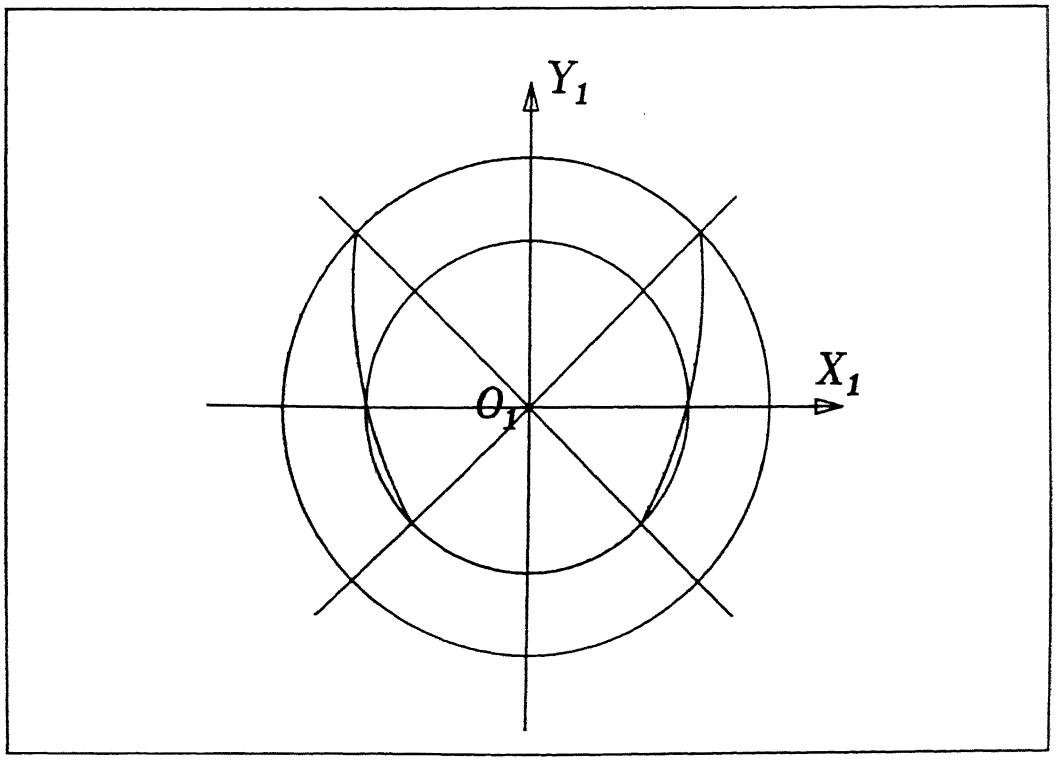

Figure 6-19. A Mono-Lobed Unsymmetrical Screw I for m = 2.

The tip and root radii of screw II $r_{t,2}$ and $r_{r,2}$ for this case are respectively 133.333

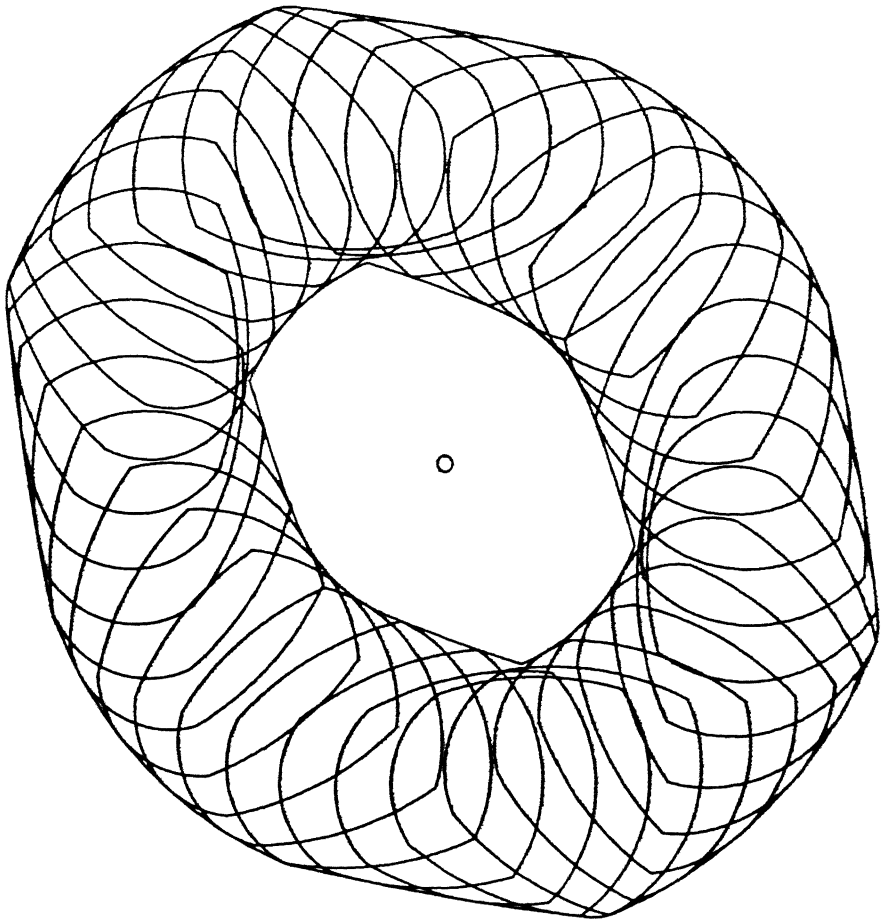

Figure 6-20. Generation of the Profile of Bi-Lobed Screw II for a Mono-Lobed Screw I

mm. and 100.000 mm. as obtained from Equation (6-19). Hence, $m = 2$ and $k_1 = 0.5$ and $k_2 = 0.66667$. From Equation (6-45), it is calculated that $\alpha_1 + \beta_1 = 181.780°$ and hence $\alpha_1 = \beta_1 = 90.895°$. Table 6-9 describes the parametric equation of the profile of screw I in the form given in Equation (6-20). The plot of this profile is shown in Figure 6-19 and the generated the cross-sectional profile of screw II using the algorithm given in Section 6.3 is shown in Figure 6-20.

i	p_i	q_i	r_i	u_{i1}	u_{i2}
1	0.000	0.000	100.000	0.77759	2.36401
2	127.690	49.697	200.000	3.03912	3.64491
3	0.000	0.000	66.667	3.91918	5.50560
4	-127.000	49.697	200.000	5.77986	6.38566

Table 6-9. Biparametric Definition of the Profile Shown in Figure 6-19.

6.4.3.2 Design of a Twin-Screw Extruder of Unsymmetrical Screws of Unequal Diameters and Unequal Speeds - Mono-Lobed Screw I and Velocity Ratio m = 3

Given :

The tip radius of Screw I	$r_{t,1}$	=	100 mm.
The tip radius of Screw I	$r_{r,1}$	=	26.667 mm.
Center Distance	r_0	=	266.667 mm.
Number of lobes	n_1	=	1.
Number of lobes	n_2	=	3.
Number of lobes	α_1	=	16.757°.
Number of lobes	β_1	=	16.757°.

The given data fully describe the specifications for screw I and the relative motions. Table 6-10 describes the parametric equation of the profile of screw I in the form given in Equation (6-20). The plot of this profile is shown in Figure 6-21 and the generated the cross-sectional profile of screw II using the algorithm given in Section 6.3 is shown in Figure 6-22.

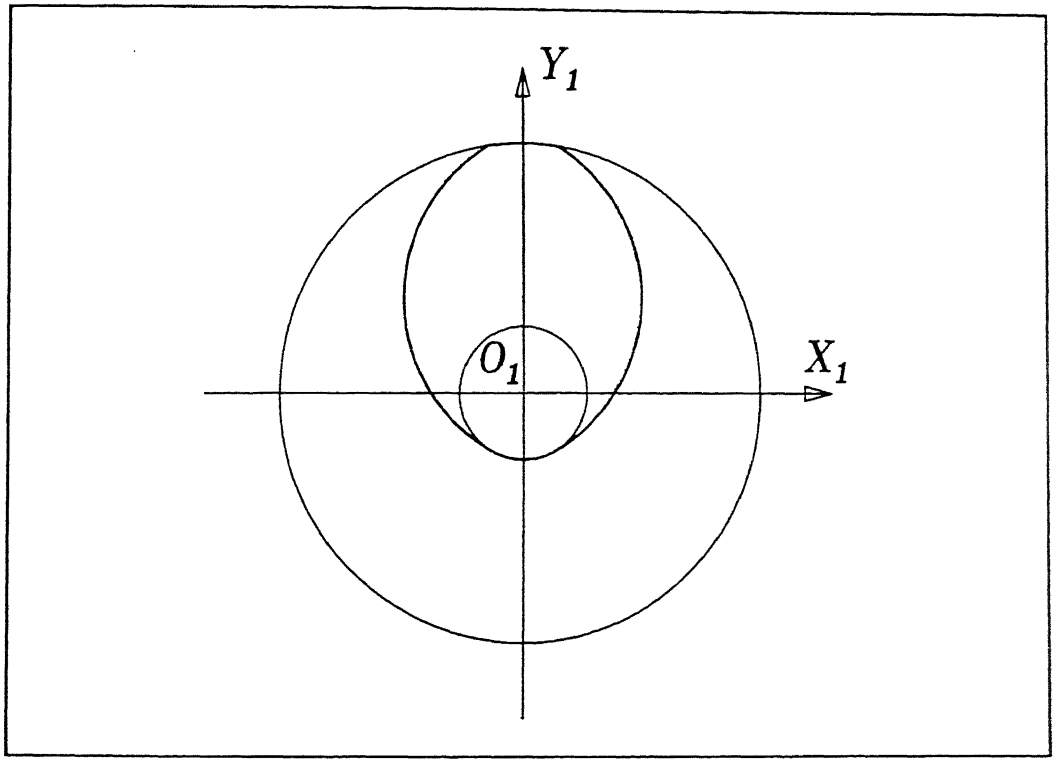

Figure 6-21. A Mono-Lobed Unsymmetrical Screw I for m = 3.

i	p_i	q_i	r_i	u_{i1}	u_{i2}
1	0.000	0.000	100.000	1.42456	1.71703
2	20.343	38.262	70.000	2.09298	4.22348
3	0.000	0.000	26.667	4.22348	5.20130
4	-20.343	38.262	70.000	5.20130	7.33180

Table 6-10. Biparametric Definition of the Profile Shown in Figure 6-21.

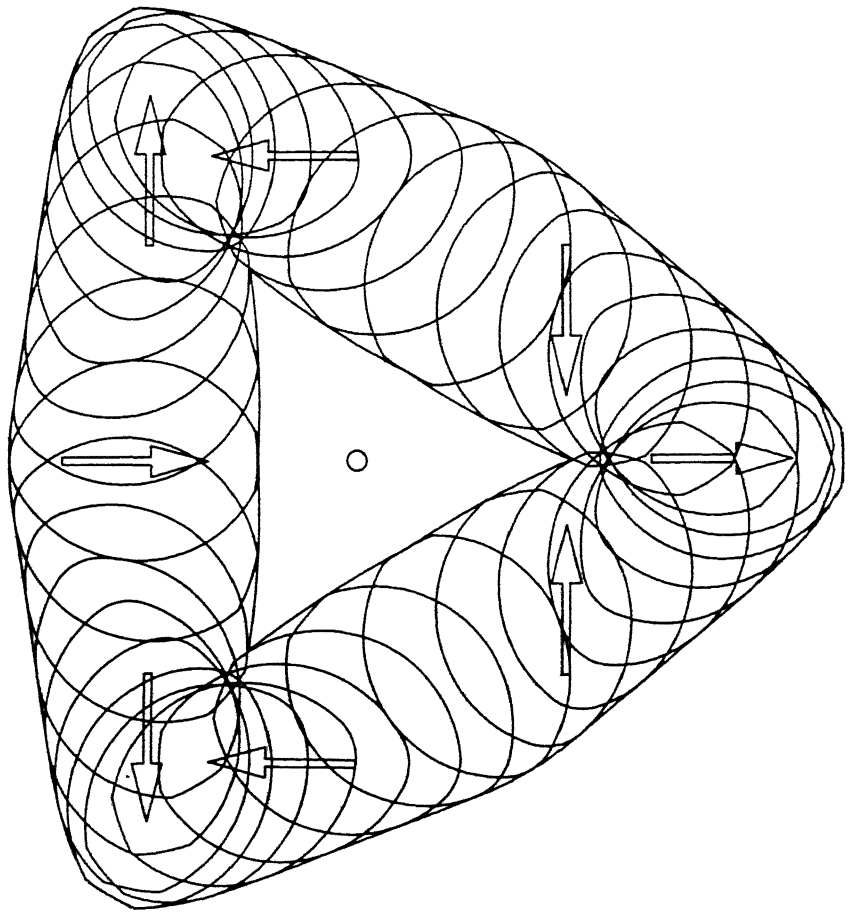

Figure 6-22. Generation of the Profile of Tri-Lobed Screw II for a Mono-Lobed Screw I

6.4.3.3 Design of a Twin-Screw Extruder of Unsymmetrical Screws of Unequal Diameters and Unequal Speeds - Mono-Lobed Screw I and Velocity Ratio m = 4

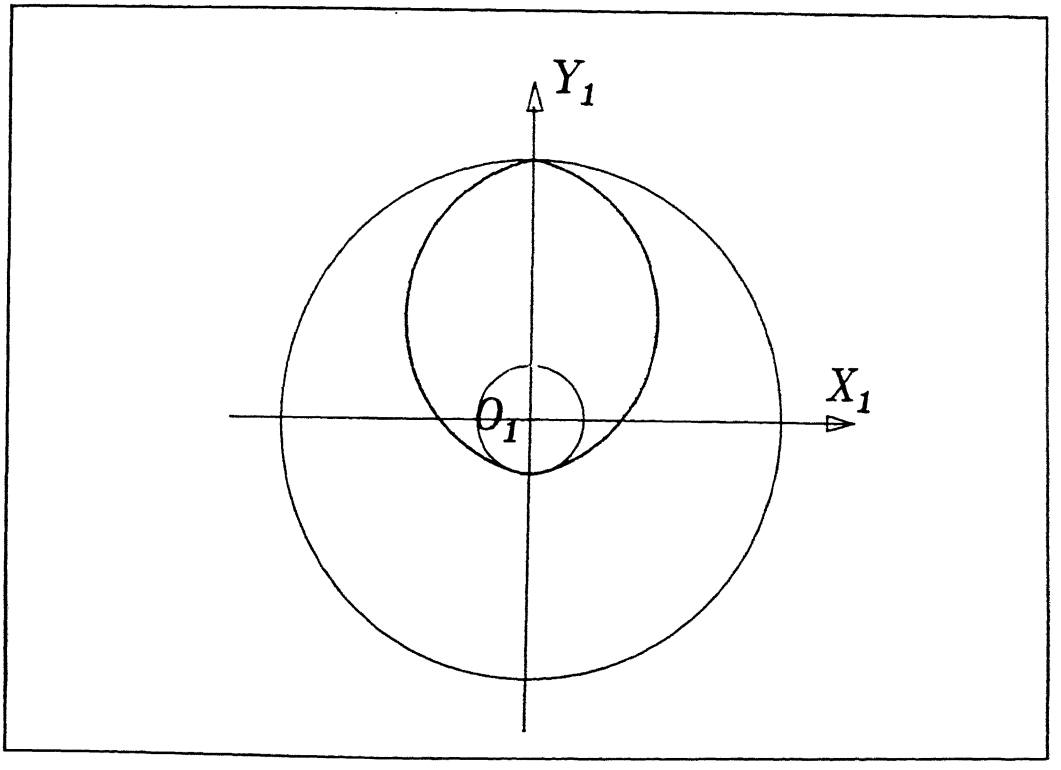

Figure 6-23. A Mono-Lobed Unsymmetrical Screw I for m = 4.

Given :

The tip radius of Screw I	$r_{t,1}$	=	100 mm.
The tip radius of Screw I	$r_{r,1}$	=	20.833 mm.
Center Distance	r_0	=	208.333 mm.
Number of lobes	n_1	=	1.
Number of lobes	n_2	=	4.
Number of lobes	α_1	=	0.34172°.
Number of lobes	β_1	=	0.34172°.

The given data fully describe the specifications for screw 1 and the relative motions. Table 6-11 describes the parametric equation of the profile of screw I in the form given in Equation (6-20). The plot of this profile is shown in Figure 6-23 and the

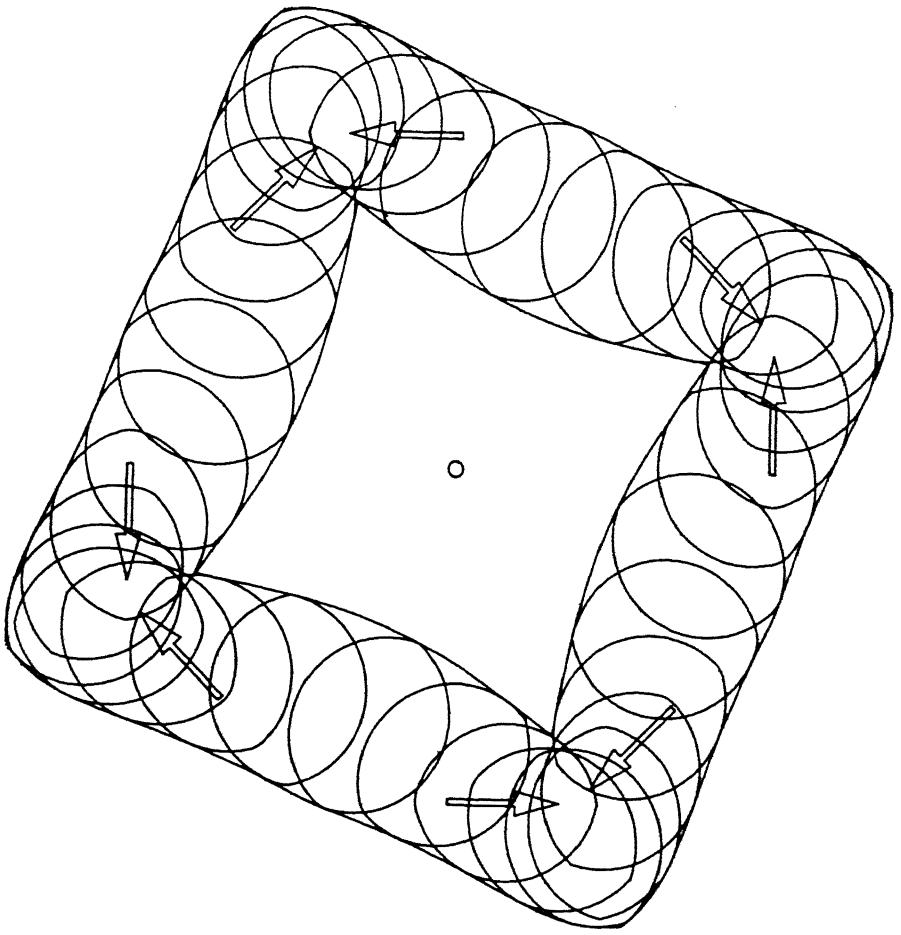

Figure 6-24. Generation of the Profile of Quadri-Lobed Screw II for a Mono-Lobed Screw I

generated the cross-sectional profile of screw II using the algorithm given in Section 6.3 is shown in Figure 6-24.

i	p_i	q_i	r_i	u_{i1}	u_{i2}
1	0.000	0.000	100.000	1.56781	1.57378
2	12.287	39.290	62.000	1.77520	4.40927
3	0.000	0.000	20.833	4.40927	5.01557
4	-12.287	39.290	62.000	5.01557	7.64958

Table 6-11. Biparametric Definition of the Profile Shown in Figure 6-23.

Chapter 7

MANUFACTURE OF EXTRUDER SCREW SURFACES

7.1 Introduction

The design of cutters for the manufacture of helicoidal surfaces such as the ones used in the extruder screws is an important area of research. These surfaces are manufactured mostly by milling processes using form cutters of the end mill type, the side mill type or the side-and-face mill type (i.e., disc type). The problem of design of cutters for machining helicoidal surfaces is not yet satisfactorily solved (Saybold, 1992). In this chapter, a methodology is proposed to solve this problem. Using this method, one can determine the two-dimensional profile of the cutter from the given cross-sectional profile of a helicoidal surface. This two-dimensional profile is similar to the profile of the generic cutter described in Chapter 4. The proposed methodology can also be used to determine the shape of the cross-sectional profile and hence the helicoidal surface that will be obtained using a given cutter. The problems of the design of both the end mill type and disc type cutters have been solved. The algorithm proposed for the design of the end mill type cutters is also valid for the design of form turning tools if it is required to realize the helicoidal surface by a turning process.

7.2 Methodology

Let ${}^{2}\underset{\sim}{g}(u)$ be the cross-sectional profile of the helicoidal surface which can be considered to be a set of C^1-continuous arc segments as given below :

$$ {}^{2}\underset{\sim}{g} = [\, x_2 \quad y_2 \quad 0 \quad 1 \,] \qquad (7\text{-}1) $$

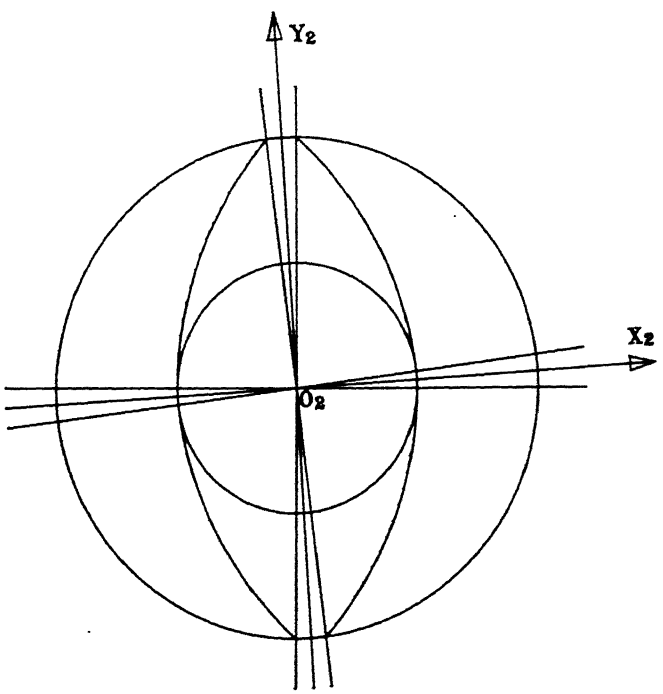

Figure 7-1. Cross-Sectional Profile of a Bi-Lobed Extruder Screw

where,

$$x_2 = p_i + r_i \cos u_i$$
$$y_2 = q_i + r_i \sin u_i$$
$$u_{i1} \le u_i \le u_{i2}$$
$$1 \le i \le 4n$$

Let S_0 (O_0- X_0, Y_0, Z_0) be a fixed coordinate frame and let S_2 (O_2- X_2, Y_2, Z_2) be a coordinate frame to which the profile ${}^2\underset{\sim}{g}(u)$ is initially attached in the X_2 - Y_2 plane as shown in Figure 7-1. If ${}^2\underset{\sim}{g}(u)$ is considered to be a generatrix of the helicoidal surface then by applying the following helical sweep to the generatrix, we can obtain the helicoidal surface ${}^0\underset{\sim}{p}(u, v)$. Note that p is the pitch of the helix.

$${}^0\underset{\sim}{p}(u, v) = {}^2\underset{\sim}{g}(u) \begin{bmatrix} \cos v & \sin v & 0 & 0 \\ -\sin v & \cos v & 0 & 0 \\ 0 & 0 & 1 & 0 \\ 0 & 0 & \frac{pv}{2\pi} & 1 \end{bmatrix} \qquad (7\text{-}2)$$

On the other hand, we can consider a plane X_c - Z_c that cuts the helicoidal surface normal to the helix (Figure 7-2). If this plane is moved along the axis of the helix, at an appropriate position, the cross-section of the helicoidal surface captured on this plane will be the cutter profile. The same helicoidal surface as the one given by Equation (7-2) will be obtained if this profile of the cutter, say ${}^c\underset{\sim}{g}(u)$, is given exactly the same helical sweep.

$${}^0\underset{\sim}{p}(u, v) = {}^c\underset{\sim}{g}(u) \begin{bmatrix} \cos v & \sin v & 0 & 0 \\ -\sin v & \cos v & 0 & 0 \\ 0 & 0 & 1 & 0 \\ 0 & 0 & \frac{pv}{2\pi} & 1 \end{bmatrix} \qquad (7\text{-}3)$$

From this, it is evident that every point of the profile ${}^2\underset{\sim}{g}(u)$ can be mapped onto the profile ${}^c\underset{\sim}{g}(u)$ and vice-versa. Therefore, if a helicoidal surface is known, one can obtain the surface of the cutter that can be used to machine it and one can also determine the geometry of a helicoidal surface that will be produced by a given cutter.

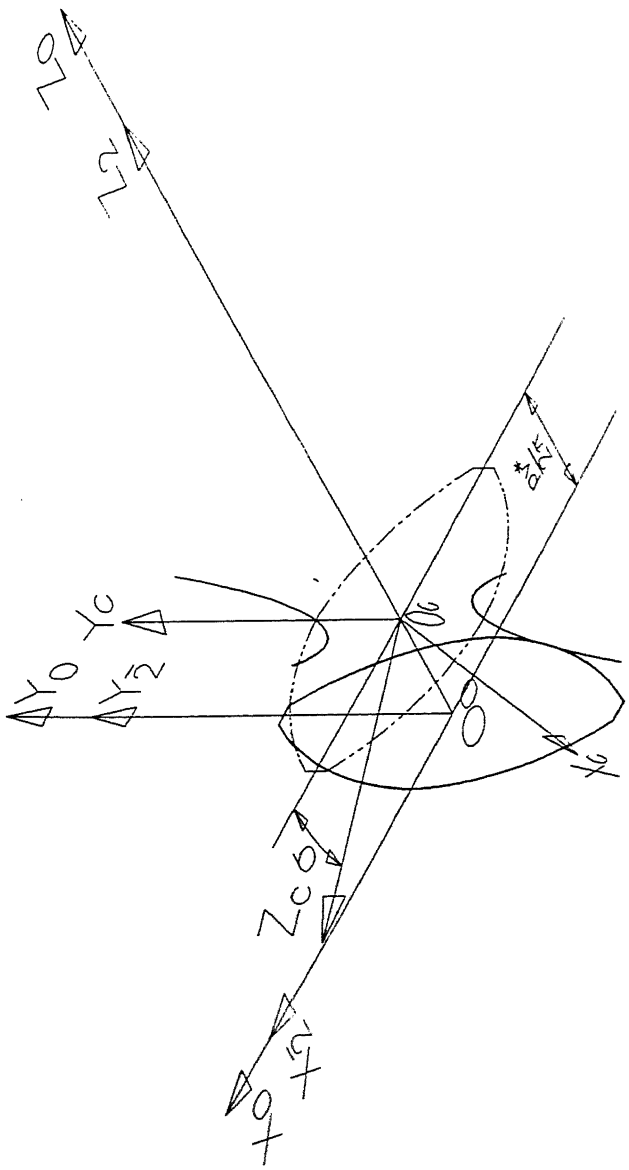

Figure 7-2. Coordinate Systems S_0, S_2 and S_c

7.2.1 Definition of the S_2 and S_c Coordinate Frames

As shown in Figures 7-1 and 7-2, S_0 (O_0- X_0, Y_0, Z_0) is a fixed frame of reference attached to the helicoidal surface. The cross-sectional profile ${}^2\underset{\sim}{g}(u)$ initially coincides with the X_0 - Y_0 plane. It is given a helical sweep described by the sweep parameter v and the pitch of the helix p in order to obtain the helicoidal surface. Let σ be the lead angle of the helix. If r is the tip radius of the cross-sectional profile ${}^2\underset{\sim}{g}(u)$, then

$$\sigma = \tan^{-1}\frac{p}{2\pi r} \tag{7-4}$$

Consider another coordinate frame S_c (O_c- X_c, Y_c, Z_c) which is obtained by applying the following two transformations to the S_0 system :

i) A rotation about Y_0 axis by an angle of $\frac{\pi}{2} + \sigma$ and

ii) A translation along Z_0 axis by a distance of $\frac{p v^*}{2\pi}$

where

$$v^* = \frac{\pi}{n} \tag{7-5}$$

Therefore any point ${}^c\underset{\sim}{p}$ in the S_c space can be mapped in the S_0 space using the following relation :

$${}^0\underset{\sim}{p} = {}^c\underset{\sim}{g}\begin{bmatrix} -\sin\sigma & 0 & -\cos\sigma & 0 \\ 0 & 1 & 0 & 0 \\ \cos\sigma & 0 & -\sin\sigma & 0 \\ 0 & 0 & \frac{p v^*}{2\pi} & 1 \end{bmatrix} \tag{7-6}$$

The initial shape of the blank on which the helicoidal surface is machined will be a cylindrical block of radius r which is the tip radius of the cross-sectional profile ${}^2\underset{\sim}{g}(u)$. The shape of the cutter profile will be decided by the root and flank arcs of the

cross-sectional profile. When $v = v^*$, the mid-point of the root arc of the cross-sectional profile will lie in the Y_c axis. Hence, the profile of the cutter will be fully obtained in the X_c - Y_c plane by finding the intersection curve of this plane with the helicoidal surface. It is enough to consider the range of v between

$$v^* - \frac{\pi}{n} \quad \text{and} \quad v^* + \frac{\pi}{n}$$

7.2.2 Determination of the Profile of the Cutter ${}^{c}\underset{\sim}{g}(u)$ Lying on a Plane Parallel to and at a Distance of w from the X_c - Y_c Plane from the given cross-sectional profile ${}^{2}\underset{\sim}{g}(u)$

The x_0, y_0 and z_0 coordinates of the helicoidal surface in terms of the cross-sectional profile ${}^{2}\underset{\sim}{g}(u)$ can be written from Equation (7-2) as

$$\begin{aligned} x_0 &= x_2 \cos v - y_2 \sin v \\ y_0 &= x_2 \sin v + y_2 \cos v \\ z_0 &= \frac{p\,v}{2\pi} \end{aligned} \tag{7-7}$$

From Equation (7-6), one can write the equation of the plane parallel to and at a distance of w from X_c - Y_c as

$$\begin{aligned} x_0 &= -x_c \sin\sigma + w \cos\sigma \\ y_0 &= y_c \\ z_0 &= \frac{p\,v^*}{2\pi} - x_c \cos\sigma - w \sin\sigma \end{aligned} \tag{7-8}$$

The profile of the cutter which is the intersection curve between the helicoidal surface and the above plane will be obtained by solving the Equations (7-7) and (7-8) for x_c and y_c as follows :

From the expressions for x_0 and y_0 of the above two equations, one can solve for x_c and y_c as

$$x_c = \frac{w}{\tan\sigma} - \frac{x_2 \cos v - y_2 \sin v}{\sin\sigma}$$
$$y_c = x_2 \sin v + y_2 \cos v \qquad (7\text{-}9)$$

Substituting these values of x_c and y_c in the z_0 expressions, we get the following equation in v.

$$y_2 \sin v - x_2 \cos v + \frac{p \tan\sigma}{2\pi} v + \left(w - \frac{p \tan\sigma}{2\pi} v^* \right) = 0 \qquad (7\text{-}10)$$

The solution of the above equation has to be found numerically to find the value of v for a given set of values. Once v is thus known, the corresponding point of the cutter profile (x_c, y_c) can be calculated. It is observed that the convergence of the solution is assured if v^* is given as the starting value for v in the iterative process.

7.2.3 Determination of the Cross-sectional Profile of the Helicoidal Surface ${}^2\underset{\sim}{g}(u)$ from the given profile of the Cutter ${}^c\underset{\sim}{g}(u)$ at $w = 0$

By comparing the expressions of Equations (7-8) and (7-9), we can find the value of v as

$$v = v^* - \frac{2\pi}{p} x_c \cos\sigma \qquad (7\text{-}11)$$

Again comparing the expressions for x_0 and y_0 of Equations (7-8) and (7-9), we can obtain the cross-sectional profile of the screw ${}^2\underset{\sim}{g}(u)$ as

$$x_2 = y_c \sin v - x_c \sin\sigma \cos v$$
$$y_2 = y_c \cos v + x_c \sin\sigma \sin v \qquad (7\text{-}12)$$

where

$$v = v^* - \frac{2\pi}{p} x_c \cos\sigma$$

7.3 Illustrative Examples for the Design of End Milling Cutters

In this section, the methodology described in Section 7.2.2 will be used to determine the cutter profile at X_c - Y_c plane (i.e at w = 0). An end milling cutter to machine the helicoidal surface will be a surface of revolution of this profile about the Y_c axis. The method of obtaining the cutter profile for this case will be illustrated by means of examples for the machining of extruder screws.

7.3.1 Design of an End Milling Cutter for the Machining of a Mono-Lobed Extruder Screw

The cross-sectional profile of a mono-lobed extruder screw is similar to the one shown in Figure 6-7. It has a tip radius of 100 mm. and a root radius of 66.667 mm. As mentioned earlier, only the root and flank arcs influence the design and the tip arc is realized in the preparation of the blank. The dimensions of one root arc and the two flank arcs adjacent to it are given in Table 7-1.

i	p_i	q_i	r_i	u_{i1}	u_{i2}
3	113.855	69.389	200.000	3.22844	3.68893
4	0.000	0.000	66.667	3.68893	5.73585
1	-113.855	69.389	200.000	5.73585	6.19634

Table 7-1. Biparametric Definition of the Root and Adjacent Flank Arcs of a Mono-Lobed Extruder Screw.

Using the method described above, the profile of the cutter was calculated for pitch p = 75 mm., p = 150 mm. and p = 225 mm. and the plots of these three profiles are shown in Figure 7-3. The coordinates of the cutter profile is listed in Table 7-2.

p = 75 mm.		p = 150 mm.		p = 225 mm.	
x_c	y_c	x_c	y_c	x_c	y_c
-25.105	99.956	-49.179	99.346	-71.330	97.066

-24.174	94.623	-47.249	94.029	-68.296	91.824
-23.169	89.549	-45.177	88.975	-65.067	86.864
-22.083	84.792	-42.951	84.244	-61.633	82.248
-20.907	80.417	-40.563	79.902	-57.988	78.044
-19.639	76.502	-38.006	76.027	-54.135	74.330
-18.274	73.129	-35.283	72.701	-50.088	71.186
-16.819	70.383	-32.408	70.008	-45.874	68.692
-15.289	68.346	-29.410	68.028	-41.536	66.920
-13.700	67.086	-26.326	66.827	-37.130	65.928
-12.082	66.651	-23.208	66.449	-32.721	65.748
-12.046	66.651	-23.140	66.450	-32.625	65.753
-9.937	66.657	-18.512	66.530	-26.107	66.083
-7.227	66.661	-13.884	66.589	-19.584	66.339
-4.818	66.664	-9.257	66.632	-13.058	66.521
-2.410	66.666	-4.628	66.658	-6.530	66.630
0.001	66.667	0.000	66.667	0.000	66.667
2.410	66.666	4.628	66.658	6.530	66.630
4.818	66.664	9.257	66.632	13.058	66.521
7.227	66.661	13.884	66.589	19.584	66.339
9.637	66.657	18.512	66.530	26.107	66.083
12.046	66.651	23.140	66.450	32.625	65.753
12.082	66.651	23.208	66.449	32.721	65.748
13.700	67.086	26.326	66.830	37.130	65.928
15.289	68.346	29.410	68.028	41.536	66.920
16.819	70.383	32.408	70.008	45.874	68.692
18.274	73.129	35.283	72.701	50.088	71.186

19.639	76.502	38.006	76.027	54.135	74.330
20.909	80.417	40.563	79.902	57.988	78.044
22.082	84.792	42.951	84.244	61.633	82.248
23.169	89.549	45.177	88.975	65.067	86.864
24.174	94.623	47.249	94.029	68.296	91.824
25.105	99.956	49.179	99.346	71.330	97.066

Table 7-2 Coordinates of the Profile of the Cutter to Machine the Mono-Lobed Extruder Screw

Since there is only one flute on this screw, the full helicoidal surface will be obtained in one steps.

7.3.2 Design of an End Milling Cutter for the Machining of a Bi-Lobed Extruder Screw

The cross-sectional profile of a bi-lobed extruder screw is similar to the one shown in Figure 6-9. It has a tip radius of 100 mm. and a root radius of 75 mm. As mentioned earlier, only the root and flank arcs influence the design and the tip arc is realized in the preparation of the blank. The dimensions of one root arc and the two flank arcs adjacent to it are given in Table 7-3.

i	p_i	q_i	r_i	u_{i1}	u_{i2}
7	-92.388	38.268	175.000	5.38513	5.89049
8	0.000	0.000	75.000	5.89049	6.67588
1	-92.388	-38.268	175.000	6.67588	7.18124

Table 7-3. Biparametric Definition of the Root and Adjacent Flank Arcs of a Bi-Lobed Extruder Screw.

Using the method described above, the profile of the cutter was calculated for pitch p=75 mm., p=150 mm. and p=225 mm. and the plots of these three profiles are shown in Figure 7-4. The coordinates of the cutter profile is listed in Table 7-4.

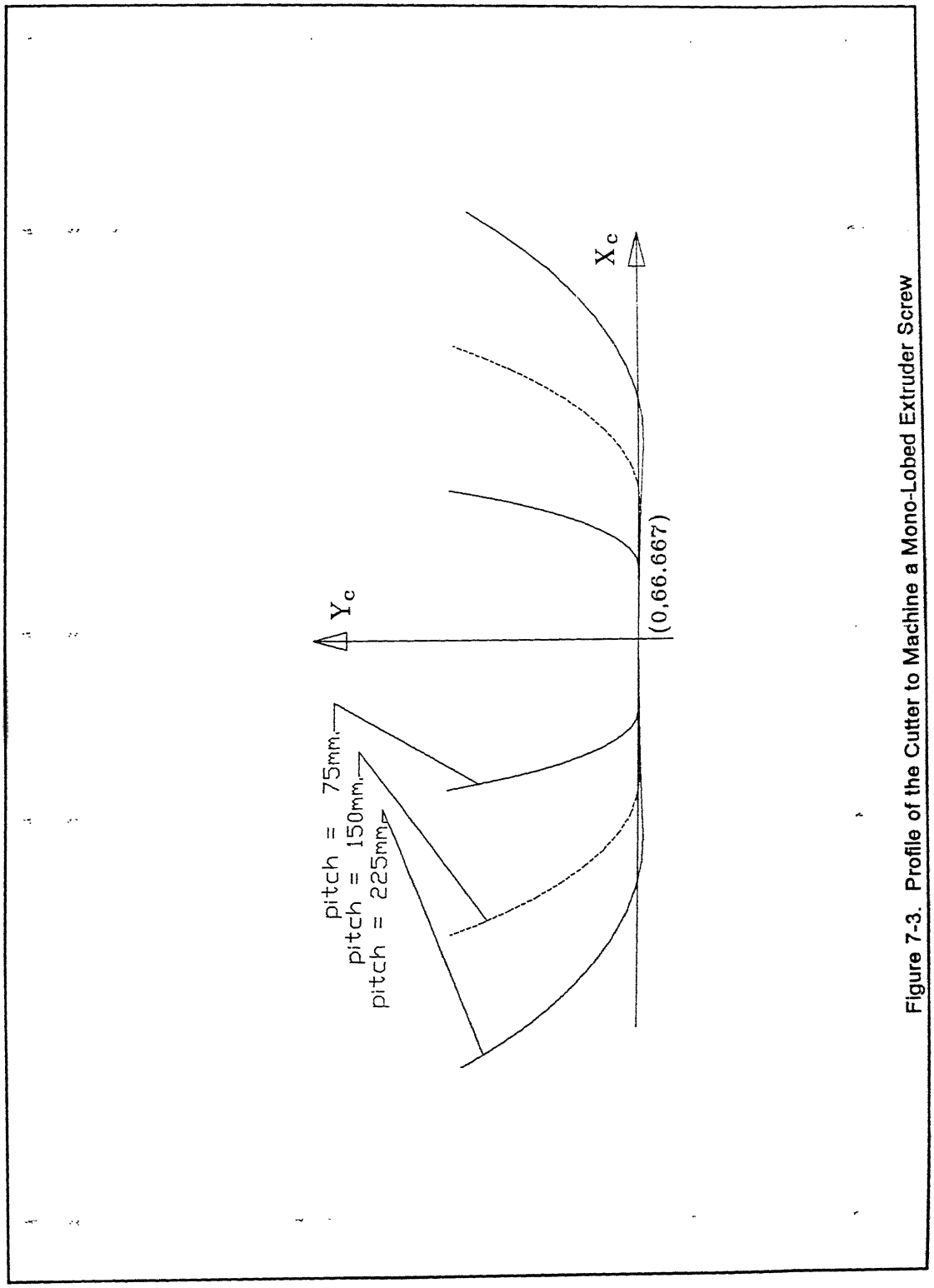

Figure 7-3. Profile of the Cutter to Machine a Mono-Lobed Extruder Screw

p = 75 mm.		p = 150 mm		p = 225 mm	
x_c	y_c	x_c	y_c	x_c	y_c
-17.115	99.979	-36.530	99.639	-58.194	93.799
-16.154	95.809	-34.547	95.492	-54.843	90.026
-15.132	91.888	-32.430	91.596	-51.221	86.568
-14.048	88.258	-30.169	87.995	-47.307	83.470
-12.898	84.966	-27.756	84.735	-43.089	80.780
-11.682	82.064	-25.188	81.867	-38.562	78.540
-10.402	79.600	-22.467	79.438	-33.745	76.792
-9.063	77.623	-19.605	77.497	-28.673	75.566
-7.676	76.176	-16.623	76.084	-23.406	74.883
-6.254	75.294	-13.552	75.231	-18.021	74.754
-4.813	74.998	-10.432	74.961	-18.022	74.754
-4.812	74.998	-10.431	74.961	-14.416	74.842
-3.849	74.999	-8.345	74.975	-10.812	74.911
-2.886	74.999	-6.259	74.986	-7.208	74.961
-1.925	75.000	-4.172	74.994	-3.604	74.990
-0.963	75.000	-2.086	74.998	0.000	75.000
0.000	75.000	0.000	75.000	3.604	74.990
0.963	75.000	2.086	74.998	7.207	74.961
1.925	75.000	4.172	74.994	10.811	74.911
2.886	74.999	6.258	74.986	14.416	74.842
3.849	74.999	8.345	74.975	18.022	74.854
4.812	74.998	10.431	74.961	18.022	74.754
4.813	74.998	10.431	74.961	23.406	74.883
6.254	75.294	13.553	75.231	28.674	75.566

7.676	76.176	16.624	76.084	33.745	76.792
9.063	77.623	19.605	77.497	38.563	78.540
10.402	79.600	22.467	79.438	43.088	80.780
11.681	82.064	25.187	81.867	47.308	83.470
12.898	84.966	27.756	84.735	51.221	86.568
14.048	88.258	30.169	87.995	54.842	90.026
15.133	91.888	32.430	91.596	58.193	93.799
16.154	95.809	34.547	95.492		
17.114	99.979	36.530	99.639		

Table 7-4 Coordinates of the Profile of the Cutter to Machine the Bi-Lobed Extruder Screw

Since there are two flutes for this screw, the full helicoidal surface will be obtained in two steps. The blank will be indexed by π radian while machining the second flute.

7.3.3 Design of an End Milling Cutter for the Machining of a Tri-Lobed Extruder Screw

The cross-sectional profile of a bi-lobed extruder screw is similar to the one shown in Figure 6-11. It has a tip radius of 100 mm. and a root radius of 87.939 mm. As mentioned earlier, only the root and flank arcs influence the design and the tip arc is realized in the preparation of the blank. The dimensions of one root arc and the two flank arcs adjacent to it are given in Table 7-5.

i	p_i	q_i	r_i	u_{i1}	u_{i2}
7	-93.969	-34.202	187.939	0.00000	0.34907
8	0.000	0.000	87.939	0.34907	0.69813
1	-76.604	-64.279	187.939	0.69813	1.04720

Table 7-5. Biparametric Definition of the Root and Adjacent Flank Arcs of a Tri-Lobed Extruder Screw.

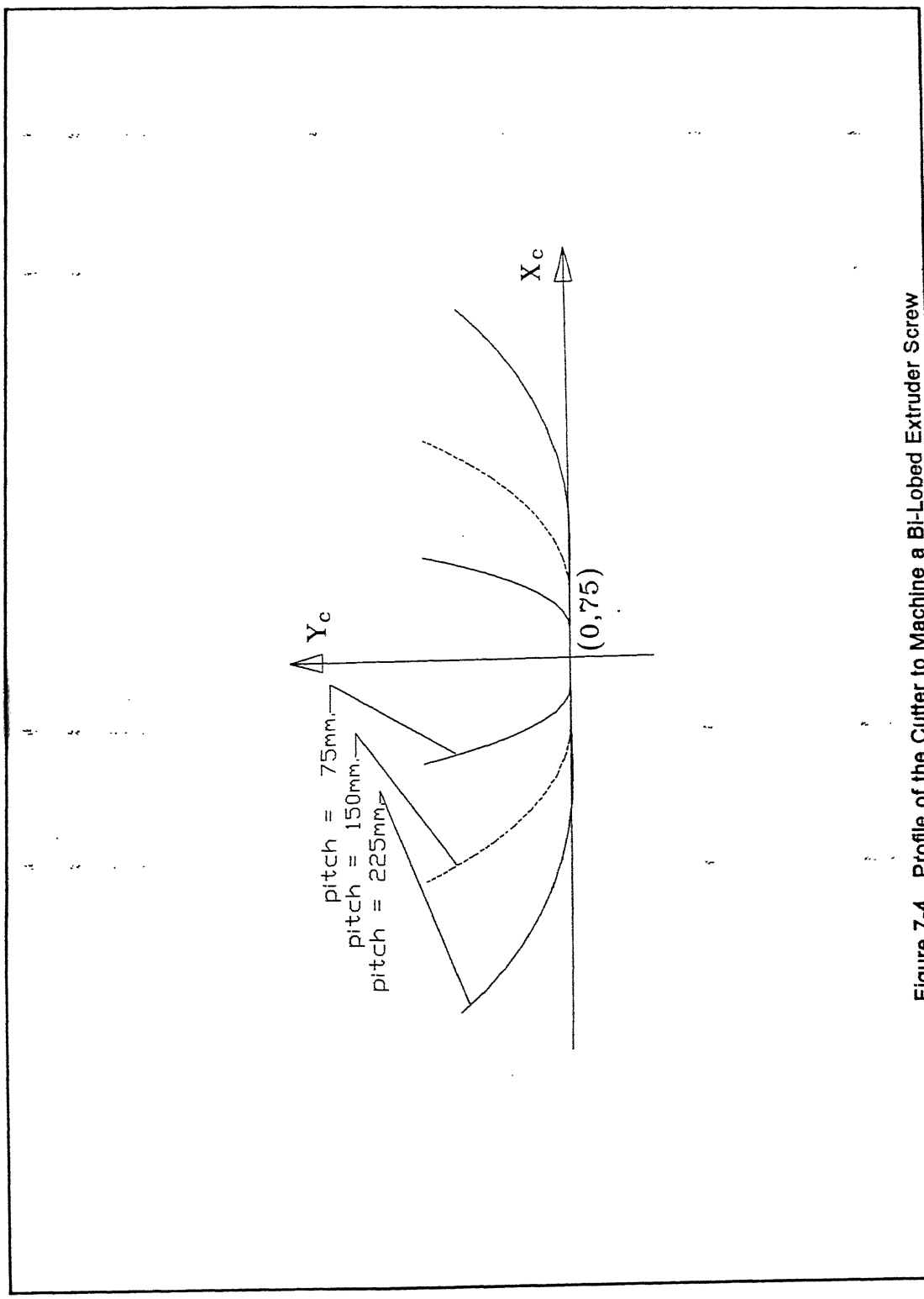

Figure 7.4 Profile of the Cutter to Machine a Bi-Lobed Extruder Screw

Using the method described above, the profile of the cutter was calculated for pitch p=75 mm., p=150 mm. and p=225 mm. and the plots of these three profiles are shown in Figure 7-5. The coordinates of the cutter profile is listed in Table 7-6.

p = 75 mm.		p = 150 mm.		p = 225 mm.	
x_c	y_c	x_c	y_c	x_c	y_c
-10.643	99.993	-22.714	99.862	-38.091	99.173
-9.882	97.835	-21.112	97.719	-35.471	97.108
-9.096	95.855	-19.453	95.755	-32.744	95.224
-8.287	94.068	-17.739	93.983	-29.910	93.532
-7.456	92.487	-15.974	92.417	-26.975	92.043
-6.603	91.125	-14.159	91.069	-23.944	90.770
-5.734	89.993	-12.301	89.950	-20.826	89.721
-4.848	89.100	-10.406	89.070	-17.634	88.904
-3.949	88.457	-8.481	88.436	-14.383	88.325
-3.044	88.069	-6.537	88.056	-11.089	87.990
-2.132	87.939	-4.581	87.933	-7.771	87.900
-2.132	87.939	-4.581	87.933	-7.772	87.900
-1.705	87.939	-3.665	87.935	-6.217	87.914
-1.280	87.939	-2.749	87.937	-4.663	87.925
-0.853	87.939	-1.833	87.939	-3.109	87.933
-0.426	87.939	-0.916	87.939	-1.554	87.937
0.001	87.939	0.000	87.939	0.000	87.939
0.426	87.939	0.916	87.939	1.554	87.937
0.853	87.939	1.832	87.938	3.109	87.933
1.280	87.939	2.748	87.937	4.663	87.925
1.706	87.939	3.664	87.935	6.218	87.914

2.133	87.939	4.580	87.933	7.772	87
2.133	87.939	4.580	87.933	7.772	87
3.043	88.069	6.536	88.056	11.089	87
3.950	88.457	8.482	88.436	14.383	88
4.848	89.100	10.405	89.069	17.634	88
5.734	89.992	12.301	89.950	20.826	89
6.604	91.125	14.159	91.069	23.943	90
7.456	92.487	15.973	92.417	26.975	92
8.287	94.068	17.739	93.983	29.910	93
9.096	95.855	19.453	95.755	32.744	95
9.882	97.834	21.112	97.719	35.472	97
10.642	99.993	22.714	99.861	38.091	99

Table 7-6 Coordinates of the Profile of the Cutter to Machine the Tri-Lobed Extruder Sc

Since there are three flutes for this screw, the full helicoidal surface w obtained in three steps. The blank will be indexed by $2\pi/3$ radian every time machining the first and second flutes.

7.3.4 Design of an End Milling Cutter for the Machining of a Quadri-L Extruder Screw

The cross-sectional profile of a bi-lobed extruder screw is similar to the one s in Figure 6-13. It has a tip radius of 100 mm. and a root radius of 90.743 mn mentioned earlier, only the root and flank arcs influence the design and the tip realized in the preparation of the blank. The dimensions of one root arc and the two arcs adjacent to it are given in Table 7-7.

i	p_i	q_i	r_i	u_{i1}	u_{i2}
15	-76.604	-64.279	190.743	0.39269	0.69813

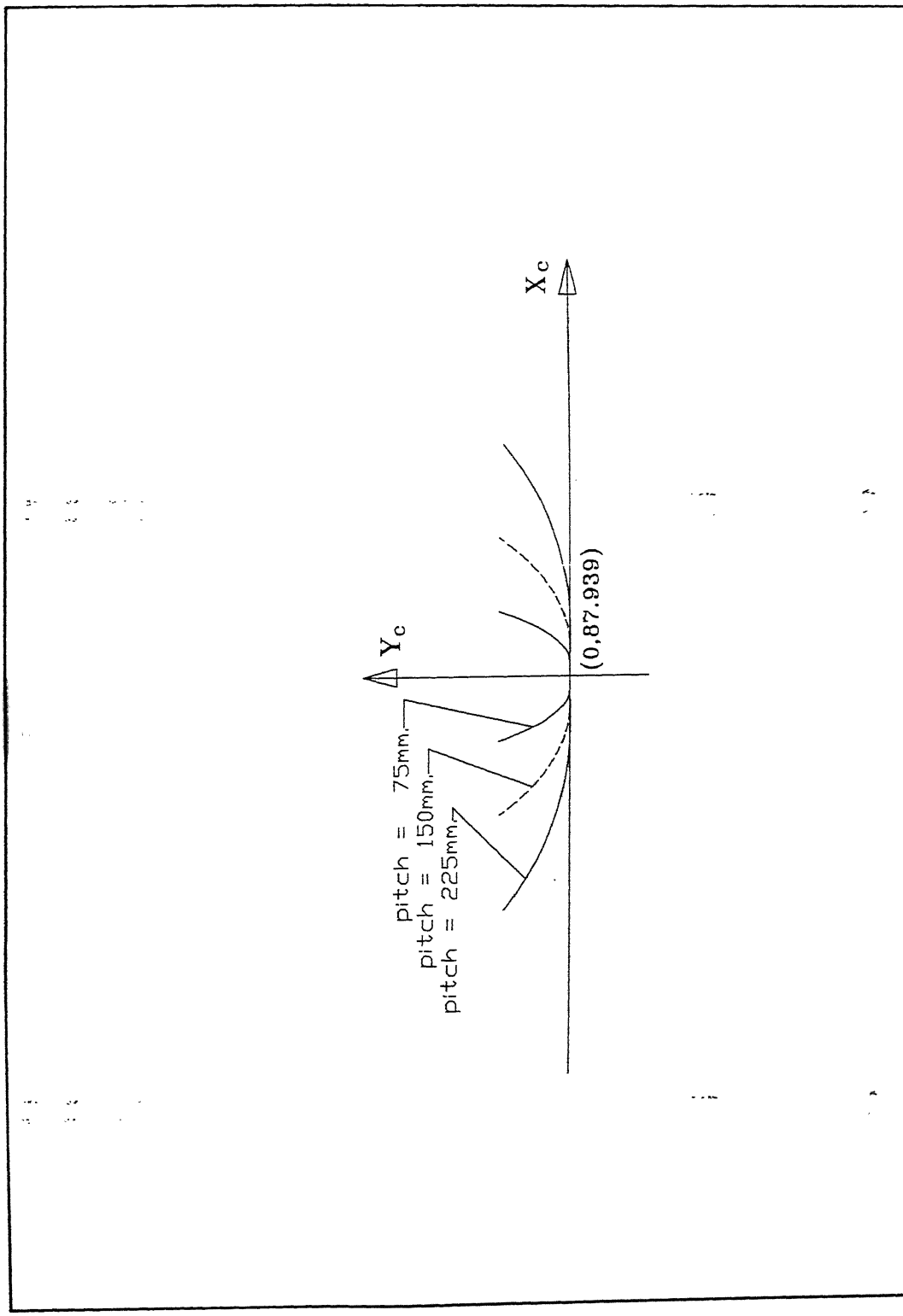
Xc
Yc
(0,87.939)
pitch = 75mm.
pitch = 150mm.
pitch = 225mm.

16	0.000	0.000	90.743	0.69813	0.87264
1	-64.281	-76.603	190.743	0.87264	1.17808

Table 7-7. Biparametric Definition of the Root and Adjacent Flank Arcs of a Quadri-Lobed Screw.

Using the method described above, the profile of the cutter was calculated f pitch p=75 mm., p=150 mm. and p=225 mm. and the plots of these three profiles a shown in Figure 7-6. The coordinates of the cutter profile is listed in Table 7-8.

p = 75 mm.		p = 150 mm.		p = 225 mm.	
x_c	y_c	x_c	y_c	x_c	y_c
-8.275	99.996	-16.211	99.930	-23.534	99.68
-7.606	98.315	-14.891	98.259	-21.596	98.05
-6.923	96.783	-13.543	96.735	-19.622	96.56
-6.223	95.407	-12.167	95.368	-17.614	95.22
-5.509	94.195	-10.768	94.165	-15.574	94.05
-4.783	93.156	-9.345	93.133	-13.508	93.04
-4.048	92.296	-7.903	92.279	-11.417	92.21
-3.302	91.620	-6.445	91.609	-9.307	91.56
-2.550	91.134	-4.976	91.127	-7.182	91.10
-1.793	90.841	-3.498	90.838	-5.048	90.82
-1.032	90.743	-2.016	90.742	-2.909	90.73
-1.033	90.743	-2.015	90.742	-2.908	90.73
-0.826	90.743	-1.612	90.742	-2.327	90.74
-0.620	90.743	-1.209	90.743	-1.745	90.74
-0.413	90.743	-0.806	90.743	-1.163	90.74
-0.207	90.743	-0.403	90.743	-0.582	90.74

-0.001	90.743	0.000	90.743	0.000	90.743
0.207	90.743	0.403	90.743	0.581	90.743
0.413	90.743	0.805	90.743	1.163	90.742
0.620	90.743	1.209	90.743	1.744	90.741
0.826	90.743	1.612	90.742	2.326	90.740
1.032	90.743	2.015	90.742	2.907	90.738
1.032	90.743	2.014	90.742	2.908	90.737
1.792	90.840	3.497	90.837	5.047	90.825
2.549	91.133	4.975	91.127	7.181	91.102
3.301	91.620	6.445	91.608	9.306	91.567
4.047	92.295	7.903	92.278	11.416	92.216
4.783	93.155	9.345	93.132	13.507	93.046
5.509	94.195	10.767	94.164	15.574	94.051
6.223	95.406	12.167	95.367	17.613	95.224
6.922	96.782	13.542	96.735	19.621	96.559
7.606	98.315	14.891	98.258	21.595	98.049
8.275	99.995	16.211	99.929	23.534	99.685

Table 7-8 Coordinates of the Profile of the Cutter to Machine the Quadri-Lobed Extruder Screw

Since there are four flutes for this screw, the full helicoidal surface will be obtained in four steps. The blank will be indexed by $\pi/2$ radian every time while machining the second, third and flutes.

7.4 Determination of the Surface of the Cutter from the Profile of the Cutter ${}^{c}\underset{\sim}{g}(u)$

The procedure to obtain the two-dimensional profile of the cutter ${}^{c}\underset{\sim}{g}(u)$ from the

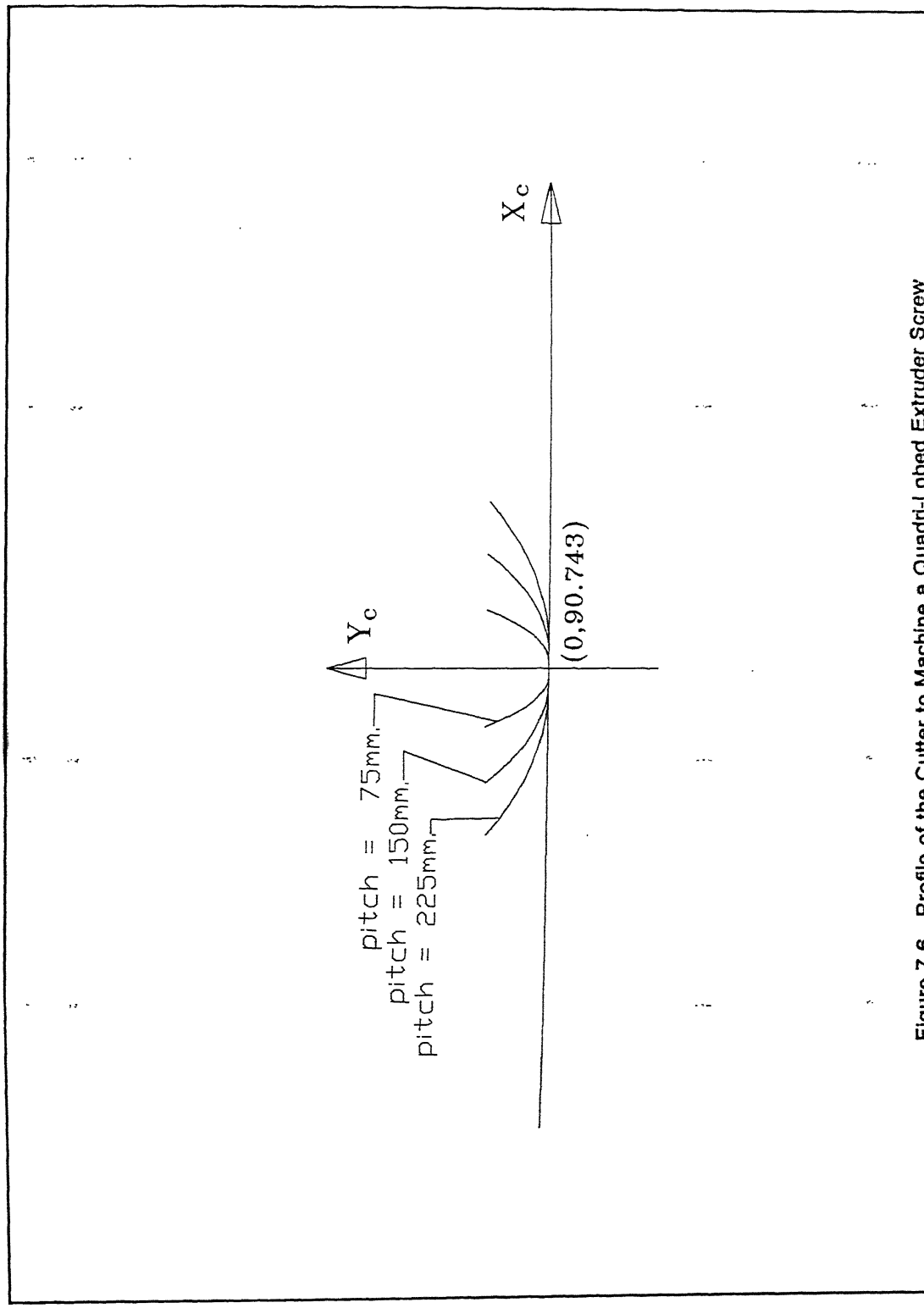

Figure 7-6. Profile of the Cutter to Machine a Quadri-Lobed Extruder Screw

given cross-sectional profile ${}^{2}\underset{\sim}{g}(u)$ of the helicoidal surface was explained earlier and this profile was determined for four extruder screws in the preceding section. This is the basic shape required to obtain various types of cutters in order to manufacture the helicoidal surface. One can obtain a turning tool, an end milling cutter, a side milling cutter or a disc type cutter by suitably manipulating this profile. In this section, the method of obtaining these different cutters and the respective manufacturing schemes are explained. In all these cases, the blank used will be a cylinder of radius equal to the tip radius of the cross-sectional profile.

7.4.1 Machining of the Helicoidal Surface Using a Turning Process

The simplest process to produce a helicoidal surface is turning since any turned surface is composed of a number of helices. The axis of the blank coincides with the Z axis (longitudinal axis) of the machine tool. The profile of the cutter is ground on the turning tool such that the plane of this profile is tilted by an angle of σ with respect to the X - Z plane of the machine tool as can be seen in Figure 7-7. The translation of the cross slide (i.e., movement of the turning tool) is coordinated with the spindle rotation to get the required pitch p. The manufacturing scheme for this case is shown in Figure 7-7.

7.4.2 Machining of the Helicoidal Surface Using a Milling Process with an End Milling Cutter

Figure 7-8 shows the end milling cutter used for the machining of the helicoidal surface. The surface of the end mill is obtained by revolving the cutter profile about the Y_c axis. While machining, the axis of the end milling cutter shall be radial to the cylinder. The tip of the end mill will be at a distance equal to the root radius of the cross-sectional profile at the final depth of cut.

7.4.3 Machining of the Helicoidal Surface Using a Milling Process with a Disc Type Cutter

Many a time, milling with a side-and-face cutter is preferred to end-milling owing to higher rate of metal removal. When a high surface finish is required, it may be required to grind the helicoidal surface after milling using a disc type of grinding wheel. The surfaces of the side-and-face cutter and the grinding wheel for machining the helicoidal surface can be obtained as surfaces of revolution of the cutter profile about an axis

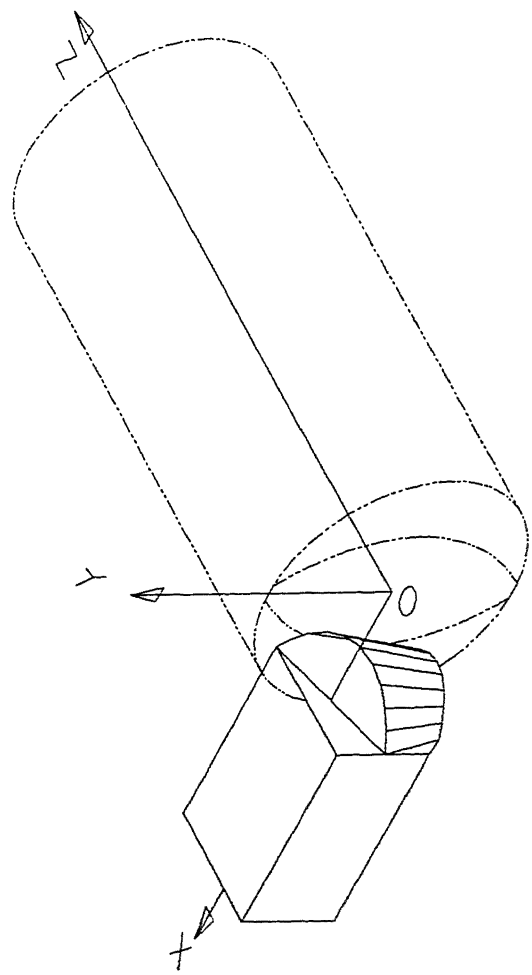

Figure 7-7. Machining of the Extruder Screw Using a Turning process

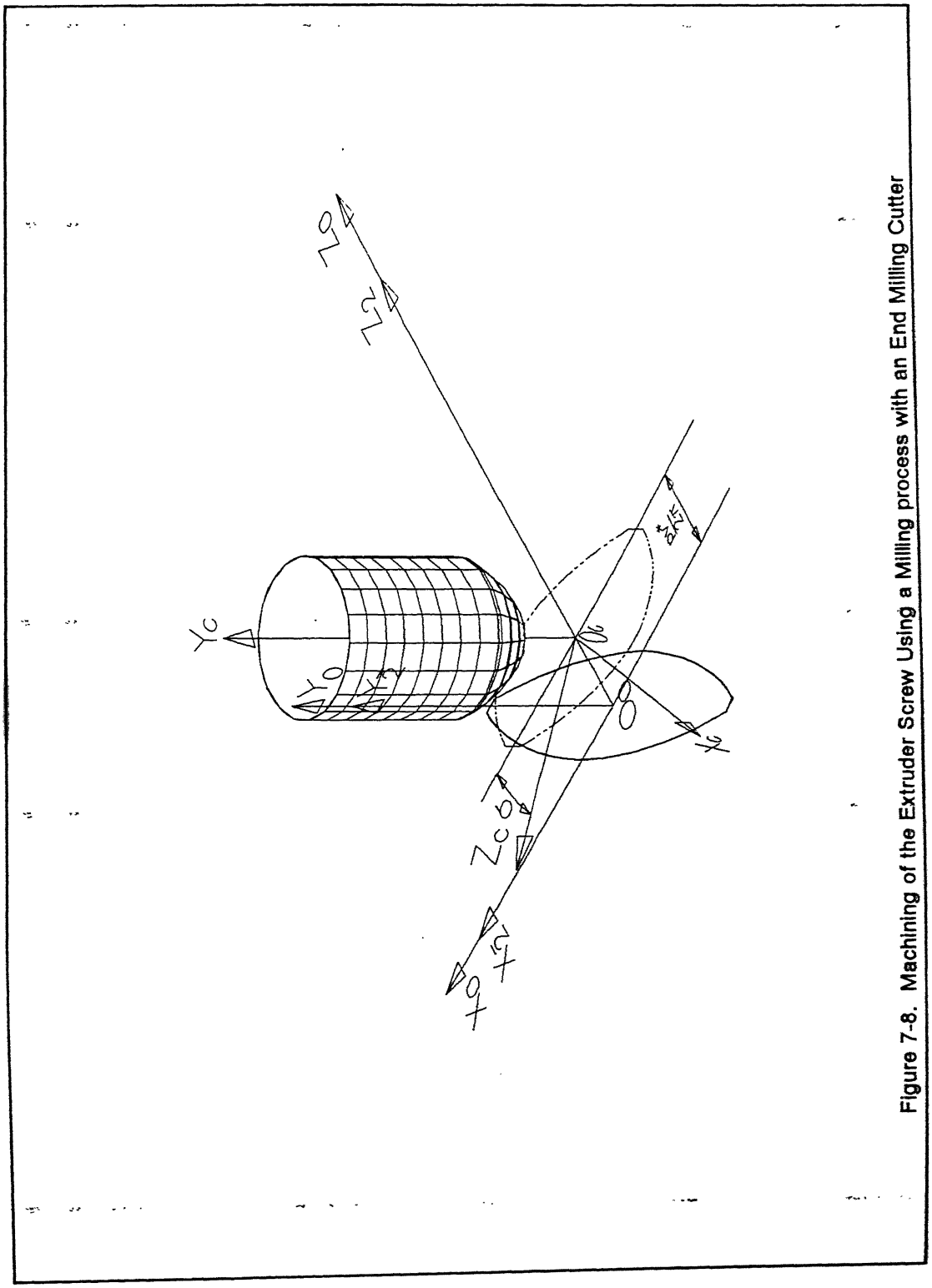

Figure 7-8. Machining of the Extruder Screw Using a Milling process with an End Milling Cutter

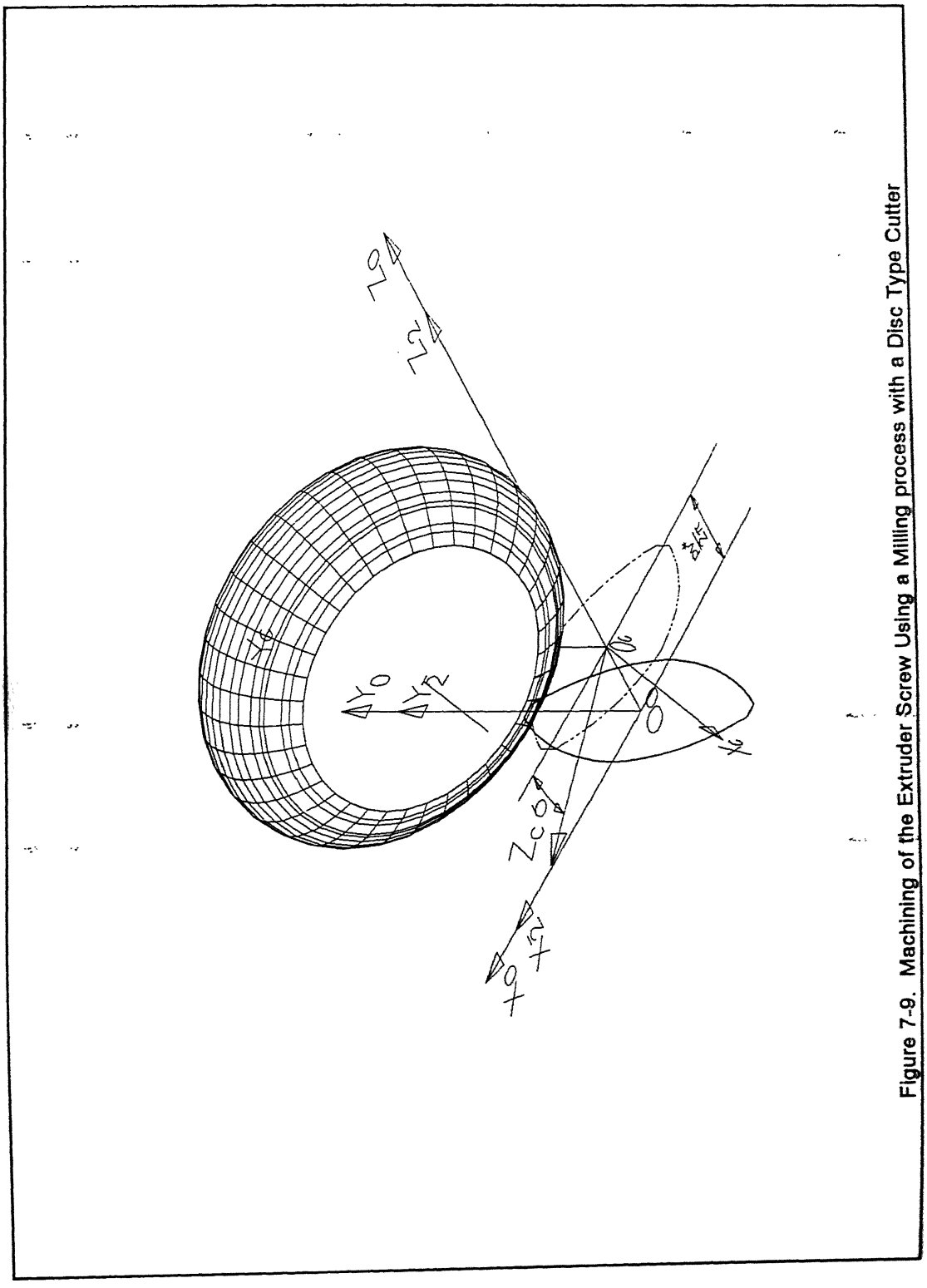

Figure 7-9. Machining of the Extruder Screw Using a Milling process with a Disc Type Cutter

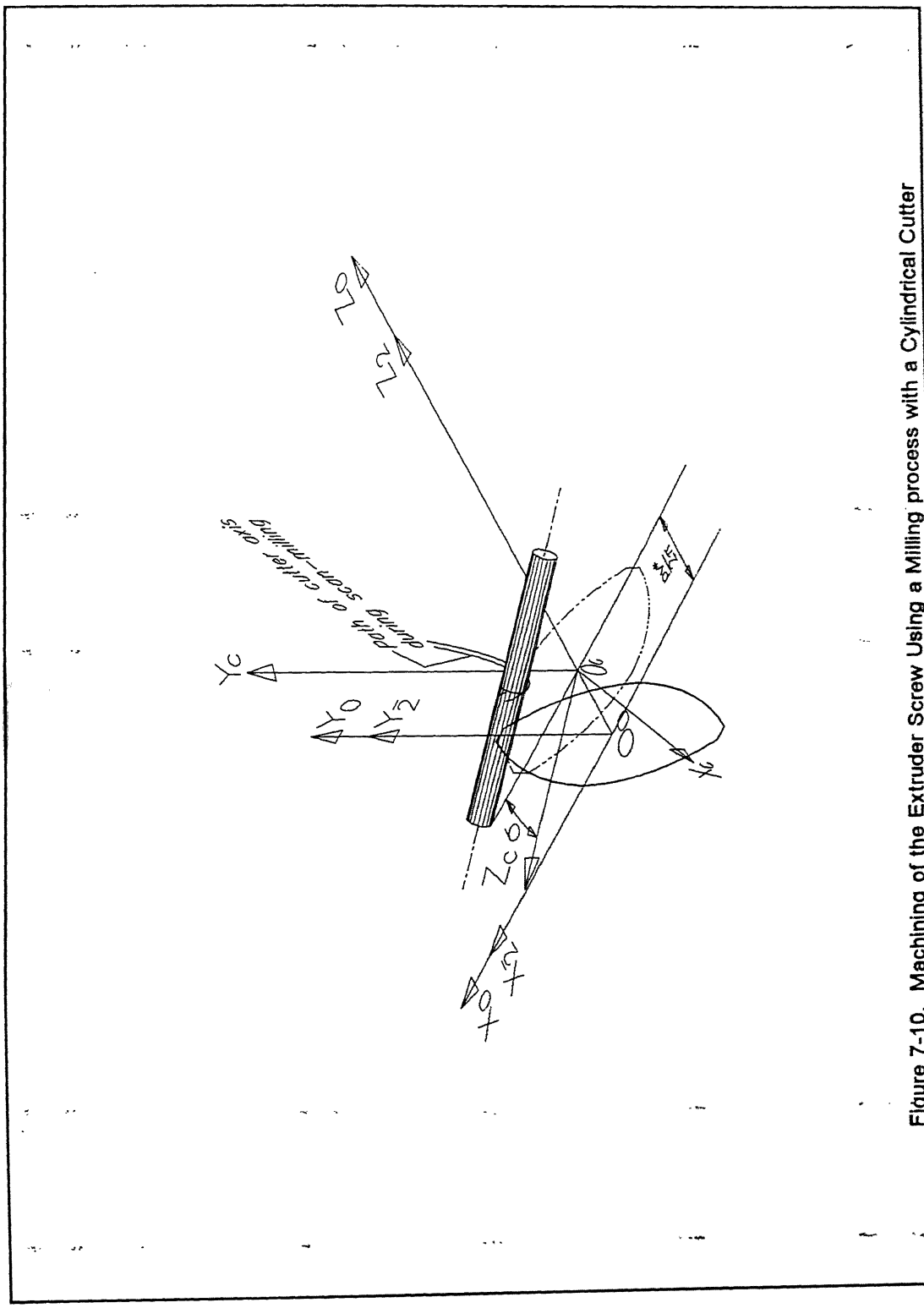

Figure 7-10. Machining of the Extruder Screw Using a Milling process with a Cylindrical Cutter

parallel to the X_c axis as shown in Figure 7-9. The axis of this disc cutter should be at an angle equal to the lead angle σ with respect to the Z_0 axis.

7.4.4 Machining of the Helicoidal Surface Using a Milling Process with a Side Milling Cutter by Scan-Milling

Scan-milling is a milling process by which the desired surface is realized by employing several passes of a cutter rather than a single pass using a form-cutter. This method gives a surface which is an approximation to the desired surface since it produces scallops on the surface. This method is employed extensively in the machining of sculptured surfaces such as the dies of car bodies and aircraft components using end milling type cutters. By suitably choosing the distance between adjacent passes and by employing dressing and deburring, sufficiently accurate surfaces can be obtained.

Since it is not possible to design a side mill which produces the helicoidal surfaces encountered in the extruder screws in single pass, these surfaces may be produced using cylindrical side mills or even by a wire-EDM process by a scanning process. In this process, the axis of the wire or the side mill is at an angle σ with respect to the X axis and it lies in a plane parallel to the X_0 - Z_0 plane as shown in 7-10. Generally, rough machining is preceded by scan-milling. A profile which is offset from the cutter profile by an amount equal to the radius of the cutter is shown in the figure. Initially, the center of the cutter is at one end of this offset profile and at this condition, the blank moves from one end to the other helically. After one pass, the cutter is moved by a small amount along the center line profile and then the blank repeats the helical motion but in the opposite direction. This process is repeated till the cutter reaches the other end of the axis profile.

7.5 Design of Side Milling Cutter for Machining the Helicoidal Surface in Single Pass

The scan-milling is an approximate method and it also takes more time to machine. Hence it is preferable to machine the helicoidal surface in single pass. This is possible for all kinds of helicoidal surfaces when we employ a turning process or a milling process either with an end milling type cutter or a disc type cutter as described in Sections 7.4.1, 7.4.2 and 7.4.3. There are some helicoidal surfaces for which a side milling cutter exists using which the helicoidal surface can be produced exactly in single pass. In this section, the procedure to determine such a side milling cutter is described (if it exists) and the procedure is illustrated by means of an example.

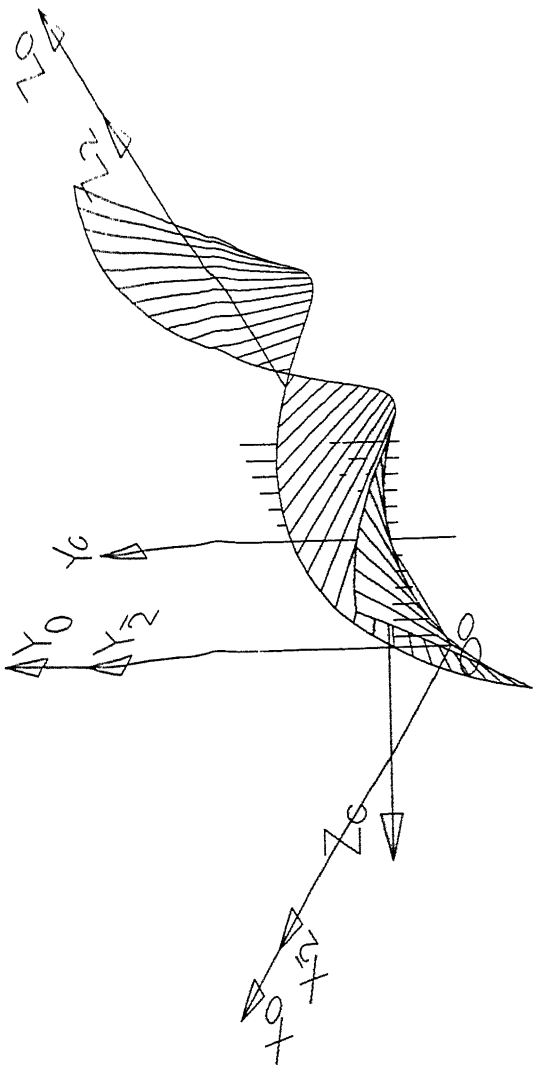

Figure 7-11. Machining of the Extruder Screw Using a Milling process with a Side Milling Cutter - Isometric View

7.5.1 Procedure for the Design of a Side Milling Cutter

In all the cases discussed earlier, the profile ${}^{c}\underset{\sim}{g}(u)$ of the cutter was obtained at the X_c - Y_c plane, i.e., at $w = 0$. This profile can be obtained for different values of w as well. The axis of the side milling cutter that is being designed will be parallel to the X_c - Z_c plane and it will make an angle σ with the X_c axis. The procedure to obtain the surface of this cutter is as follows :

1. Obtain the cutter profile ${}^{c}\underset{\sim}{g}(u)$ for various values of w at sufficiently close intervals.

2. Choose an appropriate value for d where the axis of the cutter passes through a point $(0, d, pv^{*}/2\pi)$. From the axis of the cutter, find the minimum distance of each of the cutter profiles obtained in the last step. Draw circles each with center at $(w \cos\sigma, d, pv^{*}/2\pi - w \sin\sigma)$ and the respective minimum distance as radius. These circles are drawn parallel to the Y_c - Z_c plane.

3. The cutter surface will be the surface that envelopes all these circles.

7.5.2 Illustrative Example

Consider the following generatrix ${}^{c}\underset{\sim}{g}(u)$ for a helicoidal screw whose pitch is 60π and lead angle is $\pi/4$.

$$ {}^{2}\underset{\sim}{g} = \begin{bmatrix} x_2 & y_2 & z_2 & 1 \end{bmatrix} \qquad (7\text{-}13) $$

where,

$$ x_2 = 2 $$
$$ y_2 = 4u $$
$$ z_2 = 3u $$
$$ -6 \le u \le 6 $$

Let the axis of the side mill be at 30 units from the X_c - Z_c plane.

The profile of the cutter ${}^{c}\underset{\sim}{g}(u)$ was calculated from w = -30 to w = 30 at an interval of 5 units. The resulting profiles are plotted and are shown in Figures 7-11 and 7-12. The axis of the cutter is parallel to the Z_c axis and passes through the point (0, -30, 0) with respect to the S_c coordinate system. The shortest distance between the axis of the cutter and each of these cutter profiles are given in Table 7-9.

w $(= z_c)$	Min. dist.of the profile from cutter axis
-30.0000	24.9967
-25.0000	27.1884
-20.0000	28.9538
-15.0000	30.3042
-10.0000	31.2501
-5.0000	31.8131
0.0000	32.0000
5.0000	31.8131
10.0000	31.2501
15.0000	30.3042
20.0000	28.9538
25.0000	27.1884
30.0000	24.9967

Table 7-9 Coordinates of the Profile of the Side Milling Cutter for the Example Given in Section 7.5.2.

From Table 7-9, a two-dimensional profile can be obtained in the X_c - Z_c plane at y_c = -30.000 if w is plotted along Z_c axis and the minimum distance along X_c axis. When a curve fitting was done, it was found that these points define a circle with a radius of

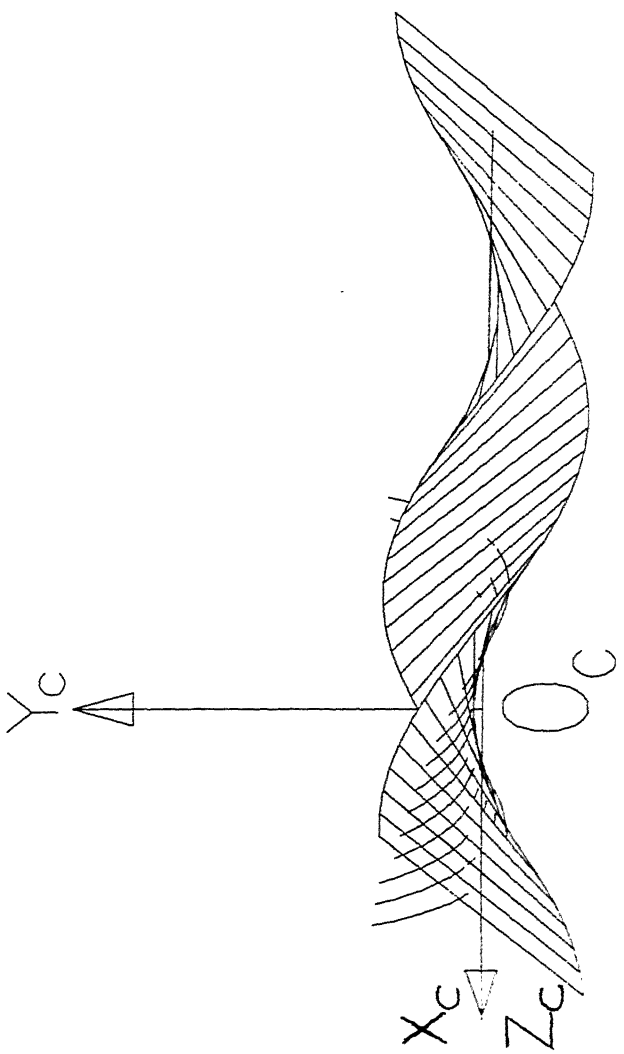

Figure 7-12. Machining of the Extruder Screw Using a Milling process with a Side Milling Cutter - Front View

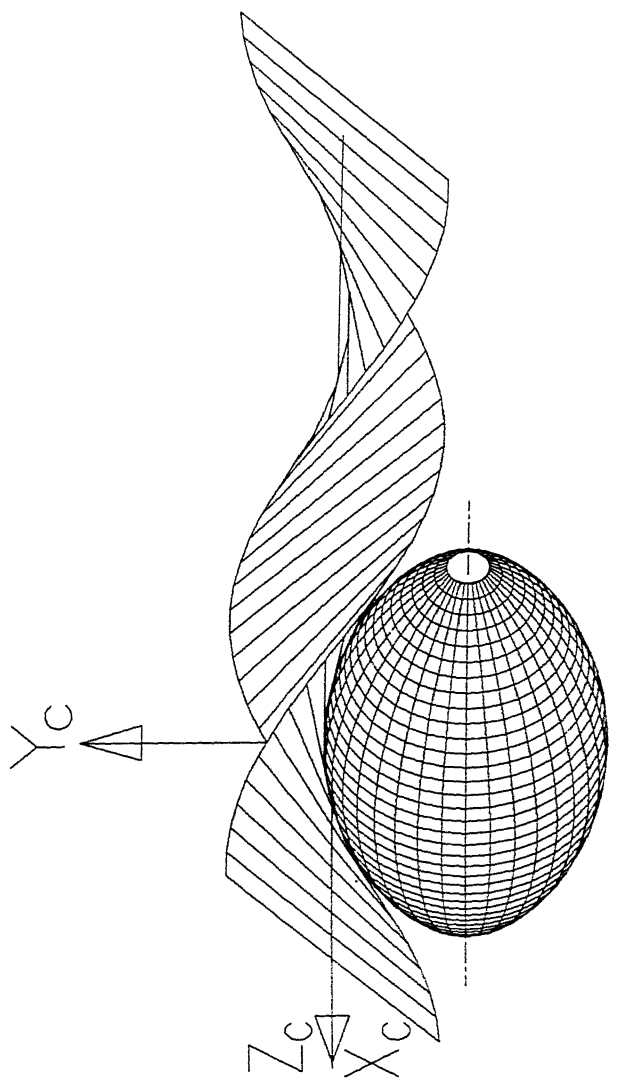

Figure 7-13. Relative Position between the Cutter and the Machined Surface

67.7857 units and center at (-35.7857, -30.0000, 0) in X_c - Z_c plane. The side mill is a surface of revolution obtained by revolving this profile about the axis of the cutter. This side milling cutter and the desired surface are depicted in Figure 7-13.

The side milling cutter described above exists only for simple surfaces such as the one shown in this example. Since most of the extruder screw surfaces are more complicated, the side milling cutter to machine them in one pass does not exist. Hence, for realizing an extruder screw surface in single pass, one has to resort to one of the other three processes, viz., a turning process, a milling process using an end milling cutter or a milling process using a disc type cutter.

Chapter 8

CONCLUSIONS AND FUTURE EXTENSIONS

8.1 Concluding Remarks

Today, the speed of computers and their graphic rendering capabilities with the help of high resolution display devices have improved so much that we are able to see the objects more realistically on the screen. What is called *Virtual Reality* in the parlance of *Computer Animation* has become possible. These advancements have triggered research in the geometric modeling of motion simulation of robots and mechanisms such as the aircraft landing gear mechanism. Extensive research is also being done by several researchers in modeling the metal removal processes geometrically (Wang, Drysdale etc.).

The geometric modeling of shape realization processes is an important aspect for a manufacturing engineer from the viewpoint of design for manufacturability. In order to be able to evaluate the feasibility of realizing a surface as defined by a designer, a manufacturing engineer is required to define the geometry of the tool, the kinematic structure of the machining process and the law of relative motion between the tool and the work piece. In many cases, the surface realized is not exact but is a close approximation of the surface defined by the designer. In such cases, it is always desirable to explore different feasible machining strategies. The model proposed in the present thesis provides a methodology for depicting the geometry of the machined surfaces for the alternative machining strategies. This has been accomplished using unified symbolic models and procedures. The proposed methodology is a useful predictive tool for selecting an appropriate machining strategy for realizing a specified surface.

8.1.1 Conjugate Geometry Formulation

The present thesis outlines the methodology of developing geometric models of several shape generating processes. The interaction of the geometric parameters of the

cutter surface as well as the kinematic parameters of the manufacturing process significantly affect the geometrical definition of the manufactured surface. It has been found that the concept of conjugate geometry enables us to distinguish between the mathematical definition, the display definition and the shape realization definition of a surface. The shape realization definition, as can be seen from the examples and the case studies, is different from the other two definitions. Generally, a design engineer is more familiar with the mathematical definition (implicit or explicit form) and the display definition (parametric form) of a shape. The shape realization definition (envelope form), it is felt, is useful in designing for manufacturability of a surface. This definition can be used for designing a machining process, the tool geometry, a feasible tool path and ensuring a smooth machined surface.

The concept of conjugate geometry has been used to define analytically four methods of realizing either a generatrix or a directrix curve of a machined surface. This classification enables us to define about twelve different groups of shape realization processes. One can see that almost all conventional as well as modern machining processes can be characterized with the help of these twelve basic groups. The proposed conjuagate geometry formulation enables the modeling of all these twelve groups of manufacturing processes in a unified manner.

As compared to the early systems such as the APT system wherein a single fixed coordinate frame is used, in the conjugate geometry formulation, three coordinate frames are used. One frame is fixed and the other two are moving coordinate frames each being attached to the blank and the cutter. The movements of the cutter and the blank are considered independent of each other. The synchronization of their movements is achieved by suitably describing the twelve parameters of motion in order to obtain the desired surface. This methodology is particularly advantageous since on many machine tools it is not only the movement of the cutter but the combined movement of both the cutter and the blank that produces the surface on the blank. Employing the homogeneous transformation matrices for transforming the position, normal and velocity vectors from one frame to the other makes the calculations simple and elegant.

8.1.2 Generic Cutter

The generic cutter definition is very elaborate and it covers a wide spectrum of cutting tools used in shape realization by metal removal. The nine parameters describing the generic cutter can also be used to store the information of cutters employed in a manufacturing shop in a data base precisely.

8.1.3 Symbolic Manipulation

The use of symbolic manipulation technique for developing conjugate geometry model of the machine tool and the generic model of the cutter for the shape realization process has been found to be an effective modeling and computational tool. The symbolic algorithm proposed here is general in nature and can be used for modeling any shape generating process. Since the algorithm is implemented symbolically, just by changing the nine parameters describing the cutter surface and the twelve motion parameters, one can obtain the algebraic expressions describing the surface produced on the blank. This is very helpful when a manufacturing engineer has to evaluate various alternatives to manufacture a surface as he or she is freed from deriving the expressions for each case.

8.2 Scope for Future Work

The theory developed in this thesis can be used in developing a user-friendly menu-driven software. The work makes some basic assumptions. It assumes that the cutter, work piece and the elements of the machine tool are rigid bodies. While cutting is taking place, it is assumed, the stresses generated are local and do not affect the neighborhood. If the elastic properties of different members of a machining process are taken into account, then the surface actually machined on the blank will be different from what is obtained using the present modeling. The proposed method for the cutter path simulation can be linked with an analysis package in order to arrive at the optimum NC code. These extensions of this thesis work are explained in the following sections.

8.2.1 Development of an Integrated Package Using the Conjugate Geometry Formulation

In its present implementation, the symbolic algorithm proposed in this thesis accepts only one expression for each of the twelve motion parameters describing the motions of the cutter and the blank. However, in reality, the surfaces machined are composite and hence they cannot be expressed by one algebraic equation. For each segment of the machined surface, there will be a different set of values for the motion parameters. Therefore an integrated software is required to be developed using the conjugate geometry theory proposed in the present thesis. Such a software will use the proposed symbolic algorithms to determine the geometry of the composite machined surface.

The conjugate surface obtained in this work is nothing but the swept volume of the cutter. In other words, the cutter is assumed to be fully immersed in the blank

material. However, actually it may no be so. Hence, in order to get the actual surface, we shall have to trim the portion of this surfaces by the surfaces defining the initial shape of the blank.

Presently, the algorithm determines only the surfaces and it does not give any indication as to which side of the surface the solid volume is present. One can determine this by following some conventions in defining sweep parameter v for the cutter profile. For instance, if v is positive in the counterclockwise direction about the Z_1 axis, then the solid material lies on the left side as one moves along the positive direction of v. By using similar conventions while defining the initial shape of the blank, we can obtain the required information that indicates on which side of the blank surface the material is present.

8.2.2 Modeling the Effect of Tolerances

No dimension can be produced exactly and hence each dimension has a tolerance limit within which it is produced. Each of the eight parameters describing the generic cutter will have a tolerance. There will be clearance on the spindle bearing which causes spindle run-out. These two tolerances will influence the geometry of the cutter surface Σ_1. Each of the links forming the kinematic chain of the machine tool will also have a tolerance. Similarly, there will be clearances on the bearings between the links. All these tolerances will influence the definition of the twelve motion parameters. However, For the modeling of a manufacturing process in this work, it has been assumed that all the dimensions are deterministic. Hence the actual machined surface Σ_2 will be slightly different from the one predicted by the conjugate geometry model here. In order to obtain more realistic results, the effect of the tolerances of the cutter surface and the kinematic links of the machine tools will have to be taken into consideration using the stochastic approach.

8.2.3 Modeling of Mechanistic Properties and NC Code Optimization

What is considered in this thesis is the solution to a geometric problem. The surface of the cutter is considered to be a continuous surface without flutes which create the cutting edges. The mechanics of cutting is not dealt with. However, under the influence of the cutting forces, the cutter, the blank and the elements of the machine tool structure will have deflections. Due to the combined effect of these deflections, the shape of the surface produced will be different from what is predicted by the present symbolic algorithm. It is required to ensure that the deviation of the actual surface is well within the tolerance requirements. Under extreme conditions, the deflection may exceed the

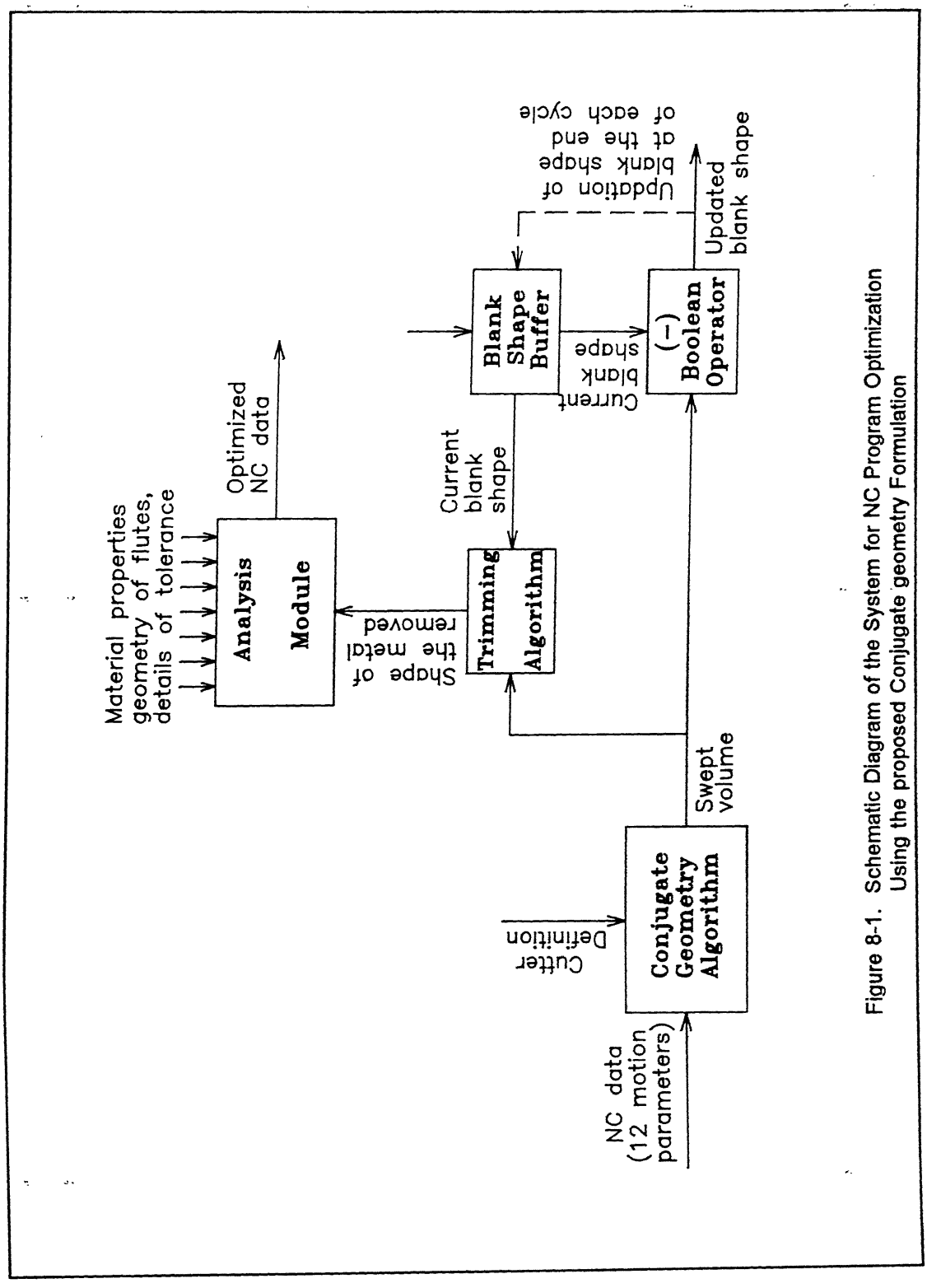

Figure 8-1. Schematic Diagram of the System for NC Program Optimization Using the proposed Conjugate geometry Formulation

elastic limit and cause the breakage of the cutter or even damage to the machine tool. It is essential to predict the cutting stresses beyond which this damage might occur so that preventive measure such as reduction of cutting speed, feed rate and depth of cut could be done.

In order to take the elasto-dynamic behavior of the manufacturing process in to account, a system similar to the one shown in the block diagram of Figure 8-1 is to be used. The primary requirement of such a system is a solid modeler preferably of the B-rep type. Initially, the conjugate geometry algorithm receives the description of the cutter and the system is fed with the initial shape of the blank. The analysis module is fed with data related to the material properties of the cutter and the blank, the number, shape and size of flutes and the allowable deviation of the actual surface from the desired surface. After the initialization, the first two NC blocks are read and they are converted into the twelve algebraic expressions as a function of time and fed to the twelve degrees of freedom model. Using the definition of the cutter and these twelve expressions, the twelve degrees of freedom model calculates the swept volume.

The swept volume of the cutter generated and the current shape of the cutter are sent to two modules, one is a trimming algorithm which trims the swept volume in order to get the actual shape of the metal removed from the blank; the other module is a difference Boolean operator which calculates the shape of the blank after the metal is removed. The output of this module will be used to update the current shape of the blank at the end of the cycle.

The most vital part of this system is the analysis module. The input to the analysis module is the shape of the metal removed by the current NC block. The analysis module will calculate the deflection of the cutter at every instant of cutting. The module will break the current NC block into suitable number of NC blocks and fit optimal feed rate values for each of them so that the cutter deflection is within the allowable limit. Thus, it converts each NC block which may be unoptimal to several NC blocks which are optimized.

There are two approaches for the analysis of cutting forces for this situation. One approach is the lumped mass approach. In this method, the analysis is done only at few representative points. All the forces that are induced during the cutting and the resulting deflections are transformed to these points by incorporating suitable factors. After this, the static and dynamic analyses are performed. This approach is approximate but will be computationally economical. The second approach is the finite element analysis. In this approach, the matrix of the volume is broken into very small elements and each of these finite elements are analyzed. This approach will give the most accurate results but this will be computationally intensive.

Since the conjugate geometry algorithm generates the surface as a first step, it will be more appropriate if the integrated software proposed is based on a B-rep solid modeler incorporating the Boolean operators.

REFERENCES

COMPUTATIONAL GEOMETRY & GEOMETRIC MODELING :

1. Ayala, D., 1988, "Boolean Operations between Solids and Surfaces by Octrees : Models and Algorithms", *CAD*, Vol. 20, No. 8, pp. 452-465.

2. Faux, I.D. and Pratt, M.J., 1983, *Computational Geometry for Design and Manufacture*, Ellis Horwood Ltd., Chichester.

3. Forrest, A.R., 1971, "Computational Geometry", *Proceedings of Royal Society*, London, A321, pp. 187-195.

4. Krzysztof Marciniak, 1992, *Geometric Modeling for NC Machining*, Oxford Science Publication.

5. Mäntylä M, 1988, *An Introduction to Solid Modeling*, Computer Science Press, Inc.

6. Mortenson, M.E., 1985, *Geometric Modeling*, John Wiley and Sons, New York.

7. Requicha, A.A.G., 1980, "Representation of Rigid Solid Objects", *Lecture Notes in Computer Science*, No. 89, Springer-Verlag, 1980.

8. Requicha, A.A.G. and Voelcker, H., 1983, "Solid Modeling : Current Status and Research Direction", *IEEE Computer Graphics & Applications*, Vol. 3, No. 7.

9. Requicha, A.A.G. and Chan, S.C., 1986, "Representation of Geometrical Features, Tolerances and Attributes in Solid Modelers on Constructive Geometry", *IEEE Journal of Robotics & Automation*, Vol. RA-2, No. 3.

10. Wozny, M.J., Turner, J.U. and Preiss, K., (editors), 1990, *Geometric Modeling for Product Engineering*, North-Holland.

11. Yap, K.T., 1988, *Computational Geometry : An Introduction with Applications to NC and Robotics*, Allison Wesley.

CONJUGATE GEOMETRY :

12. Boltyanskii, V.C., 1964, *Envelopes*, Macmillan Company.

13. Chakraborty, J. and Dhande, S. G., 1977, *Kinematics and Geometry of Planar and Spatial Cam Mechanisms*, Wiley Eastern Limited, New Delhi.

14. Chen, C.H., 1990, "Application of Complementary Conjugate Surface in Surface Generation", *M190 Conference*, Vol. 4, Atlanta, GA, pp. 21-25.

15. Dhande, S. G. and Rajaram, N., 1984, "Kinematic analysis of Constant-Breadth Follower Mechanisms", *ASME Journal of Mechanisms, Transmissions and Automation in Design*, Vol. 106, June, pp. 214-221.

16. Dudley and Darle, W., 1962, *Gear Handbook: The Design, Manufacture and Application of Gears*, N. Y. McGraw Hill.

17. Dyson, A., 1969, *Kinematics and Geometry of Gears in Three-Dimensions*, Clarendon Press, Oxford.

18. Fan Y. Chen, 1982, *Mechanics and Design of Cam Mechanisms*, Pergamon Press, New York.

19. Ghosh, P. and Mudur, S.P., 1984, "The Brush-Trajectory Approach to Figure Specification : Some Algebraic Solutions", *ACM Transactions on Graphics*, Vol. 3, No. 2 (April).

20. Harold A. Rothband, 1956, *Cams - Design, Dynamics and Accuracy*, John Wiley & Sons, New York.

21. Kaul, A., 1992, "Minkowski Sums : A Simulation Tool for CAD/CAM", *Proc. ASME Computers in Engineering Conference*, San Francisco, (August).

22. Mabie, H.H. and Reinholtz, C.F., 1987, *Mechanisms and Dynamics of Machinery*, John Wiley and Sons, New York.

23. Misra, B.K., Pradhan, B.S.S. and Dhande, S.G., 1992, "Computational Conjugate Geometry of Flexible Generating Curves", *Proceedings of 5th ASEE International Conference on Engineering Computer Graphics and Descriptive Geometry, August 17-21*, RMTI, Melbourne, Australia, pp. 428-432.

24. Shinan, L. and Jinguang, Z., 1990, "Envelope Method on the CAD of Profile Cutters", *Proceedings of the ASEE Conference on Computer Graphics (A New Vision on Engineering)*, Miami, FL, pp. 398-404.

25. Voruganti, R.S., 1990, "Symbolic and Computational Conjugate Geometry for Design and Manufacturing Applications", *M.S. Thesis*, Virginia Polytechnic Institute and State University.

26. Wagner, M. J., Ng, W. F. and Dhande, S. G., 1992, "Profile Synthesis and Kinematic Analysis of Pure Rolling Contact Gears", *ASME Journal of Mechanical Design*, Vol. 114, (June), pp. 326-333.

SYMBOLIC ALGEBRA :

27. Ashrafiuon, H. and Mani, N.K., 1989, "Applications of Symbolic Computing for Numerical Analysis of Mechanical Systems", *Applied Mechanisms & Robotics Conference*, Cincinnati, pp. 141-149.

28. Bowyer, A., Wallis, A.F. and Milne, P.S., (editors), 1987, "Symbolic Ray Tracing", *Proceedings of Computer Graphics '87 On-line Conference Publications*.

29. Brackx, F. and Constales, D., 1991, *Computer Algebra with LISP and REDUCE : An Introduction to Computer Aided Mathematics*, Kluwer Academic Publishers.

30. Buchberger, B., Collins, G.E. and Loos, R. (editors), 1982, *Computer Algebra - Symbolic and Algebraic Computation*, Springer-Verlag, New York.

31. David V. Chudnovsky and Richard D. Jenks (editors), 1989, *Computer Algebra : Lecture Notes in Pure and Applied Mathematics - Vol. 113*, Marcel Dekker, New York.

32. Inada, N. and Soma, T. (editors), 1985, *RIKEN's International Symposium on Symbolic and Algebraic Computation by Computers*, World Scientific, Philadelphia.

33. Jefferys, W.H., 1971, "Automated Algebraic Manipulation in Celestial Mechanics", *ACM Proceedings of the Symposium on Symbolic and Algebraic Manipulation*, Los Angeles, CA, pp. 328-331.

34. Martin, W.A. and Fateman, R.J., 1971, "The MACSYMA System", *ACM*

Proceedings of the Symposium on Symbolic and Algebraic Manipulation, Los Angeles, CA, pp. 59-73.

35. Moses, J., 1971a, "Symbolic Integration : The Stormy Decade", *ACM Proceedings of the Symposium on Symbolic and Algebraic Manipulation*, Los Angeles, CA, pp. 427-435.

36. Moses, J., 1971b, "Algebraic Simplification : A Guide for the Perplexed", *Communications of the ACM*, Vol. 18, No. 8, pp. 527-537.

37. Raphael, B., Bobrow, D.G., Fein, L. and Young, J.W., 1966, "A Brief Survey of Computer Languages for Symbolic and Algebraic Manipulation", *Symbol Manipulation Languages and Techniques*, Proceedings of the IFIP Working Conference on Symbol Manipulation Languages, North-Holland Publishing Company, Amsterdam, pp. 1-54.

38. Richard Pavelle, Symbolics, Inc., (editor), 1984, *Applications of Computer Algebra*, Kluwer Academic Publishers, Boston.

39. Symbolics, Inc, 1988, *MACSYMA Reference Manual Version 13*, Computer Aided Mathematics Group, Symbolics, Inc, Birlington, M A.

40. Wako-Shi, (editor), 1984, *RIKEN's International Symposium on Symbolic and Algebraic Computation by Computers*, Saitama, World Scientific, Philadelphia.

41. Wallis, A.F., Bowyer, A. and Davenport, J.H., 1989, "The Use of Symbolic Computation in Geometric Modeling", *Mathematics of Surfaces - Vol. 3*, Oxford University Press.

42. Wooff, C. and Hodgkinson, 1988, *muMATH : A Microcomputer Algebraic System*, Academic Press.

METAL CUTTING & MACHINE TOOL DESIGN :

43. Acherkan, N. et al., 1973, *Machine Tool Design, Vol. 2*, M I R Publisher.

44. Ber, A., Rotberg, J. and Zomback, S., 1988, "A Method for Evaluation of End Mill Cutting", *CIRP Annals*, Vol. 37, No. 1, pp. 37-40.

45. Dhande, S.G., Karunakaran, K.P. and Misra, B.K., 1992, "Geometric Modeling

of Manufacturing Processes Using Symbolic and Computational Conjugate Geometry", submitted to the *ASME Journal of Engineering for Industry*, (Accepted for publication in February, 1994).

46. Ghosh, A. and Mallik, A. K., 1981, *Manufacturing Science*, E W P, New Delhi.

47. Geoffrey Boothroyd, 1985, *Fundamentals of Metal Machining and Machine Tools*, Scripta Book Company, Washington.

48. Iwata, K., Sugimura, N. and Peng, L., 1988, "A Mathematical Analysis of Product Surfaces for Machine Design", *Manufacturing International*, ASME, Vol. I, pp. 1-8.

49. Pandey, P. C., and Shah, H. S., 1980, *Modern Machining Processes*, Tata McGraw Hill, New Delhi.

50. Sen, G. C. and Bhattacharyya, A., 1969, *Principles of Metal Cutting*, New Central Book Agency, Calcutta.

51. Waldrich Siegen, 1988, *Waldrich Siegen 3 Spindle 5 Axes CNC Profiler - Programming Manual*, Waldrich siegen, Burbach, West Germany.

CUTTER PATH GENERATION :

52. An-Chen Lee, Da-Pan Chen and Chih-Lung Lin, 1990, "A CAD/CAM System from 3-D Coordinate Measuring Data", *International Journal of Production Research*, Vol. 28, No. 12, pp. 2353-2371.

53. B. Ae., 1982, *APT 140 NC Machining System - User Reference Guide Release no. VSV1M4*, British Aerospace, U.K.

54. Bedi, S. and Vickess, G.W., 1987, "Post-processor for Numerically Controlled Machine Tools", *Computers in Industry*, Vol. 9, No. 1, pp. 3-18.

55. Chao-Hwa Chang and Michael A. Melkanoff, 1989, *NC Machine Programming and Software Design*, Prentice Hall, Los Angeles.

56. Choi, B.K., Lee, C.S., Hwang, J.S. and Jun, C.S., 1988, "Compound Surface Modeling and Machining", *CAD*, Vol. 20, No. 3, pp. 127-136.

57. CimPoint, 1991, *G-POST Generic NC Post Processor - User Reference Manual*, CimPoint, U.S.A.

58. David D. Grossman, 1986, "Opportunities for Reasearch on NC Machining", *Communications of the ACM*, Vol. 29, No. 6, pp. 515-522.

59. Geoffrey W. Vickers, 1977, "Computer Aided Manufacture of Marine Propellers", *CAD*, Vol. 9, No. 4, pp. 267-274.

60. Gregory C. Loney and Tulga M. Ozsoy, 1987, "NC Machining of Free Form Surfaces", *CAD*, Vol. 19, No. 2, March, pp. 85-90.

61. IBM Corporation, 1982, *IBM Manual SH20-1414-1, System/370 Automatically Programmed Tool - Advanced Contouring (APT-AC) Numerical Control Processor : Program Reference Manual*, Rye Brook, New York.

62. IBM Corporation, 1985, *IBM Manual SH20-1414-2, Automatically Programmed Tool - Advanced Contouring (APT-AC) Numerical Control Processor : Program Reference Manual*, Rye Brook, New York.

63. James P. Duncan, J.P. and Forsyth, D.G., 1977, "Machining Shoe Molds by Numerical Control", *NC from Users' Point of View, Proc. of 14th Annual Conference of NC Society*, Pittsburg, pp. 331-342.

64. Karunakaran, K.P., 1987, "Development of a Macro in FAPT for Machining 3-D Pockets with Islands", *M.Tech. Thesis*, IIT, Madras (India).

65. Kruth, J.P., Snoeys, R. Lauwers, B., Juwet, M. and Leuven, K.U., 1988, "A Generalized Post-processor and Process Planner for 5 Axes Wire EDM Machine", *CIRP Annals*, Vol. 37, No. 1, pp. 203-208.

66. Lin-Lin Chen and Woo, T. C, 1992, "Computational Geometry on the Sphere with Application to Automated Machining", *ASME Journal of Mechanical Design*, Vol. 114, (June), pp. 288-295.

67. Loney, C. and Tulga Mozsoy, 1987, "NC Machining of Free Form Surfaces", *CAD*, Vol. 19, No. 2, pp. 85-90.

68. Michael Puttré, 1992, "Computer Aided Manufacturing : Sculpting Parts from Stored Patterns", *Mechanical Engineering*, CIME, April, pp. 66-70.

69. Persson, H., 1978, "NC Machining of Arbitrarily Shaped Pockets", *CAD*, Vol. 10, No. 3, pp. 169-174.

70. Yap, K.T. and Venkatesh, V.C., 1989, "On the formulation of NC Algorithms Using Computational Geometry", *CIRP Annals*, Vol. 38, No. 1, pp. 433-436.

71. Yong Seok Suh and Kunwoo Lee, 1990, "NC Milling Tool Path Generation for Arbitrary Pockets Defined by Sculptured Surfaces", *CAD*, Vol. 22, No. 5, pp. 273-284.

CUTTER PATH SIMULATION AND ITS APPLICATIONS :

72. Blackmore, D., Leu, M.C. and Wang, K.K., 1992, "Application of Flows and Envelopes to NC Machining", *CIRP Annals*, Vol. 41, No. 1, pp. 493-496.

73. Blackmore, D. and Leu, M.C., 1990, "A Differential Equations Approach to Swept Volumes", *Proceedings of the Second International CIM Conference, May 20-23*, R P I, Troy, New York, pp. 143-149.

74. Chappel, I.T., 1983, "Use of Vectors to Simulate Material Removed by NC Milling", *CAD*, Vol. 15, No. 3, pp. 156-158.

75. Drysdale, R., Jerard, R., Schaudt, B. and Hauck, K., 1989, "Discrete Simulation of NC Machining", *Algorithmica*, 4, pp 33-60.

76. Hook, T.V., 1986, "Real Time Shaded NC Milling Display", *Proceedings of SIGGRAPH '86, Computer Graphics*, Vol. 20, No. 4, pp. 15-19.

77. Jerard, R.B., Drysdale, R.L. and Magawick, J., 1989, "Method for Detecting Errors in NC Machining of Sculptured Surfaces", *IEEE Computer Graphics & Applications*, Vol. 9, No. 1, pp. 26-39.

78. KlÖf, F., 1986, "Two Moving Coordinate Frames for Sweeping along a 3D Trajectory", *CAGD*, Vol. 3, pp. 217-229.

79. Leu, M.C. and Wang, K.K., 1988, "Robot Motion Simulation and Planning Based on Solid Modeling", *CIRP Annals*, Vol. 37, No. 1, pp. 41-44.

80. Leu, M.C., Park, S.H. and Wang, K.K., 1986, "Representation of Swept Volumes and Its Applications", *ASME Journal of Engineering for Industry*, Vol. 108, No.

2, pp. 113-119.

81. Martin, R.R. and Stephenson, P.C., 1990, "Sweeping of 3D Objects", *CAD*, Vol. 22, No. 4, pp. 223-234.

82. Oliver, J.H. and Goodman, E.D., 1990, "Direct Dimensional NC Verification", *CAD*, Vol. 22, No. 1, pp. 3-10.

83. Oliver, J.H., 1986, "Graphical Verification of NC Milling Programs for Sculptured Surface Parts", *Ph.D. Dissertation*, Michigan State University.

84. Oliver, J. H., 1992, "Efficient Intersection of Surface Normals with Milling Tool Swept Volumes for Discrete Three-Axis NC Verification", *ASME Journal of Mechanical Design*, Vol. 114, (June), pp. 283-287.

85. Robert B. Jerard, Robert L. Drysdale and John Magewick, 1989, "Methods for Detecting Errors in Numerically Controlled Machining of Sculptured Surfaces", *IEEE Computer Graphics & Applications*, Vol. 9, No. 1, January, pp. 26-39.

86. Shpitalni, 1987, "Switching Functions Based on Geometric Modeling and Its Application to NC Program Verification", *CIRP Annals*, Vol. 36, No. 1, pp. 73-76.

87. Takata, S., Tsai, M.D. and Inui, M., 1989, "A Cutting Simulation System for Machinability Evaluation Using a Work Piece Model", *CIRP Annals*, Vol. 38, No. 1, pp. 417-420.

88. Voelcker, H.B. and Hunt, W.A., 1981, "The Role of Solid Modeling in Machining - Process Modeling and NC Verification", *Proceedings of SAE International Congress Exposition*, M I, U.S.A., (February).

89. Voelcker, H.B. and Requicha, A.A.G., 1977, "Geometrical Modeling of Mechanical Parts and Processes", *Computer Surveys*, No. 10, (December).

90. Wang, W. P., and Wang, K. K., 1986, "Geometric Modeling of Swept Volume of Moving Solids", *IEEE Computer Graphics & Applications*, Vol. 6, # 2, pp. 8-17.

91. Wang, W.P. and Wang, K.K., 1986, "Real Time Verification of Multi-axes NC Program with Raster Graphics", *Proceedings of IEEE International Conference on Robotics & Automation*, San Francisco, (April).

92. Wang, K.K., 1987, "Application of Solid Modeling to Automate Machining Parameters for Complex Parts", *Proceedings of CIRM Manufacturing Seminar*, Pennsylvania State, U.S.A., pp. 33-37.

COMPUTER AIDED PROCESS PLANNING :

93. Chang, T.C. and Wysk, R.A., 1985, *An Introduction to Automated Process Planning Systems*, Prentice Hall, Inc. Englewood, New Jersey.

94. Choi, B.K., Barash, M.M. and Anderson, D.C., 1984, "Automatic Recognition of Machined Surfaces from a 3-D Solid Model", *CAD*, Vol. 16, No. 2, pp. 81-86.

95. James E. Bobrow, 1985, "NC Machine Tool Path Generation from CSG Part Representations", *CAD*, Vol. 17, No. 2, pp. 69-75.

96. Joshi, S. and Chang, T.C., 1988, "Graph Based Heuristics for Feature Recognition of Machined Features from a 3D Solid Model", *CAD*, Vol. 20, No. 2, March, pp. 58-66.

97. Kanumury, M. and Chang, T.C., 1991, "Process Planning in an Automated Manufacturing Environment", *Journal of Manufacturing Systems*, Vol. 10, No. 1.

98. Perng, D., Chen, Z., and Li, R., 1990, "Automatic 3D Machining Feature Extraction from 3D CSG Solid Input", *CAD*, Vol. 22, No. 5, (June), pp. 285-295.

99. Ramesh Srinivasan and Placid Ferreira, 1990, "Geometric Models of Machining Processes for Computer Aided Process Planning", *Geometric Modeling for Production Engineering*, Elsevier Science Publishers, pp. 423-450.

100. Shah, J.J., 1991, "Assessment of Feature Technology", *CAD*, Vol. 23, No. 5, pp. 331-343.

101. Zeidner, L.E., 1990, "Automatic Process Generation - the Surround Problem" *Second International CIM Conference*, RPI, Troy (May).

MANUFACTURE OF EXTRUDER SCREWS :

102. Barr, R.A. and Chung, C.I., 1966, "Effect of radial Screw Clearance on Extruder Performance", *SPE Journal*, June, pp. 71-73.

103. Battle, J.A., Foix, S.C. and Sanz, C.V., 1984, "On the Design of Milling Cutters or Grinding Wheels for Twist Drill Manufacture : A CAD Approach", *Proceedings of IMTDR*, pp. 315-320.

104. Booy, M.L., 1978, "Geometry of Fully Wiped Twin-Screw Equipment", *Polymer Engineering and Science*, Vol. 18, No. 12, pp. 973-984.

105. Brydson, J.A., 1966, "Some Uses and Abuses of Rheology in Polymer Processing", *Transactions of Journal of Plastics Inst.*, March, pp. 65-71.

106. Clegg, P.L., 1966b, "The Interdependent Processing Variables and Their Rheological Influence", *Transactions of Journal of Plastics Inst.*, August, pp. 179-182.

107. Clegg, P.L., 1966a, "Flow in Various Extrusion Processes", *British Plastics*, February, pp. 96-103.

108. Janssen, L.P.B.M., 1978, *Twin-Screw Extrusion*, Elsevier Scientific Publishing Company, Amsterdam.

109. Saybold, H., 1990, "Suggestions for the CAD of Cutters for the Milling of Helical Slots", Presented in the *4th ASEE International Conference on Engineering Computer Graphics and Descriptive Geometry*, Miami, USA.

110. Saybold, H., 1992, "Geometry for Engineers: What Do They Need Tomorrow ? What Do We Have to Teach Today ?", *Proceedings of 5th ASEE International Conference on Engineering Computer Graphics and Descriptive Geometry, August 17-21*, RMTI, Melbourne, Australia, pp. 327-330.

111. Stevens, M.J., 1985, *Extruder Principles and Operation*, Elsevier Applied Science Publishers, London.

112. Voruganti, R.S., Dhande, S.G. and Reinholtz, C.F., 1990, "Symbolic and Computational Conjugate Geometry for the Manufacture of Helically Swept Surfaces", *Second International CIM Conference*, RPI, Troy (May).

COMPUTER AIDED DESIGN AND MANUFACTURE :

113. Aomura, S. and Uehara, 1990, "Self-Intersection of an Offset Surface", *CAD*, Vol. 22, No. 7, pp. 417-422.

114. Dhande, S.G., Padmanabhan, B., Reinholtz,C.F. and Voruganti, R.S., 1990, "Computer Aided Design and Manufacture of Approximate Ruled Surfaces", *Proceedings of the Second International CIM Conference, May 20-23*, R P I, Troy, New York.

115. Dhande, S.G. and Karunakaran, K.P., 1993, "Realizability in Computer Aided Design", an Invited Talk in the *International Conference on Computer Graphics 1993 (ICCG-93)*, Bombay (February).

116. Farin, G., 1988, *Curves and Surfaces for Computer Aided Design - A Practical Guide*, Academic Press, San Diego, CA.

117. Gregory, J.A., (editor), 1986, *Mathematics of Surfaces - Vol. 1*, Oxford University Press.

118. Gurunathan, B., 1986, "Computer Aided Geometric Methods for Development of Certain Classes of Ruled Surfaces", *Ph.D. Dissertation*, I I T, Kanpur (India).

119. Handscomb, D.C., (editor), 1989, *Mathematics of Surfaces - Vol. 3*, Oxford University Press.

120. Joe Rooney and Philip Steadman, 1987, *Principles of Computer Aided Design*, Pitman/ Open University, London.

121. Kochan, D., (editor), 1986, *CAM : Development in Computer Integrated Manufacturing*, Springer-Verlag, Berlin.

122. Kondo. T, Kishisamy, T. and Saito, K., 1988, "A Machining System Based on Inverse Offset Method", *Journal of Japan Society of Precision Engineering*, Vol. 55, No. 5, pp. 167-172.

123. Kyprianou, L.K., 1983, "Shape Classification in CAD", *Ph.D. Dissertation*, University of Cambridge.

124. Ravani, B. and Chen, Y. J., 1986, "Computer Aided Design and Machining of Composite Ruled Surfaces", *Journal of Mechanisms, Transmissions and Automation in Design*, Vol. 108, June, pp. 217-223.

125. Ravani, B. and Wang, J. W., 1991, "Computer Aided Geometric Design of Line Constructs", *ASME Journal of Mechanical Design*, Vol.113, December, pp. 363-371.

126. Rogers, D.F. and Adams, J.A., 1974, "Mathematical Elements of Computer Graphics", McGraw Hill, New York.

127. Saeed, S.E.O., A de Pennington and Dodsworth, J.R., 1988, "Offsetting in Geometric Modeling", *CAD*, Vol. 20, No. 2, pp. 67-74.

128. Susan Finger and John R. Dixon, 1989b, "A Review of Research in Mechanical Engineering Design. Part II: Representations, Analysis and Design for the Life Cycle" *Research in Engineering Design*, Springer-Verlag.

129. Susan Finger and John R. Dixon, 1989a, "A Review of Research in Mechanical Engineering Design. Part I: Descriptive, Prescriptive and Computer-Based Models of Design Processes" *Research in Engineering Design*, Springer-Verlag.

130. Tavakkoli, S. and Dhande, S. G., 1991, "Shape Synthesis and Optimization Using Intrinsic Geometry" *ASME Journal of Mechanical Design*, Vol.113, December, pp. 379-386.

131. Yehonathan Hazony, 1990, "Geometric Modeling for Design for Manufacturability" *Second International CIM Conference*, RPI, Troy (May), pp. 131-136.

Definition of the Model of the Generic Machine Tool - Listing of MACSYMA Program

```
                        /************************/
                        /* FILE NAME : MCHN.MAC */
                        /************************/

kill(all);

/* Declaring Dependencies of variables */
/* on Parameters u1,v1,u2,v2, and t    */
/* ----------------------------------- */
depends ( [x1, y1, z1], [u1, v1] );
depends ( [x2, y2, z2], [u2, v2] );
depends ( [aa1, bb1, cc1, theta1, phi1, si1], t );
depends ( [aa2, bb2, cc2, theta2, phi2, si2], t );

/* CUTTER SURFACE: */
/* =============== */
/* Defining Point P on Cutter Surface in M1 system */
p1 : matrix ([x1, y1, z1, 1]);
/* Position Transformation matrix from M1 to M0 */
r_theta1_x1 : matrix ( [1,            0,              0,            0],
                       [0,        cos(theta1), sin(theta1),        0],
                       [0,       -sin(theta1), cos(theta1),        0],
                       [0,            0,              0,            1]);

r_phi1_y1   : matrix ( [cos(phi1),    0,         -sin(phi1),       0],
                       [0,            1,             0,            0],
                       [sin(phi1),    0,          cos(phi1),       0],
                       [0,            0,             0,            1]);

r_si1_z1    : matrix ( [cos(si1),    sin(si1),       0,            0],
                       [-sin(si1),   cos(si1),       0,            0],
                       [0,            0,             1,            0],
                       [0,            0,             0,            1]);

tr_01_to_00 : matrix ( [1,            0,             0,            0],
                       [0,            1,             0,            0],
                       [0,            0,             1,            0],
                       [aa1,        bb1,           cc1,            1]);

t10         : r_theta1_x1 . r_phi1_y1 . r_si1_z1 . tr_01_to_00;

/* Position Transformation matrix from M0 to M1 */
```

```
t01          : t10^^-1;
t01          : trigsimp (t01);

/* Transformation matrix for normal from M1 to M0: */
m10          : matrix ( [t10[1,1],  t10[1,2],  t10[1,3],        0],
                        [t10[2,1],  t10[2,2],  t10[2,3],        0],
                        [t10[3,1],  t10[3,2],  t10[3,3],        0],
                        [       0,          0,          0,      0]);

/* Transformation matrix for normal from M0 to M1: */
m01          : matrix ( [t01[1,1],  t01[1,2],  t01[1,3],        0],
                        [t01[2,1],  t01[2,2],  t01[2,3],        0],
                        [t01[3,1],  t01[3,2],  t01[3,3],        0],
                        [       0,          0,          0,      0]);

/* Velocity Tranformation Matrix from M1 to M0: */
tmp11        : 'diff (t10[1,1], t);
tmp12        : 'diff (t10[1,2], t);
tmp13        : 'diff (t10[1,3], t);
tmp14        : 'diff (t10[1,4], t);
tmp21        : 'diff (t10[2,1], t);
tmp22        : 'diff (t10[2,2], t);
tmp23        : 'diff (t10[2,3], t);
tmp24        : 'diff (t10[2,4], t);
tmp31        : 'diff (t10[3,1], t);
tmp32        : 'diff (t10[3,2], t);
tmp33        : 'diff (t10[3,3], t);
tmp34        : 'diff (t10[3,4], t);
tmp41        : 'diff (t10[4,1], t);
tmp42        : 'diff (t10[4,2], t);
tmp43        : 'diff (t10[4,3], t);
tmp44        : 'diff (t10[4,4], t);

t10v         : matrix ( [tmp11, tmp12, tmp13, tmp14],
                        [tmp21, tmp22, tmp23, tmp24],
                        [tmp31, tmp32, tmp33, tmp34],
                        [tmp41, tmp42, tmp43, tmp44]);

/* Velocity of P in Cutter Surface w.r.t. M0: */
v0p1         : p1 . t10v;

/* BLANK  SURFACE: */
/* =============== */
/* Defining Point P on Blank Surface in M2 system */
p2           : matrix ([x2, y2, z2, 1]);
/* Transformation matrix from M2 to M0 */
r_theta2_x2  : matrix ( [   1,          0,              0,          0],
                        [   0,     cos(theta2),  sin(theta2),       0],
                        [   0,    -sin(theta2),  cos(theta2),       0],
                        [   0,          0,              0,          1]);

r_phi2_y2    : matrix ( [ cos(phi2),    0,        -sin(phi2),       0],
                        [   0,          1,              0,          0],
                        [ sin(phi2),    0,         cos(phi2),       0],
                        [   0,          0,              0,          1]);

r_si2_z2     : matrix ( [ cos(si2), sin(si2),        0,          0],
                        [-sin(si2), cos(si2),        0,          0],
```

```
                          [   0,          0,          1,          0],
                          [   0,          0,          0,          1]);

tr_02_to_00 : matrix ( [   1,          0,          0,          0],
                       [   0,          1,          0,          0],
                       [   0,          0,          1,          0],
                       [  aa2,        bb2,        cc2,          1]);

t20         : r_theta2_x2 . r_phi2_y2 . r_si2_z2 . tr_02_to_00;

/* Transformation matrix from M0 to M2 */
t02         : t20^^-1;
t02         : trigsimp (t02);

/* Transformation matrix for normal from M2 to M0: */
m20         : matrix ( [t20[1,1],  t20[1,2],  t20[1,3],        0],
                       [t20[2,1],  t20[2,2],  t20[2,3],        0],
                       [t20[3,1],  t20[3,2],  t20[3,3],        0],
                       [       0,          0,          0,        0]);

/* Transformation matrix for normal from M0 to M1: */
m02         : matrix ( [t02[1,1],  t02[1,2],  t02[1,3],        0],
                       [t02[2,1],  t02[2,2],  t02[2,3],        0],
                       [t02[3,1],  t02[3,2],  t02[3,3],        0],
                       [       0,          0,          0,        0]);

/* Transformation matrix for normal from M0 to M1: */
/* Velocity Tranformation Matrix from M2 to M0: */
tmp11       : ,diff (t20[1,1], t);
tmp12       : 'diff (t20[1,2], t);
tmp13       : 'diff (t20[1,3], t);
tmp14       : 'diff (t20[1,4], t);
tmp21       : 'diff (t20[2,1], t);
tmp22       : 'diff (t20[2,2], t);
tmp23       : 'diff (t20[2,3], t);
tmp24       : 'diff (t20[2,4], t);
tmp31       : 'diff (t20[3,1], t);
tmp32       : 'diff (t20[3,2], t);
tmp33       : 'diff (t20[3,3], t);
tmp34       : 'diff (t20[3,4], t);
tmp41       : 'diff (t20[4,1], t);
tmp42       : 'diff (t20[4,2], t);
tmp43       : 'diff (t20[4,3], t);
tmp44       : 'diff (t20[4,4], t);
t20v        : matrix ( [tmp11, tmp12, tmp13, tmp14],
                       [tmp21, tmp22, tmp23, tmp24],
                       [tmp31, tmp32, tmp33, tmp34],
                       [tmp41, tmp42, tmp43, tmp44]);

/* Velocity of P in Blank Surface in M0: */
v0p2        : p2 . t20v;

/* CUTTER SURFACE NORMAL: */
/* ====================== */
/* Normal of Cutter Surface in M1: */
dx1_du1     : 'diff (x1, u1);
dy1_du1     : 'diff (y1, u1);
dz1_du1     : 'diff (z1, u1);
```

```
dx1_dv1      : 'diff (x1, v1);
dy1_dv1      : 'diff (y1, v1);
dz1_dv1      : 'diff (z1, v1);
n1p          : matrix ( [dy1_du1 * dz1_dv1  -  dy1_dv1 * dz1_du1,
                         dx1_dv1 * dz1_du1  -  dx1_du1 * dz1_dv1,
                         dx1_du1 * dy1_dv1  -  dx1_dv1 * dy1_du1,
                                                              0]);

/* Magnitude of Normal of Cutter Surface: */
magnitude_n1p : sqrt (n1p[1,1]^2 + n1p[1,2]^2 + n1p[1,3]^2);

/* Unit Normal of Cutter Surface in M2:*/
unit_n1p     : matrix ( [n1p[1,1]/magnitude_n1p,
                         n1p[1,2]/magnitude_n1p,
                         n1p[1,3]/magnitude_n1p,
                                                0]);

/* Unit Normal of Cutter Surface in M0: */
n0p1         : unit_n1p . m10;

/* BLANK SURFACE NORMAL: */
/* ===================== */
/* Normal of Blank Surface in M2: */
dx2_du2 : 'diff (x2, u2);
dy2_du2 : 'diff (y2, u2);
dz2_du2 : 'diff (z2, u2);
dx2_dv2 : 'diff (x2, v2);
dy2_dv2 : 'diff (y2, v2);
dz2_dv2 : 'diff (z2, v2);
n2p : matrix ( [dy2_du2 * dz2_dv2  -  dy2_dv2 * dz2_du2,
                dx2_dv2 * dz2_du2  -  dx2_du2 * dz2_dv2,
                dx2_du2 * dy2_dv2  -  dx2_dv2 * dy2_du2,
                                                      0]);

/* Magnitude of Normal of Blank Surface: */
magnitude_n2p : sqrt (n2p[1,1]^2 + n2p[1,2]^2 + n2p[1,3]^2);

/* Unit Normal of Blank Surface in M2:*/
unit_n2p     : matrix ( [n2p[1,1]/magnitude_n2p,
                         n2p[1,2]/magnitude_n2p,
                         n2p[1,3]/magnitude_n2p,
                                                0]);

/* Unit Normal of Blank Surface in M0: */
n0p2         : unit_n2p . m20;

/* CONDITION OF CUTTING: */
/* ===================== */
/* Relative Velocity in M0: */
v0p12 : v0p2 - v0p1;

constraint1 : v0p12 . transpose(n0p1) = 0;
constraint1 : trigsimp (constraint1);

constraint2 : v0p12 . transpose(n0p2) = 0;
constraint2 : trigsimp (constraint2);

save ("mchn.sav", all);
```

Definition of the Model of the Generic Cutter - Listing of MACSYMA Program

```
                        /**********************/
                        /* FILE NAME : CU.MAC */
                        /**********************/

kill(all);

/* NOMENCLATURE */
/* ============ */

/* u11     : value of u1 at point P for the generic cutter        */
/* u12     : value of u1 at point Q for the generic cutter        */
/* u13     : value of u1 at point S for the generic cutter        */
/* u14     : value of u1 at point T for the generic cutter        */

/* s1      : value of u1 at point P for the current cutter        */
/* s2      : value of u1 at point Q for the current cutter        */
/* s3      : value of u1 at point S for the current cutter        */
/* s4      : value of u1 at point T for the current cutter        */


/* GENERIC CUTTER */
/* ============== */

eqn_OcP             : Zc = Xc * tan(a);
eqn_PQ              : (Xc - e)^2 + (Zc - f)^2 = r^2;
eqn_QS_when_b_is_0  : Xc = Zc * tan(b) - d/2 * tan(a) * tan(b) +d/2;
eqn_QS_for_others   : Zc = Xc * cot(b) + d/2 * (tan(a) - cot(b));
eqn_ST              : Xc = h * tan(b) - d/2 * tan(a) * tan(b) + d/2;

Point_Oc   : [0,0,0];

XcA        : e;
ZcA        : f;
Point_A    : [XcA, 0, ZcA];

XcR        : d/2;
ZcR        : d/2 * tan(a);
Point_R    : [XcR, 0, ZcR];

dist_AR    : sqrt ( (XcA-XcR)^2 + (ZcA-ZcR)^2 );

XcS        : h * tan(b) - d/2 * (tan(a) * tan(b)) + d/2;
```

```
ZcS        : h;
Point_S    : [XcS, 0, ZcS];

convert_a_b_to_radians () := BLOCK( a : a * %pi / 180,
                                    b : b * %pi / 180);

calculate_e_f () :=
        BLOCK (if Is_Fillet_Radius then
                  (e : d/2 - r * (cos(a) - sin(b))/cos(a+b),
                   e : ev(e),
                   f : (e * sin(a) + r)/cos(a),
                   f : ev(f) ) );

calculate_h    () :=
     BLOCK (if b = 0 and Is_Fillet_Radius then h : f,
            if b = 0 and Is_Fillet_radius = FALSE then h : ZcQ);

Xc(u1) :=BLOCK (
          if (u1 >= 0  and u1 <  s1)
             then ('u1 * cos(a))
          else if (u1 >= s1 and u1 <  s1+s2)
             then
             if r = 0 then ('u1 * cos(a))
             else if r = INF then XcP + ((XcQ-XcP)/s2)*('u1-s1)
             else (e + abs(r) * cos ( atan2(s1*sin(a)-f, s1*cos(a)-e)
                                    + ('u1-s1)/r))
          else if (u1 >= s1+s2 and u1 <  s1+s2+s3)
               then (('u1-s1-s2-s3)*sin(b) + ev(XcS))
          else if (u1 >= s1+s2+s3 and u1 <= s1+s2+s3+s4)
               then '(ev(XcS)));

Zc(u1) :=BLOCK (
          if (u1 >= 0  and u1 <  s1)
             then ('u1 * sin(a))
          else if (u1 >= s1 and u1 <  s1+s2)
             then
             if r = 0 then ('u1 * sin(a))
             else if r = INF then ZcP + ((ZcQ-ZcP)/s2)*('u1-s1)
             else (f + abs(r) * sin ( atan2(s1*sin(a)-f, s1*cos(a)-e)
                                    + ('u1-s1)/r))
          else if (u1 >= s1+s2 and u1 <  s1+s2+s3)
               then (('u1-s1-s2-s3)*cos(b) + ev(ZcS))
          else if (u1 >= s1+s2+s3 and u1 <= s1+s2+s3+s4)
               then (('u1-s1-s2-s3) +ev(ZcS)));

X1(u1,v1) := Xc(u1) * (cos('v1));
Y1(u1,v1) := Xc(u1) * (sin('v1));
Z1(u1,v1) := Zc(u1);

save("cu.sav",all);
```

```
                    /**************************/
                    /* FILE NAME : CUTTER.MAC */
                    /**************************/


numer : TRUE;
convert_a_b_to_radians ();

/* CALCULATION OF E & F: */
/* ===================== */
calculate_e_f ();

/* POINT P: */
/* ======== */
      check_P    : ((e + f*tan(a)) * (cos(a)^2))^2
                   -(e^2 + f^2 - r^2) * (cos(a)^2);
      check_P    : ev(check_P);
      if abs(check_P) < 0.000001 then check_P : 0
      else if asksign(check_P) = 'NEG
           then check_P : POINT_P_INVALID;
      XcP        : (e + f*tan(a)) * (cos(a)^2) - sqrt (check_P);
      ZcP        : XcP * tan(a);

/* POINT Q: */
/* ======== */
      check_Q    : ((f + (e + (d/2)*(tan(a)*tan(b)-1))*tan(b))
                     * (cos(b)^2))^2
                   - ((f^2 + (e + (d/2)*(tan(a)*tan(b)-1))^2 - r^2)
                     * (cos(b)^2));
      check_Q    : ev(check_Q);
      if abs(check_Q) < 0.000001 then check_Q : 0
      else if asksign(check_Q) = 'NEG
           then check_Q : POINT_Q_INVALID;
      ZcQ        : (f + (e + (d/2)*(tan(a)*tan(b)-1)) * tan(b))
                   * (cos(b)^2) + sqrt (check_Q);
      XcQ        : ZcQ * tan(b) - (d/2) * (tan(a)*tan(b)-1);

/* CALCULATION OF H */
/* ================ */
calculate_h ();

/* CALCULATION OF S1, S2, S3 & S4: */
/* =============================== */
s1         : sqrt (XcP^2 + ZcP^2);
s1         : ev(s1);
if abs(b) = 0 then s3 : 0
else s3    : sqrt ( ( (h - d/2*(tan(a)-cot(b)))*tan(b) - XcQ)^2
                 +  (h - ZcQ)^2 );
s3         : ev(s3);

if r = 0 then s2 : 0
else  s2   : r * ( atan2(ZcQ - f, XcQ - e) - atan2(ZcP - f,XcP - e));
s2         : ev(s2);

s4 : h1;
numer : FALSE;
```